Development of Steel Slag –Bonded Wood Composites as Sustainable Building Products

By

Nada Zod

Department of Civil Engineering and Applied Mechanics

McGill University, Montreal

Quebec, Canada

August, 2022

A thesis submitted to McGill University in partial fulfillment of the requirements of the degree of Doctor of Philosophy.

Abstract

The aim of this study was to provide a deeper understanding of the mechanisms of strength gain in steel slag pastes subjected to combined carbonation-hydration curing, bringing this binder system a step closer towards recognition as sole binder. Furthermore, two building products: slag-bonded strand boards (SBSB) and lightweight structural masonry units (SMU) with recycled wood aggregates, were developed using steel slag as the sole primary binder. Lastly, different carbonation parameters were examined to optimize the flue gas carbonation curing process in SBSB. Steel slag paste achieved an ultimate strength of 70 MPa following 24 hours of carbonation curing and 28 days of subsequent hydration. Prolonged carbonation curing for 24 hours was found to improve the over-all strength and reaction degree, reduce the porosity, and promote subsequent hydration. The reaction product was found to be a hybrid between calcium silicate hydrate and calcium carbonates ($CaCO_3$) where the latter acted as seeds that promoted subsequent hydration. Results of the SBSB revealed that carbonation activated steel slag can be used as sole binder for the production of strand boards. Accelerated ageing tests performed on SBSB revealed excellent performance owing to carbonate precipitation and the weakly hydraulic nature of the steel slag. The developed SBSBs were carbon negative, cost efficient and able to store carbon dioxide. SMU with recycled wood as partial replacement of fine aggregates could sequester more carbon dioxide than wood-free SMU. Carbonation curing in wood-SMU enhanced the strength and led to the development of a lightweight loadbearing SMU. The interfacial zone between wood and carbonated steel slag paste was shown to have minimal compositional difference with that of the bulk steel slag matrix. Furthermore, flue gas was successfully used to replace pure carbon dioxide gas for the steel slag curing process of SBSB. The results revealed that an elevated temperature of

40 °C and pressure of 350 KPa could improve the carbonation efficiency and result in SBSB that demonstrated comparable performance to those cured with pure carbon dioxide gas.

Résumé

Le but de cette étude était d’acquérir une connaissance des mécanismes de gain de résistance dans les pâtes de laitier d'acier soumises à un durcissement combiné carbonatation-hydratation et la reconnaissance de ce système en tant que liant unique. De plus, le laitier d'acier a été utilisé comme seul liant pour le développement de deux produits de construction: les éléments de maçonnerie légère (SMU) avec des granulats et des panneaux de particules de bois recyclés (SBSB). La pâte de laitier d'acier a atteint une résistance ultime de 70 MPa après 24 heures de durcissement par carbonatation et 28 jours d'hydratation ultérieure. Un durcissement prolongé par carbonatation pendant 24 heures a amélioré la résistance globale et le degré de réaction, réduit la porosité et a favorisé l’hydratation ultérieure. Le produit de la réaction est un hybride entre le gel de silice modifié par Ca et les carbonates de calcium ($CaCO_3$) où ces derniers servent de des germes pour favoriser l'hydratation ultérieure. La SMU avec du bois recyclé, pour remplacer les granulats fins, pourrait séquestrer plus de dioxyde de carbone que la SMU sans bois. Il a été démontré que la zone interfaciale entre le bois et la pâte de laitier d'acier carbonaté présentait une différence minimale avec celle de la matrice de laitier d'acier en vrac. Les résultats du SBSB ont montré que le laitier d'acier activé par carbonatation peut être utilisé comme seul liant pour la production de panneaux de copeaux. Les tests de vieillissement accéléré effectués sur SBSB ont révélé d'excellentes performances en raison de la précipitation de carbonate et de la nature faiblement hydraulique du laitier d'acier. Les SBSB développés étaient négatifs en carbone, rentables et capables de stocker le dioxyde de carbone. Enfin, les gaz de combustion ont été utilisés avec succès pour remplacer le dioxyde de carbone pur dans le procédé de durcissement des scories d'acier de SBSB. Différents paramètres de carbonatation ont été testés pour optimiser le processus de durcissement par carbonatation des gaz de combustion dans les scories d'aciérie. Les résultats ont démontré qu'une température (40 °C) et une pression élevées pourraient améliorer l'efficacité de la carbonatation et

aboutir à des SBSB, qui ont des performances comparables à celles durcies avec du gaz carbonique pur.

Acknowledgments

First and foremost, I would like to thank GOD, who has so generously bestowed me with countless blessings among which was the completion of this thesis.

I would like to express my deepest gratitude to my supervisor, Professor Yixin Shao, for his immeasurable patience, invaluable guidance, insightful comments, and support throughout this academic journey. I am extremely grateful for our discussions that helped develop my intellectual thinking. I also would like to thank you for believing in me and always encouraging me to give my best.

To my beloved parents, my mother Rawaa El-Rifai and my father Mohamad Zod, I dedicate this thesis to you. You are my biggest blessing in this world. You are my first teachers and the lessons that I was so blessed to learn from you are numerous. Your unconditional love and selfless devotion are forever acknowledged. To my precious, loving, and supportive husband, Ramy Kheir: my deepest gratitude. Your encouragement and comfort when the times got rough are much appreciated and duly noted. To my beloved kids, Mazhar and Malak: I am very fortunate to have you. I hope I make you proud. To my brothers and sisters, my backbone, thank you for putting up with my constant nagging! Without such a supportive team behind me, I wouldn’t have made it this far.

I would like to thank Professor Alfonso Mucci for reviewing this thesis and for providing insightful comments. I would also like to extend my gratitude to Dr. Bill Cook, John Baratzak, William Dumais, and Lucie Riffard for all their help in the lab. Additionally, I would like to thank my colleagues Dr. Zaid Ghouleh, Dr. Xiangping Xian and Dr. Shipeng Zhang for our discussions. Lastly, big thanks to my dear sister, Samar Zod, for all the help in Photoshop.

Contribution to Original Knowledge

This work presents a feasibility study on use of steel slag to replace Ordinary Portland Cement as a sole binder for the production of various wood-slag products. The performance and microstructure of products synthesized using steel slag and wood submitted to a regime of carbonation-hydration curing were studied. The aim was to produce performance effective, sustainable and durable products that could replace cement-based products. Investigating the combined carbonation-hydration behavior of steel slag paste and wood-slag products contributes to the technological advances relating to the following findings:

1. The mechanism of strength gain in combined carbonation-hydration curing regimes in steel slag paste compacts was studied. It was found that the carbonation duration affected the ultimate strength recorded after 28 days of subsequent hydration. Prolonged carbonation duration promoted subsequent hydration and contributed towards an over-all higher strength and reaction degree. It was inferred that formed $CaCO_3$ acted as nucleation sites to promote hydration.
2. Carbonation activated steel slag was used to replace cement towards the production of slag-bonded strand boards. The production parameters were determined. The slag-bonded strand boards offer CO_2 sequestration and permanent storage, carbon footprint reduction, green house gas mitigation, industrial waste recycling and natural resource preservation.
3. Durability of wood-slag composites was improved owing to the carbonation reaction which effectively mitigated weathering carbonation. Furthermore, the long-term durability of wood within the steel slag matrix was preserved owing to the low hydraulic properties of used binder.

4. Carbonation curing was adopted to promote the use of wood in steel slag masonry units. The developed units could incorporate high volumes of wood owing to the improved interface between wood and steel slag resulting in an end-product that is performance equivalent to load-bearing commercial cement blocks and superior to non-loadbearing lightweight cement blocks. The masonry units provided a suitable outlet for the recycling and valorization of industry products such as steel slag and wood chips.

5. Flue gas carbonation was employed for the curing of slag-bonded strand boards. The optimal curing conditions were determined, and the microstructural development induced by the carbonation curing and subsequent hydration curing was investigated.

Contribution of Authors

This thesis is a manuscript-based thesis. Papers based on Chapters 3 to 7 have been submitted or will be submitted for publication in peer-reviewed journals. The author was responsible for conducting the experiments, analyzing the data, and preparing the manuscripts. The author's supervisor, Professor Yixin Shao, provided guidance and editorial revisions throughout the entire process. The submitted paper is:

Nada Zod, Alfonso Mucci, Olivier Bahn, Richard Provençal, Yixin Shao, 2021, "Steel slag-bonded strand board as a carbon-negative building product", Construction and Building Materials, Published. https://doi.org/10.1016/j.conbuildmat.2022.127695. Professor Alfonso Mucci contributed towards the writing-revision and editing. Professor Olivier Bahn provided editorial revisions. Mr. Richard Provençal provided resources for the conduction of the research.

Table of Contents

List of Tables

List of Figures

1. Chapter 1 Introduction

1.1 Overview

Slag is a major by-product of the steel industry. There are two types of slags: blast furnace slag from the iron-making process (iron slag) and converter furnace slag from the steel refining process (steel slag). Whereas iron slag is commonly used as a cementitious material for cement blends, steel slag is only used as coarse aggregates in road construction and significant amounts are disposed of in landfill. Dumping steel slag in landfills could lead to soil and water contamination, environmental pollution and could ultimately affect the quality of life for the local population [1]. Compared to iron slag, steel slag is highly undervalued. This is because steel slag is not a pozzolanic material, has high free-lime content and does not show value-added cementitious behaviour [2, 3].

Numerous approaches had been investigated to make best use of the cementitious properties of this calcium-silicate rich material. Alkali-activation had been successfully employed on ladle slag [4]. Heat treatment with controlled cooling rate had also been proven to ameliorate the cementitious properties of steel slag [5]. Furthermore, mechanical activation through prolonged milling in ethanol suspension of ladle slag and argon-oxygen decarburization of stainless steel slag had proved effective to activate its hydraulic strength [6].

Meanwhile, accelerated carbonation curing is an auspicious technique for strength improvement and permanent CO_2 sequestration in calcium-silicate rich materials. To this end, Carbonation curing had been investigated as a possible mean to activate the strength of steel slag. In fact, it was shown that the calcium silicate phases in steel slag react with CO_2 in the presence of water to form thermodynamically stable calcium carbonates and strength contributing calcium silicate hydrate gels (C-S-H). The principal reactions are given in Eq. 1 and Eq. 2. [7]

$$2(2CaO \cdot SiO_2) + (2\text{-}x)\ CO_2 + yH_2O \rightarrow x\ CaO \cdot SiO_2 \cdot yH_2O + (2\text{-}x)\ CaCO_3 \quad (1)$$

$$3(3CaO \cdot SiO_2) + (3\text{-}x)\ CO_2 + yH_2O \rightarrow x\ CaO \cdot SiO_2 \cdot yH_2O + (3\text{-}x)\ CaCO_3 \quad (2)$$

On the other hand, production of ordinary Portland cement (OPC) is an energy-intensive and CO_2-emitting process. It is estimated that production of one ton of OPC generates one ton of carbon dioxide, requires one and half tons of raw materials including limestone, clay, silica, iron ore and gypsum and consumes 105 kg of coal-equivalent fuel and 99 kWh of electric power. Furthermore, the construction industry contributes 7 % of the total carbon dioxide emissions. With global warming becoming a serious threat to oceans, water supplies, agriculture and human health to name a few, reducing the overall CO_2 emissions has become a must [8]. In this light, it would be gratifying if CO_2-activated steel slag could be used as a cementing material to completely replace Portland cement in structural concrete applications. This would significantly reduce CO_2 emissions, promote CO_2 capture and permanent sequestration, and conserve natural resource as substantial environmental and economic benefits [9].

1.2 Research Objectives

Following the global trend to preserve natural resources and mitigate carbon emissions, the objective of this research is to investigate the feasibility of producing slag-bonded wood composites using carbonation activated steel slag as sole binder. The decrease in the demand for wood chips and the need to avoid wood incineration has sparked the need to find suitable outlets for this burdensome waste material. This provides an opportunity to use wood chips, a by-product of the lumber industry, by extending the storage of carbon to wood products. Wood-strand cement boards with average cement content of 60-70 % are potential ideal candidates. Also, wood-slag masonry unit will be developed for use in structural and load-bearing purposes. The developed products should be performance equivalent or superior to commercially available cement-based products. All the products will be subjected to accelerated early carbonation curing, hydration curing and a regime of combined carbonation-hydration curing to maximize strength performance. Standard tests will be performed to compare with industry specifications and microstructure analysis will be conducted to study the new products.

Use of steel slag as a sole binder to develop wood-slag composites would entail a thorough understanding of this binder system as a first step. Although previous research had already shown the ability of carbonation curing to activate the early strength of steel slag to serve as a binder with great benefit [10, 11], most research focused on strength development rather than the microstructural phases development. To this end, the aim of this research is to study the microstructural development of the binding phases present in this binder system when subjected to various curing schemes, an essential step for wide-range acceptance of this binder. A multi-technique investigation will be employed to explore the chemical aspects of the microscopic phases present in steel slag binder as well as the mechanism of strength gain. Lastly, a process to develop slag-bonded strand board and a wood-slag masonry block will be developed where both pure carbon dioxide gas and flue gas carbonation curing will be explored.

1.3 Thesis Structure

The thesis is manuscript-based where each chapter is a stand-alone paper targeted for publication. A preface is included in each chapter to introduce the objectives and the background. Chapter 1 is an introduction to the research along with the research objectives, problem statement and the structure of thesis. Chapter 2 presents a detailed literature review pertaining to the previous work related to this research. The literature review on wood-cement composites includes the wood cement compatibility, causes of the incompatibility, measures to overcome incompatibility, applications, and advantages of wood cement composites. The literature review on steel slag covers production, properties, applications and curing procedures of steel slag. Chapters 3 focuses on the microstructural phases in carbonated and hydrated steel slag pastes. The as-received steel slag was examined for its carbon sequestration potential and the feasibility of recycling this material into a high-performance binder. The chemical composition and structural information of formed carbonation products is examined. Chapters 4 through 6 address the development of steel slag bonded wood products. In Chapter 4, the slag bonded strand board as a carbon negative building product is developed. The effect of water to slag ratio on the strength of this product is explored and the mechanical, physical and durability performance are evaluated in light of the microstructural changes taking place. Lastly, cost and carbon-balance analysis were performed on slag bonded strand boards to assess the feasibility and implications of industrial adoption. In Chapter 5, steel slag masonry units with different wood ratios are examined to study the impact of wood addition on the overall performance of steel slag masonry units subjected to various carbonation scenarios. The effect of wood on the CO_2 uptake potential of the developed masonry units is explored. The microstructure of this product is investigated through the interfacial transition zone properties of both carbonated and hydrated wood-slag pastes. Moreover, in order to contribute further to a cleaner production process, flue gas carbonation was used to replace pure caron dioxide gas in the production of slag bonded strand boards in Chapter 6. To this end, several carbonation curing conditions are studied. Lastly, Chapter 7 is a summary of the main conclusions drawn by this work along with suggestions for future work and statement of originality.

References

1. Grubeša, I.N., I. Barisic, A. Fucic, and S.S. Bansode, *Characteristics and uses of steel slag in building construction*. 2016: Woodhead Publishing.
2. Humbert, P.S. and J. Castro-Gomes, *CO2 activated steel slag-based materials: A review*. Journal of Cleaner Production, 2019. **208**: p. 448-457 DOI: https://doi.org/10.1016/j.jclepro.2018.10.058.
3. Song, Q.F., M.Z. Guo, L. Wang, and T.C. Ling, *Use of steel slag as sustainable construction materials: A review of accelerated carbonation treatment.* Resources Conservation and Recycling, 2021. **173**: p. 105740 DOI: https://doi.org/10.1016/j.resconrec.2021.105740.
4. Najm, O., H. El-Hassan, and A. El-Dieb, *Ladle slag characteristics and use in mortar and concrete: A comprehensive review.* Journal of Cleaner Production, 2021. **288**: p. 125584.
5. Mahoutian, M., Z. Ghouleh, and Y.X. Shao, *Carbon dioxide activated ladle slag binder*. Construction and Building Materials, 2014. **66**: p. 214-221 DOI: https://doi.org/10.1016/j.conbuildmat.2014.05.063
6. Kriskova, L., Y. Pontikes, Ö. Cizer, G. Mertens, W. Veulemans, D. Geysen, P.T. Jones, L. Vandewalle, K. Van Balen, and B. Blanpain, *Effect of mechanical activation on the hydraulic properties of stainless steel slags.* Cement and Concrete Research, 2012. **42**(6): p. 778-788.
7. Young, J.F., R.L. Berger, and J. Breese, *Accelerated Curing of Compacted Calcium Silicate Mortars on Exposure to Co2.* Journal of the American Ceramic Society, 1974. **57**(9): p. 394-397 DOI: https://doi.org/10.1111/j.1151-2916.1974.tb11420.x
8. Dincer, I., C.O. Colpan, and F. Kadioglu, *Causes, impacts and solutions to global warming*. 2013: Springer Science & Business Media.

9. Mahoutian, M. and Y.X. Shao, *Production of cement-free construction blocks from industry wastes.* Journal of Cleaner Production, 2016. **137**: p. 1339-1346 DOI: 10.1016/j.jclepro.2016.08.012.

10. Ghouleh, Z., R.I.L. Guthrie, and Y.X. Shao, *High-strength KOBM steel slag binder activated by carbonation.* Construction and Building Materials, 2015. **99**: p. 175-183 DOI: https://doi.org/10.1016/j.conbuildmat.2015.09.028

11. Mahoutian, M., Y.X. Shao, A. Mucci, and B. Fournier, *Carbonation and hydration behavior of EAF and BOF steel slag binders.* Materials and Structures, 2015. **48**(9): p. 3075-3085 DOI: https://doi.org/10.1617/s11527-014-0380-x

2. Chapter 2 Literature Review

2.1. Steel Slag

During steel and iron production, the slag that forms during the conversion of hot metal to crude steel or during the melting of scrap metal is known as the steel slag [1]. With an estimated worldwide production of 1.8 billion tons of steel, approximately 130-200 million tons of steel slag are produced annually [2]. Steel slags are classified into three categories based on the furnace used i.e., the basic oxygen furnace slag (BOF), electric arc furnace slag (EAF) and the ladle furnace slag (LS).

2.1.1 Steel slag properties

Properties of steel slag depend on their chemical and mineralogical compositions. Most slags contain CaO, MgO, SiO_2 and FeO as the main oxides [3]. BOF and EAF have similar composition while the composition of ladle slag is highly variable [4]. In general, the starkest difference is in the FeO and Al_2O_3 contents [3]. The former was found to be very low in LS compared to BOF and EAF while the latter was highest in LS. The difference in the chemical composition is due to the alloys added in the production of various grades of steel [1]. The mineralogy is also dependent on the nature of the deoxidizing agents and the cooling process [5]. BOF and EAF are commonly found to be rich in wustite, di-calcium silicate, di-calcium ferrite, merwinite and olivine [1]. In LS, di-calcium silicates in its different polymorphs were present in high amounts [1]. Steel slag is also rich in free calcium and magnesium oxides whose hydration reaction can cause expansion and is highly compromising for the dimensional stability[6]. Steel slag is also featured for its high bulk specific gravity and medium water absorption [1].

Steel slag possesses no pozzolanic activity and has high free-lime content which significantly limits the applications of this material. Currently, steel slag is used as aggregate for road construction while large amounts are still landfilled [7].

2.1.2 Steel slag hydration

The hydration activity of steel slag is affected by the mineralogy [2]. The low alite content and high belite content rendered steel slag as a latent hydraulic material [8]. The weak hydraulic activity is mainly attributed to the amorphous nature of its SiO_2 content [9]. Moreover, studies revealed that ladle slags, when undergoing a slow cooling process, experience the conversion of beta-C_2S to gamma-C_2S. This conversion reduces the hydraulic activity of ladle slag. A study targeting the hydration reaction of BOF slag revealed a prolonged dormant phase and retardation of setting time [10]. Adesanya et al. suggested that the mechanism of hydration in ladle slags is similar to that of calcium sulfoaluminate cements owing to the mayenite and tricalcium aluminate content [11]. Bjorkman et al. studied the hydraulic activity of ladle slag and of a 50-50 blend of ladle slag (LS) and ground granulated blast furnace slag (GGBFS) and concluded that the ladle slag or the LS/GGBFS can be used as a supplement in binder applications [12]. Furthermore, the hydraulic properties of steel slag can be inferred from its CaO/SiO_2 ratio. Steel slags with a CaO/SiO_2 ratio above 2.7 are expected to display good hydraulic properties [13, 14].

To enhance the hydraulic activity, some studies reported on the efficacy of alkali activation [5, 15]. Another approach was a mechanical activation by prolonged milling in ethanol suspension which resulted in an increase in surface area and amorphous phases [16].

2.1.3 Steel Slag Carbonation

In terms of strength, early strength of steel slag could be unleashed by carbonation curing. Owing to the free-CaO/MgO, hydraulic calcium silicate, non-hydraulic calcium silicate, and portlandite content, steel slag could react with CO_2 at early ages developing rapid early strengths. The principal reaction is given in Eq. (1) [17]

$$2(2CaO.SiO_2) + (2-x)\ CO_2 + y\ H_2O \rightarrow xCaO.SiO_2.\ yH_2O + (2-x)\ CaCO_3 \quad (1)$$

Electric arc furnace (EAF) slag paste compacts, after 2 hours of carbonation, achieved a strength of 17 MPa and a carbon uptake of 11 % [18]. After 24 hours of carbonation curing, LS paste compacts achieved a strength of 35 MPa [4]. Klockner Oxygen Blown Maxhutte (KOBM) slag paste compacts recorded a compressive strength of 80 MPa and CO_2 uptake of 13 % after just 2 hours of carbonation [19]. It was also concluded that the calcium-silicate phases present in the as-received slags were the primary contributors to strength and CO_2 uptake, not the calcium oxide content. This was explained by the fact that not all calcium phases were CO_2 reactive like merwinite and gehlenite [20]. A study on carbon sequestration of steel slag revealed that carbonation was also capable of activating the RO phase [21]. The CO_2 uptake of slag powder was proven to be enhanced when curing was performed at elevated temperatures [22]. Slag fineness was also found to influence the CO_2 uptake capacity.

Accelerated carbonation curing of steel slag had been reported to improve strength [19], enhance dimensional stability [23] and limit the leachability of hazardous metals present in alkaline slags (i.e., Cr, Se, Mo…)[7]. Several studies targeted the carbonation and subsequent hydration activity of steel slag. [19], [8], and [4] reported that carbonation did not hinder subsequent hydration.

The carbonation mechanism depends on the diffusion/permeation of CO_2 through the solid where CO_2 is dissolved in the pore spaces then hydrated to form carbonic acid (H_2CO_3). The carbonic acid subsequently ionizes to H^+, HCO_3^- and CO_3^{2-} which causes the pH to typically drop by 3 units. It is believed that the drop in pH stimulates the dissolution of calcium silicates, releasing Ca^{2+} and SiO_4^{2-} ions, that is followed by nucleation of C-S-H with simultaneous precipitation of calcium carbonates [24]. Various end products had been reported in literature. Goto et al. described the formed product by the carbonation reaction of calcium silicates as a one phase product of calcium silicate hydro-carbonate[25]. Berger et. al, in their various studies on calcium silicate systems, identified the formation of a low lime C-S-H gel and/or amorphous Si-gel [26, 27]. The formed C-S-H was different in composition and structure from the C-S-H formed by traditional Portland Cement (PC) hydration [28]. Ashraf et al. reported, in their study on non-hydraulic low-lime calcium silicate systems, the formation of a three phased product: Ca-modified silica gel, calcium carbonate and a composite phase resulting from the intermixing of both products [29].

All three crystalline polymorphs of $CaCO_3$ were reported but vaterite and aragonite tend to revert to the stable polymorph calcite [30]. Amorphous $CaCO_3$ was also detected [31]. The precipitation of $CaCO_3$ led to an improved packing density and reduction in porosity in the carbonate matrix which, in turn, augmented the strength [32].

2.1.4. Steel slag carbonation by flue gas

Tian et al. explored the feasibility of using flue gas CO_2 in steel-making plants for the direct gas-solid carbonation of steel slag [33]. The temperature was the most influencing factor on carbonation conversion and reaction rate [33]. Nielsen et al. explored the influence of CO_2 concentration on the mineral carbonation of steel slag monoliths [34]. Their main conclusion was that the CO_2 concentration affected the rate of the reaction, as the rate decreased with decreasing CO_2 concentration. They also noted that in long-duration carbonation (100 hours), steel slag cured at lower CO_2 concentrations performed better than steel slag cured at 100 % CO_2 concentration [34]. Myers at el. reported that basic oxygen furnace slag and electric arc furnace slag could achieve high net CO_2 mineralization by flue gas within one hour [35]. Nonetheless, mineral carbonation, despite its high feasibility, is expensive and energy intensive compared to other carbon dioxide capture and storage methods [36]. To this end, Moon et al. investigated the direct flue gas carbonation curing of a blended cement containing Portland cement and stainless-steel argon oxygen decarburization slag [37]. In this study, however, carbonation curing was extended to 28 days which is not viable for industrial production cycles.

2.2 Wood-cement composites

Huge amounts of waste are amassed yearly from various processes which makes waste disposal a challenge for many of communities. Recycling wastes into building products can be greatly beneficial. Some of the benefits include: cutting down on cost of construction materials, reducing the burden on landfills and preserving natural resources [38]. Wood-cement composites (WCC) present an excellent opportunity to recycle wood waste from various sources such as waste timber formwork [39], wood-working activities [38], construction and demolition wood waste [40] to name a few.

WCC had been used in the construction field since the early 1900s [41]. These composites had been divided into two main categories: wood particle-cement composites and wood fiber-cement composites [42]. Whereas wood fiber-cement composites were mainly produced to replace asbestos cement, wood particle-cement composites were developed for use in architectural, fire-resistant and acoustic panels [42, 43].

2.2.1 Wood-cement incompatibility

Perhaps the most prominent limitation for WCC is the variable compatibility between the two base materials. Different wood species contain varying amounts of extractives that are soluble in water. Extractives like hemicelluloses, sugars, acids, starches and phenols to list a few, can hinder the hydration reaction of cement or can affect the formation of crystals. These inhibitors cause the formation of impermeable calcium-silicate hydrates around the un-hydrated cement particles, thus preventing further hydration [44]. Investigations on different types of wood revealed that it is not only the level of extractives present in the wood that matters, but also the type of the extractive. Different chemical compounds have different effects on cement setting and hydration[45-47].

Studies showed that lignin, fatty acid, resin acid, sterol and terpene present at less than 1 % concentration did not significantly reduce the tensile strength of WCC. In contrast, glucose caused a huge drop in tensile strength [46]. On the other hand, another investigation revealed that the presence of 7 % of soluble extractives rendered the wood inapt [45]. Hemicellulose, found in varying amounts in different woods, is readily dissolved in high alkaline solutions such as wet cement which leads to a considerable reduction in cement hydration. Furthermore, terpenes and resins could migrate to the surface of wood particles forming an incapsulating layer that impedes the bond between wood and cement [40, 48].

Softwoods, in general, showed better compatibility with cement than hardwoods since the latter are rich in hemicellulose [47]. Typical examples of softwood include pine, fir, spruce, larch and cedar. Typical examples of hardwoods include oak, ash, elk, beech, birch and teak. Hardwoods are usually characterised by higher densities and porosity in comparison to softwoods [42].

Research on wood-cement compatibility revealed that tree species, geographical location, time of harvest and pre-treatment (i.e. drying of wood) are all factors that highly influence their compatibility [44, 47].

The long-term compatibility, on the other hand, follows an opposite to norm trend. Whereas it is known that concrete tends to gain strength with age, wood-cement composites degrade with time. The cement damages the wood particles. A study showed that the alkalinity of a cement board severely affected Sisal fibers [48]. The alkaline environment of the cement causes the disintegration of cellulose, thus releasing soluble carbohydrates [46]. The growth of hydration products, namely $Ca(OH)_2$, around the lignocellulosic material is one of the leading causes of embrittlement and degradation [47, 49]

2.2.2 Approaches to overcome incompatibility

Due to the inhibitor contents in some woods, special treatments were proposed to make them appropriate for coupling with cement. The sought compatibility can be achieved by:

1. Removing the soluble compounds from the wood. This could be achieved by rinsing the wood with hot or cold water to remove the extractives [44-48]. This method, however, was not deemed effective for all types of wood.
2. Adding chemicals to the mix, also known as the mineralization process, such as soluble silicate [46, 50], $CaCl_2$, $MgCl_2$, $SnCl_2$, $FeCl_3$ and $AlCl_3$ whereas $Al_2(SO_4)_3$ had been found to inhibit the effect of soluble sugars on cement hydration and ultimately cement durability [47]. It was found that soaking the wood particles until saturation with 3-5 % solution of calcium chloride or 3-6 % solution of aluminum sulfate prior to adding to the mix was enough to improve the wood-cement compatibility [40, 41]. However, it should be noted that all those different salts may facilitate corrosion in metals such as nails or beams used for the installation of some wood-cement composites [39].
3. Treating wood with substances of low pH such as chromated-copper arsenate (CCA) enhanced the compatibility. CCA caused the disintegration of hemicelluloses and other extractives inhibiting the full hydration [46, 51].
4. Partial replacement of Portland cement with supplementary cementitious materials such as silica fume, fly ash or rice husk ash to improve the bond [46, 52, 53]. Wei. et al explored the effect of the addition of 30 % metakaolin to the wood-cement matrix on the degradation

and concluded that the addition of metakaolin reduced the $Ca(OH)_2$ content and decreased the pH of the matrix which effectively improved the longevity of the composite and lessened the deterioration [54].

5. Coating the wood particles with isolating layers. This approach however, weakens the bond between cement and wood and would ultimately lead to reduced mechanical properties [44]. Nonetheless, a study on the effect of treating the rice straw surface with polymer emulsions improved the mechanical properties and proved the viability of this approach [53]
6. Treating with gaseous carbon dioxide had been proven to have a positive effect on setting as well as curing of the composite. The superior properties resulting from the carbonation of the composites had been linked to the formation of hydration products. The resulting calcium silicate hydrate and calcium carbonates had been found to bond well with the wood particles [44]. According to Filho et al., early CO_2 curing improves the durability of fiber cement composites to ageing because carbonation consumes $Ca(OH)_2$ and reduces pH [49]. Nevertheless, the long-term durability remains questionable since the subsequent hydration of Portland cement following carbonation curing re-alkalizes the medium and subjects the wood to alkali-degradation.

2.2.3 Strength of wood-cement composites

The mechanical properties of wood-cement composites are highly linked to the interfacial bonding zone, cement/wood ratio, water/cement ratio and types of wood particles [42, 43, 52]. If the wood used is dry, wood tends to draw the water in the mix thus limiting the water needed for the hydration reaction leading to a reduced strength [44]. Furthermore, density and overall strength were observed to decrease with the increase in wood/cement ratio [55]. The interfacial zone between wood and hydrated cement paste was found to be highly porous and rich in $Ca(OH)_2$ [56, 57].

2.2.4 Durability of wood-cement composites

Numerous investigations had been carried out on the durability of WCC. In general, it had been shown that the cement encapsulates the wood particles providing them with necessary protection against biodegradability [48]. However, the alkaline medium surrounding the wood could cause embrittlement and ultimately compromise the long-term durability of the composite. In this regard, carbonation curing proved to enhance the durability through lowering the alkalinity of the medium. Furthermore, carbonation curing of wood-cement composites decreased the volumes of capillary pores contributing towards an enhanced durability [58].

2.2.5 Merits of wood-cement composites

Advantages of these composites include improved thermal insulation [39], resistance to decay, water and fire [41, 42, 52], and sound absorbance which promotes them for noise insulation applications [39, 41, 59]. Also, compared to concrete and reinforced concrete products, wood-cement composites have lower densities, within the range of light weight concrete [39, 44, 60]. WCC are resistant to fungi and moisture which are limiting conditions for external application [61]. In addition, WCC are sustainable since the used wood is recyclable, ecofriendly and a renewable material [39, 42].

2.2.6 Wood Strand Cement Board (WSCB)

WSCB is a board marketed under the trade name Eltoboard and is made by mixing wood strands which are wider and thinner than wood wool fiber with cement and water. Despite its medium density (1100 kg/m^3), it has high strength [62]. Applications for the WSCB include flooring, tile backing; roofing; permanent shuttering; prefabricated houses; exterior and partition walls; acoustic and thermal insulation; fire resistant construction; facades and cladding.

A study conducted to investigate the mechanical properties of WSCB concluded that the cement-to-wood ratio used for the WSCB is less than that required for other types of boards due to the geometry of the strands. It was also found that the increase in the cement-to-wood ratio improved all the mechanical properties of the board except for the flexural strength [63].

Another study concluded that wood added at 40 % by weight yielded the optimum bending strength [64]. Increasing the wood content further negatively affected the internal bond and the water absorption properties of the board. It was deduced that the internal bond was affected by increasing the wood content due to the reduced bonding ability of wood strands compared to cement [64].

2.2.7 Wood-cement masonry block

Wood as partial replacement of sand and coarse aggregate in masonry units has been ventured before. Most research targeted wood ash and saw dust [65], [66], [67], [68]. A study concluded that the addition of 25 wt.% of wood fiber waste reduced the weight of the masonry block by almost 30 % [67]. Nowadays, burning of wood residues has become less acceptable, therefore research is oriented towards valorizing these residues. Studies had investigated the use of olive wood waste, wood chipping and recycled wood towards the production of masonry blocks [48, 69, 70]. The main conclusions were that that the addition of wood to the cementitious matrix retarded the hydration reaction and negatively affected the mechanical strength. Furthermore, the slump increased with the increase in wood aggregates as partial replacement of coarse aggregates [71, 72]. Finally, the increase in wood aggregates to the mix design led to a weakening of the cohesion between aggregates and cement matrix, thus the loss in workability [72]. There seems to be a consensus among researchers that the developed wood-concrete is suitable for non-load bearing purposes [73]. Stahl et al. developed a non-loadbearing concrete masonry block that complies with ASTM C129 requirements by replacing a conventional mix volume of coarse aggregate with wood aggregate [48].

References

1. Grubeša, I.N., I. Barisic, A. Fucic, and S.S. Bansode, *Characteristics and uses of steel slag in building construction*. 2016: Woodhead Publishing.DOI: https://doi.org/10.1016/c2014-0-03994-9
2. Wang, J., M. Zhong, P. Wu, S. Wen, L. Huang, and P. Ning, *A Review of the Application of Steel Slag in CO_2 Fixation.* ChemBioEng Reviews, 2021. **8**(3): p. 189-199 DOI: https://doi.org/10.1002/cben.202000021.
3. Shi, C., *Steel slag—its production, processing, characteristics, and cementitious properties.* Journal of Materials in Civil Engineering, 2004. **16**(3): p. 230-236.
4. Mahoutian, M., Z. Ghouleh, and Y.X. Shao, *Carbon dioxide activated ladle slag binder*. Construction and Building Materials, 2014. **66**: p. 214-221 DOI: https://doi.org/10.1016/j.conbuildmat.2014.05.063
5. Najm, O., H. El-Hassan, and A. El-Dieb, *Ladle slag characteristics and use in mortar and concrete: A comprehensive review.* Journal of Cleaner Production, 2021. **288**: p. 125584 DOI: https://doi.org/10.1016/j.jclepro.2020.125584
6. Jin, P., S. Zhang, Y. Liu, W. Zhang, and R. Wang, *Application of Bacillus mucilaginosus in the carbonation of steel slag.* Applied Microbiology and Biotechnology, 2021. **105**(23): p. 8663-8674 DOI: https://doi.org/10.1007/s00253-021-11641-z
7. Mahoutian, M. and Y. Shao, *Production of cement-free construction blocks from industry wastes.* Journal of Cleaner Production, 2016. **137**: p. 1339-1346 DOI: https://doi.org/10.1016/j.jclepro.2016.08.012
8. Mahoutian, M., Y.X. Shao, A. Mucci, and B. Fournier, *Carbonation and hydration behavior of EAF and BOF steel slag binders.* Materials and Structures, 2015. **48**(9): p. 3075-3085 DOI: https://doi.org/10.1617/s11527-014-0380-x

9. Humbert, P.S. and J. Castro-Gomes, *CO_2 activated steel slag-based materials: A review.* Journal of Cleaner Production, 2019. **208**: p. 448-457 DOI: https://doi.org/10.1016/j.jclepro.2018.10.058.

10. Han, F., Z. Zhang, D. Wang, and P. Yan, *Hydration heat evolution and kinetics of blended cement containing steel slag at different temperatures.* Thermochimica Acta, 2015. **605**: p. 43-51 DOI: https://doi.org/10.1016/j.tca.2015.02.018

11. Adesanya, E., H. Sreenivasan, A.M. Kantola, V.V. Telkki, K. Ohenoja, P. Kinnunen, and M. Illikainen, *Ladle slag cement - Characterization of hydration and conversion.* Construction and Building Materials, 2018. **193**: p. 128-134 DOI: https://doi.org/10.1016/j.conbuildmat.2018.10.179

12. Adolfsson, D., F. Engström, R. Robinson, and B. Björkman, *Cementitious phases in ladle slag.* Steel research international, 2011. **82**(4): p. 398-403.

13. Vlček, J., R. Švrčinová, J. Burda, M. Topinková, M. Klárová, H. Ovčačíková, D. Jančar, and M. Velička, *Hydraulic properties of ladle slags.* Metalurgija, 2016. **55**(3): p. 399-402.

14. Muhmood, L., S. Vitta, and D. Venkateswaran, *Cementitious and pozzolanic behavior of electric arc furnace steel slags.* Cement and Concrete Research, 2009. **39**(2): p. 102-109.

15. Jiang, Y., T.-C. Ling, C. Shi, and S.-Y. Pan, *Characteristics of steel slags and their use in cement and concrete—A review.* Resources, Conservation And Recycling, 2018. **136**: p. 187-197.

16. Kriskova, L., Y. Pontikes, Ö. Cizer, G. Mertens, W. Veulemans, D. Geysen, P.T. Jones, L. Vandewalle, K. Van Balen, and B. Blanpain, *Effect of mechanical activation on the hydraulic properties of stainless steel slags.* Cement and Concrete Research, 2012. **42**(6): p. 778-788.

17. Young, J., R. Berger, and J. Breese, *Accelerated curing of compacted calcium silicate mortars on exposure to CO_2*. Journal of the American Ceramic Society, 1974. **57**(9): p. 394-397.

18. Chang, J., S. Wang, and Y. Shao, *Manufacture of electric arc furnace slag aggregate and concrete through carbonation curing*. JOURNAL-CHINESE CERAMIC SOCIETY, 2007. **35**(9): p. 1264.

19. Ghouleh, Z., R.I.L. Guthrie, and Y.X. Shao, *High-strength KOBM steel slag binder activated by carbonation.* Construction and Building Materials, 2015. **99**: p. 175-183 DOI: https://doi.org/10.1016/j.conbuildmat.2015.09.028

20. Mahoutian, M., Y. Shao, A. Mucci, and B. Fournier, *Carbonation and hydration behavior of EAF and BOF steel slag binders.* Materials and Structures, 2015. **48**(9): p. 3075-3085.

21. Chen, Z., R. Li, X. Zheng, and J. Liu, *Carbon sequestration of steel slag and carbonation for activating RO phase.* Cement and Concrete Research, 2021. **139**: p. 106271.

22. Huijgen, W.J., G.J. Ruijg, R.N. Comans, and G.-J. Witkamp, *Energy consumption and net CO_2 sequestration of aqueous mineral carbonation.* Industrial & Engineering Chemistry Research, 2006. **45**(26): p. 9184-9194.

23. Pan, S.Y., Y.H. Chen, C.D. Chen, A.L. Shen, M. Lin, and P.C. Chiang, *High-Gravity Carbonation Process for Enhancing CO_2 Fixation and Utilization Exemplified by the Steelmaking Industry*. Environment Science and Technology, 2015. **49**(20): p. 12380-7 DOI: https://doi.org/10.1021/acs.est.5b02210

24. Fernandez Bertos, M., S.J. Simons, C.D. Hills, and P.J. Carey, *A review of accelerated carbonation technology in the treatment of cement-based materials and sequestration of*

CO_2. Journal of Hazardous Materials, 2004. **112**(3): p. 193-205 DOI: https://doi.org/10.1016/j.jhazmat.2004.04.019

25. Goto, S., K. Suenaga, T. Kado, and M. Fukuhara, *Calcium silicate carbonation products.* Journal of the American Ceramic Society, 1995. **78**(11): p. 2867-2872.

26. Young, J.F., R.L. Berger, and J. Breese, *Accelerated Curing of Compacted Calcium Silicate Mortars on Exposure to CO_2*. Journal of the American Ceramic Society, 1974. **57**(9): p. 394-397 DOI: https://doi.org/10.1111/j.1151-2916.1974.tb11420.x

27. Bukowski, J.M. and R.L. Berger, *Reactivity and Strength Development of CO_2 Activated Non-Hydraulic Calcium Silicates.* Cement and Concrete Research, 1979. **9**(1): p. 57-68 DOI: https://doi.org/10.1016/0008-8846(79)90095-4

28. Ghouleh, Z., M. Celikin, R.I. Guthrie, and Y. Shao, *Microstructure of carbonation-activated steel slag binder.* Journal of Materials in Civil Engineering, 2018. **30**(9): p. 04018217 DOI: https://doi.org/10.1061/(asce)mt.1943-5533.0002421

29. Ashraf, W., J. Olek, and J. Jain, *Microscopic features of non-hydraulic calcium silicate cement paste and mortar.* Cement and Concrete Research, 2017. **100**: p. 361-372 DOI: https://doi.org/10.1016/j.cemconres.2017.07.001

30. Bertos, M.F., S. Simons, C. Hills, and P. Carey, *A review of accelerated carbonation technology in the treatment of cement-based materials and sequestration of CO_2.* Journal of hazardous materials, 2004. **112**(3): p. 193-205.

31. He, Z., H. Yang, Y. Shao, and M. Liu, *Early carbonation behaviour of no-clinker steel slag binder.* Advances in Cement Research, 2013. **25**(6): p. 342-351.

32. Shao, Y., A. El-Baghdadi, Z. He, A. Mucci, and B. Fournier, *Carbon Dioxide–Activated Steel Slag for Slag-Bonded Wallboard Application.* Journal of Materials in Civil Engineering, 2014. **27**(3): p. 04014119.

33. Tian, S., J. Jiang, X. Chen, F. Yan, and K. Li, *Direct Gas–Solid Carbonation Kinetics of Steel Slag and the Contribution to In situ Sequestration of Flue Gas CO_2 in Steel-Making Plants.* ChemSusChem, 2013. **6**(12): p. 2348-2355 DOI: https://doi.org/10.1002/cssc.201300436

34. Nielsen, P., M.A. Boone, L. Horckmans, R. Snellings, and M. Quaghebeur, *Accelerated carbonation of steel slag monoliths at low CO_2 pressure-microstructure and strength development.* Journal of CO_2 Utilization, 2020. **36**: p. 124-134 DOI: https://doi.org/10.1016/j.jcou.2019.10.022

35. Myers, C.A., T. Nakagaki, and K. Akutsu, *Quantification of the CO_2 mineralization potential of ironmaking and steelmaking slags under direct gas-solid reactions in flue gas.* International Journal of Greenhouse Gas Control, 2019. **87**: p. 100-111 DOI: https://doi.org/10.1016/j.ijggc.2019.05.021

36. Mouedhen, I., N. Kemache, L.-C. Pasquier, E. Cecchi, J.-F. Blais, and G. Mercier, *Effect of pCO_2 on direct flue gas mineral carbonation at pilot scale.* Journal of Environmental Management, 2017. **198**: p. 1-8 DOI: https://doi.org/10.1016/j.jenvman.2017.04.048

37. Moon, E.-J. and Y.C. Choi, *Development of carbon-capture binder using stainless steel argon oxygen decarburization slag activated by carbonation.* Journal of Cleaner Production, 2018. **180**: p. 642-654 DOI: https://doi.org/10.1016/j.jclepro.2018.01.189

38. Bederina, M., B. Laidoudi, A. Goullieux, M. Khenfer, A. Bali, M.J.C. Quéneudec, and B. Materials, *Effect of the treatment of wood shavings on the physico-mechanical characteristics of wood sand concretes.* 2009. **23**(3): p. 1311-1315.

39. Wang, L., S.S. Chen, D.C.W. Tsang, C.S. Poon, and K. Shih, *Recycling contaminated wood into eco-friendly particleboard using green cement and carbon dioxide curing.* Journal of Cleaner Production, 2016. **137**: p. 861-870 DOI: https://doi.org/10.1016/j.jclepro.2016.07.180

40. Frank, R.E. *Construction and Demolition Wood Waste Used in Wood Cement Composites*. in *Sustainable Construction—Proceedings of the First International Conference of CIB TG16. Kibert, CJ (ed)(University of Florida) pp*. 1994.

41. Kosny, J., *Wooden concrete: High thermal efficiency using waste wood*. 1994, Oak Ridge National Lab., TN (United States).

42. Asif, M., *Sustainability of timber, wood and bamboo in construction*, in *Sustainability of construction materials*. 2009, Elsevier. p. 31-54.

43. Wolfe, R.W. and A. Gjinolli, *Cement-bonded wood composites as an engineering material.* The use of recycled wood paper in building applications. Madison, WI: Forest Products Society, 1996: p. 84-91.

44. Frybort, S., R. Mauritz, A. Teischinger, and U. Müller, *Cement bonded composites–A mechanical review.* BioResources, 2008. **3**(2): p. 602-626.

45. Ahmad, Z., L. Wee, and M.J.A.S.J. Fauzi, *Mechanical properties of wood-wool cement composite board manufactured using selected Malaysian fast grown timber species.* ASM Science Journal, 2011. **5**(1): p. 27-35.

46. Jorge, F., C. Pereira, and J. Ferreira, *Wood-cement composites: a review*. Holz als Roh-und Werkstoff, 2004. **62**(5): p. 370-377.

47. Wei, Y.M., Y.G. Zhou, and B. Tomita, *Hydration behavior of wood cement-based composite I: Evaluation of wood species effects on compatibility and strength with ordinary Portland cement.* Journal of Wood Science, 2000. **46**(4): p. 296-302.

48. Stahl, D.C., G. Skoraczewski, P. Arena, and B. Stempski, *Lightweight concrete masonry with recycled wood aggregate.* Journal of Materials in Civil Engineering, 2002. **14**(2): p. 116-121.

49. Toledo Filho, R.D., K. Ghavami, G.L. England, and K. Scrivener, *Development of vegetable fibre–mortar composites of improved durability*. Cement and Concrete Composites, 2003. **25**(2): p. 185-196 DOI: https://doi.org/10.1016/s0958-9465(02)00018-5

50. Stahl, D.C., G. Skoraczewski, P. Arena, and B.J.J.o.M.i.C.E. Stempski, *Lightweight concrete masonry with recycled wood aggregate*. 2002. **14**(2): p. 116-121.

51. Zhou, Y. and D.P. Kamdem, *Effect of cement/wood ratio on the properties of cement-bonded particleboard using CCA-treated wood removed from service.(Composites and Manufactured Products).* Forest Products Journal, Vol. 54, No. 2, p. 89-94, 2002. **52**(3): p. 77-82.

52. Simatupang, M.H. and R.L. Geimer. *Inorganic binder for wood composites: feasibility and limitations*. in *Proceedings of Wood Adhesive Symposium, Forest Product Resources Society*. 1990.

53. Na, B., Z. Wang, H. Wang, and L. Xiaoning, *WOOD-cement compatibility review*. Vol. 59. 2014. 813-825.

54. Wei, J.A. and C. Meyer, *Degradation mechanisms of natural fiber in the matrix of cement composites.* Cement and Concrete Research, 2015. **73**: p. 1-16 DOI: https://doi.org/10.1016/j.cemconres.2015.02.019

55. Lee, A.W., Z. Hong, D.R. Phillips, and C.Y. Hse, *Effect of cement/wood ratios and wood storage conditions on hydration temperature, hydration time, and compressive strength of wood-cement mixtures.* Wood Fiber Science, 2007. **19**(3): p. 262-268.

56. Del Bosque, I.S., W. Zhu, T. Howind, A. Matías, M.S. De Rojas, and C. Medina, *Properties of interfacial transition zones (ITZs) in concrete containing recycled mixed aggregate.* Cement and Concrete Composites, 2017. **81**: p. 25-34 DOI: https://doi.org/10.1016/j.cemconcomp.2017.04.011

57. Kottititum, B., Q.T. Phung, N. Maes, W. Prakaypan, and T. Srinophakun, *Early Age Carbonation of Fiber-Cement Composites under Real Processing Conditions: A Parametric Investigation.* Applied Sciences-Basel, 2018. **8**(2): p. 190 DOI: https://doi.org/10.3390/app8020190

58. Soroushian, P., J.-P. Won, and M. Hassan, *Durability and microstructure analysis of CO2-cured cement-bonded wood particleboard.* Cement Concrete Composites, 2013. **41**: p. 34-44.

59. Li, M., M. Khelifa, and M. El Ganaoui, *Mechanical characterization of concrete containing wood shavings as aggregates.* International Journal of Sustainable Built Environment, 2017. **6**(2): p. 587-596.

60. Mahzuz, H. and M. Ahmed, *Production of light weight concrete by bio-materials.* International Journal of Civil Environmental Engineering, 2012. **12**(5): p. 2077-1258.

61. Okino, E.Y., M.R. de Souza, M.A. Santana, M.V.d.S. Alves, M.E. de Sousa, and D.E. Teixeira, *Physico-mechanical properties and decay resistance of Cupressus spp. cement-bonded particleboards.* Cement Concrete Composites, 2005. **27**(3): p. 333-338.

62. Saunders, A., *Global Cement Brochure: Cement Boards 101.* Global Cement Magazine, 2014.

63. Papadopoulos, A.N., G.A. Ntalos, and I. Kakaras, *Mechanical and physical properties of cement-bonded OSB.* Holz als Roh-und Werkstoff, 2006. **64**(6): p. 517-518 DOI: https://doi.org/10.1007/s00107-005-0092-6

64. Ashori, A., T. Tabarsa, and S. Sepahvand, *Cement-bonded composite boards made from poplar strands.* Construction and Building Materials, 2012. **26**(1): p. 131-134.

65. Berra, M., T. Mangialardi, and A.E. Paolini, *Reuse of woody biomass fly ash in cement-based materials.* Construction and Building Materials, 2015. **76**: p. 286-296 DOI: https://doi.org/10.1016/j.conbuildmat.2014.11.052

66. Ramos, T., A.M. Matos, and J. Sousa-Coutinho, *Mortar with wood waste ash: Mechanical strength carbonation resistance and ASR expansion.* Construction and Building Materials, 2013. **49**: p. 343-351 DOI: https://doi.org/10.1016/j.conbuildmat.2013.08.026

67. Torkaman, J., A. Ashori, and A.S. Momtazi, *Using wood fiber waste, rice husk ash, and limestone powder waste as cement replacement materials for lightweight concrete blocks.* Construction and Building Materials, 2014. **50**: p. 432-436 DOI: https://doi.org/10.1016/j.conbuildmat.2013.09.044

68. Page, J., C. Djelal, and Y. Vanhove, *Optimisation of vibrocompaction process for wood-based concrete blocks.* International Journal of Advanced Manufacturing Technology, 2020. **109**(3-4): p. 1189-1204 DOI: https://doi.org/10.1007/s00170-020-05674-3

69. Antoun, M., C.A. Issa, G. Aouad, and N. Gerges, *Sustainable masonry blocks: Olive wood waste as substitute for fine aggregates.* Case Studies in Construction Materials, 2021. **15**: p. e00590 DOI: https://doi.org/10.1016/j.cscm.2021.e00590

70. Mohammed, B.S., M. Abdullahi, and C.K. Hoong, *Statistical models for concrete containing wood chipping as partial replacement to fine aggregate.* Construction and Building Materials, 2014. **55**: p. 13-19 DOI: https://doi.org/10.1016/j.conbuildmat.2014.01.021

71. Thandavamoorthy, T., *Wood waste as coarse aggregate in the production of concrete.* European Journal of Environmental

Civil Engineering, 2016. **20**(2): p. 125-141.

72. Fapohunda, C., B. Akinbile, and A. Oyelade, *A Review of the Properties, Structural Characteristics and Application Potentials of Concrete Containing Wood Waste as Partial Replacement of one of its Constituent Material.* YBL Journal of Built Environment, 2018. **6**(1): p. 63-85.

73. Aigbomian, E.P. and M.Z. Fan, *Development of wood-crete from treated sawdust.* Construction and Building Materials, 2014. **52**: p. 353-360 DOI: https://doi.org/10.1016/j.conbuildmat.2013.11.025

3. Chapter 3 Mechanism of Strength Gain in Steel Slag Pastes Under Combined Carbonation-Hydration Curing

Preface

Steel slag is increasingly acknowledged as a promising binder that hardens upon carbonation. To this end, this chapter provides an insight into the mechanism of strength gain in steel slag subjected to combined carbonation and hydration curing. A combined carbonation-hydration curing regime was employed on paste compacts immediately after casting. Reaction products and properties were examined through strength gain, CO_2 uptake, and microstructural development by multiple techniques. Steel slag displayed a latent hydraulic activity of 17 MPa after 28 days of hydration and an ultimate strength of 70 MPa after 28 days with a combined regime of carbonation and hydration curing. Analysis showed that the steel slag can sequester almost 13.6 % of CO_2 by dry slag mass following 24 hours of carbonation curing. Microstructural investigations revealed that both C-S-H and Ca-modified silica gel phases co-existed in carbonated samples albeit with varying concentrations which was found to be a function of the carbonation degree. SEM microanalysis revealed that the major product phase by carbonation was a hybrid of gel phases (C-S-H and Ca modified silica gel) and $CaCO_3$. It was inferred that a 24-hour carbonation promoted subsequent hydration and contributed towards an over-all higher strength and reaction degree as well as reduced porosity. These could be ascribed to the formed $CaCO_3$ that act as nucleation sites to promote subsequent hydration.

3.1 Introduction

Steel slag is a calcium silicate rich material that is a good candidate for carbon storage. In fact, several studies had highlighted the potential of steel slag to serve as a carbon sink. Ghouleh et al. demonstrated the feasibility of producing carbonated aggregates from CO_2-activated steel slag [1]. Monkman et al. employed ladle slag fines as a possible feedstock for carbon capture and used these carbonated fines as a sand substitute [2]. However, considering the high-cost of the carbonation process, high- value end- products are more favorable. In this light, more research effort was put in maximizing the investment of carbonation through recycling steel slag into a high performing binder that could replace ordinary Portland cement (OPC), limit natural resources consumption and halt burdensome landfilling; ultimately contributing towards a sustainable production [3].

To this end, steel slag was studied for its carbonation activity. Previous studies had investigated the carbonation curing of various types of steel slag from basic oxygen furnace slag (BOF) [4], electric arc furnace slag (EAF) [5], stainless steel slag (AOD) [3, 6], Klockner Oxygen Blown Maxhutte slag (KOBM)[7] and ladle slag [8, 9]. In general, it had been demonstrated that carbonation curing is a promising approach for steel slag reclamation as a binder. The calcium/magnesium silicates available in steel slag react with CO_2 in the presence of water to form thermodynamically stable calcium carbonates and strength contributing calcium silicate hydrate (C-S-H), as represented by eq. 1[10].

$$2(2CaO.SiO_2) + (2-x)\,CO_2 + y\,H_2O \rightarrow xCaO.SiO_2.yH_2O + (2-x)CaCO_3 \qquad (1)$$

Young et al. reported that the Ca/Si of the C-S-H that forms in the first 3 min bears resemblance to that formed by normal hydration then the composition changes as the C-S-H gradually decalcifies with the increase in carbonation duration [10]. Furthermore, accelerated carbonation curing of steel slag had been reported to improve strength [7], enhance dimensional stability [11] and limit the leachability of hazardous metals present in alkaline slags (i.e., Cr, Se, Mo…)[12]. Several studies targeted the carbonation and hydration activity of steel slag. [7], [5], and [8] reported that carbonation did not hinder subsequent hydration.

The carbonation mechanism depends on the diffusion/permeation of CO_2 through the solid where CO_2 is dissolved in the pore spaces then hydrated to form carbonic acid (H_2CO_3). The carbonic acid subsequently ionizes to H^+, HCO_3^- and CO_3^{2-} which causes the pH to typically drop by 3 units. It is believed that the drop in pH stimulates the dissolution of calcium silicates, releasing Ca^{2+} and SiO_4^{2-} ions, that is followed by nucleation of C-S-H with simultaneous precipitation of calcium carbonates[13, 14]. Various end products had been reported in literature. Goto et al. described the formed product by the carbonation reaction of calcium silicates as a one phase product of calcium silicate hydro-carbonate[15]. Berger et al., in their various studies on calcium silicate systems, identified the formation of a low lime C-S-H gel and/or amorphous Si-gel [10, 16]. Ashraf et al. reported the formation of a three phased product from non-hydraulic low-lime calcium silicate systems: Ca-modified silica gel, calcium carbonate and a composite phase resulting from the intermixing of both products [17].

In view of the paramount attention that steel slag as binder is experiencing, an understanding of the mechanism of strength gain is essential. Although few previous studies had been conducted on carbonation and/or hydration of steel slag, these studies focused on the valorization of this binder focusing on the performance of this potential binder system. The work presented in this chapter has focused on the mechanism of strength gain in combined carbonation-hydration curing regimes in steel slag compacts. Freshly compacted samples of steel slag were subjected to carbonation, hydration and combined curing scenarios. Multiple analytical techniques were consulted to monitor the mechanical properties, changes in mineralogy and microstructural evolutions incurred for each scenario. This study provides deeper understanding of the physio-chemical behavior of steel slag subjected to combined carbonation-hydration curing scenario, bringing steel slag a step closer towards recognition as a sole binder.

3.2 Experimental Program

3.2.1 Materials

Steel slag used in this study was typically a ladle slag that was sourced from Harsco Environmental, Quebec, Canada. The as-received slag was mainly powdery with a percentage of clumps. The clumps were sieved and only powders passing a 850-µm sieve were used. To ensure homogeneity, the sieved portion was pulverized to a finer powder using a ring-and-puck mill (90 s per half-kilogram slag). Sieve analysis showed that 30 % of the pulverized slag passed the 150-µm sieve. The oxide composition of as-received ladle slag was determined by X-ray fluorescence (XRF) spectrometry. The mineral composition was determined by quantitative X-ray diffraction (QXRD) analysis. Data were collected using a Bruker D8 Endeavour diffractometer with a Cu radiation source and an X'celerator detector operating at 40 kV and 40 mA. The samples were scanned over a range of 4-70 deg 2θ. Step size was set to 0.02 deg 2θ at a rate of 0.5 sec per step. Corundum, as an internal standard, was added to the samples to determine the amorphous content. The PDF-4 Minerals ICDD database was consulted for mineral phase identification. The Rietveld method was used for refined quantitative phase analysis.

3.2.2 Sample preparation

Paste samples were targeted in this study to exclude the effect of aggregate addition. Steel slag was mixed with water at a 0.15 water to slag ratio (by weight). The selected water-to-slag ratio was based on results of previous studies where optimal water-to-slag ratios were found to lie between 0.1-0.2 [18]. Water to slag ratio is one of the most sensitive parameters in steel slag carbonation and it is strongly linked to the fineness of the slag particles [19]. This sensitivity is due to the nature of the carbonation reaction which is mostly a diffusion dependent reaction thus an optimal value for water content is deemed crucial. Cylinder samples were 15 mm in diameter and 25 mm in height and were prepared in a custom-designed mould by continuous compaction force of 3 KN. Each freshly compacted cylinder had a bulk density of 2.2 g/cm^3. Each batch consisted of 6 compacts and the whole mixing, compacting and demolding process took under 20 min.

3.2.3 Curing Procedure

Three main curing scenarios were employed in this study:

1) Conventional hydration curing: Freshly compacted cylinders were placed in air-tight plastic bags with no moisture loss at ambient conditions (24 ± 2 °C; RH= 30 %) for 24 hours (24H) and 28 days (28dH). Thus, 24 hours was referred to as early age whereas 28 days represented the late age.
2) Accelerated carbonation curing: Specimens were transferred immediately after forming to carbonation chamber. The chamber was injected with 99.9 % pure CO_2 gas at a pressure of 1.5 atm. The chamber pressure was kept constant by means of a regulator. The set-up is shown in Fig 3-1. The curing time was carried out for different durations (2h, 4h, …24h) at ambient conditions (24 ± 2 °C; RH= 30 %). Compacts obtained immediately after carbonation were referred to as early age compacts.
3) Accelerated carbonation curing followed by conventional hydration curing: The freshly carbonated samples were transferred to airtight plastic bags and allowed to cure for total of 28 days at ambient conditions (24 ± 2 °C; RH= 30 %). Compacts obtained at the end of the 28 days were referred to as late age compacts.

3.2.4 CO_2 uptake

Quantification of CO_2 uptake was done based on the mass gain method. The formula used for the calculation is provided in Eq. 1. The collected water represents water loss due to exothermic nature of carbonation reaction and was recovered by absorbent paper. Since not all vaporized water can be collected, values obtained by mass gain method represent a minimum conservative estimate and could comprise a margin of error.

$$CO_2 \text{ Uptake } (\%) = \frac{Mass\ carbonated\ specimen\ (g) + Mass\ collected\ water (g) - Mass\ initial\ specimen (g)}{Mass\ slag\ powder\ (g)}$$

(1) Where Mass $_{\text{carbonated specimen}}$ referred to the mass of the sample immediately after the carbonation curing, Mass $_{\text{initial specimen}}$ was the mass of the sample before carbonation curing, Mass $_{\text{collected water}}$ was the collected water which was condensed on the internal walls of the carbonation curing chamber was due to the exothermic carbonation reaction and Mass $_{\text{slag powder}}$ was the initial slag content in grams.

The carbon content was further determined using the pyrolysis method[16] and adjusted to exclude the carbon content of the as-received slag. The pyrolysis method allows for quantification of non-evaporable water content (W_n) as well as the CO_2 content (W_c). This method is considered more representative of the samples since more grams are being ignited compared to the few mg samples by TGA. Approximately 3 compacts from each batch were crushed in a mortar and pestle then sieved to pass a 150 µm mesh and placed separately in ceramic crucibles. The same amount of each powder sample (9g) was analyzed to exclude the effect of material size. The crucibles were run in a muffle furnace at 105, 430, 800 and 1050 ℃ at a heating rate of 30 ℃/min holding for 1 hour at each temperature. The weight was measured following each ignition period. Three compacts from each batch were tested to obtain statistical data. It was indicated by TG/MS curves discussed in section 3.3.2 that mass loss below 430 ℃ was induced by the de-hydration of reaction products while mass loss above 430 ℃ was induced by de-carbonation. Thus, calculated W_c was obtained as the mass loss between 430 to 800 ℃ normalized by the mass after being heated to 1050 ℃ following the recommendation of [20]. The mass loss between 105 to 1050 ℃ excluding the CO_2 mass and normalized by the mass after being heated to 1050 ℃ was used to calculate the W_n.

3.2.5 Compressive Strength

Compressive strength tests were conducted on compacts at their respective curing ages. The MTS-SINTECH 30/G equipped with a 150 KN load cell used for the moulding of the compacts was utilized for the compressive strength tests. The test was run at a loading rate of 0.5 mm/min. At least 5 samples were tested and averaged from each batch to generate reproducible results.

3.2.6 Microstructural characterization

Following structural failure, compacts were crushed using a mortar and pestle to obtain a fine powder which was further sieved to pass a 150 μm sieve. The obtained powder fines were used in subsequent analyses.

To understand the mechanism behind strength development in steel slag, quantitative x-ray diffraction (Q-XRD) analysis was carried out using the Rietveld method. By adding corundum as an internal standard, identification of the amorphous content is more viable. A Panalytical X'Pert Pro diffractometer coupled to a Cu X-ray source and an X'celerator detector was utilized. The diffractograms were obtained over a range of 5 to 70 deg 2θ at a voltage of 40 kV and current of 40 mA. Step size was set to 0.017 deg 2θ with corresponding 50 s per step.

Thermogravimetric analysis (TG) allows for phase identification where each phase is characterized by a specific temperature range of decomposition. A thermal analyzer TG-Q500 coupled to a Discover mass spectrometer (MS) detector was utilized. Approximately 30 mg of powdered sample were run under argon atmosphere (20 ml/min) over a temperature span of 30 to 1050 ℃

at a heating rate of 10 °C/min. The same amount of powder was used for each run to exclude the effect of material size. MS curves, corresponding to the release of CO_2 and water (MS=44 and MS=18 respectively), were interpreted to distinguish the decarbonation temperature onset. The first derivative of thermogravimetry (DTG) curves served to identify the reaction products based on their respective decomposition temperature.

Apparent porosity of samples subjected to various curing regimen was determined by the water boiling test as per ASTM C642. The pores size distribution profile was determined using nitrogen adsorption desorption (NAD) analysis. A small piece (< 5 mm) was cut from each compact using a diamond saw with alcohol as lubricant. The cut piece obtained from the same location for each compact was crushed into smaller pieces using a mortar and pestle and then the pieces were sieved. Pieces retained on a 150 μm sieve were oven dried for 12 hours at 105 °C and then submitted for NAD analysis. A TriStar 3000 Micrometrics instrument was used with the analysis bath temperature adjusted to 77.3 K. The total pore volume and pore size distribution were derived from the desorption isotherm derived using the Barrett-Joyner-Halenda (BJH) method [21] that is deemed to be more accurate than the adsorption isotherm.

To identify the functional groups within amorphous and crystalline phases of the steel slag, Fourier transform infrared spectroscopy (FTIR) measurements were performed on a Nicolet 6700 FTIR spectrometer coupled to a Smart iTR module (FTIR-ATR). Spectra were recorded over the range of 4000 to 650 cm^{-1}.

To determine the chemical composition of amorphous products formed by carbonation and hydration, samples were examined using a Hitachi SU3500 scanning electron microscope (SEM) coupled with an energy dispersive X-ray spectrometer (EDS) for elemental compositional analysis. Carbonated and hydrated compacts of varying ages were cut using a diamond saw with alcohol as lubricant to obtain a disc of approximately 3 mm thick. These samples were embedded in resin disks of diameter 42 mm. When hardened, the samples were polished in an automatic grinder/polisher machine. For microstructural morphology, samples were about 5 mm in size and were obtained from the surface layer of compacts. Prior to SEM examination, all samples were coated with a thin layer of gold.

3.3 Results and discussions

3.3.1 Characteristic of as-received slag

The oxide and mineral composition of the as-received slag are shown in Table 3-1. Almost 50 % by weight of the slag oxide composition was CaO which could be traced back to the addition of lime during the steel processing phase. The second most abundant phase, at 25 % by weight, was SiO_2. The third dominant phase was MgO. Other phases present in less percentages like FeO and Al_2O_3 were also detected. The high CaO and MgO content (57.7 wt. %) lent this slag its high reactivity to carbonation [3]. Its hydraulic properties could be inferred from its CaO:SiO_2 ratio. The CaO/SiO_2 of as-received slag was 1.99 which was much less than the threshold, of 2.7, for hydraulicity identified by other studies [22, 23]. Thus, this slag was not expected to display good hydraulic activity.

Table 3-2 presents the mineral composition of raw steel slag. In terms of CO_2 uptake, the maximum theoretical CO_2 uptake capacity calculated based on the alkali metals present in the raw slag were 12.1 % for MgO and 36.6 % for CaO leading to a total of up to 48.7 %.

The oxides present in the as-received steel slag were primarily in the form of calcium silicates (65.7 wt. %). Almost 81 % of these were in the form of calcio-olivine, 15 % were in the form of jasmundite and the remining percentage belonged to larnite and cuspidine. Other oxides were present in the form of mayenite and periclase at lower percentages. All of the present mineral phases were reported to be CO_2 reactive [24] albeit to varying degree. Calcio-olivine was reported to display no hydraulic activity [10, 25] while jasmundite displayed a poorly hydraulic activity [26].

3.3.2 CO_2 uptake and non-evaporable water content

The CO_2 uptake recorded in samples subjected to various carbonation curing periods is depicted in Fig. 3-2. The CO_2 uptake increased with the increase in CO_2 curing duration, but the increase seemed to be rapid in the first 2 hours of the reaction and then afterwards CO_2 uptake rate declined. Almost 11.5 % by dry slag mass of CO_2 were sequestered in the first 2 hours of carbonation curing. Extending the carbonation curing duration to 24 hours resulted in an additional CO_2 uptake of 1.8 % by dry slag mass only.

The cut-off temperatures to distinguish the onset of the dehydration and the decarbonation phases were realized after consulting the typical MS curves of carbonated samples shown in Fig 3-3. The mass loss below 415 ℃ was associated with the decomposition of calcium aluminate hydrates (C-A-H), portlandite and gel phases (calcium silicate hydrates (C-S-H), Ca-modified silica gel) [7, 8, 27]. Above 415 ℃, de-carbonation was considered as the primary cause of mass loss induced by decomposition of amorphous $CaCO_3$, vaterite and aragonite, and well crystallized calcite respectively [27]. Based on the MS curves, the onset of CO_2 release (MS=44) occurred at 430 ℃ nearly intersecting with the decaying H_2O (MS=18) release curve.

Accordingly, the pyrolysis method was adopted and mass loss below 430 ℃ was attributed to non-evaporable water content (W_n) whereas mass loss between 430 ℃ and 800 ℃ was attributed to chemically bound CO_2 (W_c). Results of chemically bound CO_2 content and non-evaporable water content as a function of CO_2 curing duration are presented in Fig 3-4.

It could be seen that after 2 hours of carbonation curing W_c was 11.7 % and reached 13.6 % following 24 hours of carbonation curing. Results by pyrolysis method were almost the same as those of the mass gain method. Extending the carbonation curing duration led to further increase in CO_2 uptake albeit not substantial. This reflected that $CaCO_3$ nucleation and growth was fast at the start of the reaction due to the unobstructed calcium silicate minerals, but with the progression of the reaction and the continued deposition of $CaCO_3$s on the rim of said minerals, CO_2 diffusion was hindered and further dissolution of Ca^{2+} decelerated, effectively slowing down the reaction but not stopping it [28].

The early age (within 24-hour) W_n increased as the carbonation duration increased which implied an increase in formed products. The highest W_n content was noted in 24-hour hydrated-only sample (6.39 %); nonetheless, the W_n in 24-hour CO_2-cured sample was very close (5.76 %). The same trend was also seen in late age (up to 28 days subsequent hydration) samples. The W_n observed in samples subjected to 28 days of hydration curing (7.71 %) was marginally higher than that observed in samples subjected to an initial 24 hours of carbonation curing (6.84 %). Nonetheless, the W_n increment induced by subsequent hydration seemed to be on the same order of magnitude regardless of the carbonation duration. This demonstrated that carbonation curing did not hinder subsequent hydration.

3.3.3 Compressive strength

Compressive strength is the most critical property in any construction material. Results of compressive strength of compacts subjected to different CO_2 curing durations and to 28 days of subsequent hydration are given in Fig. 3-5. The reactivity of steel slag to CO_2 curing was reflected by a significant and rapid strength gain recorded in compacts immediately after carbonation. Carbonation curing for 2 hours yielded a strength of 29 MPa. The strength gain steadily increased with the carbonation duration reaching an ultimate strength of 46.8 MPa after 24 hours of carbonation curing. The corresponding strength recorded after 24-hour of hydration in hydrated-only counterparts was 3.6 MPa. Carbonation strength was almost 13 times higher than the hydration strength for the same curing duration.

Subsequent 28 days of hydration seemed to further reinforce the performance of carbonated compacts. The overall strength induced by 2 hours of carbonation followed by 28 days of hydration was 42 MPa. The strength steadily increased with the increase in the initial carbonation curing duration to 70 MPa, recorded in samples subjected to an initial 24 hours of carbonation curing. Interestingly, the hydrated-only compacts attained a strength of 17 MPa following 28 days of sealed curing which displayed the latent hydraulic potential of the used steel slag as hypothesized by the XRF and QXRD data of as-received slag.

The variation in the CO_2 curing duration affected the subsequent hydration performance of steel slag where a more pronounced increase in strength was recorded in samples subjected to longer periods of carbonation curing namely 12 and 24 hours. This finding contradicts the findings of other studies performed on cement-based materials where it was shown that the ultimate compressive strengths attained after subsequent hydration were almost on the same order of magnitude regardless of the variation in CO_2 curing period [20]. In the referenced study, this was attributed to the barrier effect of the formed carbonation products limiting Ca^{2+} ions dissolution in subsequent hydration phase. Whereas this hypothesis could be valid for hydraulic materials, the same cannot be projected to steel slag, a weak latent hydraulic material because the main mineral targeted by carbonation curing in steel slag does not possess inherent hydraulic activity on its own. The steel slag under study contained almost 53.1 % of gamma-C_2S, a mineral proven to have no hydraulic activity [16, 29, 30]. The engagement of this predominant mineral was solely dependent on CO_2 activation unlike the minerals in cement which do not require activation for engagement and can thus engage in hydration and carbonation reactions simultaneously. Moreover, the formation of $CaCO_3$ by carbonation reaction could promote subsequent hydration by providing nucleation sites for reaction product deposition which might reduce the gel rim of C-S-H and C-A-H that encapsulates the active slag minerals. The linear relation (Fig. 3-6) established between compressive strength and W_c/W_n seemed to further reinforce this interpretation. The trend established in steel slag-based materials was much steeper than the cement-based results reproduced by Wang et al. [20], suggesting that the aforementioned barrier effect theory was more applicable to cement-based substrates than steel slag (owing to its heterogeneous mineral composition). Furthermore, the similarity in the trend established between W_c and W_n (Fig. 3-6) also suggested that the formed products by carbonation and hydration could possibly belong to the same phase, possibly carbonate modified C-S-H.

3.3.4 *Porosity characterization*

Apparent porosity greatly reflects the physical strength of construction materials [3]. The porosity of samples subjected to various periods of carbonation curing and to hydration curing is shown in Fig 3-7. The employed test was performed on the whole compacts and thus the porosity gradient could not be determined, and the obtained results represented the average porosity per sample. It should also be mentioned that the adopted dry cast compaction method was responsible for the introduction of large air voids into the system which increased the total average porosity per sample. Carbonation for 2 hours resulted in an apparent porosity of 36 % which dropped to 29 % when carbonation duration was extended to 24 hours. The highest porosity was recorded in 24-hour hydrated-only samples at 38 %. Subsequent hydration led to a pore reduction in all samples. The porosity in hydrated only samples dropped to 36 % after 28 days of hydration. The most significant pore reduction was recorded in samples subjected to an initial 24 hours of carbonation.

The obtained results were in good agreement with strength and CO_2 uptake results, implying that extending the carbonation curing duration induced pore densification and promoted strength gain in early and late ages.

The pore size distribution for several samples subjected to various curing scenarios were analyzed by NAD which detects the porosities between 4 and 100 nm[31]. The cumulative pore volume distribution as a function of the pore diameter is illustrated in Fig. 3-8A. For pore sizes between 4 and 7 nm, samples subjected to 24 hours of carbonation curing had less porosity than samples carbonated for 2 hours. With subsequent hydration, porosity further reduced with the lowest porosity recorded in samples subjected to an initial 24 hours of carbonation curing.

The pore size distribution defined by the incremental pore volume as a function of pore diameter is shown in Fig 8B. The carbonated samples with or without subsequent hydration displayed a non-symmetric bimodal distribution whereas hydrated-only samples displayed a multimodal distribution. At early age, the first peak occurring at 4 nm was of higher intensity for samples carbonated for 24 hours compared to 2 hours of carbonation. Pores occurring at this scale are an intrinsic part of C-S-H [32, 33]’ thus the increase in carbonation duration was expected to increase the deposition of carbonation and hydration products conforming with the obtained results. The influence of carbonation curing duration on porosity was more pronounced on the pores with diameter a between 7 to 70 nm associated with the smaller capillary pore sizes [33]. Compared to samples carbonated for 2 hours, 24-hour carbonated samples demonstrated a weaker smoother peak signifying refinement of pores whereas 2-hour carbonated samples displayed sharper distinct peaks. This observation revealed that the increase in CO_2 uptake generated more nano-pores (10 nm) and less micropores (1 μm).

Subsequent hydration in carbonated samples had different effect on pore sizes. Compared to 24-hour carbonated samples, samples carbonated for 2 hours showed no change in pore sizes between 7 and 20 nm but a reduction over the range 20 to 70 nm. Meanwhile, 24-hour carbonated sample displayed pore reduction over the whole 7 to 70 nm pore size range reflecting the lowest porosity associated with smaller capillary pores. When a longer period of CO_2 curing was adopted, this led to higher refinement with smaller capillary pores almost disappearing in samples 24C28dH. Thus, prolonging the CO_2 curing duration did not negatively affect the subsequent hydration and after exposure to CO_2, hydration continued and led to an overall reduced smaller-capillary pores which was reflected in an enhanced mechanical strength. This observation was consistent with other studies [32] where it was shown that minor changes in porosities had a profound effect on strength at later ages.

3.3.5 *Reaction products characterization*

XRD spectra of several samples at the early age were acquired in order to study the variation in hydration/carbonation products of steel slag pastes initiated by selected curing methods (CO_2 curing and sealed-hydration curing). Fig. 3-9 presents these data. By comparing the CO_2-cured and the hydration-cured diffractograms, the most noticeable difference was the weakening in γ-C_2S peak intensity (sharpest characteristic diffraction peak at $2\theta = 29.5$ ° and 33 °) in samples 2C and 24C accompanied by an abundant emergence of calcite peak ($2\theta = 29.3$ °), reflecting the occurrence of the carbonation reaction of calcium silicates described in eq. 1. The former peak experienced no apparent change in intensity in hydrated-only samples emphasizing the non-hydraulic nature of this mineral. Other minerals such as jasmundite, periclase, cuspidine, mayenite and larnite experienced a drop in intensities to varying degrees, which was accompanied by the appearance of new peaks of varying intensities, namely calcite, katoite and vaterite (albeit not in all samples). Although no calcium carbonates were detected in hydrated-only samples, their formation cannot be ruled out, especially knowing that XRD can only identify crystalline phases and knowing that no strict measures to restrict weathering carbonation during preparation and curing of samples were taken.

Vaterite, a calcium carbonate polymorph, was only observed in samples subjected to 24 hours of carbonation curing. Several studies [7, 9, 34, 35, 36] also observed vaterite upon carbonation of steel slag matrix. It is worth mentioning that vaterite is regarded as the less stable polymorph of $CaCO_3$ which upon heating to 350 ℃ transforms to the stable polymorph calcite [15]. Vaterite had been previously identified as the main product of C-S-H carbonation [37, 38]. Therefore, the presence of vaterite in samples subjected to prolonged carbonation curing (24C early and late) might suggest the onset of C-S-H carbonation in these samples.

The DTG curves of samples subjected to various curing schemes are plotted in Fig. 3-10. The most prominent peak in carbonated samples was the peak corresponding to the decomposition of well crystallized $CaCO_3$ centered at about 700 ℃ attributed mainly to calcite [7]. Moreover, a low and broad maximum on all DTG curves of carbonated samples was observed around 100 to 430 ℃, which was associated with the decomposition of gel phases (C-S-H and Ca-modified silica gel), C-A-H, and katoite [7, 8]. Hydrated-only samples displayed a multi-peak trend in the dehydration zone ($T < 430$ ℃, Fig 3-3). XRD diffractograms (Fig 3-9) revealed a clear drop in mayenite peaks ($2\theta = 18$ °) accompanied by the emergence of new peaks of katoite. According to [22, 39], the hydration reaction in ladle slags bears resemblance to calcium sulfoaluminate cements where mayenite hydrates form aluminum hydroxide and katoite whose decomposition temperature is in the range 200-250 ℃ and 300-380 ℃ respectively. Accordingly, the multi-peak profile in hydrated-only steel slag samples could be attributed to C-S-H and C-A-H, aluminum hydroxide and katoite respectively. It is worth mentioning that the shifts noted in the DTG curves of hydrated-only samples were ascribed to the unstable initial formation of calcium-aluminate hydrates that subsequently convert at later ages to the stable polymorph katoite [40]. QXRD results of raw, carbonated and hydrated steel slag samples at early and late ages are presented in Table 3-4. In general, these data complied well with TG data, apart from the quantification of formed $CaCO_3$. Only well crystalline $CaCO_3$ can be detected by XRD, but all polymorphs of $CaCO_3$ can be detected by TGA and thus quantified. The difference in quantified $CaCO_3$ could be attributed to the formation of amorphous or poorly crystalline calcium carbonates. Also, it seemed that the divergence between wt. % of $CaCO_3$ measured by TG and QXRD increased with the increase in carbonation duration. This observation was consistent with the findings of [41] who noted the same trend in carbonated blast oxygen furnace slag. In samples subjected to different carbonation curing durations, the amount of precipitated, well-crystalline $CaCO_3$ crystals, namely calcite, were on the same order of magnitude (Table 3-4). DTG curves displayed an increase in poorly crystalline $CaCO_3$ with the increase in carbonation duration. It seemed that increasing the duration of CO_2 exposure mainly led to the formation of poorly crystalline $CaCO_3$ crystals which indicated the tendency of the matrix to shift to a more amorphous phase (Table 3-4).

The results of FTIR analysis of samples subjected to various curing scenarios at early and late ages are shown in Fig. 3-11. The peaks at 815 and 846 cm^{-1} correspond to γ-C_2S [42]. A huge drop in the intensities of these peaks in carbonated samples indicated the reaction of this mineral by carbonation curing. The peaks at about 875 and 712 cm^{-1} correspond to the out-of-plane bending vibration of CO_3^{2-} [17] in calcite while the broad absorption band at 1410 cm^{-1} can be ascribed to the symmetric stretching vibration of C-O bond in amorphous $CaCO_3$ [43, 44]. The carbonation reaction of steel slag formed mainly calcite and amorphous $CaCO_3$. The calcite peaks were almost on the same order of magnitude in samples carbonated for 2 and 24 hours, consistent with the

QXRD results. Extending the carbonation reaction from 2 to 24 hours increased the amorphous $CaCO_3$ content. In hydrated-only samples, minor peaks attributed to amorphous $CaCO_3$ could be detected at lower frequency of 1380 cm^{-1} which could be attributed to weathering carbonation occurring during the preparation of these samples. The double peaks occurring over the range 920-1100 cm^{-1} were typical of the asymmetric and symmetric stretching vibrations in Si-O bonds. The peak centered between 920 and 960 cm^{-1} could be attributed to the C-S-H [42]. This phase was present in hydrated and carbonated samples at early and late ages albeit with varying intensities. Also, it was interesting to note that the C-S-H in 24-hour carbonated-only sample was less than that in the 2-hour carbonated only sample. This finding might suggest carbonation of this phase, consistent with the observation that vaterite (a product of C-S-H carbonation) was only detected in the former sample (Fig. 3-9). Nonetheless, at the late age, the peak at about 945 cm^{-1} increased in both samples and the increase was more prominent in 24-hour carbonated sample. A peak located between 1020 and 1100 cm^{-1} observed in carbonated-only samples was correlated with the occurrence of Ca-modified silica gel or a highly polymerized Si- gel [45, 46]. The broad peak was lower in the 2-hour carbonated sample, and it increased in intensity and in wavenumber when the carbonation duration was increased to 24 hours. This could be interpreted as increased polymerization of calcium-silica gel phase with the increase in carbonation duration. According to [17, 46, 47], the degree of polymerization of silicate compound is a function of the Ca:Si atomic ratio of the calcium-silica gel phase. These observations confirmed that C-S-H and Ca-modified silica gel co-existed in samples subjected to 2 and 24 hours of carbonation while the trend established by the spectra suggested that C-S-H formed first, and it tended to de-calcify with the increase in carbonation duration to form Ca-modified silica gel. The definition of the product referred to herein as Ca-modified silica gel is a low lime Ca/Si C-S-H. Interestingly, the subsequent hydration reaction seemed to cause significant changes to the matrix for samples carbonated for longer durations (24-hour) than samples carbonated for shorter durations (2-hours) (Fig. 3-11). There was a slight increase in intensity accompanied by a shift to lower wavenumbers recorded in the frequency range 1020 to 1100 cm^{-1} in 2 and 24-hour carbonated samples at late ages.

SEM-BSE imaging coupled with EDS analysis were carried out to identify carbonation reaction products. Fig. 3-12A is a higher magnification photomicrograph of the surface. The lighter grey areas correspond to higher atomic number entities namely unreacted steel slag grains while the darker areas represent the reaction products. The darkest areas represent the cracks and voids in the matrix. In the zoomed-in photomicrograph shown in Fig. 3-12B, a partially reacted calcium-silicate grain can be observed surrounded by the reaction product rim. All points used in EDS analysis were collected from these rims from different locations, with more than 100 points collected from each sample subjected to different curing scenarios to present statistical data. EDS analysis (Fig 3-12) revealed that the reaction product phase contained Ca, Si, O, and C as the main elements with varying intensities which implied that the reaction product was a hybrid of gel phases (C-S-H and Ca-modified silica gel) and $CaCO_3$. Similar results were reported by Rostami et al. and Ashraf et. al [17, 48]. As established by the FTIR analysis (Fig. 3-11), Ca-modified silica gel or highly polymerized C-S-H gel was present in carbonated samples, thus it seemed logical to represent the Ca:Si atomic ratio of the carbonated samples as Ca/(Ca + Si) atomic ratios to avoid very small or very big ratios. The values of Ca/(Ca + Si) ranged between 0 to 1 with 0 approaching a de-calcified silica gel while 1 represented $CaCO_3$. Fig. 3-13 displays the atomic ratio distribution of (Al + Fe)/Ca vs. Ca/(Ca + Si) for 2 and 24-hour carbonated samples both at early and late ages. The variability in the pattern of Al could be interpreted as a substitution of Al by Si in gel phases which might help in the identification of the formed product phases. The distribution of the data sets hinted at the formation of a major product phase that was a hybrid between gel phases (C-S-H and Ca-modified silica gel) and $CaCO_3$ (with the Ca/(Ca + Si) atomic ratio ranging between 0.42 to 0.85). Minor phases of Ca-modified silica gel and $CaCO_3$ seemed to be present (with the Ca/(Ca + Si) atomic ratio less than 0.42 for the former and greater than to 0.85 for the latter). The distribution of (Al + Fe)/Ca atomic ratios implied that these values were highly variable in the Ca-modified silica gel phase compared to the composite and $CaCO_3$ phases. A similar observation was made by Ashraf et al [17]. Furthermore, it seemed that the subsequent hydration phase caused the lower Ca/(Ca + Si) atomic ratios to shift towards higher values. To follow up on this revelation, the frequency distribution of Ca/(Ca + Si) atomic ratios of samples subjected to 2 and 24 hours of carbonation curing at early and late ages are shown in Fig. 3-14. In general, the frequency distribution plot confirmed the presence of a major phase (II on the graph) that was the composite phase and two minor phases (I and III on the graph) that were the Ca-modified silica gel and $CaCO_3$. Low Ca/(Ca + Si) atomic ratios were scarce in 2-hour and 24-hour carbonated samples. However, it was evident that increasing the carbonation duration to 24 hours led to a higher decalcification, as indicated by the FTIR results. Subsequent hydration, on the other hand, led to an increase in Ca/(Ca + Si) atomic ratio with the simultaneous disappearance of the lower Ca/(Ca + Si) atomic ratios, signifying a vigorous subsequent hydration reaction. Changes in Ca:Si and O:C atomic ratios of the hybrid phase are summarized in Table 3-5. The Ca:Si ratio of the hybrid phase of gel (C-S-H and Ca-modified silica gel) and $CaCO_3$ was 1.8 after 2 hours of carbonation curing. Extending the carbonation duration to 24 hours reduced the Ca:Si ratio to 1.7. Subsequent hydration increased the Ca/Si ratios to 2.0 and 1.9 in 2C and 24C, respectively. The subsequent hydration phase played an important role in the reinforcement of the structure (as evident by compressive strength increases: Fig. 3-5). Interestingly, the resultant

Ca:Si atomic ratio of the hybrid phase was within the same range as the regular C-S-H i.e. 1.5 to 2.0 [49, 50]. Simultaneously, an increase in O/C atomic ratios accompanied the subsequent hydration phase which served to confirm that carbonation did not hinder subsequent hydration.

3.3.6 Morphological characterization

SEM photomicrographs shown in Fig. 3-15 and 3-16 are typical of the surface layer of compacts. The morphological evolution of the carbonation-cured steel slag samples with time is presented in Fig. 3-15. Samples subjected to 2 hours of carbonation curing were less dense with an aggregated overall morphology (Fig. 3-15A). Increasing the carbonation duration to 24 hours led to a denser matrix and locating $CaCO_3$ become harder as the matrix experienced more amorphous or poorly crystalline product deposition (Fig. 3-15B). Subsequent hydration (Fig. 3-15C) led to a monolithic amorphous matrix dominated by a honeycomb-like morphology, interpreted as the deposition of post-carbonation products that engulfed the already densified matrix. This observation was consistent with results of porosity analysis (section 3.4), the increase in W_n content recorded by TGA and pyrolysis methods (Fig 3-4 and Table 3-3) as well as FTIR (Fig. 3-11) and BSE-EDS analyses (Fig. 3-13).

The photomicrographs of samples after 28 days of hydration with and without subsequent hydration are shown in Fig 3-16. The difference in reaction product morphology between carbonated and hydrated samples could be clearly seen. Katoite (Fig. 3-16A) was the dominant product in hydrated samples, as indicated by the QXRD (Table 3-4) results. The other product found in much less abundance was C-S-H (Fig. 3-16B), as revealed by TG (Table 3-3) and FTIR (Fig. 3-11) analyses. It is also worth mentioning that the hydrated sample was dominated by unreacted slag particles even after 28 days of hydration, reflecting the poor hydraulicity of steel slag. In carbonated samples at the late age, the dominant product was a continuous gel phase which, according to EDS analysis, contained variable quantities of Ca and Si while also containing C. This phase was identified as a hybrid between gel phases (C-S-H and Ca-modified silicate gel) and $CaCO_3$.

3.4 Discussion

Table 3-6 summarizes the strength increase developed upon the subsequent 27-day hydration curing following carbonation, with hydrated-only sample strength shown as reference. The definition of the strength increase is the late age strength deducted from the early age strength which denoted the contribution of the subsequent hydration to the ultimate strength recorded at 28 days. The strength of the reference hydrated-only sample increased 13.4 MPa between day-1 and day-28 of curing. The strength increase recorded in samples subjected to combined carbonation-hydration curing was 13 MPa for samples subjected to an initial 2 hours of carbonation and increased steadily to 23.2 MPa in samples subjected to an initial 24 hours of carbonation curing. Subsequent hydration strength increased with the increase in the carbonation duration.

The microstructural evolution of steel slag pastes subjected to hydration and carbonation both at early and late ages is shown in Fig. 3-17. The mechanism of strength gain is discussed below.

Scenario (1) Hydration-only: Since steel slag is a latent hydraulic material then at the end of the 24 hours of hydration hardly any hydration products (namely C-S-H) had started to form on the steel slag grain, as inferred from the low engagement of reactant minerals by QXRD. Supplemented by 27 days of subsequent hydration, steel slag slowly hydrated, and a hydration product rim was formed on steel slag particles. This is backed-up by the results of QXRD, DTG and FTIR analyses.

Scenario (2) Short-term carbonation (2C, 4C, 6C): Unlike commonly studied hydraulic systems (cement), in steel slag systems (latent poorly hydraulic) carbonation and hydration are not expected to proceed simultaneously during these short CO_2 exposures. Accordingly, upon exposure to CO_2 curing (early age), CO_3^{2-} reacts with fully exposed steel slag particles to form C-S-H and calcite as revealed by DTG, QXRD, FTIR and SEM. When samples are allowed to cure for 28 subsequent days (late age), hydration proceeds, and the ultimate strength was found to be equal to the simple superposition of carbonation-only plus hydration-only strengths.

Scenario (3) Prolonged carbonation (12C, 24C): At the early age, extending the carbonation reaction duration allowed for the latent hydraulic activity to initiate with the progression of the carbonation reaction. Hydration proceeded in a matrix modified by the deposition of $CaCO_3$s. It is proposed that these carbonates acted as seeds that promote more reaction product deposition and simultaneously inhibit the formation of products on the rim of the calcium silicate particles thus promoting higher dissolution. This was found to lead to the decalcification of C-S-H to form Ca-modified silica gel as well as the deposition of amorphous $CaCO_3$ which led to a densified overall amorphous phase. At later ages, nucleation and growth explained why the 28-day strength was found to be higher than the simple superposition of carbonation-only plus hydration-only strengths. Evidence to support these hypotheses can be found in the fact that: (1) porosity was refined by extending the carbonation period and was almost diminished by the subsequent hydration in 24C samples; (2) QXRD results revealed the highest consumption of raw slag minerals in samples subjected to prolonged carbonation duration compared to samples carbonated for shorter durations and hydrated-only samples; (3) DTG and QXRD revealed that carbonation did not hinder subsequent hydration and that the extent of the subsequent hydration reaction was almost the same in both carbonated samples; (4) subsequent hydration, as shown by the frequency distribution of Ca/(Ca + Si) (Fig. 3-14), increased the Ca/(Ca + Si) atomic ratios in both samples, in agreement with results of the FTIR analysis (Fig. 3-11). Simultaneously, subsequent hydration led to a decrease in frequency of the product with high Ca/(Ca + Si) atomic ratios (between 0.85 and 1). This suggested that these $CaCO_3$-rich products might provide more nucleation sites for the subsequent hydration reaction, as confirmed by increases to the overall Ca/Si and O/C ratios following subsequent hydration reaction.

In conclusion, the deposition of $CaCO_3$s resulted in a higher reaction degree (i.e. raw slag minerals consumption as revealed by QXRD) which translated into an improved overall mechanical performance when supplemented by the subsequent hydration curing. As such, CO_2 curing for longer durations (12C and 24C) might promote hydration leading to an improvement in ultimate strength.

3.5 Conclusion

The influence of combined carbonation-hydration curing on mechanical characteristics and microstructure of steel slag-based binder prepared with low water to slag ratio was studied. The steel slag subjected to carbonation and hydration was characterized by the chemically bound calcium carbonate content, non-evaporable water content, compressive strength, pore structure and morphological phases as a function of CO_2 curing duration. The main conclusions are summarized below:

1. The CO_2 uptake in steel slag paste samples was 11.5 % after 2 hours of carbonation curing and increased to 13.3 % following 24 hours of carbonation curing. Non-evaporable water content increased with the increase in carbonation curing duration and the same trend was also seen for post-carbonation hydration. However, in all carbonated samples with and

without subsequent hydration, the non-evaporable water content was less than that in hydrated-only references emphasizing that calcium carbonates played a major role in strength reinforcement.

2. Compressive strength of carbonation-cured steel slag compacts increased linearly with the increase in carbonation duration. The ultimate strength (70 MPa) was recorded in samples subjected to 24 hours of carbonation curing followed by 28 days of subsequent sealed-hydration curing.
3. Porosity analysis showed that the lowest open porosity was recorded in samples subjected to 24 hours of carbonation curing followed by 28 days of subsequent hydration. NAD revealed that the smaller capillary pores were almost eliminated owing to the subsequent hydration phase in samples subjected to prolonged carbonation duration.
4. A difference between the calcium carbonates measured by TGA and by QXRD suggested the presence of poorly crystalline calcium carbonates. The gap increased with the increase in the carbonation curing duration.
5. The major formed product by carbonation curing was identified as a hybrid between gel phases (C-S-H and Ca-modified silica gel) and $CaCO_3$ with an average Ca/Si atomic ratio of 1.9 immediately after 24-hour carbonation curing and 2.0 after 28 days of subsequent hydration.
6. Carbonation for short durations resulted in an over-all strength equal to the superposition of hydration-only and carbonation-only strengths. However, the 28-day hydration strength of steel slag carbonated samples benefited from longer carbonation durations. The enhanced strength was associated with the nucleation and growth of carbonation-deposited calcium carbonates within the hybrid product. The final composite phase (late age), as

revealed by porosity and morphology analysis, was superior to the other phases formed by early age carbonation-only.

References

1. Ghouleh, Z., R.I.L. Guthrie, and Y.X. Shao, *Production of carbonate aggregates using steel slag and carbon dioxide for carbon-negative concrete.* Journal of CO_2 Utilization, 2017. **18**: p. 125-138 DOI: https://doi.org/10.1016/j.jcou.2017.01.009
2. Monkman, S., Y.X. Shao, and C.J. Shi, *Carbonated Ladle Slag Fines for Carbon Uptake and Sand Substitute.* Journal of Materials in Civil Engineering, 2009. **21**(11): p. 657-665 DOI: https://doi.org/10.1061/(asce)0899-1561(2009)21:11(657)
3. Salman, M., O. Cizer, Y. Pontikes, R.M. Santos, R. Snellings, L. Vandewalle, B. Blanpain, and K. Van Balen, *Effect of accelerated carbonation on AOD stainless steel slag for its valorisation as a CO_2-sequestering construction material.* Chemical Engineering Journal, 2014. **246**: p. 39-52 DOI: https://doi.org/10.1016/j.cej.2014.02.051
4. Wang, D., J. Chang, and W.S. Ansari, *The effects of carbonation and hydration on the mineralogy and microstructure of basic oxygen furnace slag products.* Journal of CO_2 Utilization, 2019. **34**: p. 87-98 DOI: https://doi.org/10.1016/j.jcou.2019.06.001
5. Mahoutian, M., Y.X. Shao, A. Mucci, and B. Fournier, *Carbonation and hydration behavior of EAF and BOF steel slag binders.* Materials and Structures, 2015. **48**(9): p. 3075-3085 DOI: https://doi.org/10.1617/s11527-014-0380-x
6. Nielsen, P., M.A. Boone, L. Horckmans, R. Snellings, and M. Quaghebeur, *Accelerated carbonation of steel slag monoliths at low CO_2 pressure-microstructure and strength development.* Journal of CO_2 Utilization, 2020. **36**: p. 124-134 DOI: https://doi.org/10.1016/j.jcou.2019.10.022

7. Ghouleh, Z., R.I.L. Guthrie, and Y.X. Shao, *High-strength KOBM steel slag binder activated by carbonation.* Construction and Building Materials, 2015. **99**: p. 175-183 DOI: https://doi.org/10.1016/j.conbuildmat.2015.09.028

8. Mahoutian, M., Z. Ghouleh, and Y.X. Shao, *Carbon dioxide activated ladle slag binder.* Construction and Building Materials, 2014. **66**: p. 214-221 DOI: https://doi.org/10.1016/j.conbuildmat.2014.05.063

9. Yi, Y.R., Y. Lin, Y.C. Du, S.Q. Bai, Z.L. Ma, and Y.G. Chen, *Accelerated carbonation of ladle furnace slag and characterization of its mineral phase.* Construction and Building Materials, 2021. **276**: p. 122235 DOI: https://doi.org/10.1016/j.conbuildmat.2020.122235

10. Young, J.F., R.L. Berger, and J. Breese, *Accelerated Curing of Compacted Calcium Silicate Mortars on Exposure to CO_2.* Journal of the American Ceramic Society, 1974. **57**(9): p. 394-397 DOI: https://doi.org/10.1111/j.1151-2916.1974.tb11420.x

11. Pan, S.Y., Y.H. Chen, C.D. Chen, A.L. Shen, M. Lin, and P.C. Chiang, *High-Gravity Carbonation Process for Enhancing CO_2 Fixation and Utilization Exemplified by the Steelmaking Industry.* Environmental Science and Technology, 2015. **49**(20): p. 12380-7 DOI: https://doi.org/10.1021/acs.est.5b02210

12. Mahoutian, M. and Y.X. Shao, *Production of cement-free construction blocks from industry wastes.* Journal of Cleaner Production, 2016. **137**: p. 1339-1346 DOI: https://doi.org/10.1016/j.jclepro.2016.08.012

13. Fernandez Bertos, M., S.J. Simons, C.D. Hills, and P.J. Carey, *A review of accelerated carbonation technology in the treatment of cement-based materials and sequestration of CO_2.* Journal of Hazardous Materials, 2004. **112**(3): p. 193-205 DOI: https://doi.org/10.1016/j.jhazmat.2004.04.019

14. Ghouleh, Z., M. Celikin, R.I.L. Guthrie, and Y.X. Shao, *Microstructure of Carbonation-Activated Steel Slag Binder.* Journal of Materials in Civil Engineering, 2018. **30**(9): p. 04018217 DOI: https://doi.org/10.1061/(asce)mt.1943-5533.0002421

15. Goto, S., K. Suenaga, T. Kado, and M. Fukuhara, *Calcium silicate carbonation products.* Journal of the American Ceramic Society, 1995. **78**(11): p. 2867-2872.

16. Bukowski, J.M. and R.L. Berger, *Reactivity and Strength Development of CO_2 Activated Non-Hydraulic Calcium Silicates.* Cement and Concrete Research, 1979. **9**(1): p. 57-68 DOI: https://doi.org/10.1016/0008-8846(79)90095-4

17. Ashraf, W., J. Olek, and J. Jain, *Microscopic features of non-hydraulic calcium silicate cement paste and mortar.* Cement and Concrete Research, 2017. **100**: p. 361-372 DOI: https://doi.org/10.1016/j.cemconres.2017.07.001

18. Humbert, P.S. and J. Castro-Gomes, *CO_2 activated steel slag-based materials: A review.* Journal of Cleaner Production, 2019. **208**: p. 448-457 DOI: https://doi.org/10.1016/j.jclepro.2018.10.058.

19. Johnson, D., *Accelerated carbonation of waste calcium silicate materials*. 2000: Society of Chemical Industry Science Lecture Series.

20. Zhan, B.J., D.X. Xuan, C.S. Poon, and C.J. Shi, *Mechanism for rapid hardening of cement pastes under coupled CO_2-water curing regime.* Cement and Concrete Composites, 2019. **97**: p. 78-88 DOI: https://doi.org/10.1016/j.cemconcomp.2018.12.021

21. Barrett, E.P., L.G. Joyner, and P.P. Halenda, *The determination of pore volume and area distributions in porous substances. I. Computations from nitrogen isotherms.* Journal of the American Chemical society, 1951. **73**(1): p. 373-380 DOI: https://doi.org/10.1021/ja01145a126

22. Vlček, J., R. Švrčinová, J. Burda, M. Topinková, M. Klárová, H. Ovčačíková, D. Jančar, and M. Velička, *Hydraulic properties of ladle slags*. Metalurgija, 2016. **55**(3): p. 399-402.

23. Muhmood, L., S. Vitta, and D. Venkateswaran, *Cementitious and pozzolanic behavior of electric arc furnace steel slags.* Cement and Concrete Research, 2009. **39**(2): p. 102-109.

24. Song, Q.F., M.Z. Guo, L. Wang, and T.C. Ling, *Use of steel slag as sustainable construction materials: A review of accelerated carbonation treatment.* Resources Conservation and Recycling, 2021. **173**: p. 105740 DOI: https://doi.org/10.1016/j.resconrec.2021.105740.

25. Odler, I., *Special Inorganic Cements*. 2000: CRC Press, https://doi.org/10.1201/9781482271942.

26. Liska, M., A. Wilson, and J. Bensted, *Special cements.* Lea's Chemistry of Cement and Concrete, 5th ed.; Hewlett, PC, Liska, M., Eds, 2019: p. 618.

27. Zhang, D., X.H. Cai, and B. Jaworska, *Effect of pre-carbonation hydration on long-term hydration of carbonation-cured cement-based materials.* Construction and Building Materials, 2020. **231**: p. 117122 DOI: https://doi.org/10.1016/j.conbuildmat.2019.117122.

28. Huijgen, W.J.J., G.J. Witkamp, and R.N.J. Comans, *Mechanisms of aqueous wollastonite carbonation as a possible* CO_2 *sequestration process.* Chemical Engineering Science, 2006. **61**(13): p. 4242-4251 DOI: https://doi.org/10.1016/j.ces.2006.01.048

29. Na, S., S. Kang, S. Lee, and M. Song. *Gamma-*C_2S *synthesis from fly ash of fluidize-bed boiler for* CO_2 *capture*. in *Proceedings of the 4th International Congress APMAS, Fethiye, Turkey*. 2014. Citeseer.

30. Chang, J., Y. Fang, and X. Shang, *The role of* β-C_2S *and* γ-C_2S *in carbon capture and strength development.* Materials and Structures, 2016. **49**(10): p. 4417-4424.

31. Xian, X.P. and Y.X. Shao, *Microstructure of cement paste subject to ambient pressure carbonation curing.* Construction and Building Materials, 2021. **296**: p. 123652 DOI: https://doi.org/10.1016/j.conbuildmat.2021.123652

32. Zhao, S., Z. Liu, F. Wang, S. Hu, and C. Liu, *Effect of Extended Carbonation Curing on the Properties of γ-*C_2S *Compacts and Its Implications on the Multi-Step Reaction Mechanism.* ACS Sustainable Chemistry & Engineering, 2021. **9**(19): p. 6673-6684 DOI: https://doi.org/10.1021/acssuschemeng.1c00200.s001

33. Kumar, R. and B. Bhattacharjee, *Porosity, pore size distribution and in situ strength of concrete.* Cement and Concrete Research, 2003. **33**(1): p. 155-164 DOI: https://doi.org/10.1016/s0008-8846(02)00942-0

34. Chang, J., C. Xiong, Y.Y. Zhang, and D. Wang, *Foaming characteristics and microstructure of aerated steel slag block prepared by accelerated carbonation.* Construction and Building Materials, 2019. **209**: p. 222-233 DOI: https://doi.org/10.1016/j.conbuildmat.2019.03.077

35. Shtepenko, O., C. Hills, A. Brough, and M. Thomas, *The effect of carbon dioxide on β-dicalcium silicate and Portland cement.* Chemical Engineering Journal, 2006. **118**(1-2): p. 107-118 DOI: https://doi.org/10.1016/j.cej.2006.02.005

36. Borges, P.H., J.O. Costa, N.B. Milestone, C.J. Lynsdale, and R.E. Streatfield, *Carbonation of CH and C–S–H in composite cement pastes containing high amounts of BFS.* Cement and Concrete Research, 2010. **40**(2): p. 284-292.

37. Black, L., C. Breen, J. Yarwood, K. Garbev, P. Stemmermann, and B. Gasharova, *Structural features of C–S–H (I) and its carbonation in air—a Raman spectroscopic study.*

Part II: carbonated phases. Journal of the American Ceramic Society, 2007. **90**(3): p. 908-917 DOI: https://doi.org/10.1111/j.1551-2916.2006.01429.x

38. Zhang, J., C. Shi, N. Li, Z. Zhang, and N. Farzadnia, *Carbon dioxide sequestration by alkali-activated materials*, in *Carbon dioxide sequestration in cementitious construction materials*. 2018, Elsevier. p. 279-298.DOI: https://doi.org/10.1016/b978-0-08-102444-7.00012-5

39. Adesanya, E., H. Sreenivasan, A.M. Kantola, V.-V. Telkki, K. Ohenoja, P. Kinnunen, and M. Illikainen, *Ladle slag cement–Characterization of hydration and conversion.* Construction and Building Materials, 2018. **193**: p. 128-134.

40. Shi, C.J., *Characteristics and cementitious properties of ladle slag fines from steel production.* Cement and Concrete Research, 2002. **32**(3): p. 459-462 DOI: https://doi.org/10.1016/s0008-8846(01)00707-4

41. Wang, Q., P. Yan, and S. Han, *The influence of steel slag on the hydration of cement during the hydration process of complex binder*. Science China Technological Sciences, 2011. **54**(2): p. 388-394 DOI: 10.1007/s11431-010-4204-0.

42. Ashraf, W., J. Olek, and V. Atakan. *A comparative study of the reactivity of calcium silicates during hydration and carbonation reactions*. in *14th International Congress on Cement Chemistry, Beijing, China*. 2015.DOI: https://doi.org/10.1021/acssuschemeng.8b06841.s001

43. Cizer, Ö., C. Rodriguez-Navarro, E. Ruiz-Agudo, J. Elsen, D. Van Gemert, and K. Van Balen, *Phase and morphology evolution of calcium carbonate precipitated by carbonation of hydrated lime.* Journal of Materials Science, 2012. **47**(16): p. 6151-6165 DOI: https://doi.org/10.1007/s10853-012-6535-7

44. Wehrmeister, U., D. Jacob, A. Soldati, N. Loges, T. Häger, and W. Hofmeister, *Amorphous, nanocrystalline and crystalline calcium carbonates in biological materials.* Journal of Raman Spectroscopy, 2011. **42**(5): p. 926-935 DOI: https://doi.org/10.1002/jrs.2835

45. Ibáñez, J., L. Artús, R. Cuscó, Á. López, E. Menéndez, and M.C. Andrade, *Hydration and carbonation of monoclinic* C_2S *and* C_3S *studied by Raman spectroscopy.* Journal of Raman Spectroscopy: An International Journal for Original Work in all Aspects of Raman Spectroscopy, Including Higher Order Processes, and also Brillouin and Rayleigh Scattering, 2007. **38**(1): p. 61-67 DOI: https://doi.org/10.1002/jrs.1599

46. Ashraf, W. and J. Olek, *Carbonation behavior of hydraulic and non-hydraulic calcium silicates: potential of utilizing low-lime calcium silicates in cement-based materials.* Journal of Materials Science, 2016. **51**(13): p. 6173-6191.

47. Yu, P., R.J. Kirkpatrick, B. Poe, P.F. McMillan, and X. Cong, *Structure of calcium silicate hydrate (C-S-H): Near-, Mid-, and Far-infrared spectroscopy.* Journal of the American Ceramic Society, 1999. **82**(3): p. 742-748 DOI: https://doi.org/10.1111/j.1151-2916.1999.tb01826.x

48. Rostami, V., Y.X. Shao, A.J. Boyd, and Z. He, *Microstructure of cement paste subject to early carbonation curing.* Cement and Concrete Research, 2012. **42**(1): p. 186-193 DOI: https://doi.org/10.1016/j.cemconres.2011.09.010

49. Taylor, H.F., *Cement Chemistry Academic Press.* London, England, 1990: p. 5-22.

50. Kunther, W., S. Ferreiro, and J. Skibsted, *Influence of the Ca/Si ratio on the compressive strength of cementitious calcium–silicate–hydrate binders.* Journal of Materials Chemistry A, 2017. **5**(33): p. 17401-17412 DOI: https://doi.org/10.1039/c7ta06104h

Tables

Table 3-1 Chemical composition of as-received steel slag.

XRF analysis (wt. %)								
SiO_2	Al_2O_3	Fe_2O_3	MnO	MgO	CaO	Na_2O	K_2O	LOI
23.37	4.02	7.71	1.208	11.09	46.59	0.04	< 0.01	3.53

Table 3-2 Mineral composition of as-received steel slag.

Q-XRD Rietveld analysis (wt. %)		
Mineral Compound	Chemical formula	
Calcio-olivine	γ-Ca_2SiO_4	53.1
Mayenite	$Ca_6Al_7O_{16}F$	15.3
Periclase	MgO	10
Jasmundite	$Ca_{10.5}Mg_{0.5}Si_4SO_{18}$	9.7
Larnite	β-Ca_2SiO_4	1.9
Cuspidine	$Ca_4(Si_2O_7)F_2$	1
Portlandite	$Ca(OH)_2$	n.d.
Calcite	$CaCO_3$	n.d.
Amorphous		9

Table 3-3 Reaction products in steel slag pastes subjected to different curing scenarios by TG analysis.

Reaction Products (%)		2C		24C		24H	
		early	late	early	late	early	late
Mass loss in de-hydration	105-430 ℃	2.13	2.45	3.01	3.27	5.04	6.13
Mass loss in de-carbonation	430-800 ℃	10.28	10.78	11.84	12.97	0.84	0.70
Total precipitated $CaCO_3^*$		23.36	24.50	26.91	29.48	1.91	1.59

Table 3-4 Mass fractions (wt. %) of mineral phases in various steel slag compacts estimated by Q-XRD analysis.

QXRD (wt. %)		Raw	2C		24C		24H	
Mineral Compound	Chemical Formula		early	late	early	late	early	late
Calcio-olivine	γ-Ca_2SiO_4	53.1	37.7	36.8	30.1	28.8	52.6	44.9
Larnite	β-Ca_2SiO_4	3	1.8	2.1	1.1	n.d.	2.7	1.2
Jasmundite	$Ca_{10.5}Mg_{0.5}(Si_4)SO_{18}$	9.7	6.5	5.9	3.1	3	9.4	5.8
Mayenite	$Ca_{5.65}Al_7O_{16.15}$	15.3	13.9	12.5	10.5	10.7	2.7	2.1
Periclase	MgO	10	8.9	8.6	7	6.9	8.7	5.6
Cuspidine	$Ca_4Si_2O_7(F, OH)_2$	1	1.8	1.6	n.d.	n.d.	1	n.d.
Portlandite	$Ca(OH)_2$	n.d.	n.d.	n.d.	n.d.	n.d.	n.d.	n.d.
Katoite	$Ca_3Al_2SiO_4(OH)_{12}$	n.d.	2.1	1.3	1.8	1.3	4.5	8.5
Calcite	$CaCO_3$	n.d.	14.6	14.1	13.9	15	n.d.	n.d.
Vaterite	$CaCO_3$	n.d.	n.d.	n.d.	2.4	1.9	n.d.	n.d.
Gypsum	$CaSO_4.2H_2O$	n.d.	n.d.	n.d.	n.d.	n.d.	1	0.5
Amorphous		7.9	12.7	17.1	30.1	32.4	17.4	31.4

Table 3-5 Summarized atomic ratios of hybrid gel phase with CaCO3 in steel slag samples subjected to various curing scenarios.

Atomic ratio	2C		24C	
	early	late	early	late
Ca/Si	1.8	2.0	1.7	1.9
O/C	2.1	2.4	2.6	3.5

Table 3-6 Strength increase in steel slag samples due to subsequent hydration.

	Early age strength (MPa)	Late age strength (MPa)	Strength increase (MPa)
24H	4	17	13
2C	29	42	13
4C	30	45	15
6C	39	50	12
12C	44	63	19
24C	47	70	23

Figures

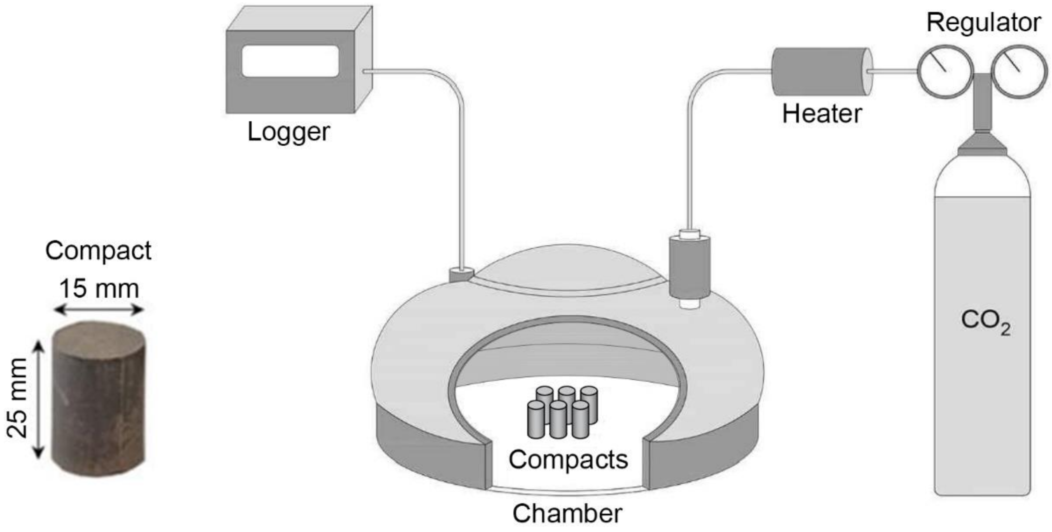

Figure 3-1 Carbonation setup for steel slag compacts.

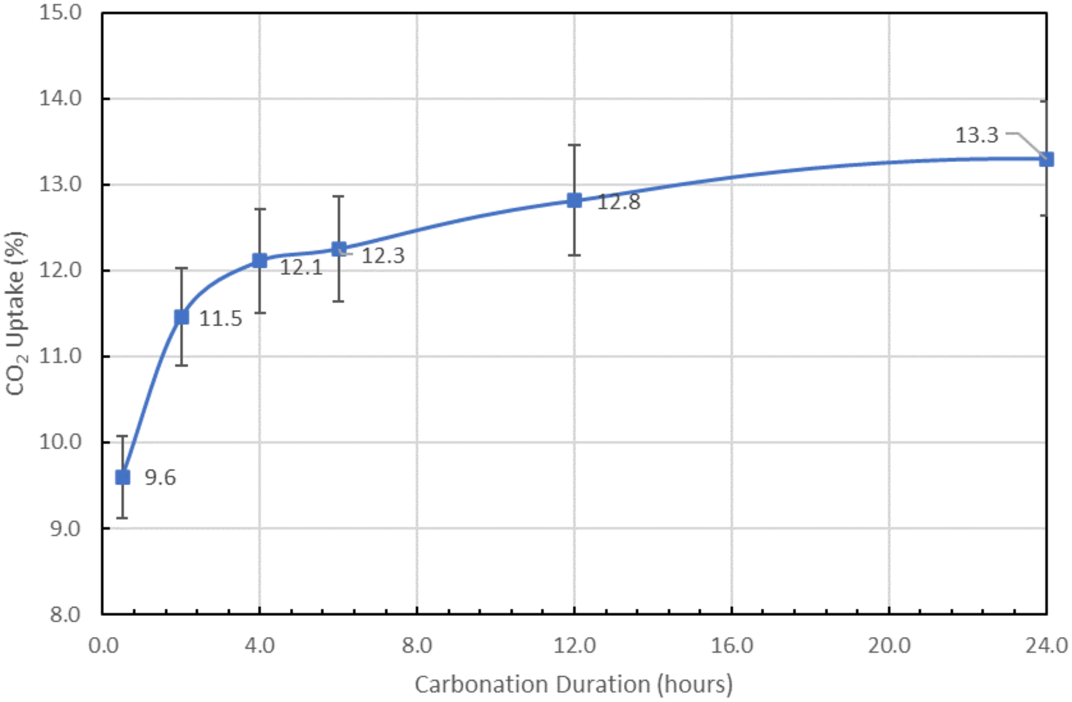

Figure 3-2 Variation in CO_2 uptake with carbonation duration in freshly carbonated steel slag compacts.

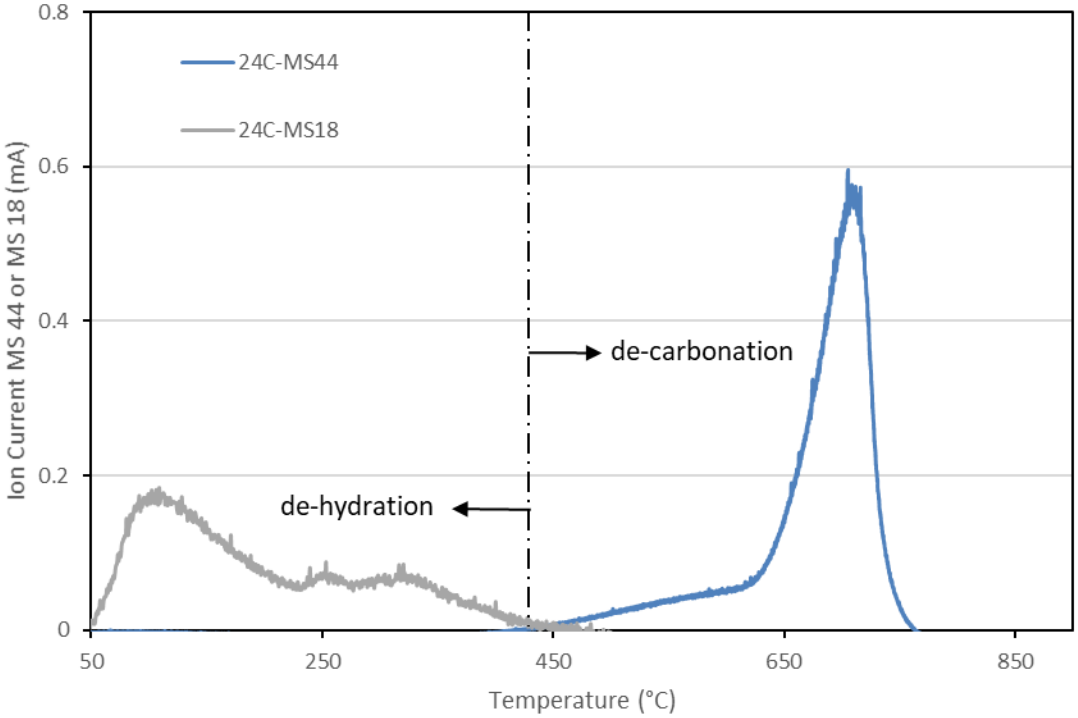

Figure 3-3 Typical MS-curves of carbonated steel slag at early and late age.

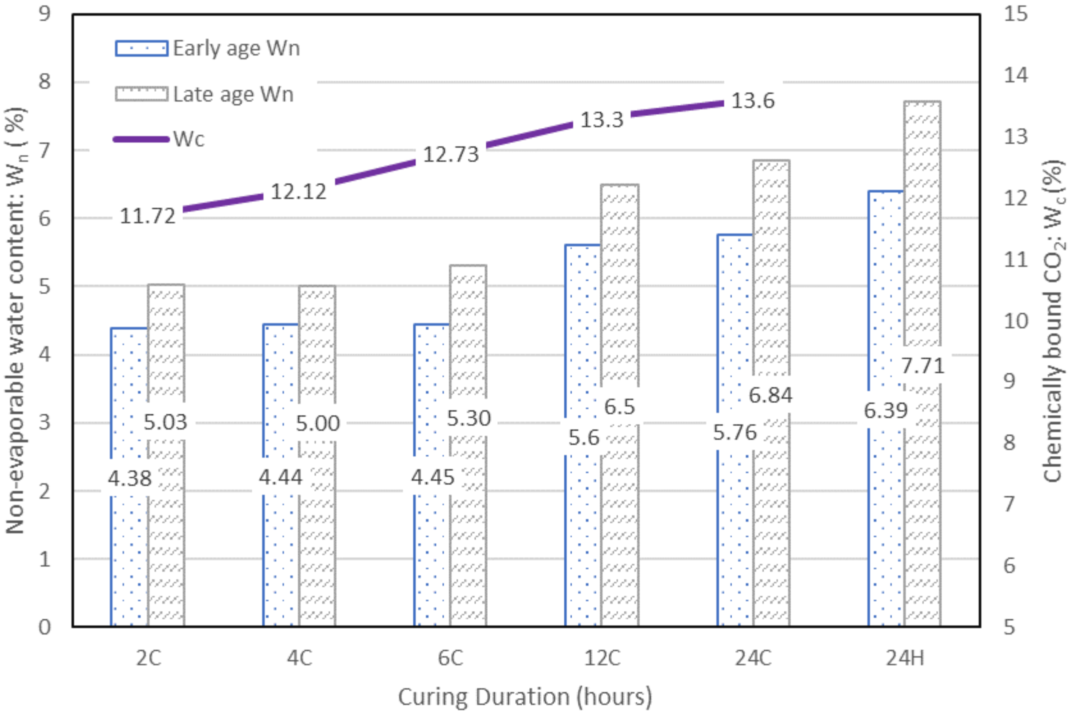

Figure 3-4 Variation of non-evaporable water content and chemically bound CO_2 in carbonated and hydrated steel slag from pyrolysis method.

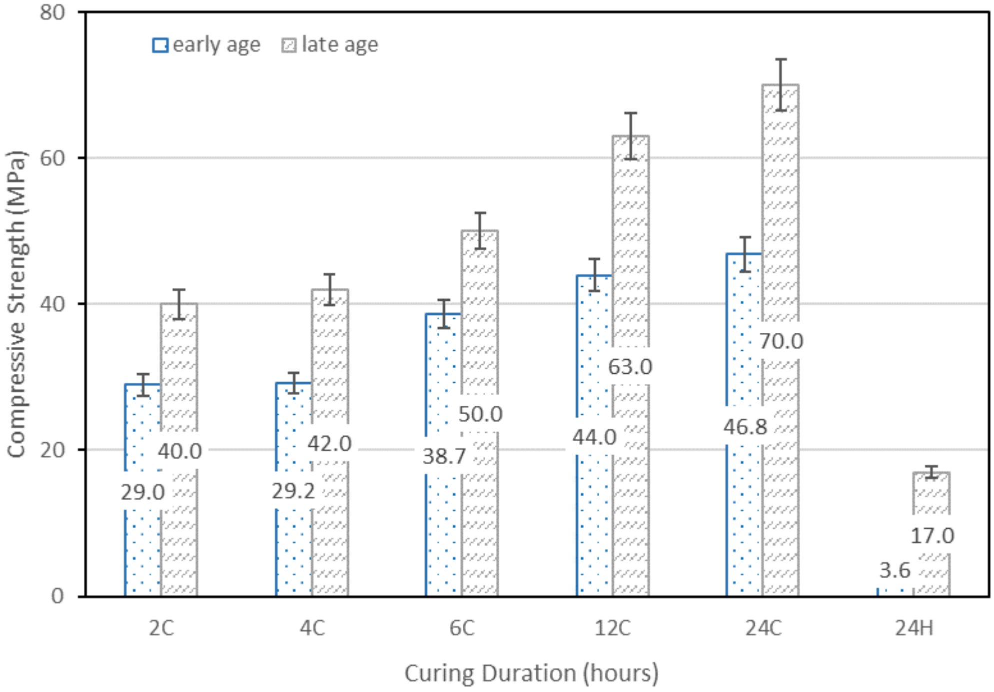

Figure 3-5 Evolution of Strength of steel slag compacts subjected to various curing durations.

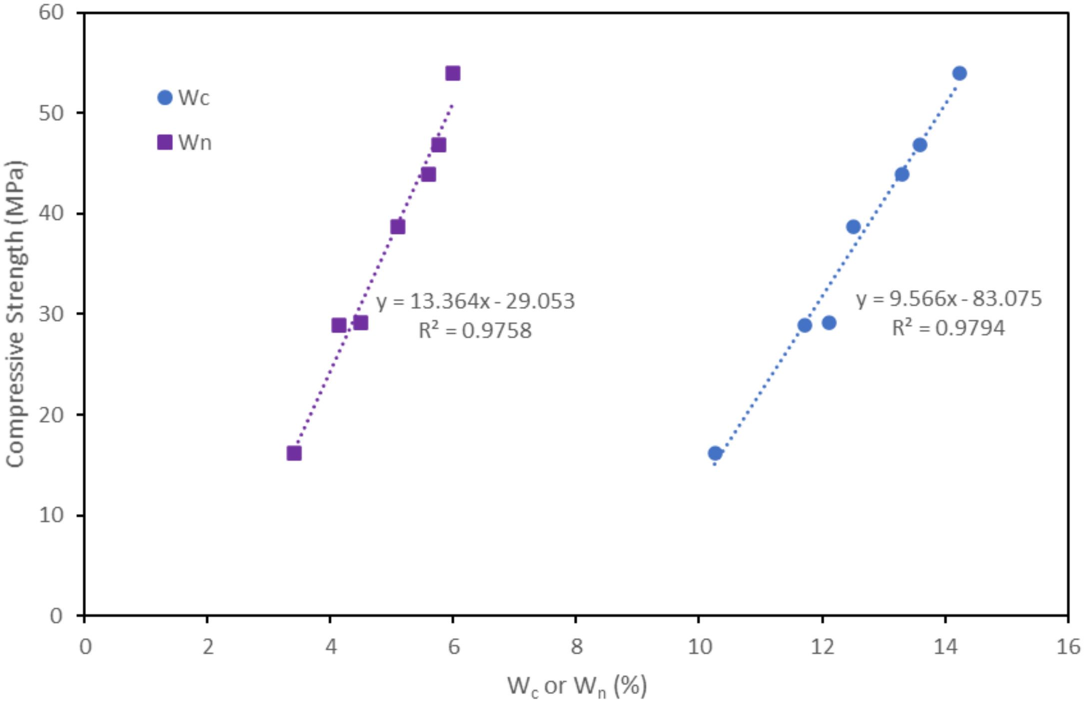

Figure 3-6 Correlation between compressive strength and non-evaporable water content (Wn) / chemically bound CO_2 (Wc).

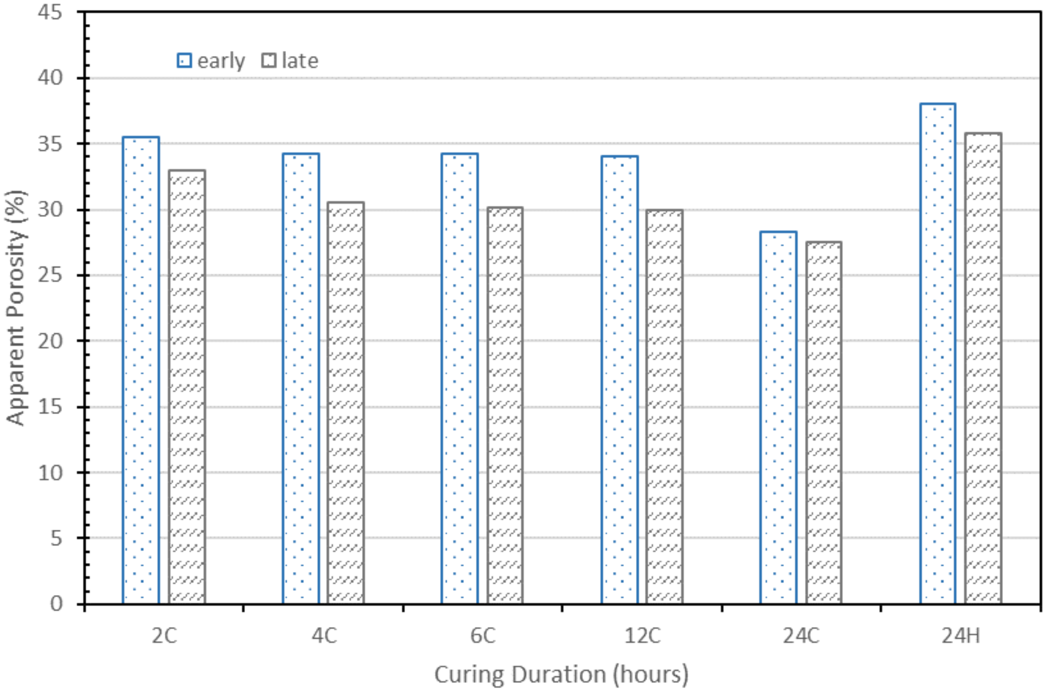

Figure 3-7 Apparent porosity of carbonated and hydrated steel slag compacts.

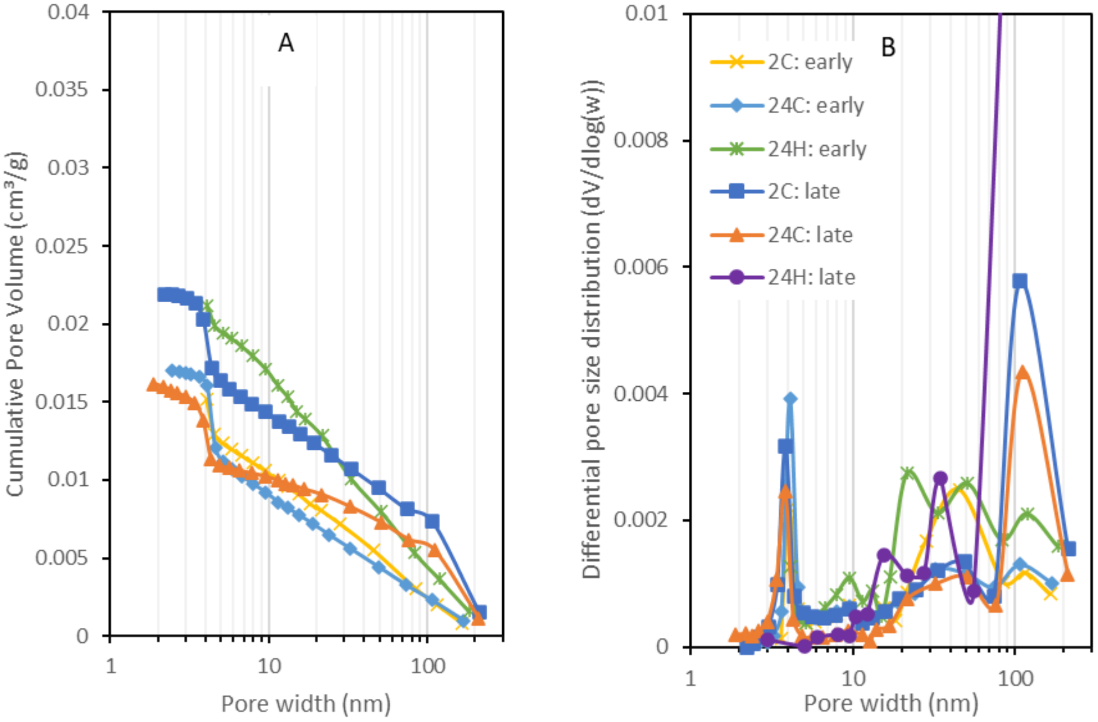

Figure 3-8 NAD results of carbonated and hydrated steel slag compacts: (A) Cumulative pore size distribution, (B) Differential pore size distribution.

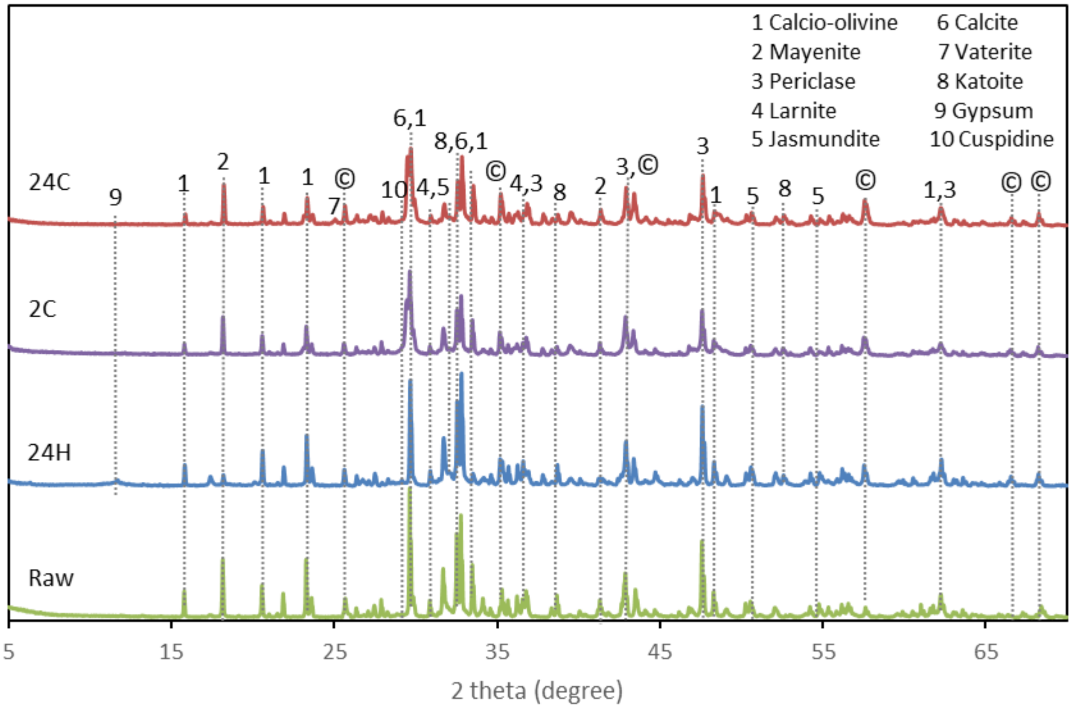

Figure 3-9 X-ray diffractograms of raw and carbonated slag at early age (© represents the internal standard corundum).

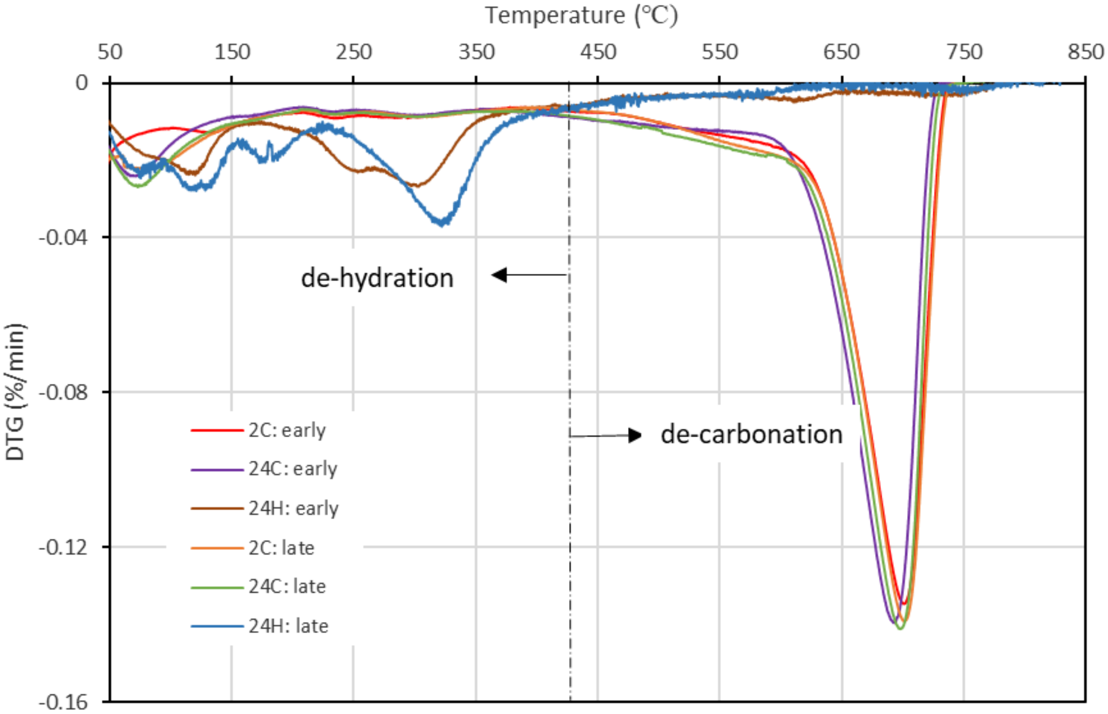

Figure 3-10 Thermal analysis of steel slag compacts subjected to different curing scenarios.

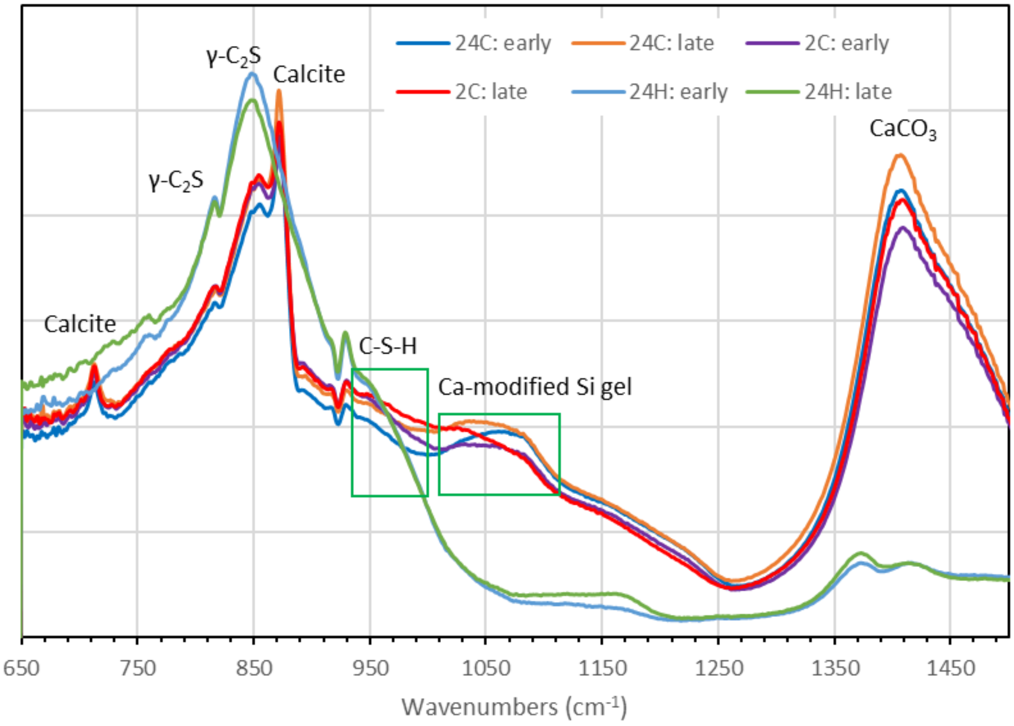

Figure 3-11 FTIR spectra of steel slag compacts subjected to various curing scenarios.

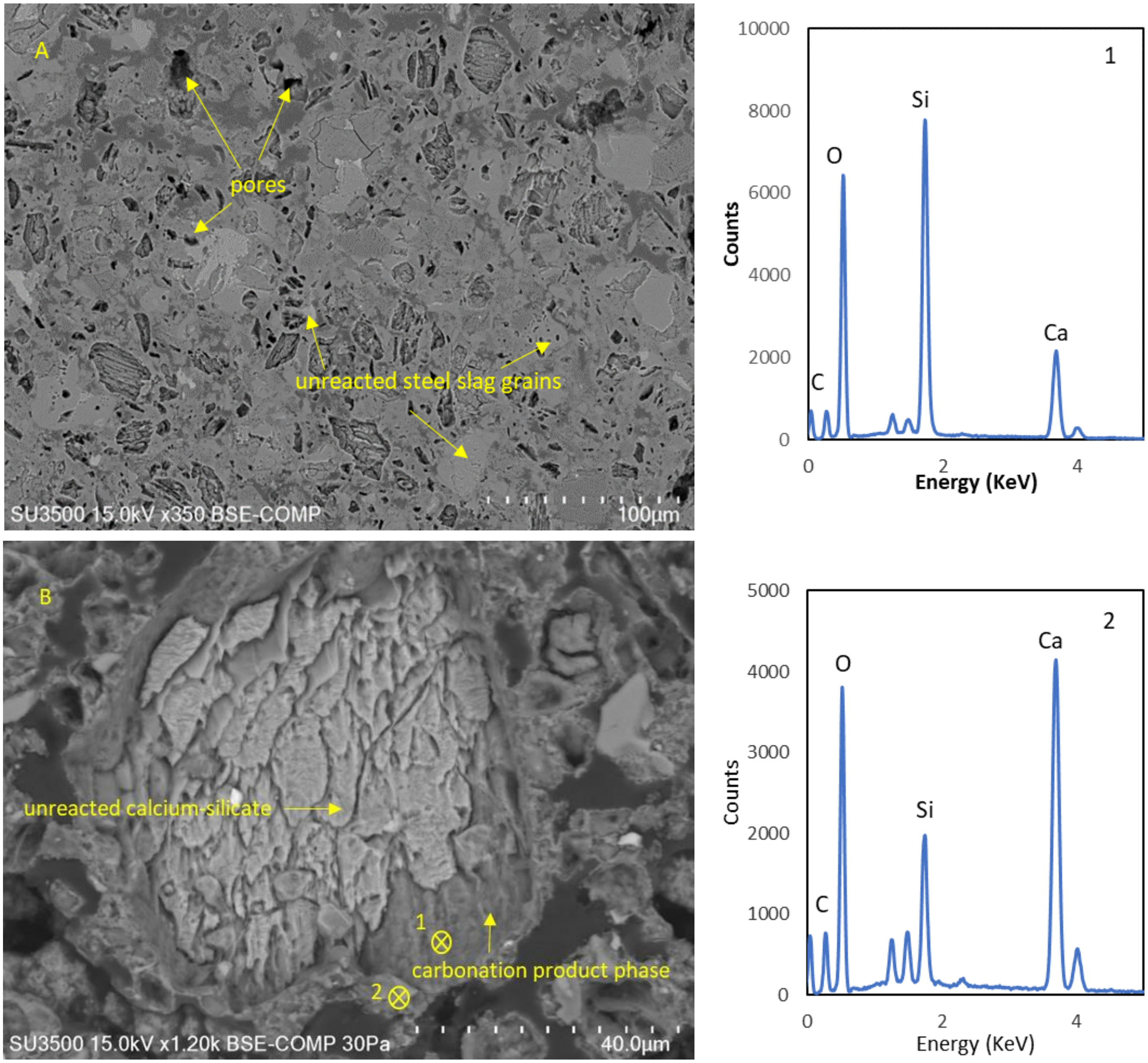

Figure 3-12 Typical SEM-BSE micrographs of 24-hour carbonated samples after 28 days of hydration: (A) higher magnification, (B) lower magnification

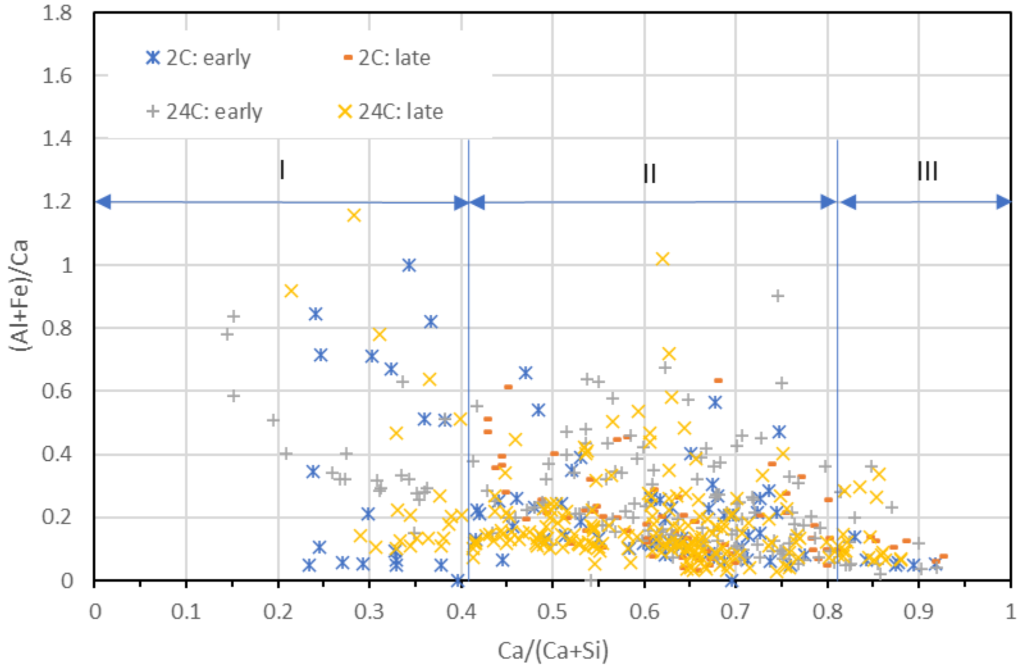

Figure 3-13 Atomic ratio distribution of (Al + Fe)/Ca as a function of Ca/(Ca + Si), where: I: Ca-modified silica gel, II: composite phase (gel phases + $CaCO_3$), III: $CaCO_3$.

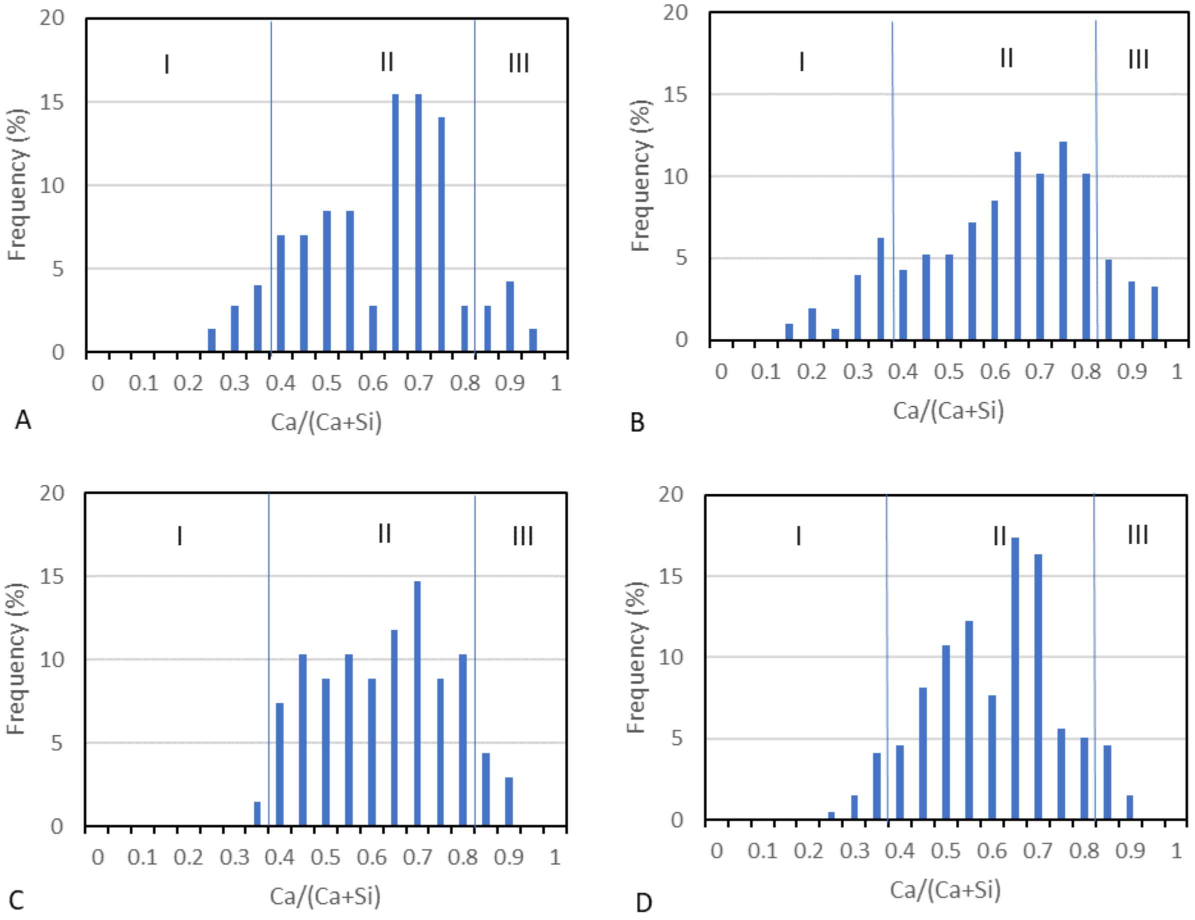

Figure 3-14 Frequency distribution of the Ca/(Ca + Si) atomic ratio of carbonation reaction products of steel slag (bin size 0.05) in (A) 2-hour carbonated only sample, (B) 24-hour carbonated only sample, (C) 2-hour carbonated sample followed by 28 days of hydration; (D) 24-hour carbonated sample followed by 28 days of hydration, where: I: Ca-modified silica gel, II: composite phase (gel phases +$CaCO_3$), III: $CaCO_3$.

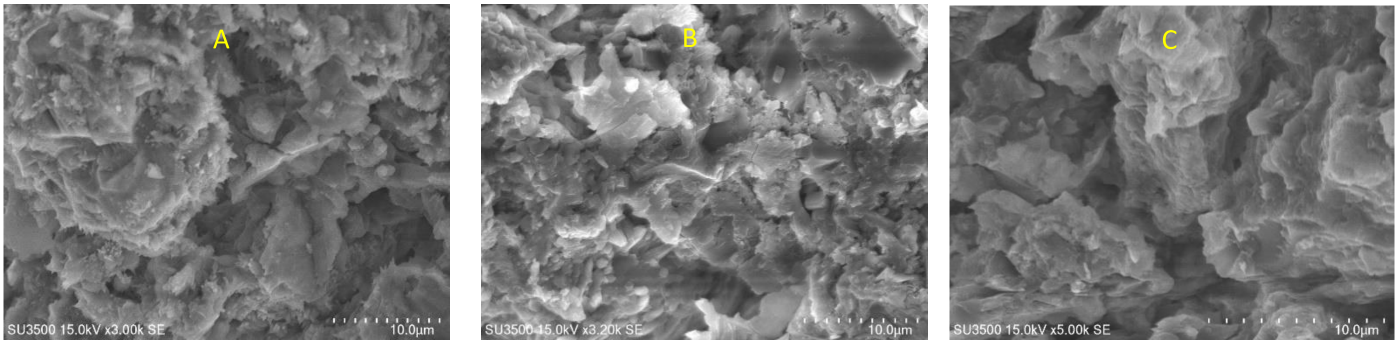

Figure 3-15 Morphological evolution featuring: (A) 2-hour carbonated sample, (B) 24-hour carbonated sample, (C) 24-hour carbonated sample followed by 28 days of hydration.

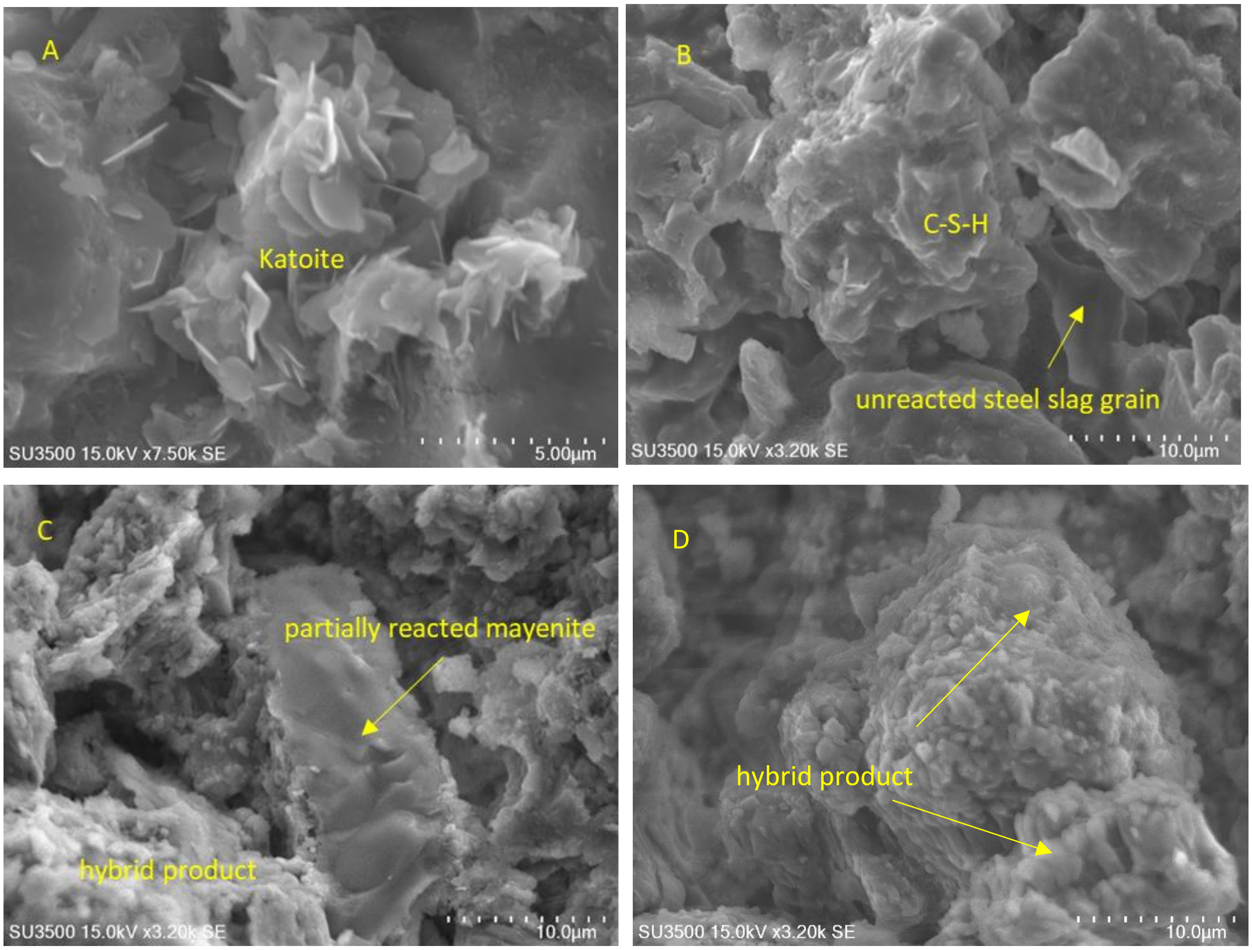

Figure 3-16 Micrographs of samples at 28 days of hydration: (A) and (B) with no prior carbonation, (C) and (D) with 24-hour carbonation prior to hydration.

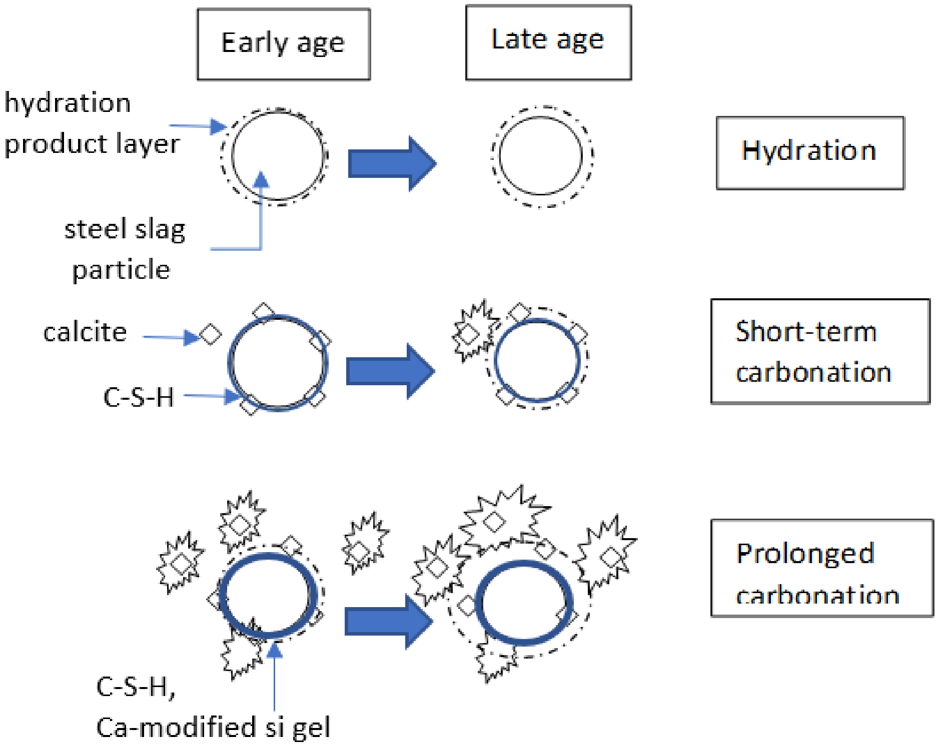

Figure 3-17 Proposed schematic illustration of microstructural evolution in steel slag paste subjected to different curing scenarios.

4. Chapter 4 Steel Slag-Bonded Strand Board as a Carbon-Negative Building Product

Preface

In Chapter 3, the characteristics of steel slag as a sole binder were studied and reaction products identified. It was found that prolonged carbonation curing promoted higher strength in steel slag paste which was attributed to the formed calcium carbonates acting as seeds to promote subsequent hydration. Based on the findings of Chapter 3, the feasibility of using carbonation-activated steel slag as the exclusive binder for the production of slag-bonded strand boards was studied in an attempt to replace cement-bonded fiberboards and resin-bonded strand boards. After a 12-hour carbonation, the developed slag-bonded strand board displayed excellent compatibility and enhanced performance owing to the slag chemistry. Carbonated boards successfully met international standard requirements for mechanical strength and physical performance. Durability of the composite was examined through accelerated ageing by warm water test and soak-dry cycles. Microstructure development was monitored through X-ray diffraction (XRD), thermogravimetric analysis (TGA), Fourier transform infrared spectroscopy (FTIR) and scanning electron microscopy (SEM). The study demonstrated that carbonation curing successfully reduced the production time, activated the dormant γ-C_2S, contributed towards superior dimensional stability, and sequestered almost 10.8 % of CO_2 by dry slag mass. A further 28 days of hydration improved the mechanical characteristics of the composite and contributed towards a superior end-product. It was found that slag-bonded strand boards are resistant to ageing owing to carbonation-induced precipitation and are carbon-negative with higher carbon storage capacity and lower production cost.

4.1. Introduction

Steel slag is the by-product of the steel making process. With an estimated worldwide production of 1.8 billion tons of steel, approximately 130-200 million tons of steel slag is produced annually [1]. Steel slag is a calcium silicate-rich material with latent hydraulic but no pozzolanic activity [2]. The weak hydraulic activity is mainly attributed to the amorphous nature of its SiO_2 content [3]. Furthermore, steel slag is rich in free CaO/MgO phases which, upon its addition to other building materials, can cause expansion and volume instability[4]. These drawbacks de-valued steel slag and limited its application as a binder. However, research has shown that carbonation curing can activate this material's early strength, giving rise to a binder with great benefits [2, 3, 5]. Carbonation curing consumes free lime content thus mitigating the expansion problem [6]. Furthermore, during the curing process, CO_2 reacts with the calcium silicate phases in steel slag to form thermodynamically stable calcium carbonate ($CaCO_3$) crystals and calcium silicate hydrate (C-S-H) [2, 7, 8]. The principal reaction is given in Eq (1) [9].

$$2(2CaO \cdot SiO_2) + (2\text{-}x)\ CO2 + yH_2O \rightarrow xCaO \cdot SiO_2 \cdot yH_2O + (2\text{-}x)\ CaCO_3 \qquad (1)$$

The carbonation mechanism depends on the diffusion/permeation of CO_2 through the solid where CO_2 is dissolved in the pore spaces then hydrated to form carbonic acid (H_2CO_3). The carbonic acid subsequently ionizes to H^+, HCO_3^- and CO_3^{2-} which causes the pH to typically drop by 3 units. This is followed by a nucleation of C-S-H and the precipitation of $CaCO_3$ [9, 10]. A study on KOBM (Klockner Oxygen Blown Maxhutte) steel slag carbonation has shown that a compressive strength of 109 MPa could be achieved after 2 hours of carbonation curing followed by 28 days of hydration, thus surpassing the OPC (Ordinary Portland Cement) industry standard [5].

This chapter proposes the use of steel slag as sole binder to develop a carbon-negative building product through carbonation activation. Wood cement composites are a good target for this application since they are widely used in construction and are comprised of a relatively high cement to wood ratio.

The use of wood as reinforcement within a cementitious matrix is particularly attractive since wood is renewable, non-toxic, and biodegradable, thus contributing towards a sustainable production. Unlike commonly used reinforcement in cementitious matrices, the biodegradable aspect of wood renders the wood production process waste free. Among the commonly used composites are cement-bonded particle boards, wood-fiber cement boards, wood-strand cement board and wood-wool cement boards (also called Excelsior board). Wood strands are also used in making oriented strand board (OSB) using a resin adhesive as binder. Whereas each board has its own characteristics and applications, the wood strand cement board is unique because, despite its medium density, it possesses high strength [11]. The high strength is attributed to the interlayered structure of the board which promotes inter-particle contact and ultimately improves the adhesive bonding of the strands [12]. Applications of this board include but are not limited to flooring, tile backing, roofing, permanent shuttering, exterior and partition walls, and acoustic and thermal insulation.

Wood-cement composites (WCC) have some drawbacks namely dimensional stability, low wood-cement compatibility and long term degradation of wood fibers in the alkaline environment of cement [13]. The growth of hydration products, namely $Ca(OH)_2$, around the lignocellulosic material is one of the leading causes of embrittlement and degradation [14, 15]. According to Filho et al. early CO_2 curing improves the durability of fiber cement composites to ageing because carbonation consumes $Ca(OH)_2$ and reduces pH [14]. However, the long-term durability remains questionable since the subsequent hydration of Portland cement, following the carbonation curing, re-alkalizes the medium and subjects the wood to alkali-degradation. Other mitigation techniques include the addition of supplementary cementitious materials to the mix, whose addition contributes towards the reduction of $Ca(OH)_2$. In this light, Wei. et al, explored the effect of the addition of 30 % metakaolin to the wood-cement matrix on the degradation and concluded that the addition of metakaolin reduced the $Ca(OH)_2$ content and decreased the pH of the matrix which effectively improved the longevity of the composite and lessened the deterioration [15]. However, research on replacing the hydraulic binder by a weakly-hydraulic one, namely steel slag, has not been investigated before.

This chapter is to explore the feasibility of using the weakly hydraulic steel slag as an exclusive binder in making slag-bonded strand boards via carbonation curing to achieve enhanced mechanical and physical properties. The adopted binder and curing conditions were jointly investigated to develop a board that combines excellent performance with carbon negativity, carbon storage capacity and relatively low cost.

4.2 Experimental program

4.2.1 Materials

The steel slag was sourced from Harsco Environmental Quebec, Canada. It was identified as a ladle slag, a by-product of the steel refining process. Its mineralogy is dependent on the appended fluxes, deoxidizing agents, and cooling process. The as-received slag contained clumps that were first sieved out using an 850-µm sieve. The powder passing through the sieve was pulverized to a finer powder using a ring-and-puck mill (60 s per half-kilogram slag) to ensure homogeneity. Only slag powder that passed through a 150-µm sieve was used in this study. The major oxide components of the slag were identified by X-ray fluorescence (XRF) and are presented in Table 4-1. The mineralogical phases were determined by X-ray diffraction (XRD) and are presented in Fig. 4-1.

Poplar strands were selected for this study. Poplar trees have appealing physical characteristics for a variety of industrial applications such as board production as well as pulp and paper [16]. These trees grow fast and are moisture-loving making it easier to cut strands, as the wood does not require steaming which is ideal for OSB production. Poplar species are also known for their low densities which promote a good bond when manufacturing a composite because pressing will force the strands into close contact and thus yield a medium density-board with improved properties[17]. Table 4-2 summarizes the characteristics of the poplar strands used. The as-received strands were chopped down to a length of 5 to 10 cm to facilitate forming into lab-scale boards.

4.2.2 Production and curing process

Table 4-3 summarizes the laboratory production parameters while the production process of slag-bond strand board (SBSB) is illustrated in Fig. 4-2. Almost 30 % of the total mix water were used to prewet the chopped poplar strands prior to mixing. The strands were then hand-mixed with steel slag and the remaining mix water for 10 min. Subsequently, the mix was placed into a 127 x 76 mm steel mold and evenly distributed to ensure a consistent density. The combined prewetting, mixing and forming process took less than 30 min. The mat was compact formed to a thickness of 12 mm using a vibrating hammer and then left under a pressure of 10 KPa for 3 hours to avoid spring back of strands. After pressing, the board samples were demolded and trimmed to remove any out-of-plane strands. The boards were then subjected to three distinct curing scenarios to obtain: carbonated boards, combined carbonated-hydrated boards and hydrated-only boards.

For carbonated boards, the trimmed boards were transferred to a pressure chamber for carbonation curing which was conducted under ambient temperature conditions (25 ± 2 °C). The experimental apparatus used is presented in Fig. 4-3. In the chamber, the samples were subjected to 12 hours of pure CO_2 gas at a pressure of 150 KPa. The regulator assured that the pressure was maintained in the chamber such that CO_2 was continuously replenished to counter the pressure drop arising from the reaction. The carbonation duration was selected to represent overnight curing if implemented at an industrial scale.

Half of the produced boards, referred to as SBSB-12C, were tested immediately to evaluate the properties of the carbonated-only boards. The remaining half, referred to as SBSB-12C28dH, were transferred to airtight plastic bags for subsequent hydration curing for 28 days at 25 ± 2 °C. Subsequent hydration was employed to maximize strength gain. Fig. 4-4 shows the materials used and the produced SBSB.

Hydrated boards, referred to as SBSB-28dH, were placed in air-tight plastic bags, immediately after demolding, for 28 days of sealed curing at 24 ± 2 °C. These boards served as reference and aimed at highlighting the effect of carbonation curing on the properties of produced boards.

4.2.3 CO_2 uptake

CO_2 uptake was assessed on the basis of the mass gain method. The formula used for the calculation is provided in Eq 1. Due to the exothermic nature of carbonation reaction, water was condensed on the internal walls of the carbonation chamber. This water was recovered by an absorbent paper and referred to as mass of collected water. Since not all vaporized water can be collected, values obtained by the mass gain method represent a conservative estimate.

$$CO_2\ \text{Uptake}\ (\%) = (mass_{\text{carbonated specimen}} + mass_{\text{collected water}} - mass_{\text{initial specimen}}) / (mass_{\text{slag powder}}) \qquad (1)$$

4.2.4 Mechanical performance

Modulus of rupture (MOR) or flexural strength tests were performed as per ASTM D-1037 (2012). A three-point bending test was carried out over a span of 101 mm using an MTS-

SINTECH 30/G tension and compression tester equipped with a 75 KN load cell. Tests were performed following dry conditioning. A minimum of 5 specimens were tested and results averaged for each curing condition to obtain reproducible and representative results.

Screw holding power (SHP) was determined on boards following ASTM D-1037 (2012) requirements using an MTS-SINTECH 30/G equipped with a 75 KN load cell at a testing rate of 1.5 mm/min. Screws of nominal diameter 3.4 mm were threaded through the boards and the pullout tensile force was recorded. The screw holding power of the board represents the withdrawal resistance of screws and is presented as the maximum pullout force divided by the depth of penetration in N/mm where the depth is the thickness of the board. For all durability tests listed in the sections below, anti-rust screws were embedded prior to the start of aging cycles as per the ASTM recommendations.

4.2.5 Physical performance

Water absorption and thickness swelling tests were performed as per ASTM D-1037 (2012) requirements to evaluate the dimensional stability of the composites. Boards of various curing ages were submerged in water at 20 ± 1 °C for 24 hours. After submersion, the boards were withdrawn from water and left to drain in air for 10 ± 2 min before excess surface water was dabbed with a paper towel. Water absorption values are reported as the percentage increase in weight based on the weight after conditioning. Thickness swelling of boards is expressed as percentage of conditioned thickness.

4.2.6 Warm water test

The purpose of the warm water test is to accelerate the chemical reactions (ageing) between the constituents of this newly developed board. Specimens were immersed in water saturated with excess lime and maintained at 60 ± 2 °C for 56 ± 2 days. Performance evaluation is based on the relative changes of the mechanical, physical, and microstructural properties/characteristics of the boards before and after the accelerated ageing process following dry conditioning. A total of fifteen specimens were cast: 5 specimens were tested at the end of the 28-day curing regime and served as reference, and10 specimens were subjected to accelerated ageing as per ASTM C-1185.

4.2.7 Soak-dry test

The soak-dry test followed the recommendation of BS-EN 494 (2012). Ten boards were subjected to 50 soak-dry cycles. Each cycle consisted of immersion in water at ambient temperature for 18 hours followed by drying in an oven at 60 ℃ for 6 hours. These alternating ageing cycles endeavour to simulate the service life conditions of the boards if subjected to severe environmental conditions. Evaluation of board performance is carried out on a comparative basis, where mechanical, physical, and microstructural performance of aged boards following dry conditioning were compared to unaged boards following 28 days of curing.

4.2.8 pH evaluations

The elevated alkalinity of pore solutions is known to be the main cause of degradation in wood-cement composites. The pH of composite pore solutions was evaluated by suspending 0.5 g of sieved (< 100 μm) slag powder in 10 ml of distilled water for 2 min according to the protocol described in [18]. The pH of the suspensions was measured at 25°C ± 2 ℃ with a EXTECH PH110 pH meter calibrated against three NIST-traceable buffer solutions (pH 4.0, 7.0, 10.0). Measurements were carried out in triplicates.

4.2.9 Microstructural analysis

The as-received slag as well as the carbonated (SBSB-12C28dH) and hydrated boards (SBSB-28dH) were examined by X-ray diffraction (Cu Kα radiation, scan interval 10-65° 2θ, 0.01°, and 0.5 s per step) using a Philips PW 1710 Powder Diffractometer (Philips, Amsterdam, Netherlands) to document how the mineralogy of the raw slag was modified by the curing regimen and the ageing tests. This information provided insights into the chemical reactions that led to the development of this innovative composite.

The thermogravimetric analysis (TG) allows the identification of constituent phases, including amorphous phases not detected by XRD, as each phase is characterized by a specific range of decomposition temperatures. To identify decomposition temperature ranges, differential thermogravimetric (DTG) curves were consulted. A thermal analyzer TG-Q500 with a resolution of 0.01 mg was used to obtain TG/DTG curves over the range 30-975 °C at a heating rate of 10 °C/min. All analyses were carried out in a nitrogen atmosphere.

To identify the functional groups within amorphous and crystalline phases of the steel slag, Fourier transform infrared spectroscopy (FTIR) analyses were performed with a Nicolet 6700 FTIR spectrometer coupled with a Smart iTR module (FTIR-ATR). Spectra were recorded over the range of 4000 to 650 cm^{-1}.

For all microstructural examinations, the powder slag was obtained from the center of the fractured surface after MOR testing following the procedure recommended by Mohr et al. [19].

4.2.10 Morphological and reaction product characterization

The morphology and microstructure of carbonated (SBSB-12C28dH) and hydrated boards (SBSB-28dH) were examined using a Hitachi SU3500 scanning electron microscope (SEM). Samples were obtained from fractured surfaces including wood strands and steel slag. A dispersive X-ray (EDX) detector was coupled to SEM for elemental analysis. All samples were sputter coated with a thin layer of gold prior to observation.

4.3. Results and discussion

4.3.1. Influence of water-to-slag ratio on fabrication of slag-bonded strand board

Fig. 4-5 reports the MOR recorded in hydrated and carbonated boards manufactured with varying water-to-slag ratios (w/s). Hydrated-only boards manufactured with varying w/s ratios after 28 days of sealed curing had very low strengths which fluctuated minimally around 2.5 MPa. The MOR of carbonated-only samples increased gradually with increasing w/s ratio until it peaked at a value of 0.35 after which MOR decreased. The ultimate MOR recorded was 9.7 MPa, nearly 4 times higher than that recorded for the 28-day sealed hydration reference boards, surpassing the ISO 8335 (1987) standard strength requirement of 9 MPa. MOR reflects the combined action of steel slag and wood strands, as the binder is responsible for bond stress and the wood provides tensile stress. The distribution of these stresses, however, depends on the interconnection of the strands [20] which, in turn, depends on the adhesion capabilities of the binder. The obtained results showcased that the hydrated steel slag is a weak latent hydraulic material that failed to bind the wood strands and resulted in a poor composite whereas carbonation curing activated the strength of steel slag and yielded a strong matrix that successfully bonded the wood strands. The improved strength of the carbonated SBSB can be attributed to the CO_2 activation of calcio-olivine (γ-Ca_2SiO_4), the major constituent of slag (Fig. 4-1) and the mineral with no hydraulic activity. The exothermic carbonation reaction (consistent with the thermodynamic reaction delineated in eq. 1) sharply raised the temperature inside the carbonation chamber from ambient conditions to above 30 °C (Fig. 4-6) within the first hour of curing. Likewise, the relative humidity in the chamber rose from ambient conditions to above 70 % and was maintained for 1-2 hours reflecting the initial rapid water evaporation rate. Afterwards, the temperature and relative humidity curves decreased gradually reflecting a decelerated carbonation reaction.

The highest temperature was recorded (30.5 °C) in carbonated strand boards manufactured with 0.35 w/s ratio. Likewise, the highest CO_2 uptake potential (10.8 %) was recorded in these composites (Table 4-4). Water content is a critical factor in the carbonation of wood-slag composites. The hygroscopic behaviour of wood strands changes the effective water to slag ratio of the mix [21]. Consequently, CO_2 solvation and hydration might be affected. Thus, an optimum water-to-slag ratio is deemed crucial.

A subsequent 28-day sealed curing of the 12-hr carbonated strand boards led to significant increase in MOR (Fig. 4-5). All carbonated samples were capable of exceeding the standard strength requirement (9 MPa), which confirmed that hydration after carbonation played a significant role in reinforcing the strength of strand boards. The early carbonation did not hinder subsequent hydration and the final strength resulted from the combined contribution of carbonation and hydration. Since carbonation curing accounted to almost 70 % of the ultimate strength, the w/s ratio had more influence on the carbonation reaction than the subsequent hydration reaction. An ultimate strength of 14.2 MPa was recorded in samples prepared with w/s of 0.35. Therefore, 0.35 was considered as the optimal w/s ratio and was used to prepare the SBSB subjected to accelerated ageing tests.

Thickness swelling (TS) is a physical property that reflects the dimensional stability of boards and is key to a successful new composite. Thickness swelling in boards is divided into two components: swelling induced by the wood's hygroscopic nature and swelling due to the release of compression pressure after the pressing/clamping time [22]. The latter, however, is non-reversible when boards return to drier condition and is mostly referred to as "spring back"[22]. Results of thickness swelling in boards fabricated with different w/s ratios are shown in Fig. 4-7.

Thickness swelling in all carbonated boards varied marginally, indicating a lesser dependence on the w/s ratio. Results of carbonated boards with and without subsequent hydration were well below the 2 % limit specified by the ISO 8335 (1987). A further 28-day hydration of the carbonated-SBSB did not significantly improve their physical performance, implying that early carbonation curing was mostly responsible for their dimensional stability. Conversely, TS in hydrated boards seemed to increase with the increase of w/s ratio. Lower w/s ratios led to a more compact-formed composite and ultimately decreased swelling[23]. Hydrated slag boards fabricated with w/s ratios of 0.375 and 0.4 failed to meet the TS requirement. Hence, it could be inferred that the precipitation of thermodynamically stable calcium carbonates upon carbonation curing contributed towards the superior dimensional stability of the carbonated strand boards both with and without subsequent hydration. As carbonation is a surface densification process, it contributes to porosity reduction especially at the surface [5] and thus carbonation curing could create a less permeable barrier, preventing water seepage into the composite and promoting high dimensional stability. Compared to their hydrated-only counterparts, carbonated elements have a denser microstructure due to the embedment of $CaCO_3$ within the strength contributing to C-S-H [24]. The very low thickness swelling recorded in carbonated boards, as opposed to the very high value in hydrated-only boards, highlighted the ability of carbonation curing to limit the hygroscopicity of wood strands by effectively reducing the pore sizes.

4.3.2 Durability assessment: Mechanical and physical assessment before and after ageing

Durability of construction and building materials mirrors their behavior in service life. Durability studies were carried out to monitor the behavior of carbonated (SBSB-12C28dH) and hydrated (SBSB-28dH) SBSB after accelerated ageing cycles. Two tests were performed: a warm water (WW) test and a repeated soak-dry (SD) test. Fig. 4-8 summarizes the mechanical performance of the boards before and after the accelerated ageing. In general, accelerated ageing did not have significant adverse effects on the mechanical performance of the carbonated boards. The same, however, cannot be said about the hydrated-only boards.

Placing the boards in alkaline water at elevated temperatures (60 °C) promotes hydrolysis of major amorphous components in natural fibers, namely lignin and hemicellulose, and accelerates their degradation [15]. Hydrated-only boards failed the warm water test after 28 days of submersion, as they disintegrated into rubble and, consequently, no further tests could be performed. Conversely, the carbonated SBSB showed an insignificant drop in MOR and SHP (5 % and 15 %, respectively) after the warm water test. The SHP test was included in the durability assessment because it represents the holding strength of the boards and results are indirectly related to the internal bond (IB) strength of the composite.

After repeated soak-dry cycles, carbonated boards experienced an enhanced performance in MOR. Hydrated-only SBSBs experienced no change in MOR but a drop in SHP which implied a deterioration of the bond. Repeated soak-dry cycles allowed for a continuation of hydration reactions as well as weathering carbonation [25] in hydrated-only boards, as evidenced by the apparent change in color of the boards throughout the ageing cycles. However, this was not proportionally reflected in their performance, as was the case for carbonated boards, because the acquired strength with ageing was built on a weak foundation. Before ageing, the low hydraulic activity of steel slag affected the bond-ability between wood strands and thus the boards displayed many macrocracks mirroring the poor adhesion even after prolonged pressing. Even though ageing of the hydrated-only boards allowed for a continuation of the curing process, the weak initial state of the board limited gain in mechanical performance.

The SHP performance of carbonated boards showed no apparent change after ageing whereas the SHP of hydrated-only boards decreased. Hence, carbonation curing of steel slag led to a strong internal bonding that was not affected by accelerated ageing. In contrast, hydrated-only boards displayed weak bonding from the start and, consequently, when subjected to the harsh conditions of the repeated soak-dry test, the strands experienced petrification and the bond further deteriorated.

Water absorption (WA) and thickness swelling (TS) tests were carried out as further means of evaluating the durability of the composites. Physical performance of carbonated and hydrated-only boards before and after ageing tests are shown in Fig. 4-9. In general, upon ageing, TS improved for all boards, but the WA performance decreased slightly. The small increase in water absorption after ageing could be a sign of the development of internal microcracks induced by the cyclic swelling and drying of wood strands inflicted by the accelerated ageing test. Similarly, Wang et al. reported the presence of microcracks in magnesium oxysulfate cement incorporating rice husk ash after wetting/drying cycles due to the water swelling and drying shrinkage [26]. Nonetheless, the WA values recorded after ageing of the carbonated boards were significantly less than the absorption limits specified by international standards (25 % at 24 hours) and may be ascribed to carbonation curing which effectively limited the amount of water that could be absorbed by the boards. In contrast to hydrated-only boards, early carbonation curing seems to lend the composite a higher resistance towards ageing effects.

4.3.3 Microstructural assessment before and after ageing

Fig. 4-10A shows the X-ray diffractograms of the raw slag as well as the carbonated (SBSB-12C28dH) and hydrated-only (SBSB-28dH) boards. The mineralogy resulting from the distinct curing regimes explained much of the differential mechanical performance of the boards. The raw slag was rich in calcium silicate phases with the calcio-olivine (γ-Ca_2SiO_4) being the most abundant phase, whereas larnite (β-Ca_2SiO_4) and jasmundite ($Ca_{10.5}Mg_{0.5}Si_4SO_{18}$) were present at lower concentrations. The raw slag also contained the aluminate-bearing mineral mayenite ($Ca_{5.65}Al_7O_{16.15}$) and periclase (MgO).

The distinctive feature arising in hydrated-only boards was the appearance of new peaks of katoite ($Ca_3AL_{2.85}O_{2.55}(OH)_{9.45}$), reflecting the hydration reaction of mayenite. In addition, a decrease in the larnite peaks was detected in both carbonated and hydrated boards reflecting the hydraulic potential of this mineral. The XRD spectra revealed almost no drop in calcio-olivine peaks (2 theta of 29.5° and 33°) upon hydration in hydrated-only boards whereas a clear drop was recorded in carbonated SBSB. Calcio-olivine is known to have no hydraulic properties, but carbonation curing valorizes this mineral and allows for the formation of a C-S-H like gel and calcium carbonate ($CaCO_3$) [9, 27], as expressed in equation 1. It is believed that the low pH medium induced by carbonation of steel slag drives this activation of strength [5, 7]. Thus, distinctive peaks attributed to the presence of calcium carbonate in the carbonated boards reflected that calcium silicates reacted with CO_2 in the presence of water to form calcium carbonate, as confirmed by the pore solution pH measurements. After 28 days of subsequent hydration, the pH increased from 9.8 to 11.42 but remained below value in the hydrated-only boards (11.65). It should be noted that the pH recorded in the carbonated SBSB is much lower than those reported in other studies that employed cement as binder and for which values were higher than 13, owing primarily to the $Ca(OH)_2$ content [13, 15]. Accordingly, steel slag may provide a low alkaline medium suitable for the long-term preservation of wood. This was backed up by the revelation that no peaks attributed to $Ca\ (OH)_2$ were detected in the boards carbonated and/or hydrated.

Fig. 4-10B shows the XRD patterns of carbonated and hydrated-only SBSB after the warm water (WW) test and soak-dry (SD) cycles. The WW test led to the formation of new peaks in the carbonated SBSB. Mayenite peaks (2 theta of 17 °, Fig. 4-10B) disappeared while katoite peaks, evidence of mayenite hydration, appeared. A sharp decrease in the intensity of the periclase (MgO) peak was also observed. Hydration of MgO is expansive, because the molar volume of $Mg(OH)_2$ is almost twice that of MgO[23]. This reaction, however, had little effect on the performance of carbonated boards since carbonation provided an encasing protection to the composite. Carbonated boards still contained unreacted slag minerals which, under the elevated temperature of the WW test, underwent continued hydration. The same could be projected onto the hydrated-only boards to explain why the hydrated boards failed the test. Hydrated-only SBSB comprised a large portion of un-reacted slag which, upon further WW hydration, promoted expansive reactions (namely the conversion of MgO to $Mg(OH)_2$) which accelerated the alkaline attack on the wood strands and caused the composite to fail.

SD cycles had a less significant effect on the mineralogy of carbonated SBSBs than on the hydrated-only SBSB. In general, both boards experienced an increase in $CaCO_3$ content, but the increase was much more pronounced in the hydrated-only boards (calcium carbonate peaks at 2 theta 36° and 39.5°: Fig. 4-10B). Weathering (adventitious CO_2 uptake from the atmosphere) carbonation during the soak-dry cycles was substantial in hydrated-only boards owing to their high percentage of unreacted slag minerals on one hand and the presence of macrocracks, induced by the poor adhesion between strands and steel slag, which allow for the penetration of atmospheric gases, notably CO_2, within their structure on the other. Weathering carbonation induced by the SD cycles in hydrated-only boards led to petrification of wood strands which was evidently reflected in the drop in SHP performance and the unrestored strength. XRD patterns of boards subjected to both tests showed no Ca $(OH)_2$ clearly.

Fig. 4-11A depicts the TG and DTG weight loss curves of the composites after 28 days of hydration with and without carbonation curing. Endothermic events can be identified in the two main zones of decomposition in hydrated and in carbonated composites. The DTG curves showed distinct weight loss steps at 100 °C attributed to free water, at 150 and 380 °C related to C-S-H, C-A-H and katoite respectively and at 680 °C due to decomposition of calcium carbonates. Similar results were reported by other studies on ladle slag carbonation and hydration [28, 29]. The most prominent DTG peak corresponds to the decomposition of $CaCO_3$. This peak was obviously accompanied by a higher mass loss in carbonated boards than hydrated-only boards. The decarbonation detected in hydrated-only boards is attributed to carbonation by ambient air during mixing and curing. It is interesting to note the difference in decomposition temperature of the $CaCO_3$ in the carbonated and in hydrated-only boards. The decomposition temperature reflects a difference in mineralogy or crystallinity of formed $CaCO_3$ which is affected by many factors such as the carbonation pressure and pH to name a few [30]. It is also noteworthy that the unaged hydrated-only boards recorded the highest water loss (Table 4-5) whereas their mechanical performance (MOR, SHP) was 3-4 times less than the unaged carbonated boards (SBSB-12C28dH). This suggests that $CaCO_3$ plays a major role in strengthening the amorphous C-S-H and C-A-H and ultimately contributes towards improved mechanical properties in carbonated boards [2]. Likewise, Bukowski and Berger reported that $CaCO_3$ crystals contribute towards the formation of a strong bonded matrix in calcium silicate systems [31].

Thermal decomposition of $Ca(OH)_2$ occurred between 380 and 430 °C [5]. Ca $(OH)_2$ was only present in trace amounts in both carbonated and hydrated boards, evidence of the poor hydraulic property of the raw slag. According to Mohr et al.[19], the presence of portlandite initiates the degradation of pulp during wetting/drying cycles of fiber-cement composites. Therefore, minimizing the amount of Ca $(OH)_2$ initially present, by using weakly hydraulic steel slag, promotes wood preservation and minimizes or eliminates long-term embrittlement.

Fig. 4-11B shows typical TG-DTG curves of the carbonated and hydrated-only boards after ageing cycles. In general, results of the TG analyses mirrored those of the XRD. Table 4-5 summarizes the estimated percentages of reaction products of carbonated and hydrated-only boards, as derived from the TG curves as well as estimated percentages of Ca $(OH)_2$ and $CaCO_3$ based on stoichiometric calculations. The WW test led to an increase in hydration products in carbonated boards but did not significantly affect the $CaCO_3$ content. This increased abundance of hydration products did not significantly affect the performance of the carbonated SBSB, as revealed by the mechanical and physical assessment of SBSB-12C28dH after ageing. Even after being subjected to this harsh ageing test, the properties of the carbonated boards surpassed standard requirements.

SD cycles led to weathering carbonation of the hydrated-only and carbonated boards but weathering carbonation in carbonated boards was much less. Carbonation curing seemed to lend the composite a high resistance to weathering carbonation and ageing. This was also observed in a study performed on CO_2-cured concrete where it was inferred that carbonation curing could effectively slow-down the weathering carbonation rate [32].

FTIR analyses were performed to further characterize the reaction products including the amorphous and crystalline phases of the carbonated and hydrated SBSB as well as the changes inflicted by the SD ageing test. The spectra are presented in Fig. 4-12. The peaks occurring at 711, 871, 1408 cm^{-1}, corresponding to the stretching vibration of C-O[33, 34] were evidence of carbonate formation by carbonation curing. These peaks were much stronger in carbonated boards compared to hydrated-only boards, in agreement with the results by TG and XRD. The prominent peak at 848 cm^{-1} in hydrated-only boards was associated with calcio-olivine [34]. A broad hump was observed between 3000-3650 cm^{-1} attributed to the stretching vibration of O-H in amorphous C-S-H [35]. The intensity of O-H bond absorption band was higher in SBSB-28dH, indicating more hydration products were formed in hydrated-only boards, in agreement with the results the by TG analyses. Furthermore, the broad peaks with maxima between 929 and 1050 cm^{-1} could be attributed to the Si-O bonding in C-S-H gel [36]. The very weak peak at 3645 cm^{-1} detected in hydrated-only SBSB was possibly attributed to the O-H bond in some hydration products such as calcium hydroxide [33]. As calcium hydroxide was not detected by the XRD results. Therefore, it might come from other hydrates.

The SD test led to an increase in carbonate formation in carbonated and hydrated SBSB as clearly evident by the intensity increase in the peaks corresponding to the stretching vibration of C-O. Also, an increase in intensity and wavenumber was observed in the broad peak attributed to stretching vibration of Si-O after ageing in hydrated-only boards, indicating an increased degree of polymerization of the silicate compound [36]. The degree of silicate polymerization of C-S-H gel is dependent on the Ca/Si ratio of the calcium-silica gel. These observations indicated the occurrence of weathering carbonation in both carbonated and hydrated SBSB, but the shifts in spectra revealed a higher susceptibility to weathering carbonation in hydrated-only SBSB.

pH measurements of pore solutions in the composite at the end of the ageing tests back-up these findings (Table 4-6). pH values dropped in both boards subjected to SD, but the drop was more prominent in hydrated-only boards. This further demonstrated the ability of carbonation curing in steel slag to develop a stable and durable composite. Moreover, the pH recorded after WW test, which, according to results of the TG and XRD analyses, accelerated the hydration reaction of steel slag minerals, was 11.86. This further reinforced the observation that the carbonated steel slag provided a low alkaline medium suitable for long-term durability of the composite.

4.3.4 Morphological assessment and reaction product characterization

The photomicrographs of SBSB-12C28dH and SBSB-28dH are shown in Fig. 4-13(A and B) respectively. The carbonated boards were characterized by a fine dense matrix whereas hydrated only samples displayed a coarse and highly porous matrix. It was obvious from Fig. 4-13A that slag particles adhered well to the strand surface whereas slag particles in hydrated-only SBSB (Fig. 4-13B) were dispersed with little to no adhesion to wood strands.

The microstructure of SBSB-28dH was further investigated and EDS characterization obtained. Fig 4-14 presents typical micrographs. From Fig. 4-14A, it seemed that the interface between wood and slag was highly porous implying a poor adhesion between both materials. The zoomed-in micrograph (Fig. 4-14B) revealed a coarse and aggregated microstructure. This observation is consistent with the poor mechanical and physical performance of hydrated-only SBSB. The microstructure of steel slag was dominated by unreacted slag particles which caused the weak bonding between wood and steel slag.

The SEM micrographs along with EDS characterization of SBSB-12C28dH are shown in Fig 4-15. The interface between wood strands and steel slag matrix (Fig. 4-15A) revealed a dense microstructure devoid of cracks and voids. Furthermore, the zoomed-in micrograph (Fig. 4-15B) revealed a thorough interlock between wood strands and steel slag which would explain the enhanced mechanical and durability performance of SBSB. No calcium carbonate crystals could be detected in the bulk matrix surrounding the wood strands. The matrix was dominated by a continuous film engulfing what resembled spiky extrusions. EDS analyses of these extrusions revealed strong carbon signals along with Ca and Si. Thus, it was believed that these represented calcium carbonates engulfed by a C-S-H like gel. This observation was consistent with the findings of [24], who noted that calcium carbonates formed by carbonation curing were intermingled with C-S-H. Interestingly, calcium carbonates with an amorphous morphology were detected on the walls of the wood strand. These nano-deposits could explain the improved interface between wood and steel slag contributing towards the improved mechanical, durability and physical performance of carbonated SBSB.

4.3.5 Visual assessment

Not only did the carbonated and hydrated boards differ in performance, but also in appearance. The hydrated unaged boards had yellow blotches on them possibly an oxidation reaction of one of the metal residues, probably iron oxide, present in the steel slag. This phenomenon was reported elsewhere and was attributed to the oxidation of iron in ground iron furnace slag[37]. The referenced study linked the progression of oxidation to the voids present in the matrix. In this study, carbonated SBSB did not show any color changes before the ageing cycles. After repeated soak/dry cycles, localized rust pits were observed on the surface of some of the boards (carbonated and hydrated), possibly induced by oxidation of iron-bearing mineral phases. This opens the door for future tests to be performed on the newly developed composite to overcome this shortcoming. Among the mitigation techniques could be de-ironizing the steel slag using magnetic separation techniques to reduce the ferrous content prior to use.

4.4 General Assessment of slag bonded strand board

4.4.1 Strand board compared to major commercial boards

The benchmark properties of some commercial boards are summarized in Table 4-7. In terms of mechanical strength, SBSB-12C28dH displayed comparable MOR to the commercial cement-bonded particleboard (Bison panel) but slightly lower MOR than commercial cement bonded strand board (Eltoboard) and OSB. SHP performance of SBSB-12C28dH was comparable to Eltoboard and superior to Bison panel. In terms of physical performance, the carbonated SBSB displayed superior thickness swelling resistance than all commercial boards. Health and safety wise, carbonated SBSB liberates no toxic gases, and it is worth mentioning that unlike all other boards, the carbonated SBSB is the only board in which no chemical additives (such as chemicals used to overcome wood-cement incompatibility) were utilized in the production process. The density of the carbonated SBSB, however, was the highest among all boards but was within the acceptable range for medium density boards[38, 39].

4.4.2 Economic and environmental viability

Typically, wood cement composites contain approximately 60 to 70 % ordinary cement [39]. If this cement was replaced by steel slag and carbonation curing was employed, extensive savings on environmental and economical levels could be achieved. Furthermore, steel slag is a by-product and often entails landfilling burdens on steel manufacturers. Thus, finding an outlet for these by-products would be highly beneficial, including avoidance of disposal in landfills and possible pollution inhibition. The production of commercial wood-strand cement board requires wood strands, cement and water at a ratio of 1:2:1 by dry weight [38]. To overcome the wood-cement incompatibility, additives such as waterglass can be added at concentrations of 2-4 % by weight. Table 4-8 offers a rough comparison between the cost of SBSBs-12C28dH and commercial wood-strand cement boards. These calculations exclude the cost of manufacturing, including the pressing and drying required for commercial production of wood-strand cement boards, an energy intensive process. Calculations were based on a typical strand board of size 2400 x 600 mm with a thickness of 12 mm. Raw material cost estimates revealed that carbonated SBSBs could be produced at a 40 % of the cost of the traditional boards while offering more benefits and comparable performance.

Stringent environmental policies act as an incentive towards promoting carbon negative products. Therefore, a carbon balance analysis was conducted to evaluate the footprint associated with the production of one slag-bonded strand board of size 2400 x 600 of thickness 12 mm. Production of this board entailed several CO_2 contributors from steel slag grinding to CO_2 capture and recovery, and CO_2 compression and liquefaction. The production of one board consumed approximately 15 kg of steel slag and stored approximately 1.62 kg of CO_2 through the carbonation curing process. Table 9 shows the energy consumption of each of these contributors. According to the U.S. energy information administration (2021) [40], 1 kWh of electricity from natural gas generates 0.41 Kg of CO_2, thus the CO_2 emitted at each stage was calculated. By summing up the CO_2 emitted (0.4 Kg) and that sequestered by the carbonation process (-1.62 Kg), the result was a negative uptake indicating a clean footprint. Thus, a typical 2400 x 600 mm board of 12 mm thickness could consume 1.22 kg of CO_2 from the environment. Approximately 211 m^3 of finished boards of varying thicknesses could be produced per 7-hour shift daily in fully automated plants which round up to 33 boards per 24-hour period per plant [39]. If this cement were to be replaced by steel slag and carbonation curing was adopted, significant amounts of CO_2 could be sequestered per day per plant. With the increased use of these panel products, shifting to a carbon-negative strand board could be a win-win strategy.

4.5 Conclusion

This chapter presented an innovative method to recycle steel slag into an eco-friendly medium density strand board. Renewable wood strands mixed with steel slag were formed into boards and subjected to early carbonation curing. The following conclusions can be drawn:

1. Renewable wood strands can be employed as reinforcement in CO_2-activated steel slag matrix to develop slag bonded strand board. Compatibility between wood and slag was confirmed

through performance and durability tests. Carbonated strand boards satisfied criteria set by ASTM C1185, ASTM D1037 and BS EN 494.

2. Formation of C-S-H and $CaCO_3$ by early carbonation curing led to a board that could show mechanical and physical performance in only 12 hours, thus potentially accelerating production rate and turnover.
3. Subsequent 28 days of hydration after carbonation significantly improved the mechanical performance of the composite and contributed towards an enhanced ultimate strength. Carbonation curing does not hinder subsequent hydration. The ultimate strength was a superposition of carbonation and hydration strength.
4. Accelerated ageing tests demonstrated excellent performance of carbonated strand boards, as carbonation curing enhanced the board resistance to weathering carbonation due to soak-dry cycles and preserved the embedded wood strands from hydrolysis attack in the warm water test.
5. The innovative slag-bonded wood composite displayed comparable performance to commercial wood-cement composites while preserving natural resources, recycling industrial wastes, promoting carbon negativity, and serving as a means of carbon storage. Cost analysis showed that carbonated slag-bonded strand boards can be produced at a lower cost than commercial cement bonded strand board while offering greater environmental benefits.

References

1. Wang, J., M. Zhong, P. Wu, S. Wen, L. Huang, and P. Ning, *A Review of the Application of Steel Slag in CO2 Fixation.* ChemBioEng Reviews, 2021. **8**(3): p. 189-199 DOI: https://doi.org/10.1002/cben.202000021.
2. Mahoutian, M., Y.X. Shao, A. Mucci, and B. Fournier, *Carbonation and hydration behavior of EAF and BOF steel slag binders.* Materials and Structures, 2015. **48**(9): p. 3075-3085 DOI: https://doi.org/10.1617/s11527-014-0380-x
3. Humbert, P.S. and J. Castro-Gomes, *CO_2 activated steel slag-based materials: A review.* Journal of Cleaner Production, 2019. **208**: p. 448-457 DOI: https://doi.org/10.1016/j.jclepro.2018.10.058.
4. Jin, P., S. Zhang, Y. Liu, W. Zhang, and R. Wang, *Application of Bacillus mucilaginosus in the carbonation of steel slag.* Applied Microbiology and Biotechnology, 2021. **105**(23): p. 8663-8674 DOI: https://doi.org/10.1007/s00253-021-11641-z
5. Ghouleh, Z., R.I.L. Guthrie, and Y.X. Shao, *High-strength KOBM steel slag binder activated by carbonation.* Construction and Building Materials, 2015. **99**: p. 175-183 DOI: https://doi.org/10.1016/j.conbuildmat.2015.09.028
6. Wang, R., P. Jin, H. Dong, Y. Liu, Z. Ding, and W. Zhang, *Effect of moist content on the bio-carbonated steel slag bricks.* Construction and Building Materials, 2021. **269**: p. 121313 DOI: https://doi.org/10.1016/j.conbuildmat.2020.121313
7. Ghouleh, Z., M. Celikin, R.I.L. Guthrie, and Y.X. Shao, *Microstructure of Carbonation-Activated Steel Slag Binder.* Journal of Materials in Civil Engineering, 2018. **30**(9): p. 04018217 DOI: https://doi.org/10.1061/(asce)mt.1943-5533.0002421
8. Wang, Y.-J., Y.-N. Zeng, J.-G. Li, Y.-Z. Zhang, Y.-J. Zhang, and Q.-Z. Zhao, *Carbonation of argon oxygen decarburization stainless steel slag and its effect on chromium*

leachability. Journal of Cleaner Production, 2020. **256**: p. 120377 DOI: https://doi.org/10.1016/j.jclepro.2020.120377

9. Young, J.F., R.L. Berger, and J. Breese, *Accelerated Curing of Compacted Calcium Silicate Mortars on Exposure to CO_2*. Journal of the American Ceramic Society, 1974. **57**(9): p. 394-397 DOI: https://doi.org/10.1111/j.1151-2916.1974.tb11420.x
10. Fernandez Bertos, M., S.J. Simons, C.D. Hills, and P.J. Carey, *A review of accelerated carbonation technology in the treatment of cement-based materials and sequestration of CO2*. Journal of Hazardous Materials, 2004. **112**(3): p. 193-205 DOI: https://doi.org/10.1016/j.jhazmat.2004.04.019
11. Saunders, A., *Global Cement Brochure: Cement Boards 101*. Global Cement Magazine, 2014.
12. Papadopoulos, A.N., G.A. Ntalos, and I. Kakaras, *Mechanical and physical properties of cement-bonded OSB*. Holz als Roh-und Werkstoff, 2006. **64**(6): p. 517-518 DOI: https://doi.org/10.1007/s00107-005-0092-6
13. Wang, L. and D.C. Tsang, *Carbon dioxide sequestration on composites based on waste wood*, in *Carbon Dioxide Sequestration in Cementitious Construction Materials*. 2018, Elsevier. p. 431-450.DOI: https://doi.org/10.1016/b978-0-08-102444-7.00018-6
14. Toledo Filho, R.D., K. Ghavami, G.L. England, and K. Scrivener, *Development of vegetable fibre–mortar composites of improved durability*. Cement and Concrete Composites, 2003. **25**(2): p. 185-196 DOI: https://doi.org/10.1016/s0958-9465(02)00018-5

15. Wei, J.A. and C. Meyer, *Degradation mechanisms of natural fiber in the matrix of cement composites.* Cement and Concrete Research, 2015. **73**: p. 1-16 DOI: https://doi.org/10.1016/j.cemconres.2015.02.019

16. Onuaguluchi, O. and N. Banthia, *Plant-based natural fibre reinforced cement composites: A review.* Cement and Concrete Composites, 2016. **68**: p. 96-108 DOI: https://doi.org/10.1016/j.cemconcomp.2016.02.014

17. Balatinecz, J.J., A. Leclercq, and D.E. Kretschmann. *Achievements in the utilzation of poplar wood: guideposts for the future*. in *21st Session of the International Poplar Commission (IPC 2000): poplar and willow culture: meeting the needs of society and the environment. St. Paul, Minn.: US Dept. of Agriculture, Forest Service, North Central Research Station, 2000. General technical report NC; 215: p. 11*. 2000.DOI: https://doi.org/10.5558/tfc77265-2

18. Kakade, A.M., *Measuring concrete surface pH-A proposed test method.* Concrete Repair Bulleting, 2014: p. 16-20.

19. Mohr, B.J., J.J. Biernacki, and K.E. Kurtis, *Supplementary cementitious materials for mitigating degradation of kraft pulp fiber-cement composites.* Cement and Concrete Research, 2007. **37**(11): p. 1531-1543 DOI: https://doi.org/10.1016/j.cemconres.2007.08.001

20. Caprai, V., F. Gauvin, K. Schollbach, and H.J.H. Brouwers, *MSWI bottom ash as binder replacement in wood cement composites.* Construction and Building Materials, 2019. **196**: p. 672-680 DOI: https://doi.org/10.1016/j.conbuildmat.2018.11.153

21. Caprai, V., F. Gauvin, K. Schollbach, and H.J.H. Brouwers, *Influence of the spruce strands hygroscopic behaviour on the performances of wood-cement composites.* Construction and

Building Materials, 2018. **166**: p. 522-530 DOI: https://doi.org/10.1016/j.conbuildmat.2018.01.162

22. Halligan, A., *A review of thickness swelling in particleboard.* Wood Science and Technology, 1970. **4**(4): p. 301-312 DOI: https://doi.org/10.1007/bf00386406

23. Wang, L., S.S. Chen, D.C.W. Tsang, C.S. Poon, and K. Shih, *Recycling contaminated wood into eco-friendly particleboard using green cement and carbon dioxide curing.* Journal of Cleaner Production, 2016. **137**: p. 861-870 DOI: https://doi.org/10.1016/j.jclepro.2016.07.180

24. Rostami, V., Y.X. Shao, A.J. Boyd, and Z. He, *Microstructure of cement paste subject to early carbonation curing.* Cement and Concrete Research, 2012. **42**(1): p. 186-193 DOI: https://doi.org/10.1016/j.cemconres.2011.09.010

25. Soroushian, P., J.P. Won, and M. Hassan, *Durability and microstructure analysis of CO_2-cured cement-bonded wood particleboard.* Cement and Concrete Composites, 2013. **41**: p. 34-44 DOI: https://doi.org/10.1016/j.cemconcomp.2013.04.014

26. Wang, R., L. Qin, and X.J. Gao, *Mechanical strength and water resistance of magnesium oxysulfate cement based lightweight materials.* Cement and Concrete Composites, 2020. **109**: p. 103554 DOI: https://doi.org/10.1016/j.cemconcomp.2020.103554

27. Ashraf, W. and J. Olek, *Carbonation behavior of hydraulic and non-hydraulic calcium silicates: potential of utilizing low-lime calcium silicates in cement-based materials.* Journal of Materials Science, 2016. **51**(13): p. 6173-6191 DOI: https://doi.org/10.1007/s10853-016-9909-4

28. Adesanya, E., H. Sreenivasan, A.M. Kantola, V.V. Telkki, K. Ohenoja, P. Kinnunen, and M. Illikainen, *Ladle slag cement - Characterization of hydration and conversion.*

Construction and Building Materials, 2018. **193**: p. 128-134 DOI: https://doi.org/10.1016/j.conbuildmat.2018.10.179

29. Mahoutian, M., Z. Ghouleh, and Y.X. Shao, *Carbon dioxide activated ladle slag binder.* Construction and Building Materials, 2014. **66**: p. 214-221 DOI: https://doi.org/10.1016/j.conbuildmat.2014.05.063

30. Chang, R., S. Kim, S. Lee, S. Choi, M. Kim, and Y. Park, *Calcium Carbonate Precipitation for* CO_2 *Storage and Utilization: A Review of the Carbonate Crystallization and Polymorphism.* Frontiers in Energy Research, 2017. **5**: p. 17 DOI: https://doi.org/10.3389/fenrg.2017.00017

31. Bukowski, J.M. and R.L. Berger, *Reactivity and Strength Development of* CO_2 *Activated Non-Hydraulic Calcium Silicates.* Cement and Concrete Research, 1979. **9**(1): p. 57-68 DOI: https://doi.org/10.1016/0008-8846(79)90095-4

32. Zhang, D., T.L. Liu, and Y.X. Shao, *Weathering Carbonation Behavior of Concrete Subject to Early-Age Carbonation Curing.* Journal of Materials in Civil Engineering, 2020. **32**(4): p. 04020038 DOI: https://doi.org/10.1061/(asce)mt.1943-5533.0003087

33. Xian, X.P. and Y.X. Shao, *Microstructure of cement paste subject to ambient pressure carbonation curing.* Construction and Building Materials, 2021. **296**: p. 123652 DOI: https://doi.org/10.1016/j.conbuildmat.2021.123652

34. Salman, M., O. Cizer, Y. Pontikes, R.M. Santos, R. Snellings, L. Vandewalle, B. Blanpain, and K. Van Balen, *Effect of accelerated carbonation on AOD stainless steel slag for its valorisation as a* CO_2*-sequestering construction material.* Chemical Engineering Journal, 2014. **246**: p. 39-52 DOI: https://doi.org/10.1016/j.cej.2014.02.051

35. Wang, X., W. Ni, J. Li, S. Zhang, M. Hitch, and R. Pascual, *Carbonation of steel slag and gypsum for building materials and associated reaction mechanisms.* Cement and Concrete Research, 2019. **125**: p. 105893 DOI: https://doi.org/10.1016/j.cemconres.2019.105893

36. Xian, X., D. Zhang, and Y. Shao, *Flue gas carbonation curing of cement paste and concrete at ambient pressure.* Journal of Cleaner Production, 2021. **313**: p. 127943 DOI: https://doi.org/10.1016/j.jclepro.2021.127943.

37. Savastano Jr, H., P. Warden, and R. Coutts, *Ground iron blast furnace slag as a matrix for cellulose-cement materials.* Cement and Concrete Composites, 2001. **23**(4-5): p. 389-397.

38. VAN ELTEN, I.E.B. *Cement bonded particle board (CBPB) and wood strand cement board (EltoBoard): Production, properties and applications*. in *10th Inter. Inorganic Bonded Fiber Composites Conf.(IIBCC), Sao Paulo, Brazil*. 2006.

39. Aro, M. *Wood strand cement board*. in *11th Int. Inorganic-Bonded Fiber Composites Conference (IIBCC2008), November 5-7, 2008, Madrid, Spain*. 2010.

40. van Zomeren, A., S.R. Van der Laan, H.B. Kobesen, W.J. Huijgen, and R.N. Comans, *Changes in mineralogical and leaching properties of converter steel slag resulting from accelerated carbonation at low CO2 pressure.* Waste Management, 2011. **31**(11): p. 2236-2244 DOI: https://doi.org/10.1016/j.wasman.2011.05.022

41. Halmann, M.M. and M. Steinberg, *Greenhouse gas carbon dioxide mitigation: Science and Technology*. 1998: CRC press.DOI: https://doi.org/10.1201/9781482227833

Tables

Table 4-1 Chemical composition of as-received steel slag

XRF analysis [a] (wt. %)								
SiO_2	Al_2O_3	Fe_2O_3	MnO	MgO	CaO	Na_2O	K_2O	LOI
23.37	4.02	7.71	1.208	11.09	46.59	0.04	< 0.01	3.53

[a] Panalytical PW2440 spectrometer (MagiX PRO series)

Table 4-2 Wood strand specifications

Wood-Strands	
Physical Specifications (mm)	
Length	100
Width	3
Thickness	0.17
Density (g/cm^3)	0.42
Moisture Content (%)	0
Water Absorption (%)	118.7

Table 4-3 Laboratory production parameters of slag-bonded strand board

Board Dimensions (mm)		
Length		127
Width		76
Thickness		12
Manufacture ratios		
Mixture	water/slag	wood/slag
1	0.3	0.17
2	0.35	0.17
3	0.375	0.17
4	0.4	0.17

Table 4-4 CO_2 uptake of carbonated-SBSB

Water to slag ratio		0.25	0.3	0.35	0.375	0.4
CO_2 uptake	(%)	8.1	9.9	10.8	10.2	9.6

Table 4-5 Thermogravimetric thermal analysis

Condition	Board I.D.	Water loss in hydration products [a] (%)	Water loss in $Ca(OH)_2$ (%)	CO_2 loss in $CaCO_3$ (%)	$Ca(OH)_2$ (%)	$CaCO_3$ (%)
Unaged [b]	SBSB-12C28dH	4.9	0.4	9.45	1.64	21.48
	SBSB-28dH	6.86	0.4	3.41	1.64	7.75
Aged-SD [c]	SBSB-12C28dH	4.98	0.44	10.17	1.81	23.11
	SBSB-28dH	6.53	0.49	11.86	2.01	26.95
Aged-WW [c]	SBSB-12C28dH	6.17	0.72	7.48	2.96	17.00
	SBSB-28dH	-	-	-	-	-

[a] *Based-on mass loss between 105-380 ℃.*
[b] *Unaged refers to boards at 28 days.*
[c] *Aged refers to boards after the accelerated ageing cycles.*

Table 4-6 pH of pore solutions in carbonated and hydrated-only boards at 28 days and after ageing.

pH	Unaged	Aged-WW	Aged-SD
SBSB-12C28dH	11.42	11.87	11.35
SBSB-28dH	11.65	-	11.5

Table 4-7 Comparison of SBSB-12C28dH mechanical and physical properties with commercial board products

Board	MOR (MPa)	SHP (N/mm)	Swelling 24 hr (%)	Density [a] (g/cm^3)	Health and safety
SBSB-12C28dH	14.2	65	0.17	1.3	No toxic gases
Elto-board [b]	20.31[d]	76.83	3.94	1.13	No toxic gases
Bison panel [c]	12	40	1	1.25	No toxic gases
OSB	22.4	-	0.49	0.8	Liberated toxic gases

[a] Calculated based on ISO-8335 recommendations
[b] Commercial cement bonded strand board (adapted from [39])
[c] Commercial cement bonded particleboard
[d] Based on 10 mm thick boards

Table 4-8 Price comparison between raw material in SBSB and commercial wood-strand cement board

	SBSB			Wood strand cement board		
Item	Item/board (kg)	Price ($/ton)	Total ($/board)	Item/board (kg)	Price ($/ton)	Total ($/board)
Wood strands: Poplar [a]	2.6	37	0.1	3.5	37	0.13
Cement [b]	-	-	-	7	124	0.87
Salt solution [c]	-	-	-	0.2	150	0.03
Steel slag [d]	15	5	0.08	-	-	-
Steel slag grinding [e]	15	1.8	0.027	-	-	-
CO_2 capture and transportation [f]	1.62	110	0.178	-	-	-
Total ($/board)			0.38			1.03

[a] https://senb.ca/images/MARKET_SHEET_JAN_31_2019.pdf

[b] https://www.statista.com/statistics/us-prices-of-cement

[c] https://www.alibaba.com/showroom/bulk-sodium-silicate.html

[d] *https://www.harsco-environmental.com/*

[e] *2.2 kW consumed by pulverizer for 1 kg of slag for 2 min*

[f] *https://www.iea.org/commentaries/is-carbon-capture-too-expensive*

Table 4-9 Carbon balance analysis for the production of one slag-bonded strand board

Unit		Steel slag grinding	CO_2 capture and recovery	CO_2 compression and liquefaction	Steel slag CO_2 uptake	Total CO_2 emitted for 1 board
Energy	(kWh/ton)	36.7 [a]	143 [b]	103 [b]	-	
Energy for 1 board	(kWh)	0.55	0.23	0.17	-	
CO_2 emitted for 1 board	(Kg)	0.23	0.1	0.07	-1.62	-1.22

[a] 2.2 kW consumed by pulverizer for 1 kg of slag for 2 min

[b] [41] Halmann, M., Steinberg, M., 1999. Greenhouse gas carbon dioxide mitigation: Science and Technology, Lewis Publishers: Boca Raton, 568 pp.

Figures

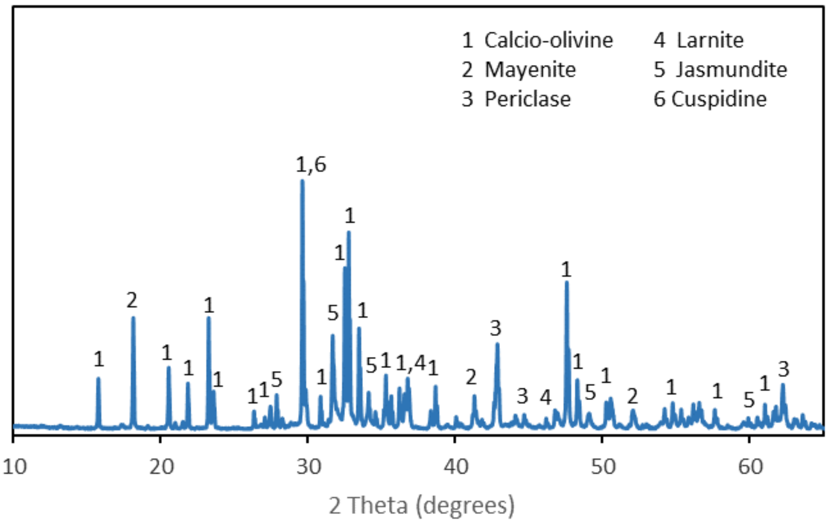

Figure 4-1 XRD diffractograms of raw ladle slag

Figure 4-2 Manufacturing process of slag-bonded strand board (SBSB).

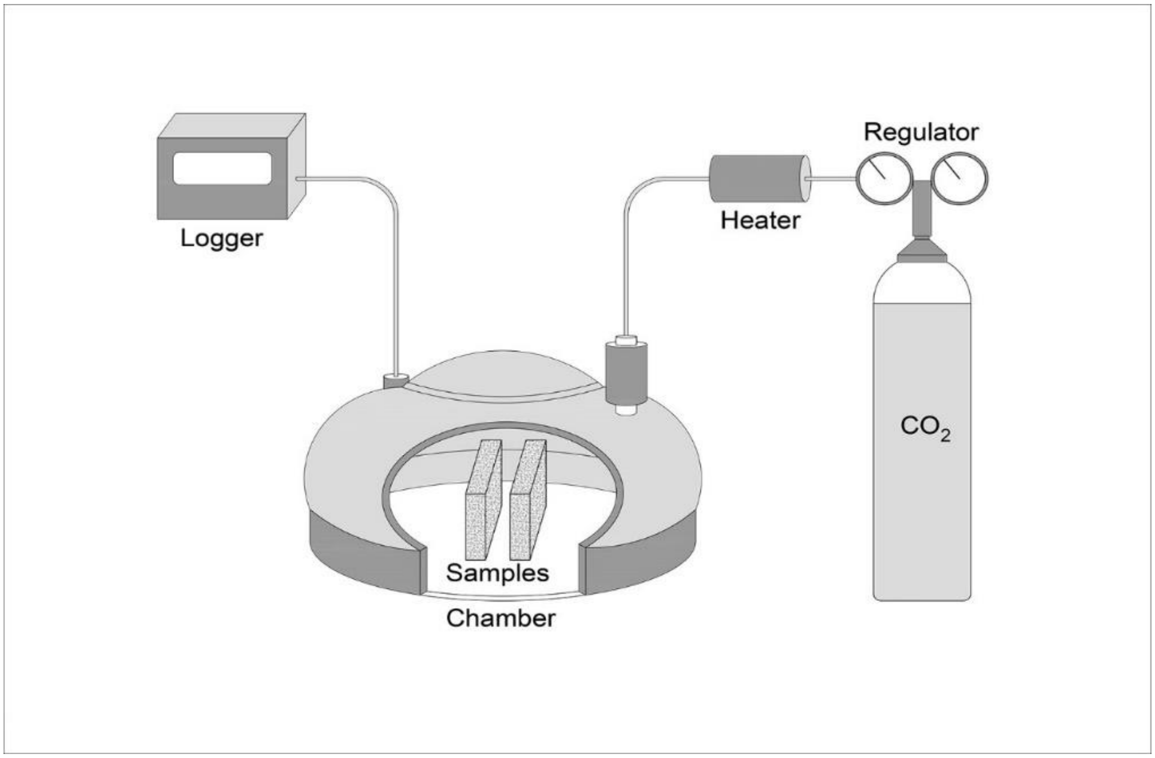

Figure 4-3 Experimental carbonation apparatus for SBSB.

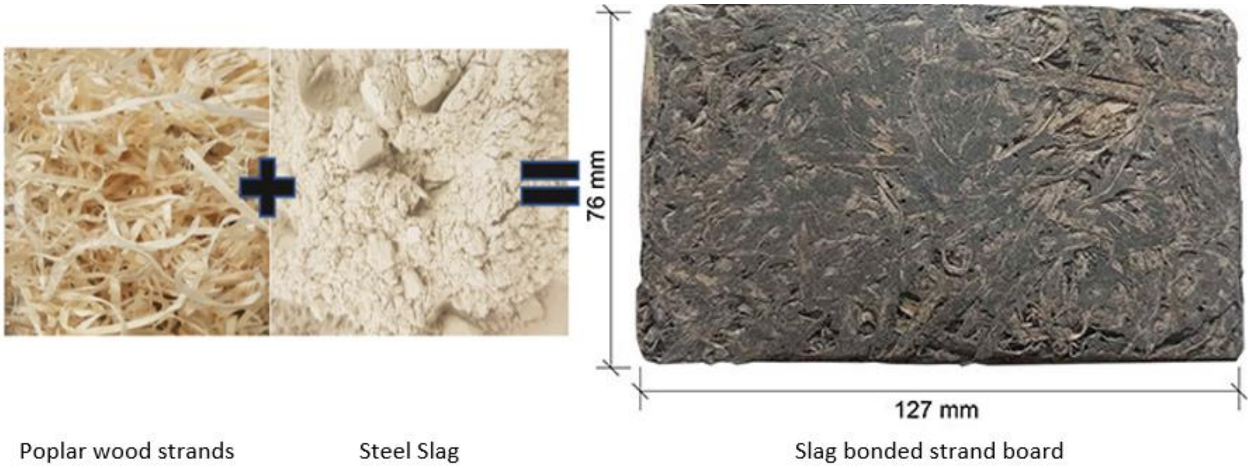

Figure 4-4 Poplar wood strands, steel slag and SBSB.

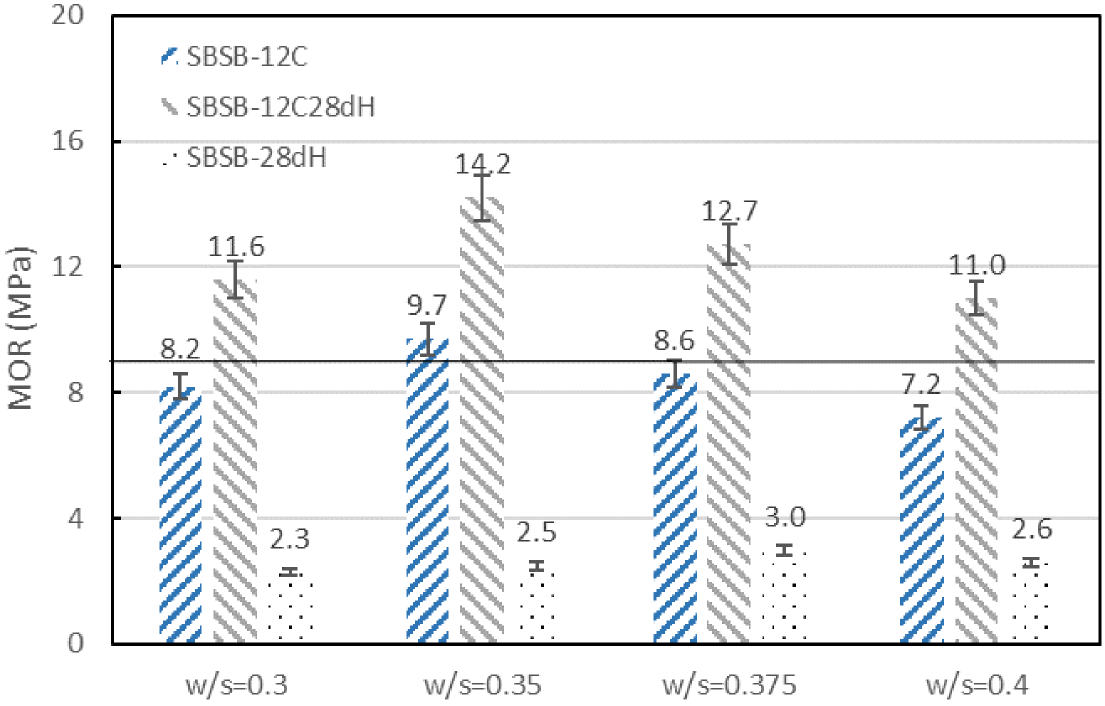

Figure 4-5 Influence of water to slag ratio on MOR of SBSB.

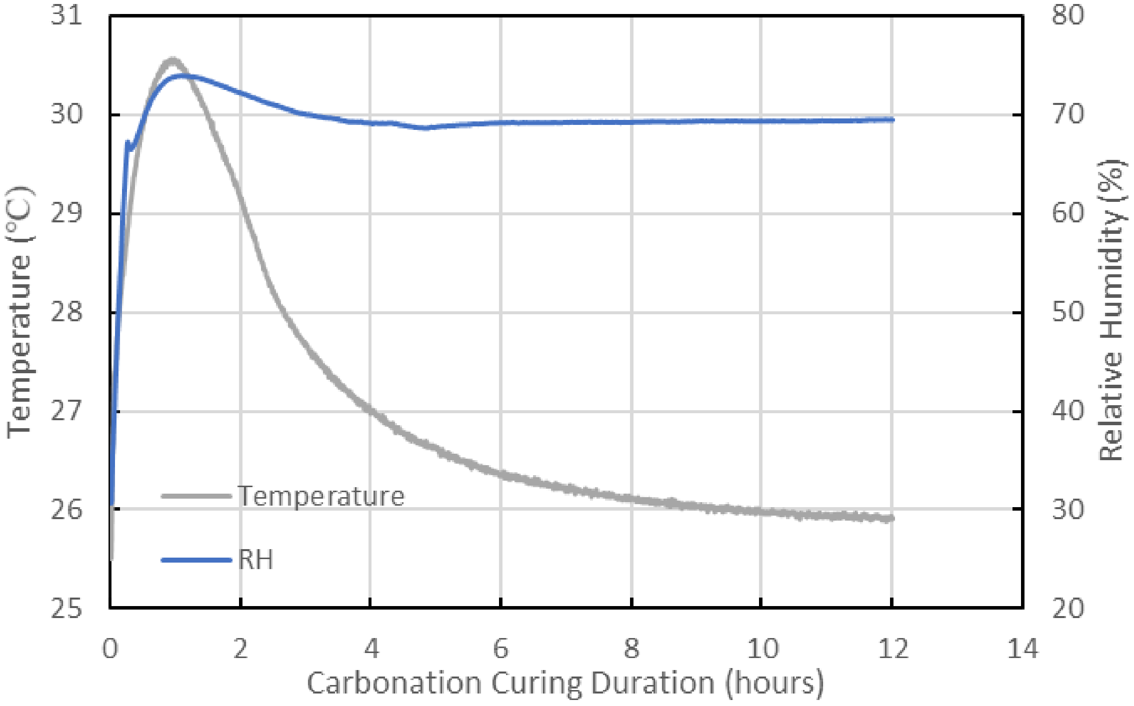

Figure 4-6 Typical temperature and relative humidity profiles during carbonation of SBSB.

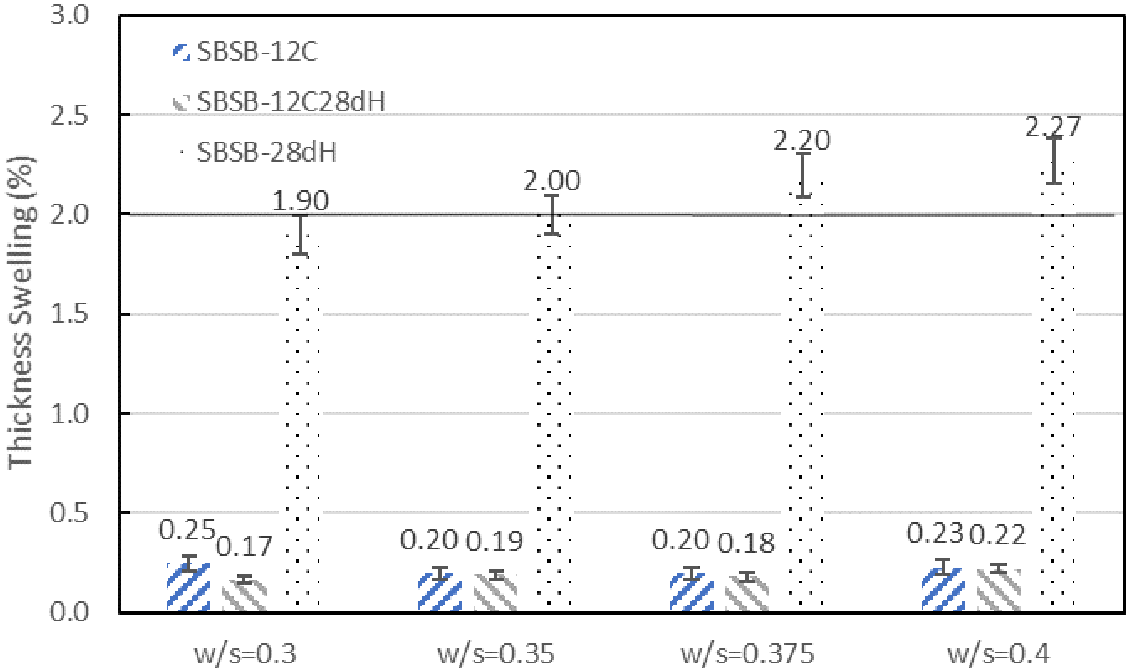

Figure 4-7 Influence of water to slag ratio on thickness swelling of SBSB.

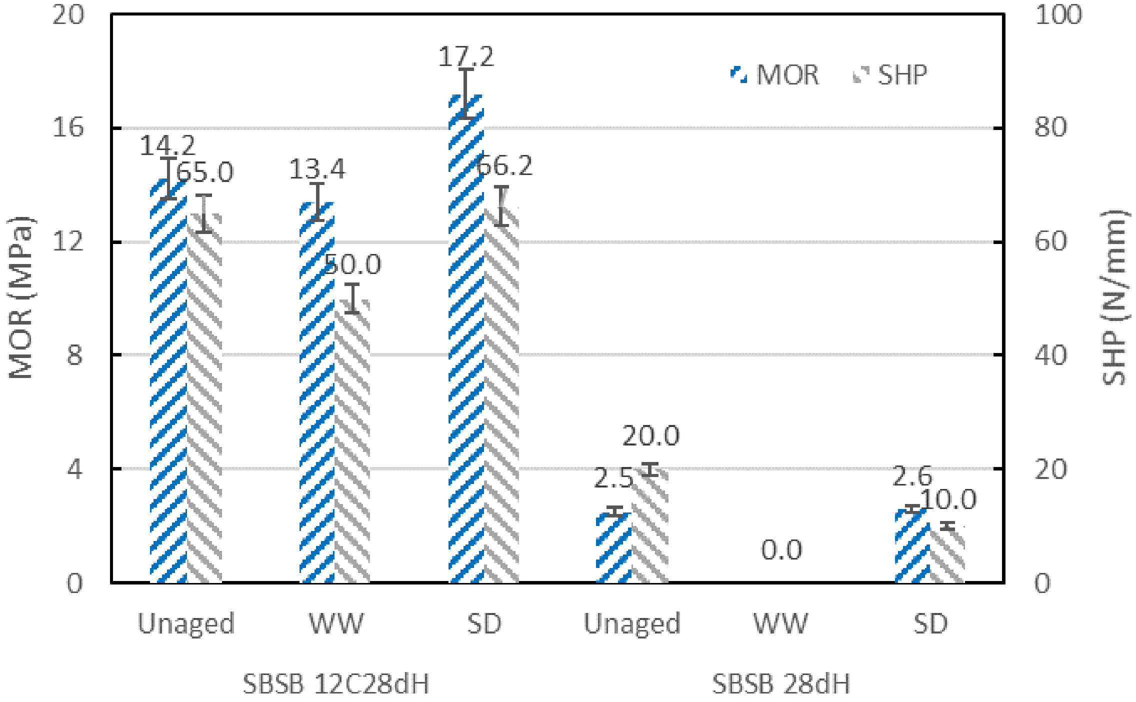

Figure 4-8 Mechanical performance of carbonated and hydrated SBSB before and after ageing.

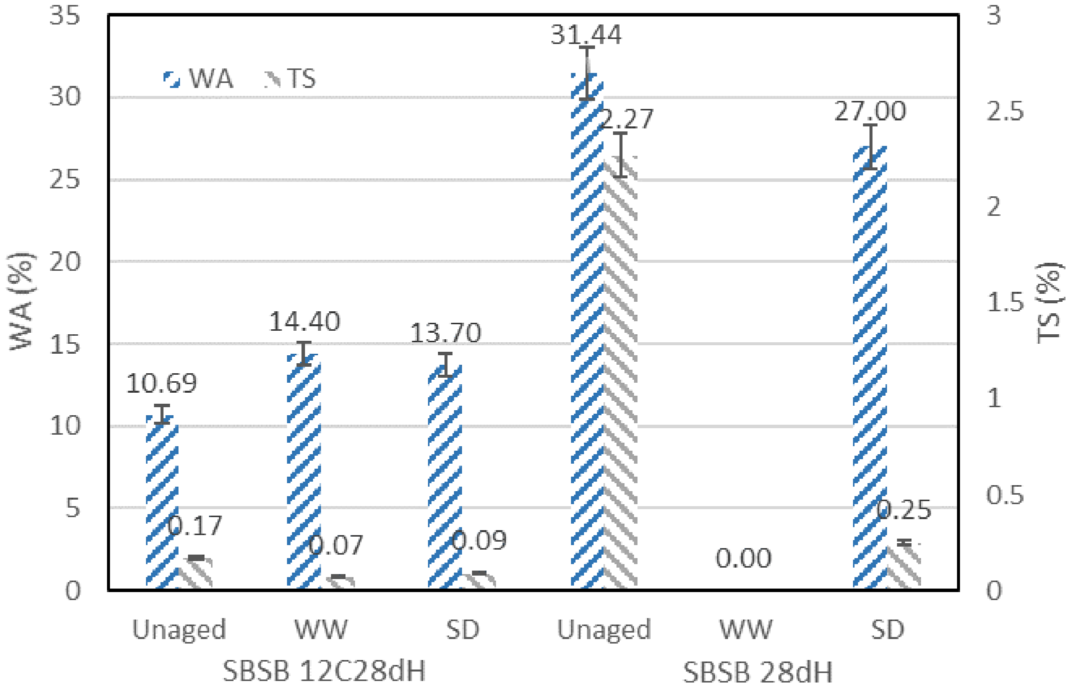

Figure 4-9 Physical performance of carbonated and hydrated SBSB before and after ageing.

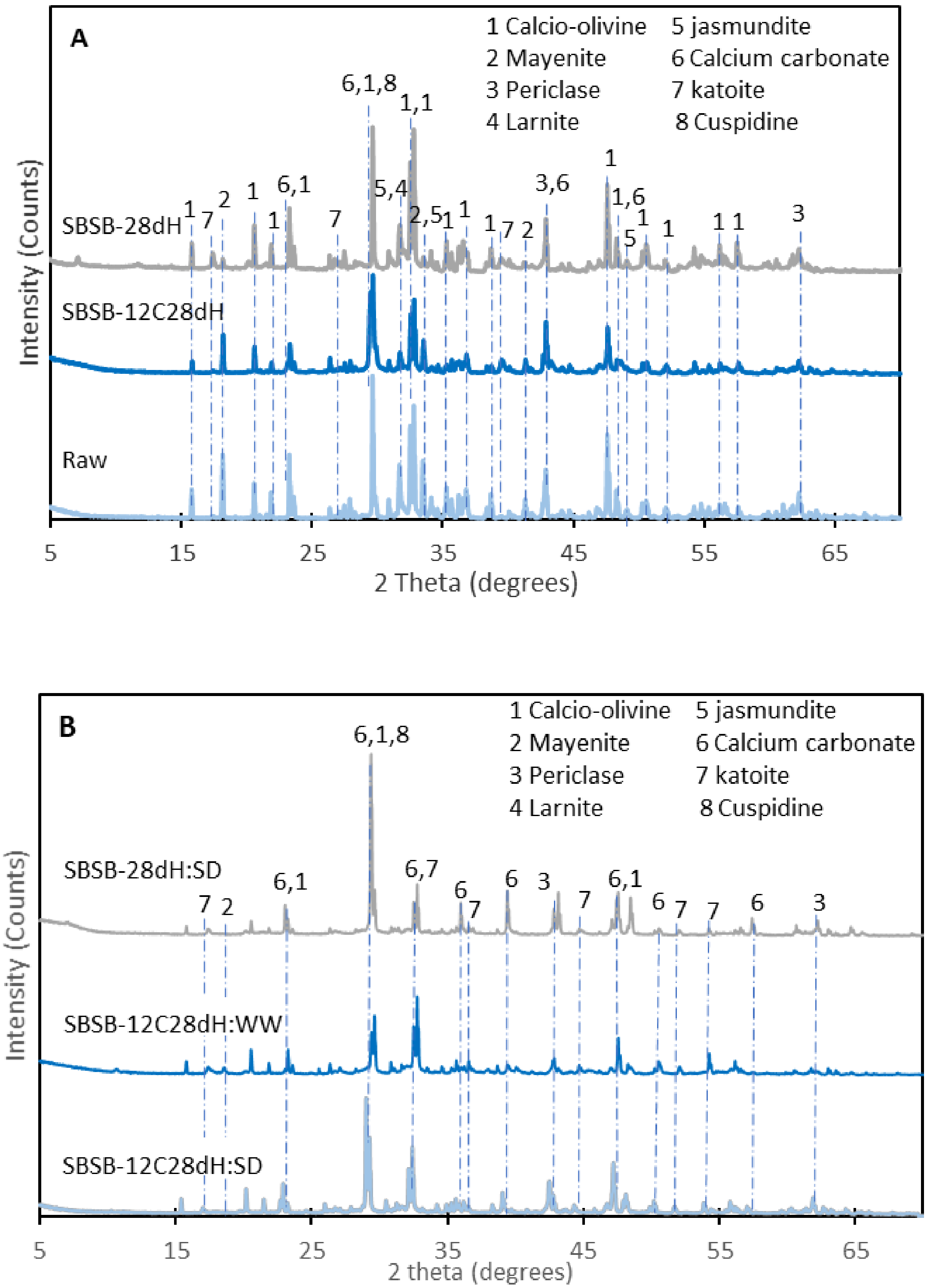

Figure 4-10 XRD of raw slag, carbonated SBSB-12C28dH and hydrated only SBSB-28dH: (A) unaged, (B) after ageing.

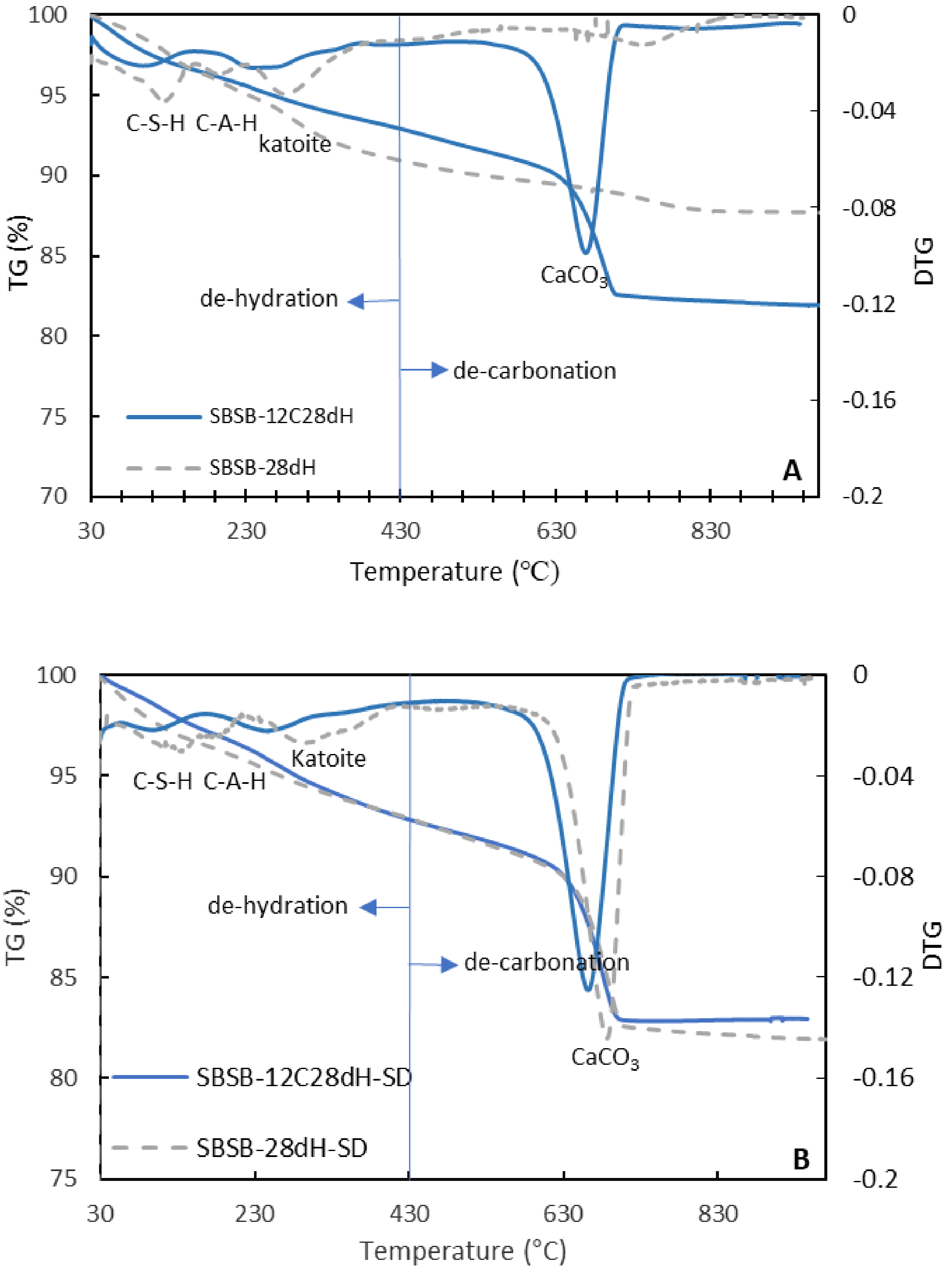

Figure 4-11 Thermal analysis of SBSB: (A)unaged at 28 days with carbonation (SBSB-12C28dH) and without carbonation (SBSB-28dH), (B) after ageing.

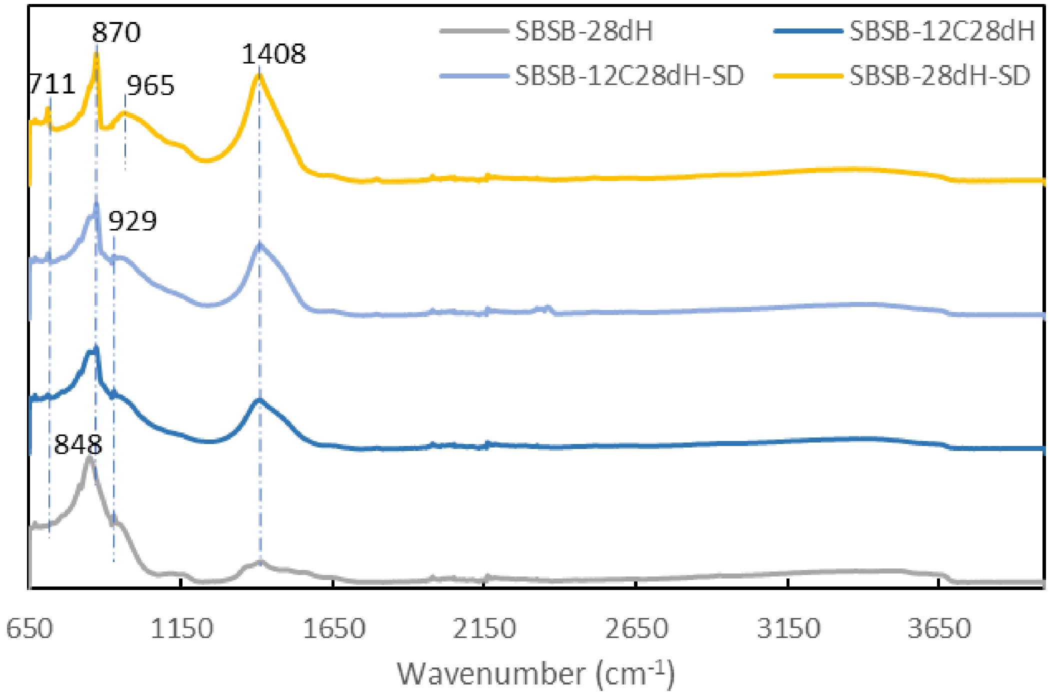

Figure 4-12 FTIR spectra of SBSB-12C28dH and SBSB-28dH before and after ageing.

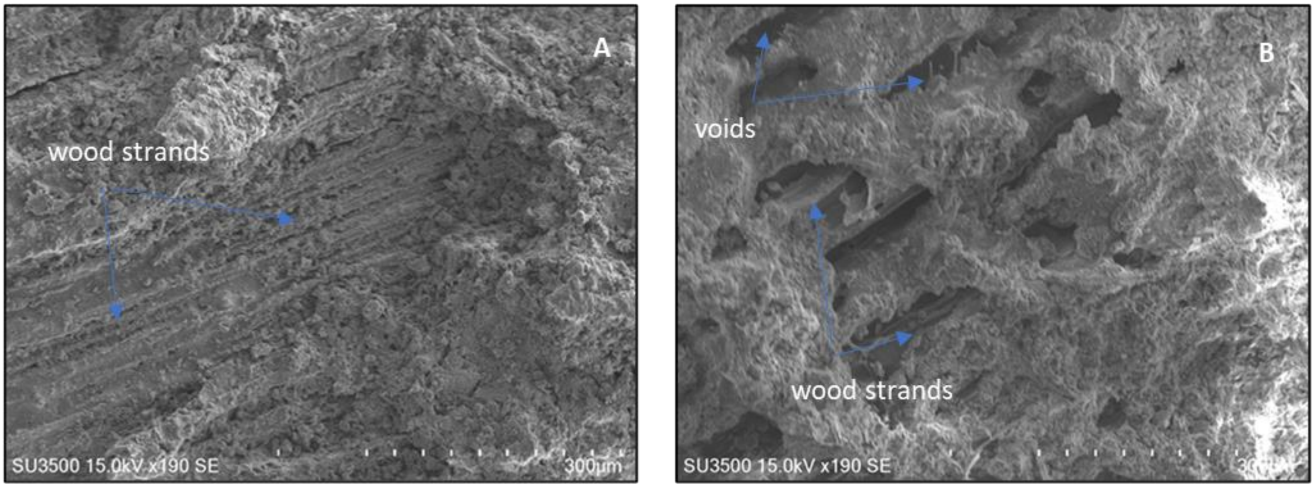

Figure 4-13 SEM micrographs of SBSB (A) 12C28dH, (B) 28dH.

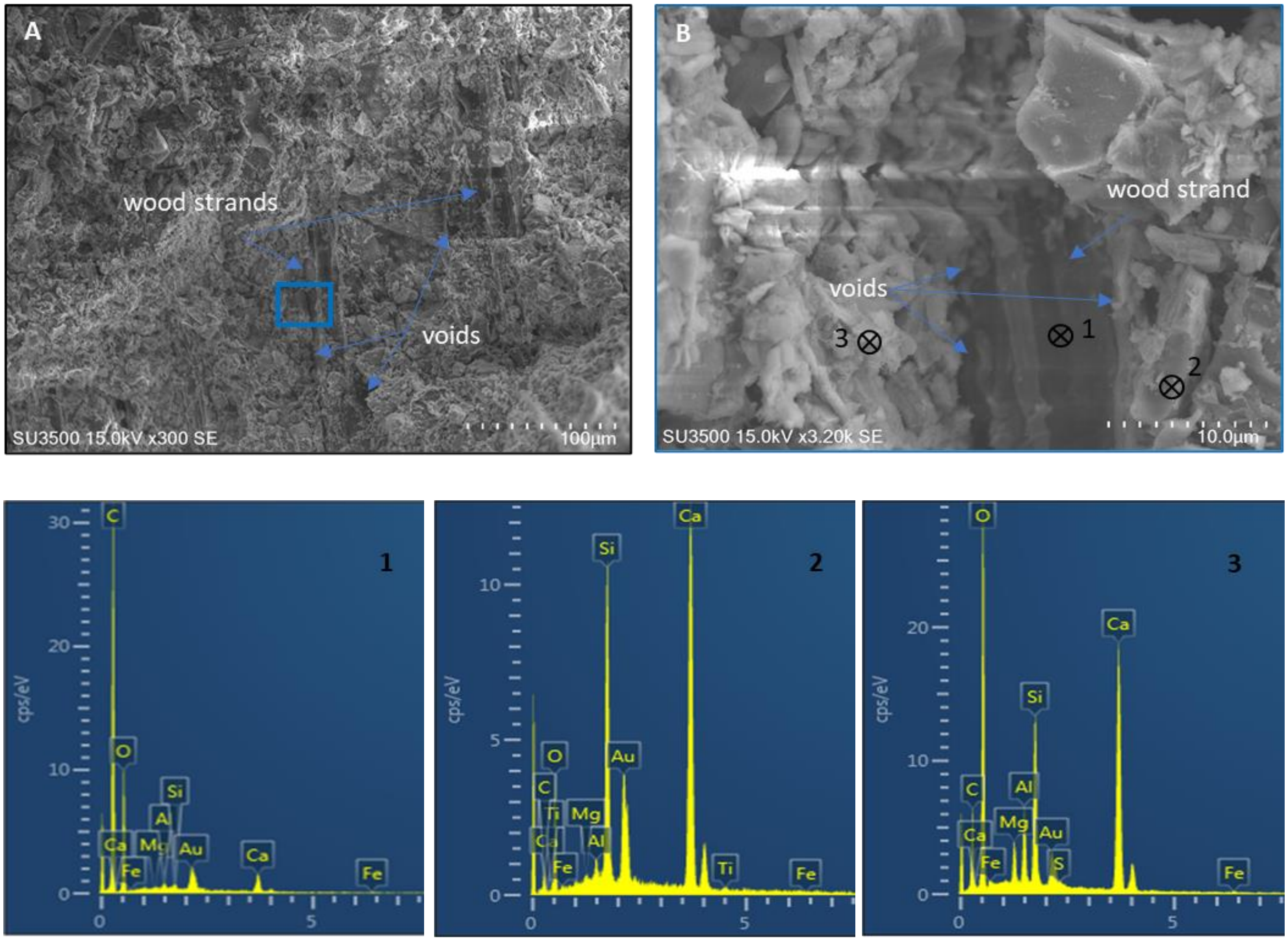

Figure 4-14 SEM micrograph of SBSB-28dH: (A) magnification 300x, (B) magnification 3200x.

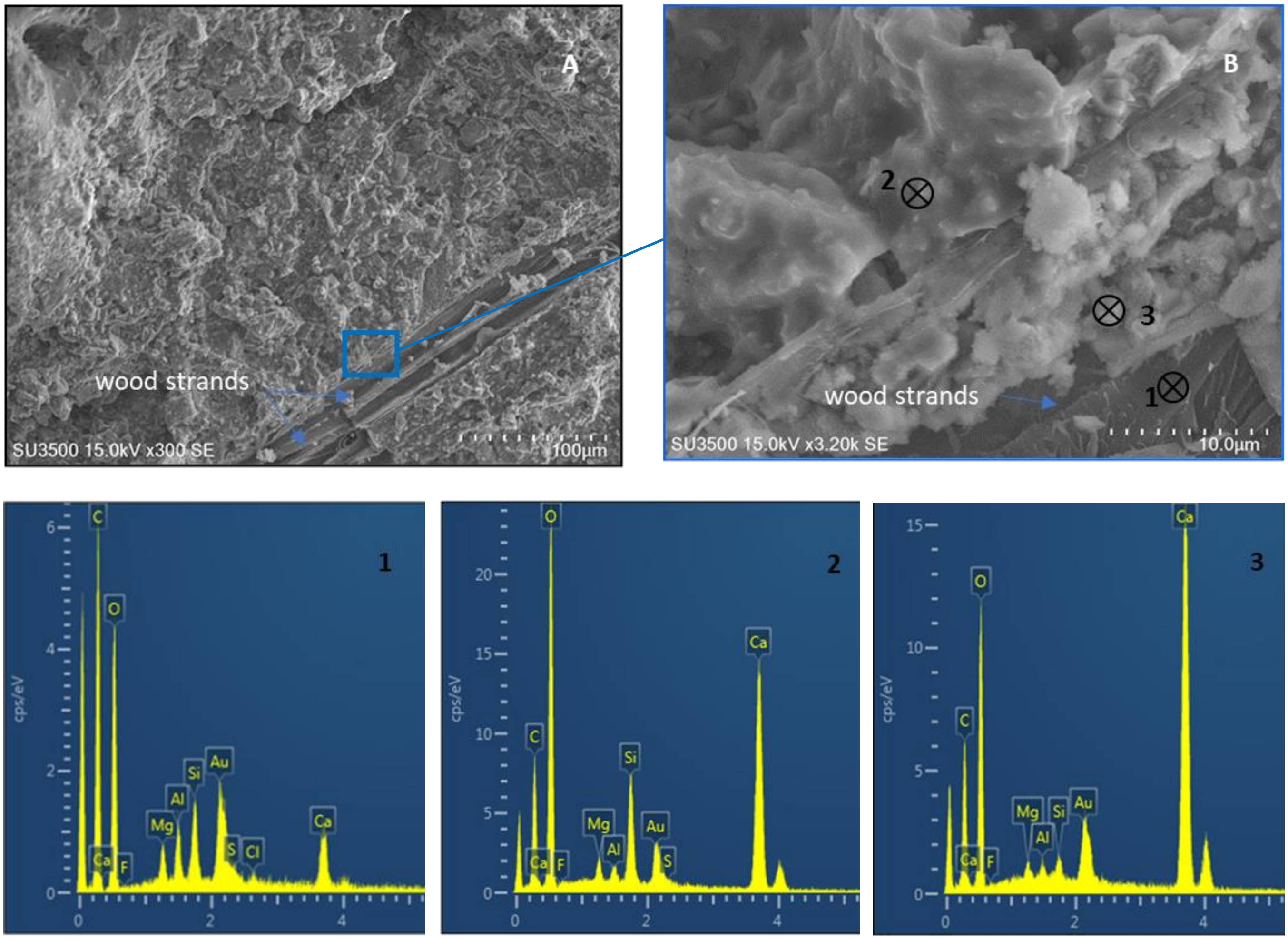

Figure 4-15 SEM photomicrographs of SBSB-12C28dH (A) magnification 300x, (B) magnification 3200x.

5. Chapter 5 Lightweight Masonry Units Using Carbon-Activated Steel Slag and Recycled Wood Aggregates

Preface

The previous chapter has shown that wood strands can be successfully employed in a carbonation-cured steel slag matrix towards the production of a slag-bonded strand board. Also, superior durability performance and carbon storage-ability were observed for these composites. To build on that, using recycled wood to partially replace fine aggregates in steel slag masonry units was investigated in this chapter. This chapter is oriented towards promoting recycling of both steel slag and lumber industry residues towards the production of a lightweight and loadbearing masonry unit. According to the literature survey on concrete masonry units, the incorporation of recycled wood, whether to reduce the dead load or to contribute towards sustainability, significantly affects the overall mechanical properties and results in a concrete suitable for non-loadbearing applications. To this end, this chapter explored the influence of carbonation curing on the mechanical performance of steel slag-bonded masonry units with recycled wood aggregates. Masonry units were prepared with steel slag as exclusive binder and with recycled wood aggregates replacing 35% and 50% by volume of crushed granite sand. The temperature and relative humidity inside the CO_2 curing chamber were reported. Compared to conventional steel slag concrete, carbonation of wood-incorporated slag concrete is deeper and more homogeneous. Experimental results revealed that incorporation of wood increased the CO_2 uptake potential of wood-steel slag masonry units; thus, effectively achieving a higher degree of carbonation. In terms of compressive strength, a decline of strength upon addition of wood was noted, but this decline was relatively counteracted by increasing the carbonation duration. It was also found that the wood-steel slag interface bond was improved owing to carbonation-deposited products.

5.1 Introduction

Considerable research effort had been put forward to find outlets for different industry generated wastes. Steel slag, the residue of the steel making industry, has particularly attracted a lot of attention recently. The steel slag's calcium-silicate constituents bear resemblance to those of cement that makes it a good target for binder innovation purposes. At present, a number of publications addressing the use of steel slag as sole binder are available in literature [1], [2], [3], [4], [5], [6]. Both the hydraulic and the accelerated carbonation activity of steel slag had been investigated. It was inferred that steel slag displayed a weak latent hydraulic activity owing primarily to the amorphous nature of its silicon content [3]. Also, the free calcium/magnesium oxide content triggers volumetric expansion which compromises the stability of steel slag. Carbonation curing activates the dormant phases and mitigates the expansion problem [3, 7, 8]. On this basis, carbonation curing is proposed as an ideal approach to valorize steel slag for certain applications.

The carbonation reaction depends on the diffusion of CO_2 into the solid which in turn relies on the permeability characteristics of the solid [9]. The diffused/permeated CO_2 dissolves into the pore solution and then hydrates to form carbonic acid (H_2CO_3). Carbonic acid subsequently ionizes into H^+, HCO_3^- and CO_3^{2-} which causes the pH to typically drop by 3 units [8, 10]. With the concomitant dissolution of the cementitious phases, the nucleation of calcium silicate hydrate (C-S-H) and the precipitation of $CaCO_3$ proceeds [11, 12]. Carbonation activated steel slag has been successfully used in masonry unit production. Compared to Portland cement masonry, steel slag bonded blocks are heavier which limits their application in construction.

Wood particles are another type of mass-produced waste from wood industry. Wood particles can be recycled as partial replacement of sand and coarse aggregate. However, most research targeted wood ash and saw dust [13], [14], [15], [16]. Other studies used olive wood waste, wood chipping and recycled wood towards the production of masonry blocks [17], [18], [19]. Main conclusions were that the addition of wood to the cementitious matrix retarded the hydration reaction and negatively affected the mechanical strength. There seems to be a consensus among researchers that the developed wood-concrete is suitable for non-load bearing purposes [20]. Other researchers used coconut shells as a replacement of coarse aggregate in concrete and noted that the strength decreased as the replacement ratio of shells increased [21]. Nonetheless, addition of wood has a positive impact on the overall weight reduction. The use of 25 % palm kernel shells as fine aggregate replacement reduced the weight of reinforced concrete slab by 17.9 % [22]. Likewise, the addition of 25 wt. % of wood fiber waste reduced the weight of the masonry block by almost 30 % [15]. Lastly, the addition of wood aggregate significantly improved the thermal insulation capacity of concrete [23].

Up to now, little to no attention has been paid to the adoption of carbonation curing to wood-masonry units. There are obvious advantages of wood as an aggregate that need to be exploited by carbonation curing. It is hypothesized that when CO_2 gas reacts with calcium silicates in the presence of water to form thermodynamically stable calcium carbonates, these might act as a nano-reinforcement possibly strengthening the weak matrix resulting from the substitution of strong granite aggregates by weaker wood particles. Moreover, it is expected that wood, owing to its geometry, may provide the composite with additional surface area and porosity to promote CO_2 diffusion and, consequently, a higher degree of carbonation [24]. Furthermore, as the long-term durability of wood is compromised in an alkaline medium, carbonation curing could solve this problem by effectively consuming $Ca(OH)_2$ and ultimately providing a low alkaline medium suitable for wood preservation. Wood is also highly hygroscopic, which would reflect negatively on the absorption characteristics of the end-product. To this end, carbonation curing could decrease the porosity of the matrix, mitigating the high absorption characteristic accompanying the replacement of granite by wood. On another hand, the interfacial transition zone (ITZ) is regarded as the weakness in composite materials. The higher porosity and defects characterizing this zone affect the mechanical as well as the durability performance of the end product and its susceptibility to various deleterious solution invasion. Thus, it is expected that carbonation curing might improve the bond and decrease the porosity in the ITZ giving rise to an improved overall performance.

In this light, the focus of this research is to valorize wood-steel slag concrete through adopting carbonation curing. The carbonation curing of steel slag masonry units incorporating recycled wood aggregates partially replacing crushed fine granite sand is studied as a function of CO_2 curing duration. The formed masonry units were subjected to a combined carbonation and hydration curing scheme to promote the ultimate strength development. The effect of the addition of wood to the matrix on the performance was studied in terms of mechanical and physical properties. Lastly, the ITZ between wood and steel slag was investigated and the Ca/Si ratios were reported.

5.2 Experimental program

5.2.1 Materials

Steel slag was sourced from Harsco Environmental Quebec, Canada and was identified by the supplier as ladle slag. Ladle slag is the by-product of the steel refining process. Its' mineralogy is dependent on the appended fluxes, deoxidizing agents, and cooling process. The as-received slag contained clumps that were first sieved out using an 850-μm sieve. The powder passing through the sieve was pulverized to a finer powder using a ring-and-puck mill (90 s per half-kilogram slag) to ensure homogeneity. Only slag powder that passed through a 150-μm sieve was used in this study. The major oxide components were identified by X-ray fluorescence (XRF) whereas the mineralogical phases were determined by quantitative X-ray diffraction (Q-XRD) analysis using 10 % TiO_2 as an internal reference and are presented in Table 5-1 and 5-2 respectively. The characteristics of the used steel slag are summarized in Table 5-3.

Wood aggregates selected for this study were sourced from a local wood mulch warehouse, Les Sciures Jutras Quebec, Canada. The facility specializes in recycled wood mulch for various uses. They receive mostly pallets and random wood waste where the wood is chopped down using a hammer mill to numerous sizes controlled by the in-feed grinder's screen size. The sourced wood aggregates were of size 2 to 5 mm and were air-dried to a constant moisture content of 5 %. The percent absorption was approximately 67 % and the oven dry unit weight was approximately 248 kg/m^3.

The fine aggregate used in this study was crushed fine granite sand with a fineness modulus of 3.55 and particle size ranging from 0 to 5 mm. The coarse aggregate was crushed coarse granite with a fineness modulus of 5.65 and particle size lying in the range of 5 to 10 mm. The percent absorption was approximately 1.12 and 1.14 % for fine and coarse granite respectively and the oven-dry unit weight was 2500 kg/m^3. The sieve analysis results are shown in Fig. 5-1. Water for different slag-bond masonry unit (SMU) mixes consisted of mix water plus water needed to bring the wood to 30 % SSD. Adding more water resulted in a wet mix that was not deemed suitable for the dry mix procedure adopted for the production of masonry units. It should be noted that water is a key parameter for the production of carbonation-cured products because carbonation curing is a diffusion-controlled phenomenon. The hygroscopic nature of wood is also expected to change the effective water to slag ratio of the mix. Therefore, after several trials and errors it was concluded that presoaked wood with 30 % SSD yielded the best carbonation outcome for the wood-steel slag matrix.

5.2.2 Wood-slag masonry unit fabrication and curing process

Several wood-slag masonry units with various wood ratios as replacement of fine aggregates were fabricated. The selection of the presented mix designs, summarized in Table 5-4, was done on the basis of the mode of failure following 24 hours of carbonation curing. Compared to sand, wood has much lower cohesion capabilities such that beyond a certain wood content the matrix becomes less cohesive and subsequently the mode of failure of the concrete slab changes and failure occurs at the wood slag interface in the form of crushing. In this context, several batches were preliminary selected, and it was noted that beyond 50 % by volume of wood replacement the mode of failure changed and thus was deemed inappropriate for this study. It should be noted that masonry units are composed of almost 70-90 % of aggregates and 10-30 % of binder, thus the success of this composite depends immensely on the cohesion capabilities of the aggregate rather than the binding capabilities of the binder.

Wood chips shown in Fig. 5-2A were prewet to a moisture content of 30 % SSD and left overnight in tight-sealed containers to absorb the water. Slag and crushed granite aggregate (fine and coarse) were added first to the mixer and dry mixed for 2 minutes. Afterwards, the prewetted wood aggregates were added to the mix and homogenized for an additional 2 minutes. Once all constituents homogenized, mix water was gradually added and mixed for 5 minutes. The mix was hand placed in the mold of dimensions 127 x 76 mm and then compacted using a jackhammer to a thickness of 30 mm such that the formed block simulated the web of a masonry unit (Fig. 5-2B). The concrete samples were then subjected to distinct curing scenarios to obtain carbonated-only SMU, combined carbonated-hydrated SMU and hydrated-only SMU.

For carbonated-only SMU, the concrete samples were preconditioned for 2 hours in mold in front of a fan to evaporate approximately 35 % of the water to create pathways to facilitate CO_2 gas penetration. Afterward, the conditioned samples were transferred to a pressure chamber for carbonation curing which was conducted under ambient conditions (25 ± 2 ℃; 30 % RH). The experimental apparatus used is presented in Fig. 5-2. In the chamber, the samples were subjected to pure CO_2 gas at a pressure of 150 KPa. The regulator assured that the pressure was maintained in the chamber such that CO_2 was continuously replenished to counter the pressure drop arising from the reaction. Several carbonation durations (4 hours, 12 hours, and 24 hours) were selected to monitor the CO_2 uptake and performance of different SMUs. Two samples were cured in the carbonation chamber each run.

For combined carbonated-hydrated SMUs samples after carbonation curing for the designated duration were transferred to airtight plastic bags for subsequent hydration curing for 28 days at 25 ± 2 ℃ to maximize strength gain.

Hydrated-only concrete blocks were placed in air-tight plastic bags, immediately after demolding for 28 days of sealed curing at 25 ± 2 ℃. These samples served as reference and served to highlight the effect of carbonation curing on the properties of produced SMU.

5.2.3. Temperature and relative humidity

Temperature and relative humidity are key parameters that influence the carbonation process of steel slag. The exothermic nature of carbonation reaction was monitored using a wireless temperature and relative humidity HOBO MX2300 data logger placed inside the carbonation chamber. The logger was configured to collect data every 30 sec during the carbonation process.

5.2.4 CO_2 uptake, water loss and curing degree

CO_2 uptake was assessed on the basis of the mass gain method according to the calculation provided by Eq. 1. The carbonation reaction in calcium silicate systems resulted in mass increase of the specimens accompanying the formation of carbonation products. Therefore, specimens' mass was tracked before and after the carbonation reaction to note this mass-change ($Mass_{initial\ specimen}$ and $Mass_{carbonated\ specimen}$ in Eq. 1). Also, when CO_2 reacted with raw slag, both water binding and water release took place during the reactions. The evaporated water that condensed on the internal walls of the carbonation chamber was carefully recovered using an absorbent paper and weighed ($Mass_{\ collected\ water}$ in Eq. 1). Since not all vaporized water can be collected, values obtained by the mass gain method represent a minimum conservative estimate. The net mass gain was normalized against the mass of slag powder present initially in the sample ($\mathrm{Mass}_{\mathrm{slag\ powder}}$ in Eq.1)

$$CO_2\ \text{Uptake}\ (\%) = \frac{Mass\ carbonated\ specimen\ (g) + Mass\ collected\ water(g) - Mass\ initial\ specimen(g)}{Mass\ slag\ powder(g)} \qquad (1)$$

5.2.5. Compressive strength

After the desired curing age, SMU specimens were tested for compressive strength using an MTS-SINTECH 30/G tension and compression tester equipped with a of 75 KN load cell. The test speed was set to 0.5 mm/min. Three specimens were tested and averaged for each curing scenario.

5.2.6 Density and water absorption

ASTM C-90 classifies masonry units into three categories based on the density: lightweight, medium weight and normal weight such that the ranges for density in each class is less than 1680 kg/m^3, between 1680 and 2000 kg/m^3, and more than 2000 kg/m^3 respectively. Acknowledging the fact that some of the water may vaporize or engage in subsequent hydration, all density measurements carried out on different SMU samples were performed following oven drying at

105 °C until samples reached constant mass. Water absorption testing was evaluated according to the recommendations of ASTM C140 (2016) on samples of age 28 days. Again, all results were average of three samples.

5.2.7 Microstructure Analysis

The microstructure of carbonated-only and hydrated-only steel slag-wood SMUs/cubes was studied through scanning electron microscope imaging. Both secondary electron (SE) and back scattered electron (BSE) modes were used to characterize the samples using a Hitachi SU3500 equipped with energy dispersive X-ray spectroscopy (EDS). EDS analysis was performed to identify the different phases in carbonated and hydrated samples.

Special samples were prepared for SEM analysis to exclude the interference of granite aggregates on the transition zone, following the recommendation of [25, 26]. Steel slag was mixed with wood particles and water and formed into small cubes of 2-cm, compacted using a vibration hammer. The cubes were subjected to 2 distinct curing scenarios. Half of the cubes were submitted to sealed hydration for of 28 days and the other half were only carbonated for 24 hours in the carbonation chamber. The aim was to study the influence of each curing scenario (hydration-only and carbonation-only) on the interface between the wood and the steel slag. It should be noted that the conditions adapted for carbonation and hydration were the same as those of the masonry unit samples. After curing, the cubes were cut through the middle using a diamond saw with alcohol applied as lubricant to obtain 3 mm thick square samples. The obtained samples were dried overnight at 105 °C and then embedded in resin disks (ø 42 mm) followed by impregnation with an epoxy resin. The resin impregnation is considered a crucial step for the preservation of the microstructure against the abrasion induced by specimen preparation. The samples were further submitted to a series of grinding and polishing with diamond particle liquid in an automatic MetPrep 4^{TM} grinder/polisher machine (ALLIED HIGH TECH).

For morphology identification in SE mode, fractured surfaces from the cube samples were used. Both fractured and polished samples were coated with a thin layer, approximately 5 µm, of gold prior to observation to improve conductivity of the samples.

5.3 Results

5.3.1 Fluctuations in temperature and relative humidity

The typical temperature and relative humidity profiles are shown in Fig. 5-4 A and B respectively. Remarkably, in all mixes the temperature peaked at around 1-2 hours after CO_2 injection and then declined gradually to almost the same temperature of 25 °C following 8 hours of CO_2 injection and remained constant till the end of the curing period. The rapid increase in temperature implied that the carbonation reaction delineated in Eq (2) is exothermic [10].

$$(2CaO \cdot SiO_2) + (2-x)\ CO_2 + yH_2O \rightarrow x\ CaO \cdot SiO_2 \cdot yH_2O + (2-x)\ CaCO_3 \qquad (2)$$

The decrease in temperature that followed the peak did not signify the end of the carbonation reaction but rather a slowing down of the reaction rate that was linked to the reduced availability of free particles. The carbonation reaction in real time was inhibited by the barrier effect [27] where the amassed precipitation of $CaCO_3$ hindered the CO_2 diffusion into the binding matrix [28] and caused a leveling off of the reaction. It should be noted that since the carbonation chamber was not insulated, the recorded temperatures were conservative estimates as the heat loss could not be controlled. Nevertheless, since all tests were run under the same conditions a comparison between specimens was nonetheless valid.

It was interesting to note the difference in the temperature peaks recorded in samples incorporating wood and those with no wood (Fig. 5-4A). The highest temperature (36 °C) was recorded in SMU50 followed by SMU15 (35 °C) whereas the lowest (31.5°C) was recorded in SMU0. Obviously, the addition of the organic particles to the steel slag matrix affected the carbonation reaction. The increase in the replacement ratio of fine aggregates by wood particles caused an increase in the peak temperature which could be interpreted as a stronger reaction of gamma-C_2S, the main constituent of the used ladle slag (Table 5-2). This could reflect a deeper penetration of the CO_2 gas in the wood-steel slag matrix. Figure 5-5 shows SMU samples after being sprayed with phenolphthalein. Phenolphthalein is a pH indicator that displays dark pink (fuchsia) at pH of 12-13, pink at pH 12 -8.2 and turns colorless at pH below 8.2. Samples with no wood after 4 hours of carbonation only had a colorless surface layer while the core was pink indicating that the carbonation reaction occurred only at the surface. Extending the carbonation reaction to 12 and 24 hours seemed to allow for a deeper CO_2 penetration such that the carbonation front reduced significantly. The high temperatures recorded in SMU35 and SMU50 (Fig. 5-4A) were corroborated with a deep and homogeneous carbonation front such that samples incorporating wood showed a completely colorless surface after 4 hours of carbonation.

Upon CO_2 injection, the relative humidity (Fig. 5-4B) in the chamber increased rapidly from 35 % to a peak of 75 % in SMU with and without wood. After almost 2 hours of carbonation, the relative humidity decreases and then was maintained at a value of 70 % for all samples throughout the carbonation duration. The jump in the relative humidity recorded was induced by the initial water evaporation from the samples caused by the heat release by the exothermic carbonation reaction. According to [29] and [30], the optimal conditions for an effective accelerated carbonation curing lies in the range of 60 to 75 % which were the conditions at which subsequent carbonation reactions were conducted.

The difference in the shape of the temperature and RH curves between the wood bearing samples and those with no wood was particularly notable. The steep slope of the dropping portion of the latter curves, as opposed to the gentle curves of samples without wood aggregates reflected the difference in the physiochemical behavior of these samples. Both granite and wood are fairly good thermal insulators, do not conduct heat readily, but the presence of water, one of the substances with the highest heat capacity, in the wood fibers could explain the observed difference. This feature could have caused the samples incorporating wood aggregates to retain heat for longer periods and ultimately led to a more efficient carbonation reaction in wood-bearing SMUs.

5.3.2 Water loss and CO_2 curing degree

The variation of the normalized water loss with carbonation duration is depicted in Fig. 5-6A. Normalized water loss was calculated as the ratio of the mass of water lost during the carbonation process to the initial mass of water present in the specimen. In general, water loss increased with carbonation duration for SMUs with and without wood. Normalized water loss of SMU50 and SMU35 increased respectively, from 24 to 30 % and from 16 to 25 % as the carbonation duration increased from 4 to 24 hours which was higher than those recorded for SMU0 (from 6.6 to 20%). Water loss increased with the increase in the wood replacement ratio.

The CO_2 uptake recorded in samples subjected to varying carbonation durations is portrayed in Fig. 5-6B. CO_2 uptake increased with the carbonation duration in samples with and without wood. The highest CO_2 uptake was recorded in SMU50 samples at 16 % per 24 hours of carbonation, followed by 15 % in SMU35 and 13 % in samples with no wood. Considering the linear relation between CO_2 uptake and normalized water loss (Fig. 5-7A), it could be inferred that with the increase in water loss a higher degree of carbonation could be achieved. The water loss contributed towards a higher porosity which, in turn, created pathways for CO_2 penetration.

Moreover, with the introduction of wood to the matrix, the CO_2 uptake capacity increased with the replacement ratio of fine aggregates by wood, irrespective of the carbonation duration. The wood replacement ratio affected the CO_2 uptake. It varied linearly for short carbonation durations of up to 4 hours but varied logarithmically for longer durations of 12 and 24 hours of carbonation curing. This behaviour seemed to comply well with the barrier effect theory which implies a decline in CO_2 uptake potential with the increase in carbonation duration attributed to the formed carbonation products limiting further reaction. Nonetheless, the correlation between CO_2 uptake and wood replacement ratio for different curing scenarios (Fig. 5-7B) along with the findings of Fig. 5-6 suggested that the addition of wood facilitated water loss and consequently promoted a higher degree of carbonation. This phenomenon could be attributed to the geometry of wood particles.

5.3.3 Compressive Strength

The results displayed in Fig. 5-8 represent the compressive strengths recorded in different SMU samples subjected to distinct curing scenarios. Compared to sealed hydration curing, carbonation curing significantly improved the performance of all SMUs. A peek at the steel slag mineral composition (Table 5-2) would aid in explaining the observed results. The main mineral in raw slag, at 53.1 wt. % was calcio-olivine (γ-Ca_2SiO_4), a mineral proven to have no hydraulic activity. Ultimately, this mineral's binding potential would not prevail unless subjected to carbonation curing. The minerals that are inherently hydraulic on their own albeit to varying degrees are: mayenite ($12CaO_7Al_2O_3$), periclase (MgO), larnite (β-Ca_2SiO_4), and jasmundite ($Ca_{10.5}Mg_{0.5}Si_4SO_{18}$). These secondary minerals make up approximately 36.9 % of the steel slag. For carbonated-only SMUs, the strength increased as the carbonation duration increased. SMU0 could meet the standard strength requirement (ASTM C90, 13.8 MPa) after 4 hours of carbonation curing only, as SMU35 met the standard after 24 hours of carbonation curing. However, SMU50 could not meet the standard requirement (13.8 MPa) after up to 24 hours of carbonation. Subsequent hydration was necessary for all samples to optimize their performance. After 4 hours of carbonation curing followed by 28 days of hydration curing, the ultimate strength recorded in SMU0 was 16 MPa which increased to 25 MPa following 24 hours of carbonation curing as opposed to 9.5 MPa for hydrated-only SMU0. The same phenomenon was also observed for SMU35 and SMU50. As the carbonation duration increased so did the ultimate strength recorded after 28 days of hydration which was much higher than the strength recorded for 28-day hydrated only samples. The ultimate strength recorded in SMU35 was 20.5 MPa and 5 MPa for carbonated and hydrated samples respectively. Measured strengths for SMU50 were 17 and 4 MPa for carbonated and hydrated samples, respectively.

Extending the carbonation period from 12 to 24 hours in SMU35 and SMU50 resulted in a respective strength gain of 4.5 MPa. In SMU0, the strength gain by extending the carbonation period was only 2 MPa, signifying minimal strength gain due to extending the carbonation curing duration in SMU0. The increase in strength noted in SMU35 and SMU50 implied a continued CO_2 penetration owed to a more porous structure resulting from the addition of wood particles and thus a higher efficiency of carbonation reaction. Extending the carbonation duration to 24 hours was beneficial for wood incorporating units, the same however cannot be said about units with no wood.

Replacement of fine aggregates by wood particles affected the compressive strength. Nonetheless, SMU35 and SMU50 at 28 days of hydration after carbonation surpassed the strength requirements of ASTM C90 for load bearing masonry units (13.8 MPa) following 12 and 24 hours of carbonation curing. Thus, it could be inferred that wood employed in a steel slag matrix could be used for load-bearing purposes owed primarily to the carbonation reaction. To study the contribution of the carbonation reaction to strength, comparing the performance of carbonated SMUs to hydrated-only SMUs would not do it justice as steel slag is a weakly hydraulic binder. Thus, evaluation was based on the performance of SMU35 and SMU50 relative to SMU0. Table 5-4 presents the strength reduction resulting from replacing fine aggregates by wood particles. Strength reduction is the percentage of decrease in the strength of SMU35 or SMU50 at 28 days of hydration after carbonation with respect to its corresponding strength in SMU0 at 28 days. In hydrated-only SMUs, the replacement of fine aggregates by wood resulted in a strength reduction of 47 % and 74 % in SMU35 and SMU50 respectively. However, with the introduction of CO_2 curing, the strength reduction was 41 % after 4 hours of carbonation curing and declined to 18 % after 24 hours of carbonation curing in SMU35. The same phenomenon was also observed in SMU50 where the strength reduction decreased to 56 % with 4 hours of CO_2 curing and further reduced to 32 % after 24 hours of carbonation curing. Thus, the introduction of CO_2 curing evidently improved the performance of masonry units. Furthermore, the increase in the carbonation duration seemed to compensate for the decrease in strength.

These observations validated the potential of using CO_2 curing process to improve the mechanical performance of wood-incorporating masonry units and ultimately resulted in a product suitable for loadbearing uses.

5.3.4 Density and water absorption

The density profiles of masonry units subjected to various carbonation durations with and without wood are presented in Fig. 5-9. The highest densities were recorded in SMU0 at 2163, 2300 and 2317 kg/m^3 following 4, 12 and 24 hours of carbonation curing, respectively. These values rendered SMU0 within the normal weight category. Introduction of 35 % by volume of wood aggregates significantly dropped the densities to 1686, 1728 and 1896 kg/m^3 respectively. The lowest densities were recorded in SMU50 at 1541, 1632 and 1680 kg/m^3 respectively. Thus, SMU35s fit the medium weight category whereas the SMU50s fit the lightweight category. As revealed by the data reported above, the density increased with the carbonation duration. Increasing the carbonation duration led to an increase in CO_2 uptake (Fig. 5-5B) which translated into more precipitated calcium carbonates and an increased density. Considering the obtained density profiles and the almost comparable strength performance (Fig. 5-8), the SMU35s were an improved version of SMU0s. SMU35 combined the elements of high performance while maintaining a low density. This was also reflected in the relationship between density and compressive strength (Fig. 5-10). The weak correlation indicated that the strength did not decrease linearly with the decrease in density owing to the carbonation induced precipitation of $CaCO_3$. This observation contrasts with the results of hydrated-only OPC wood-masonry units reported in other studies whereby the compressive strength was reported to decrease linearly with the decrease in density [15, 31].

Water absorption values recorded in different SMUs are reported in Table 5-6. The highest absorption values were recorded in hydrated-only specimens with SMU containing 35 and 50 % of wood have absorption values of 220 and 281 Kg/m^3, respectively. With the introduction of carbonation curing, the absorption values significantly decreased. This decrease seemed to increase with the increase in carbonation duration. The lowest absorption values recorded in 35 and 50 % wood SMUs were 107 and 190 Kg/m^3, respectively, following 24 hours of carbonation curing. Prolonged carbonation curing significantly decreased the absorption capacity of wood-SMU. The absorption of SMU0; however, did not seem to be affected by the carbonation duration.

Nonetheless, all masonry units met the water absorption requirements set by ASTM C90 (288, 240 and 208 Kg/m^3 for lightweight, medium weight and normal weight masonry units respectively).

5.3.5 Interfacial transition zone (ITZ)

The bonding between wood aggregates and steel slag paste has a major impact on the mechanical strength of the developed wood-slag concrete. Therefore, the enhancement of the binding properties in the ITZ can effectively improve the structural performance of wood-slag concrete. Accordingly, EDS coupled with BSE-SEM was adopted to study the Ca/Si distribution in the ITZ and the bulk slag matrix.

Typical SEM-BSE images featuring the interface between wood aggregates and steel slag matrix in both hydration-cured and carbonation-cured samples are shown in Fig. 5-11 and Fig. 5-13, respectively. The darker areas in the micrographs designated the carbon rich, wood particles, whereas the lightest areas designated the unreacted steel slag minerals. The black areas designate the presence of voids and/or cracks.

Morphological characterization of the ITZ between wood particles and hydrated steel slag matrix allowed for the identification of what seemed like a two phase ITZ-matrix: inner matrix and outer matrix. The inner ITZ matrix, adjacent to the wood particle consisted of steel slag remnants on the wall of the wood and a gap while the outer ITZ matrix consisted of a zone of loosely deposited hydration products. In Fig. 5-11A, a visible distinctive crack was observed in the hydrated-only sample in what appeared to be the inner matrix of the interface between wood and steel slag paste which probably reflected the lack of adhesion between both entities. The evident crack in the interface could also be attributed to drying shrinkage occurring in the weak and loose ITZ matrix. Furthermore, a segment of poorly packed elements was also observed which was designated as the outer matrix of the ITZ. Beyond that, a large number of unreacted steel slag minerals were observed in the bulk steel slag matrix which could be traced back to the poor hydraulic property of the used steel slag, as was confirmed through the compressive strength performance of hydrated samples (Fig. 5-8). The EDS spot 1 showed an unreacted calcium silicate grain. Fig. 5-11B displays a zoomed-in image of the ITZ between wood-slag in hydrated only sample. The adjacent EDS spot suggested that this loosely packed product was $Ca(OH)_2$. Lastly, based on data collected from more than six locations, the width of the ITZ between wood and hydrated steel slag paste matrix was estimated at 65 μm. The line analysis shown in Fig. 5-12, taken over a span of 120 μm, seemed to confirm these findings. Wood rich in carbon was located to the left of the graph, after which a void identified as the inner ITZ occupied a distance of 45 μm. The outer ITZ matrix, rich in calcium deposits, was almost 20 μm thick.

In Fig. 5-13A, a smooth continuous interface between wood and steel slag paste could be clearly observed. Hence, the carbonated steel slag appears to adhere intimately to wood aggregates leading to a compact and uniform interface. It would appear that the wood was contacted soundly and smoothly in the areas where epoxy had infiltrated. Some exposed lumina revealed evidence of mineralization by calcium rich products. EDS point 1 revealed that these deposits were likely precipitated $CaCO_3$. However, this cannot be confirmed by BSE-EDS analysis alone as the high carbon content of the wood cell walls could affect the results. Fig. 5-13B shows a zoomed-in image on the ITZ between the wood and steel slag paste. The image showed fewer unreacted steel slag particles compared to hydrated samples, confirming the ability of carbonation curing to effectively activate the reaction of steels slag minerals. The accompanying EDS spot 2 showed the presence of a C-S-H with low Ca/Si at the interface between the wood and the carbonated steel slag. To further investigate this observation, an EDS line scan was carried out on a carbonated sample. Fig. 5-14 displays the changes in elemental composition up to 70 μm from the face of wood. Wood is rich in carbon while the bulk paste matrix is a mix of silica, carbon, calcium, and oxygen. Based on the line analysis, the wood element was identified to be to the right over the span of 70 to 85 µm. In the interface and approximately over a 10 µm span, the region was rich in Si and had a low Ca/Si, as revealed by the EDS spot analysis (Fig. 5-13B, EDS spot 2). Further away from the interface and approaching the bulk steel slag matrix, an increase in Ca/Si was observed. To follow up on this finding, the Ca/Si ratio was reported in the 10 µm region surrounding the wood aggregates and in the bulk steel slag paste. At least 50 points were collected from 5 different locations for each sample. The collected data are presented in Fig. 5-15. The Ca/Si was marginally higher in the bulk matrix at around 1.8, compared to the ratio immediately at the wood-steel slag interface (1.6). This might suggest that minute differences existed between ITZ and bulk matrix in carbonated wood-steel slag.

Fig. 5-16 A and B shows the SE images obtained from the fractured surfaces of hydrated and carbonated wood-steel slag samples respectively. In Fig. 5-16A, a gap could be seen between the wood and steel slag matrix which backed up the findings of the SEM-BSE images. The wood and hydrated steel slag displayed a weak bonding, and the steel slag matrix had a highly aggregated coarse texture. The zoomed in micrograph of the interface between the wood and hydrated slag revealed the presence of crystalline deposits. The adjacent EDS spot analysis confirmed that the crystalline product was $Ca(OH)_2$. This observation confirmed the findings by SEM-BSE, the interface between wood and hydrated steel slag hosted percentages of $Ca(OH)_2$ crystals. In Fig. 5-16B, a clean smooth interface could be observed in wood-carbonated steel slag samples which reflected a good wood-steel slag bond owed primarily to carbonation curing. Furthermore, the microstructure of the bulk steel slag matrix was much refined compared to the hydrated counterpart. The zoomed in micrograph of the interface revealed the presence of a continuous gel phase which, according to the EDS analysis, was identified as C-S-H. However, the EDS yields strong peaks of carbon which suggested that the carbon was incorporated within the gel phase, giving rise to a hybrid product with improved properties. Similar results were reported by Rostami et al. [32].

To identify the product deposited inside the lumina of wood, SE imaging of the morphology could aid in the characterization. The inside of the wood aggregate (Fig. 5-17) contained an amorphous product ruling the formation of crystalline $Ca(OH)_2$ product. The amorphous product, rich in calcium and carbon, was most likely nano-scaled amorphous calcium carbonates.

5.4 Discussion

5.4.1 Enhancement of mechanical and physical performance

The recycling of wood into masonry blocks can be highly beneficial for limiting natural resource consumption as well as creating an outlet for wood waste, but the negative effects arising from the use of wood should not be overlooked. The substitution of the high-density aggregates with low density wood aggregates reduces the strength such that the developed block is not capable of competing with the commercial block. Table 5-6 presents the compressive strength and the percent reduction in strength recorded in different cement-based masonry units incorporating wood as partial replacement of one of its constituents based on several studies. The strength loss varied from 26 % with 10 % replacement by volume to 80 % with 30 % replacement by volume. However, based on the results of this study (Table 5-4) a 35 and 50 % replacement of fine crushed granite by wood aggregates resulted in an only 18 and 32 % decrease in strength. This showcased the ability of carbonation curing to ameliorate the performance of wood-steel slag masonry units. Carbonation curing also improved the physical performance of wood-steel slag masonry units (Table 5-6). Carbonation curing, owing to the induced calcium carbonate precipitation, limited the hygroscopic tendency of wood aggregates such that the water absorption values of wood-SMU decreased with the increase in carbonation duration, in contrast to the trend noted in wood-free SMU. Moreover, the developed masonry unit used steel slag instead of cement thus effectively limiting the CO_2 emissions and natural resource consumption associated with the use of ordinary Portland cement.

5.4.2 Enhancement of interfacial transition zone

BSE and SE imaging along with EDS analysis revealed a transition zone which was cracked and relatively enriched in $Ca(OH)_2$ crystals in hydrated-only wood-steel slag samples. Unlike C-S-H, $Ca(OH)_2$ does not contribute to strength and its excessive precipitation leads to deterioration in mechanical performance. However, in carbonated-only samples, the ITZ between the wood and steel slag was dense and packed with carbonation products. Upon exposure to CO_2, the calcium-bearing minerals in the ITZ were more likely to lose their Ca ions to the water saturated surface of wood, leading to the formation of C-S-H on the surface of the wood aggregate. Continued exposure to CO_2 led to further release of Ca ions which were capable of penetrating the wood cell walls and precipitating inside (Fig. 5-17). This continued release of Ca ions led to a C-S-H which had a Ca/Si 0.2 orders of magnitude less than that of the bulk steel slag matrix. Higher decalcification of C-S-H in ITZ of wood-steel slag could be explained by the higher permeability of the matrix due to the presence of wood. Nonetheless, the Ca-O binding capabilities of the gel phase were maintained [33]. EDS analysis (Fig. 5-13B, spot 2) revealed that this product was enriched in carbon which reinforced the amorphous phase giving rise to an improved final product. According to [34, 35], the formation of C-S-H is the lead contributor of mechanical strength due to its amorphous structure which promotes adhesion. On this basis, the improved performance of wood-steel slag concrete can be attributed to carbonation curing which led to the formation of C-S-H gel and calcium carbonates in the ITZ. Previous studies of the ITZ of carbonation-cured composites inferred that carbonation curing densified the ITZ and decreased the porosity [25, 36]. However, variations of the Ca/Si between ITZ and bulk matrix had scarcely been addressed, even more so when wood is used as aggregate. Based on the findings of this study, the hygroscopic nature of the wood tends to attract the calcium ions leading to the formation of C-S-H with slightly lower Ca/Si in the ITZ of carbonated wood-steel slag compared to the bulk matrix. This implied that carbonation curing could develop into a composite with little difference between ITZ and bulk matrix thus leading to a stronger bond between aggregate and paste.

5.5 Conclusion

This study explored the feasibility and implications of adopting carbonation curing of wood-steel slag matrix to produce light-weight load-bearing masonry units. Experimental results revealed the following:

1. Over the 24-hour CO_2 curing period the water loss and CO_2 curing degree increased with the increase in wood replacement ratio which could be traced back to the geometry of wood particles facilitating CO_2 diffusion as well as the compartmentalized structure of wood which provided additional space for calcium carbonate precipitation.
2. The addition of wood decreased the compressive strength of carbonated and of hydrated specimens. Carbonation curing enhanced the compressive strength of the developed masonry units. This enhancement effect was more prominent with the increase in carbonation duration.
3. Although slag-bond masonry units (SMUs) incorporating wood amassed more $CaCO_3$ than control SMU, they were not capable of surpassing the strength of control SMU which

reflected the weakness of wood aggregates; nonetheless all carbonated SMU could exceed the standard strength requirement for loadbearing masonry units (ASTM C90).

4. CO_2 curing presents a viable technique for the recycling of wood and steel slag into a high performing lightweight load-bearing masonry unit. The curing also significantly improved the water absorption performance of wood-slag masonry units.
5. BSE micrographs and EDS analyses confirmed the amelioration of the wood-slag transition zone by accelerated carbonation curing through the deposition of carbonation products in the interface. For hydrated-only samples, ITZ could be divided into an inner ITZ which was cracked and highly porous and an outer ITZ matrix that was loosely packed with hydration products namely calcium hydroxide. In carbonation-cured samples, the ITZ was rich in C-S-H and carbon which led to an improved interlocking between both entities.
6. The Ca/Si at the ITZ of carbonated wood-steel slag was almost the same as that in the bulk steel slag matrix leading to a stronger bond between wood and carbonated steel slag. This indicates a homogenous microstructure of the steel slag matrix by carbonation curing.
7. The lightweight masonry units made from carbonation activated steel slag and recycled wood aggregates are environment friendly composite products that are waste-derived, consume no natural resources, sequester carbon dioxide and can be carbon negative.

References

1. Ghouleh, Z., R.I.L. Guthrie, and Y.X. Shao, *High-strength KOBM steel slag binder activated by carbonation.* Construction and Building Materials, 2015. **99**: p. 175-183 DOI: https://doi.org/10.1016/j.conbuildmat.2015.09.028
2. Mahoutian, M., Z. Ghouleh, and Y.X. Shao, *Carbon dioxide activated ladle slag binder.* Construction and Building Materials, 2014. **66**: p. 214-221 DOI: https://doi.org/10.1016/j.conbuildmat.2014.05.063
3. Humbert, P.S. and J. Castro-Gomes, *CO_2 activated steel slag-based materials: A review.* Journal of Cleaner Production, 2019. **208**: p. 448-457 DOI: https://doi.org/10.1016/j.jclepro.2018.10.058.
4. Serjun, V.Z., B. Mirtic, and A. Mladenovic, *Evaluation of Ladle Slag as a Potential Material for Building and Civil Engineering.* Materiali in Tehnologije, 2013. **47**(5): p. 543-550, <Go to ISI>://WOS:000326005900001.
5. Shi, C.J., *Characteristics and cementitious properties of ladle slag fines from steel production.* Cement and Concrete Research, 2002. **32**(3): p. 459-462 DOI: https://doi.org/10.1016/s0008-8846(01)00707-4
6. Mahoutian, M., Y.X. Shao, A. Mucci, and B. Fournier, *Carbonation and hydration behavior of EAF and BOF steel slag binders.* Materials and Structures, 2015. **48**(9): p. 3075-3085 DOI: https://doi.org/10.1617/s11527-014-0380-x
7. Zhang, D., Z. Ghouleh, and Y. Shao, *Review on carbonation curing of cement-based materials.* Journal of CO_2 Utilization, 2017. **21**: p. 119-131 DOI: https://doi.org/10.1016/j.jcou.2017.07.003
8. Fernandez Bertos, M., S.J. Simons, C.D. Hills, and P.J. Carey, *A review of accelerated carbonation technology in the treatment of cement-based materials and sequestration of*

CO_2. Journal of Hazardous Materials, 2004. **112**(3): p. 193-205 DOI: https://doi.org/10.1016/j.jhazmat.2004.04.019

9. Elsalamawy, M., A.R. Mohamed, and E.M. Kamal, *The role of relative humidity and cement type on carbonation resistance of concrete.* Alexandria Engineering Journal, 2019. **58**(4): p. 1257-1264 DOI: https://doi.org/10.1016/j.aej.2019.10.008
10. Young, J.F., R.L. Berger, and J. Breese, *Accelerated Curing of Compacted Calcium Silicate Mortars on Exposure to CO_2*. Journal of the American Ceramic Society, 1974. **57**(9): p. 394-397 DOI: https://doi.org/10.1111/j.1151-2916.1974.tb11420.x
11. Khan, R.I., S. Siddique, and W. Ashraf, *Effects of magnesia in semi-hydraulic and non-hydraulic calcium silicate binders during carbonation curing.* Construction and Building Materials, 2022. **338**: p. 127628 DOI: https://doi.org/10.1016/j.conbuildmat.2022.127628
12. Ghouleh, Z., M. Celikin, R.I.L. Guthrie, and Y.X. Shao, *Microstructure of Carbonation-Activated Steel Slag Binder.* Journal of Materials in Civil Engineering, 2018. **30**(9): p. 04018217 DOI: https://doi.org/10.1061/(asce)mt.1943-5533.0002421
13. Berra, M., T. Mangialardi, and A.E. Paolini, *Reuse of woody biomass fly ash in cement-based materials.* Construction and Building Materials, 2015. **76**: p. 286-296 DOI: https://doi.org/10.1016/j.conbuildmat.2014.11.052
14. Ramos, T., A.M. Matos, and J. Sousa-Coutinho, *Mortar with wood waste ash: Mechanical strength carbonation resistance and ASR expansion.* Construction and Building Materials, 2013. **49**: p. 343-351 DOI: https://doi.org/10.1016/j.conbuildmat.2013.08.026
15. Torkaman, J., A. Ashori, and A.S. Momtazi, *Using wood fiber waste, rice husk ash, and limestone powder waste as cement replacement materials for lightweight concrete blocks.*

Construction and Building Materials, 2014. **50**: p. 432-436 DOI: https://doi.org/10.1016/j.conbuildmat.2013.09.044

16. Page, J., C. Djelal, and Y. Vanhove, *Optimisation of vibrocompaction process for wood-based concrete blocks.* International Journal of Advanced Manufacturing Technology, 2020. **109**(3-4): p. 1189-1204 DOI: https://doi.org/10.1007/s00170-020-05674-3
17. Antoun, M., C.A. Issa, G. Aouad, and N. Gerges, *Sustainable masonry blocks: Olive wood waste as substitute for fine aggregates.* Case Studies in Construction Materials, 2021. **15**: p. e00590 DOI: https://doi.org/10.1016/j.cscm.2021.e00590
18. Stahl, D.C., G. Skoraczewski, P. Arena, and B. Stempski, *Lightweight concrete masonry with recycled wood aggregate.* Journal of Materials in Civil Engineering, 2002. **14**(2): p. 116-121 DOI: https://doi.org/10.1061/(asce)0899-1561(2002)14:2(116)
19. Mohammed, B.S., M. Abdullahi, and C.K. Hoong, *Statistical models for concrete containing wood chipping as partial replacement to fine aggregate.* Construction and Building Materials, 2014. **55**: p. 13-19 DOI: https://doi.org/10.1016/j.conbuildmat.2014.01.021
20. Aigbomian, E.P. and M.Z. Fan, *Development of wood-crete from treated sawdust.* Construction and Building Materials, 2014. **52**: p. 353-360 DOI: https://doi.org/10.1016/j.conbuildmat.2013.11.025
21. Olanipekun, E., K. Olusola, and O. Ata, *A comparative study of concrete properties using coconut shell and palm kernel shell as coarse aggregates.* Building and Environment, 2006. **41**(3): p. 297-301 DOI: https://doi.org/10.1016/s0140-6701(06)82311-8
22. Olutoge, F., *Investigations on sawdust and palm kernel shells as aggregate replacement.* ARPN Journal of Engineering and Applied Sciences, 2010. **5**(4): p. 7-13.

23. Taoukil, D., A. El-Bouardi, H. Ezbakhe, and T. Ajzoul, *Thermal proprieties of concrete lightened by wood aggregates.* Research Journal of Applied Sciences, Engineering and Technology, 2011. **3**(2): p. 113-116.

24. Wang, L., S.S. Chen, D.C. Tsang, C.-S. Poon, and K. Shih, *Recycling contaminated wood into eco-friendly particleboard using green cement and carbon dioxide curing.* Journal of Cleaner Production, 2016. **137**: p. 861-870.

25. Chen, T.F. and X.J. Gao, *Use of Carbonation Curing to Improve Mechanical Strength and Durability of Pervious Concrete.* ACS Sustainable Chemistry & Engineering, 2020. **8**(9): p. 3872-3884 DOI: https://doi.org/10.1021/acssuschemeng.9b07348

26. Savastano Jr, H. and V. Agopyan, *Transition zone studies of vegetable fibre-cement paste composites.* Cement and Concrete Composites, 1999. **21**(1): p. 49-57 DOI: https://doi.org/10.1016/s0958-9465(98)00038-9

27. Zhan, B.J., D.X. Xuan, C.S. Poon, and C.J. Shi, *Mechanism for rapid hardening of cement pastes under coupled CO_2-water curing regime.* Cement and Concrete Composites, 2019. **97**: p. 78-88 DOI: https://doi.org/10.1016/j.cemconcomp.2018.12.021

28. Lu, B., P.P. He, J.H. Liu, Z.Y. Peng, B.X. Song, and X. Hu, *Microstructure of Portland cement paste subjected to different CO_2 concentrations and further water curing.* Journal of CO_2 Utilization, 2021. **53**: p. 101714 DOI: https://doi.org/10.1016/j.jcou.2021.101714

29. Shi, C.J. and Q.Y. Zou, *Use of CO_2 as an Accelerated Curing Agent for Concrete Blocks.* Advances in Concrete and Structures, 2009. **400-402**(2): p. 81-+ DOI: https://doi.org/10.4028/www.scientific.net/kem.400-402.81

30. Kuo, W.Y., J.S. Huang, and C.H. Lin, *Effects of organo-modified montmorillonite on strengths and permeability of cement mortars.* Cement and Concrete Research, 2006. **36**(5): p. 886-895 DOI: https://doi.org/10.1016/j.cemconres.2005.11.013

31. Aigbomian, E.P. and M. Fan, *Development of Wood-Crete building materials from sawdust and waste paper.* Construction and Building Materials, 2013. **40**: p. 361-366 DOI: https://doi.org/10.1016/j.conbuildmat.2012.11.018

32. Rostami, V., Y.X. Shao, A.J. Boyd, and Z. He, *Microstructure of cement paste subject to early carbonation curing.* Cement and Concrete Research, 2012. **42**(1): p. 186-193 DOI: https://doi.org/10.1016/j.cemconres.2011.09.010

33. Kunther, W., S. Ferreiro, and J. Skibsted, *Influence of the Ca/Si ratio on the compressive strength of cementitious calcium–silicate–hydrate binders.* Journal of Materials Chemistry A, 2017. **5**(33): p. 17401-17412 DOI: https://doi.org/10.1039/c7ta06104h

34. Prokopski, G. and J. Halbiniak, *Interfacial transition zone in cementitious materials.* Cement and Concrete Research, 2000. **30**(4): p. 579-583 DOI: https://doi.org/10.1016/s0008-8846(00)00210-6

35. Chen, X., G. Wang, Q. Dong, X. Zhao, and Y. Wang, *Microscopic characterizations of pervious concrete using recycled Steel Slag Aggregate.* Journal of Cleaner Production, 2020. **254**: p. 120149 DOI: https://doi.org/10.1016/j.jclepro.2020.120149

36. Kottititum, B., Q.T. Phung, N. Maes, W. Prakaypan, and T. Srinophakun, *Early Age Carbonation of Fiber-Cement Composites under Real Processing Conditions: A Parametric Investigation.* Applied Sciences-Basel, 2018. **8**(2): p. 190 DOI: https://doi.org/10.3390/app8020190

37. Abed, J.M. and B.A. Khaleel, *Effect of wood waste as a partial replacement of cement, fine and coarse aggregate on physical and mechanical properties of concrete blocks units.* International Journal of Integrated Engineering, 2019. **11**(8): p. 229-239.

38. Enţuc, I.-S., D.N. Isopescu, L.C. Bagdasar, G. Oprişan, I.D. Zapodeanu, and S.G. Maxineasa, *Performances of Concrete Masonry with Recycled Wood Chips (II).* Buletinul Institutului Politehnic din lasi. Sectia Constructii, Arhitectura, 2019. **65**(1): p. 9-15.

Tables

Table 5-1 Chemical composition of as-received steel slag.

SiO_2	Al_2O_3	Fe_2O_3	MnO	MgO	CaO	Na_2O	K_2O	LOI
23.37	4.02	7.71	1.21	11.09	46.59	0.04	< 0.01	3.53

Table 5-2 Mineral composition of as-received steel slag (wt. %).

Mineral Compound	Chemical formula	
Calcio-olivine	γ-Ca_2SiO_4	53.1
Mayenite	$Ca_{5.65}Al_7O_{16.15}$	15.3
Periclase	MgO	10.0
Cuspidine	$Ca_4Si_2O_7(F, OH)_2$	1.0
Jasmundite	$Ca_{10.5}Mg_{0.5}Si_4SO_{18}$	9.7
Larnite	β-Ca_2SiO_4	3.0
Amorphous		7.9

Table 5-3 Characteristics of steel slag paste.

Density (g/cm^3)	3.4
Fineness	
Passing 325 mesh (%)	65
Compressive Strength (MPa)	
24-hr carbonation	44
24-hr carbonation+ 28-day hydration	70
28-day hydration	17

Table 5-4 Mix proportions of steel slag masonry units by volume.

Mix design	Slag	Wood	Fine crushed granite	Coarse crushed granite	Mix Water
SMU0	1.0(1.0)	0.0(0.0)	3.68(2.7)	0.3(0.2)	1.1(0.3)
SMU35	1.0(1.0)	1.27(0.14)	2.41(1.74)	0.3(0.2)	1.1(0.3)
SMU50	1.0(1.0)	1.84(0.2)	1.84(1.3)	0.3(0.2)	1.1(0.3)

Table 5-5 Strength reduction inflicted by wood addition

Strength Reduction (%)							
SMU35				SMU50			
4C28dH	12C28dH	24C28dH	28dH	4C28dH	12C28dH	24C28dH	28dH
41	30	18	47	56	41	32	74

Table 5-5 Physical performance of different SMU

Absorption (Kg/m^3)											
SMU0				SMU35				SMU50			
4C28dH	12C28dH	24C28dH	28dH	4C28dH	12C28dH	24C28dH	28dH	4C28dH	12C28dH	24C28dH	28dH
106	71	80	165	193	145	107	220	256	220	190	281

Table 5-6 Comparison of literature based on studies of wood-cement masonry units

Previous work	Type	Replacement ratio	Target product	Component replaced	28-day f'c (MPa)	Percent reduction (%)	Density (kg/m^3)
Stahl. et al [18]	wood particles	6 % by weight	masonry unit	replace fine aggregate	6.7	-	-
Khaleel et al. [37]	wood waste aggregate	0 % by volume	masonry unit	replace coarse aggregate	33.8	-	2432
		10 % by volume			24.9	26	2300
		15 % by volume			21.6	36	2157
		20 % by volume			17.2	49	2047
		25 % by volume			9.3	72	1887
		30 % by volume			6.8	80	1758
Entuc et al. [38]	wood chips	50 % by volume	masonry unit	replace total volume of aggregate	2.8	-	1182
		25 % by volume			8.5	-	1739
Mohammed et al.[19]	wood chipping	0 % by volume		replace sand	40.3	-	1915
		10 % by volume			36.5	9	1808
		15 % by volume			33.2	18	1755
		20 % by volume			28.6	29	1688
		30 % by volume			17.3	57	1554

Figures

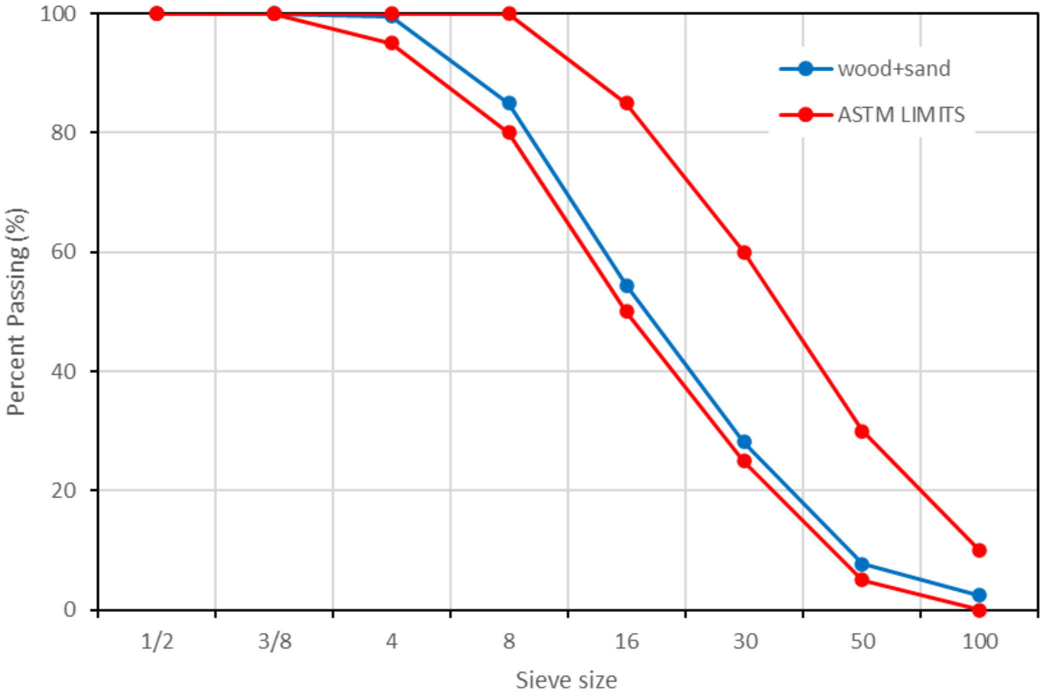

Figure 5-1 Sieve analysis of wood and crushed fine granite aggregates.

Figure 5-2 (A) Recycled wood aggregates, (B) Typical wood-SMU.

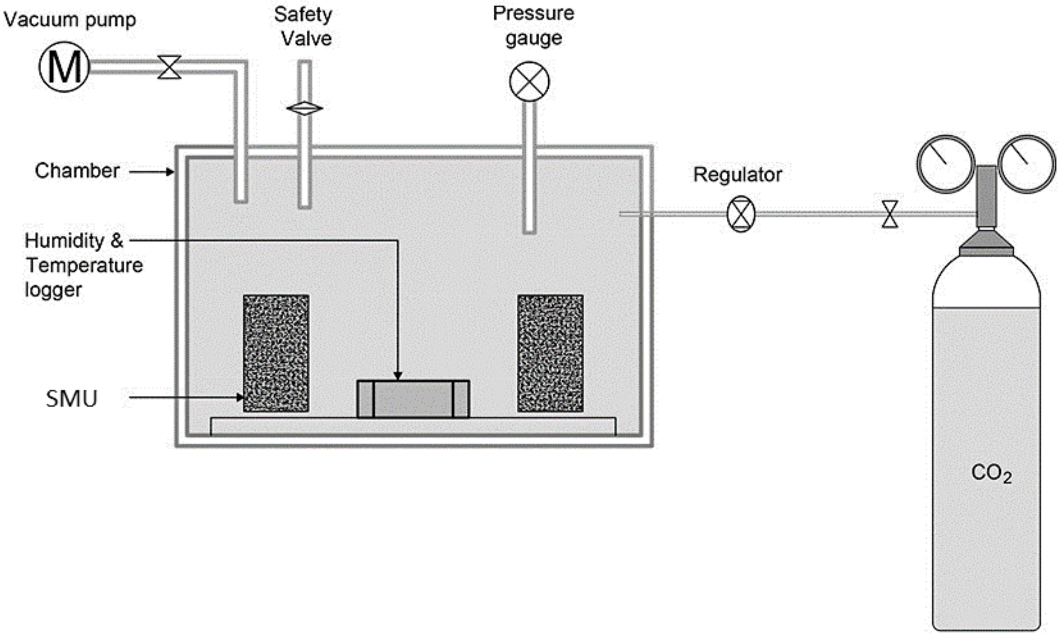

Figure 5-3 Carbonation setup for different SMU samples.

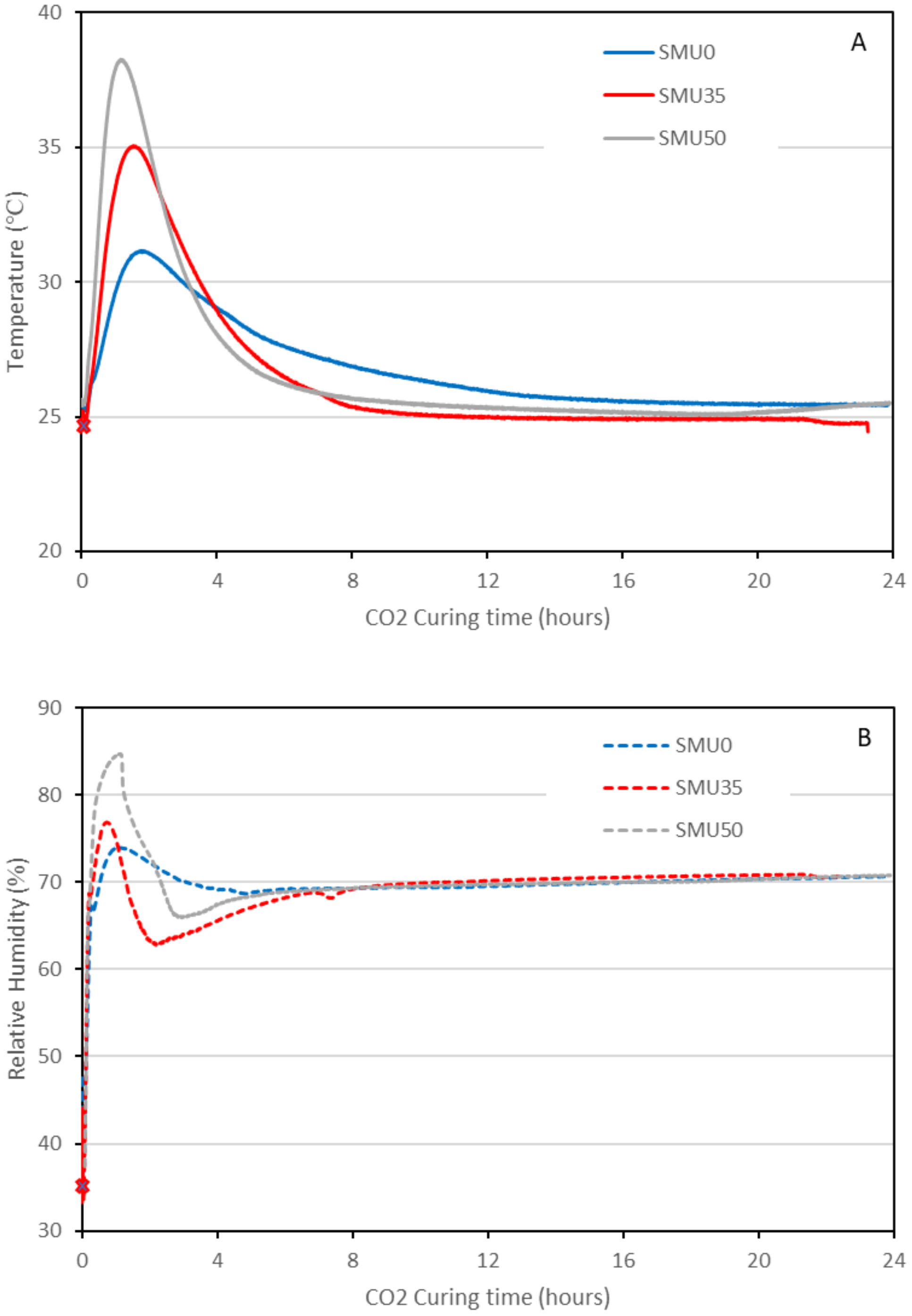

Figure 5-4 (A) Temperature and (B) Relative humidity in carbonation chamber of SMU samples.

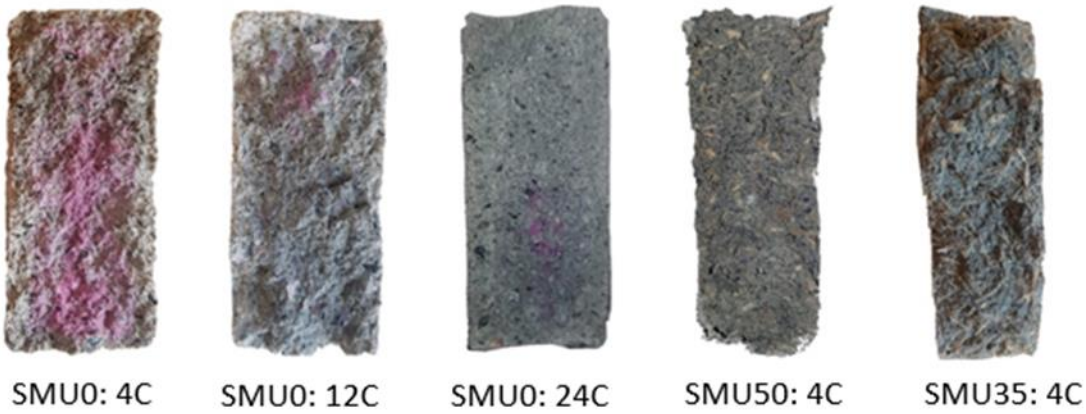

Figure 5-5 Phenolphthalein sprayed SMU blocks

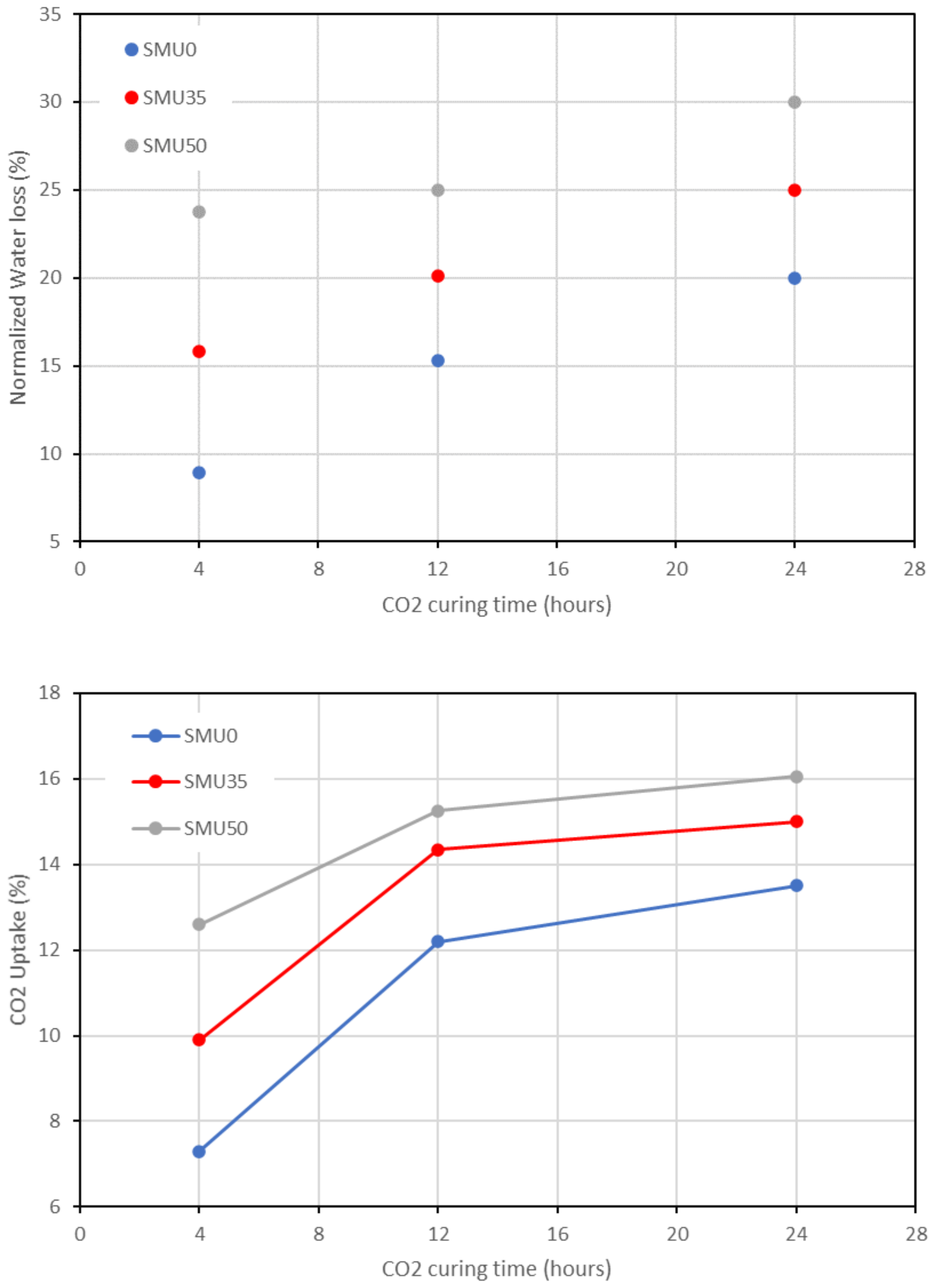

Figure 5-6 Results of SMU subjected to various carbonation durations: (A) Normalized water loss, (B) CO_2 uptake.

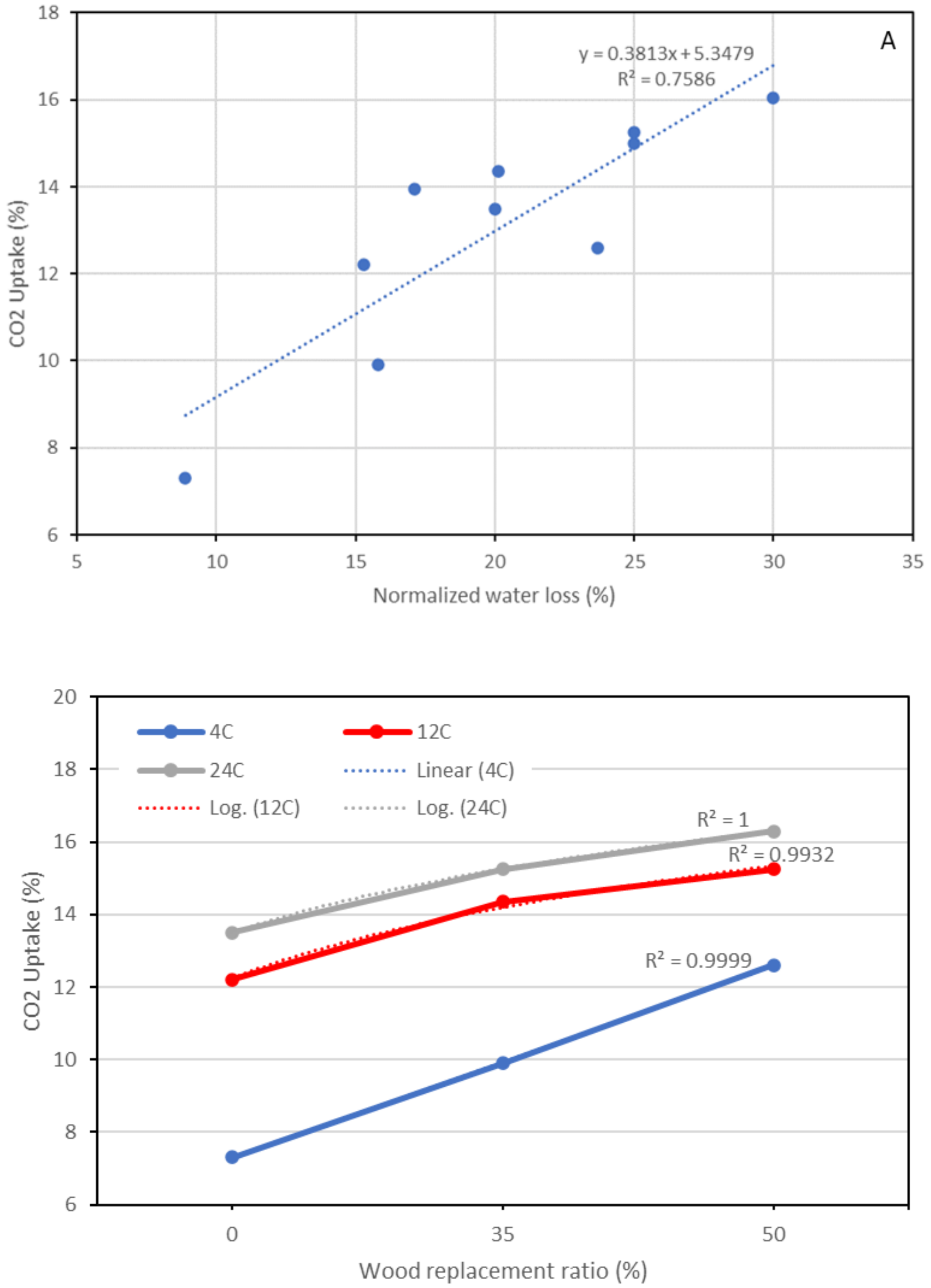

Figure 5-7 Results of different SMU: (A) CO_2 uptake as a function of water loss, (B) Correlation between CO_2 uptake and wood replacement ratio.

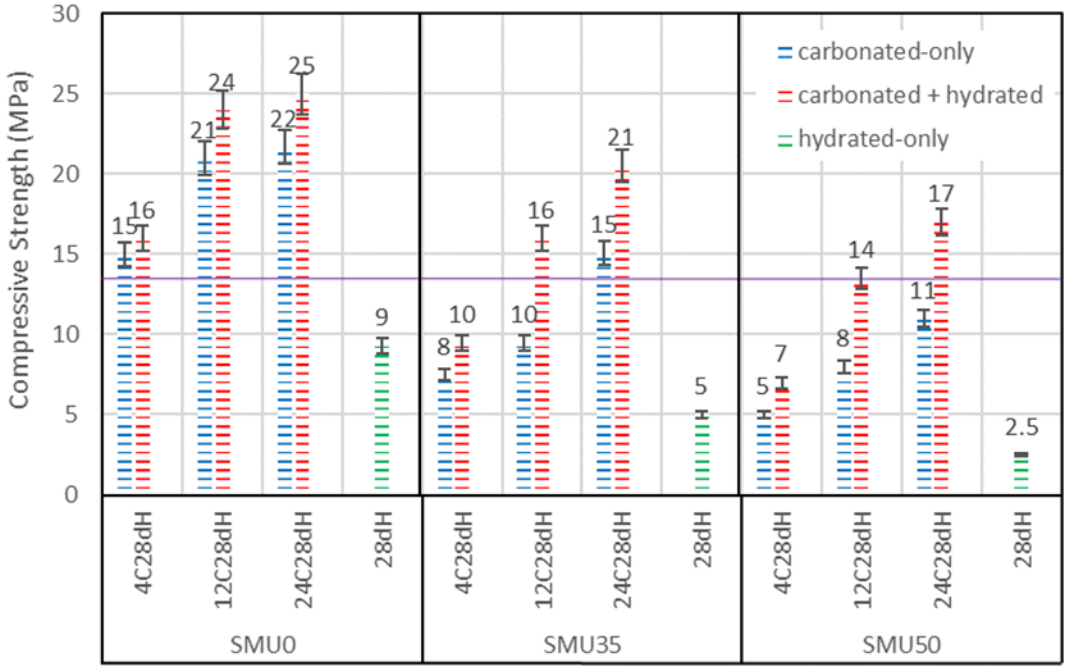

Figure 5-8 Compressive strength of SMU samples subjected to different curing scenarios.

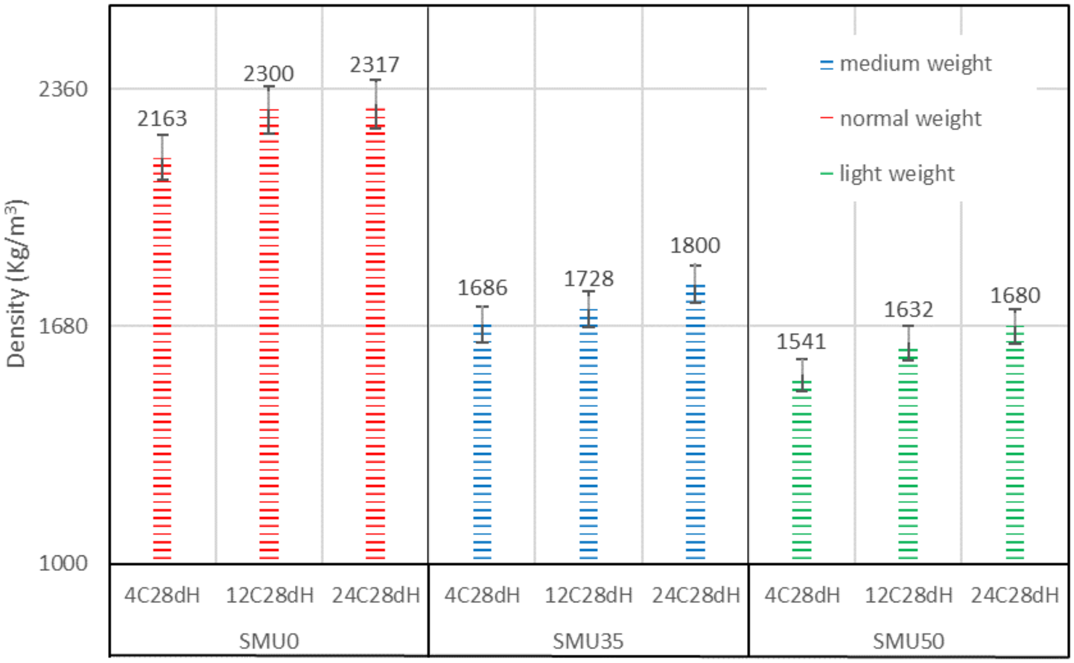

Figure 5-9 Density profiles of different SMU subjected to different curing durations.

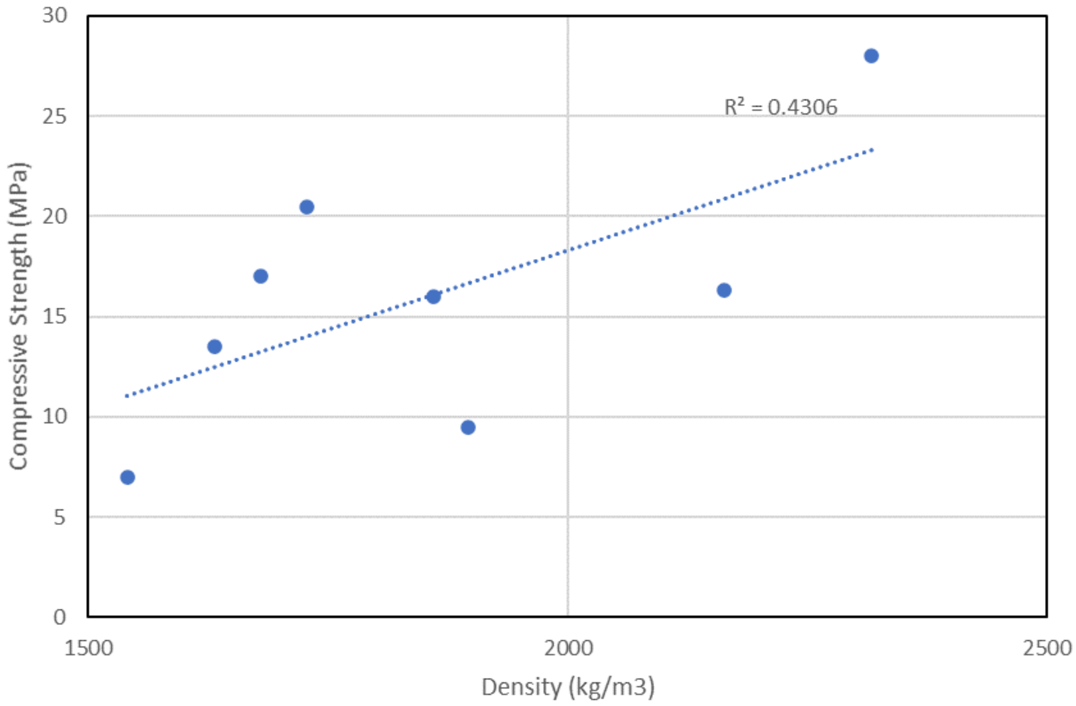

Figure 5-10 Linear correlation between compressive strength and density of different SMU.

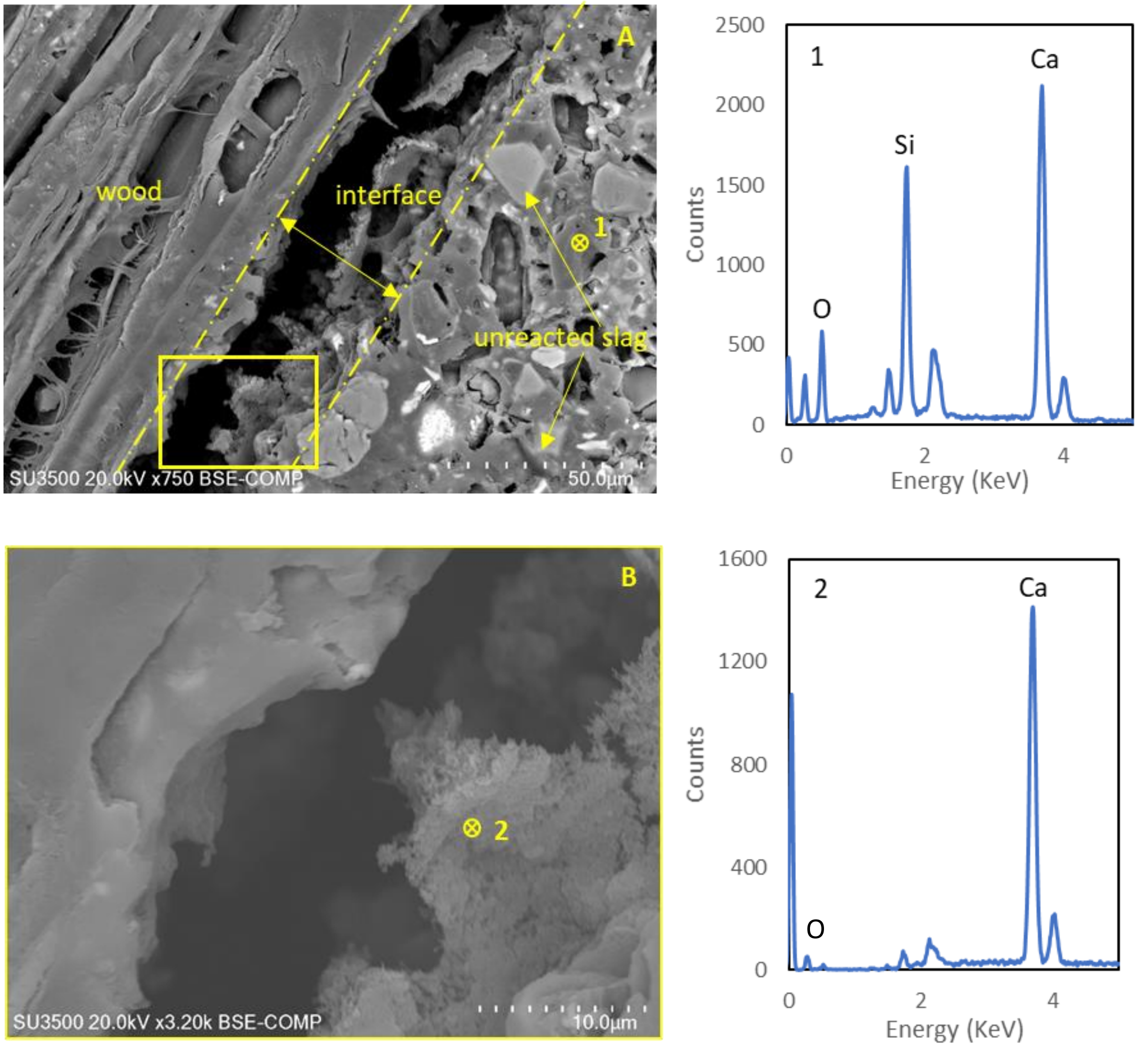

Figure 5-11 SEM-BSE of hydrated wood-slag samples (A) at 750x magnification, (B) at 3200x magnification.

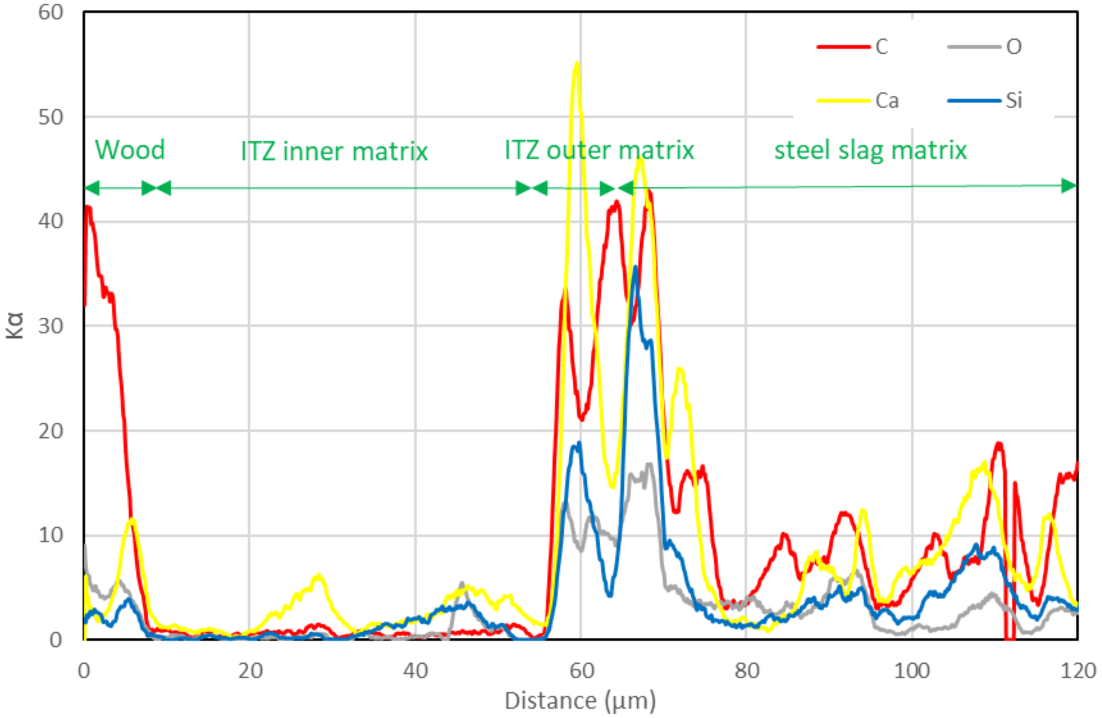

Figure 5-12 Element composition as a function of distance as obtained by line scan in hydrated sample.

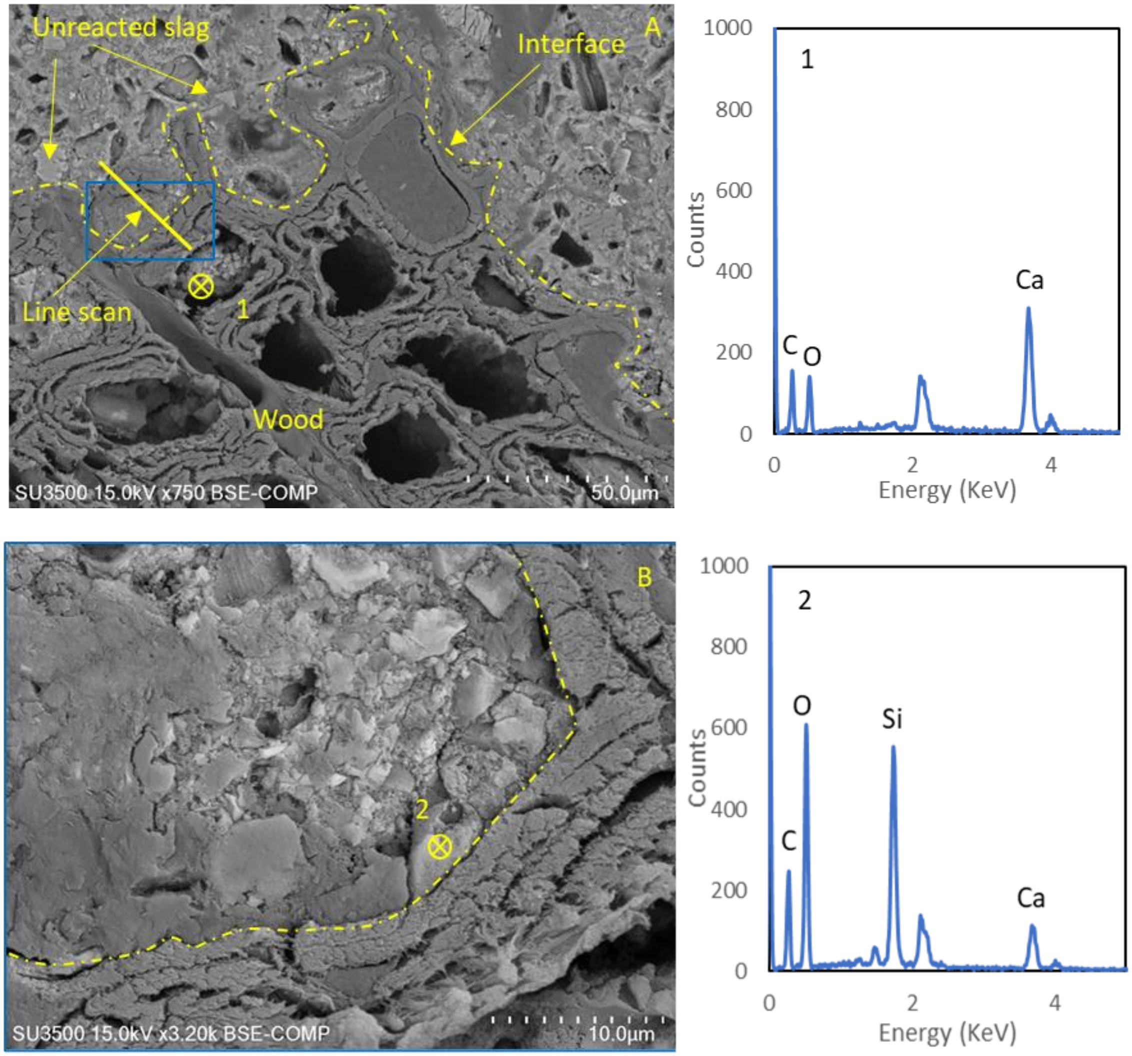

Figure 5-13 SEM-BSE of carbonated wood-slag samples (A) at 750x magnification, (B) at 3200x magnification.

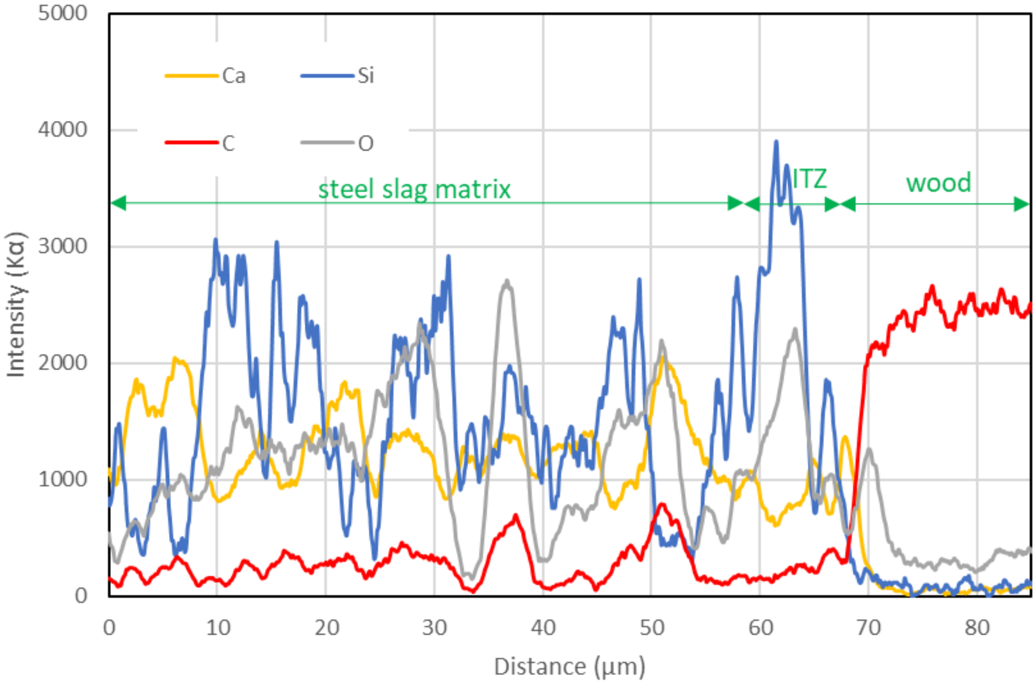

Figure 5-14 Element composition as a function of distance as obtained by line scan in carbonated sample.

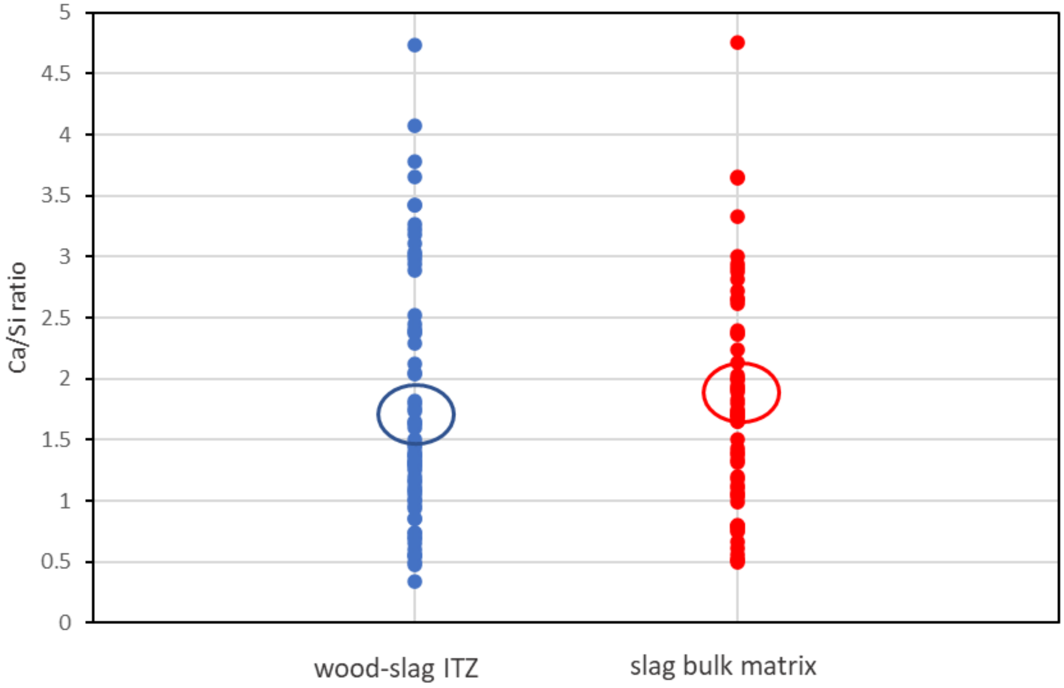

Figure 5-15 Ca/Si at wood-steel slag interface (blue) and Ca/Si in steel slag matrix (red) of carbonated samples.

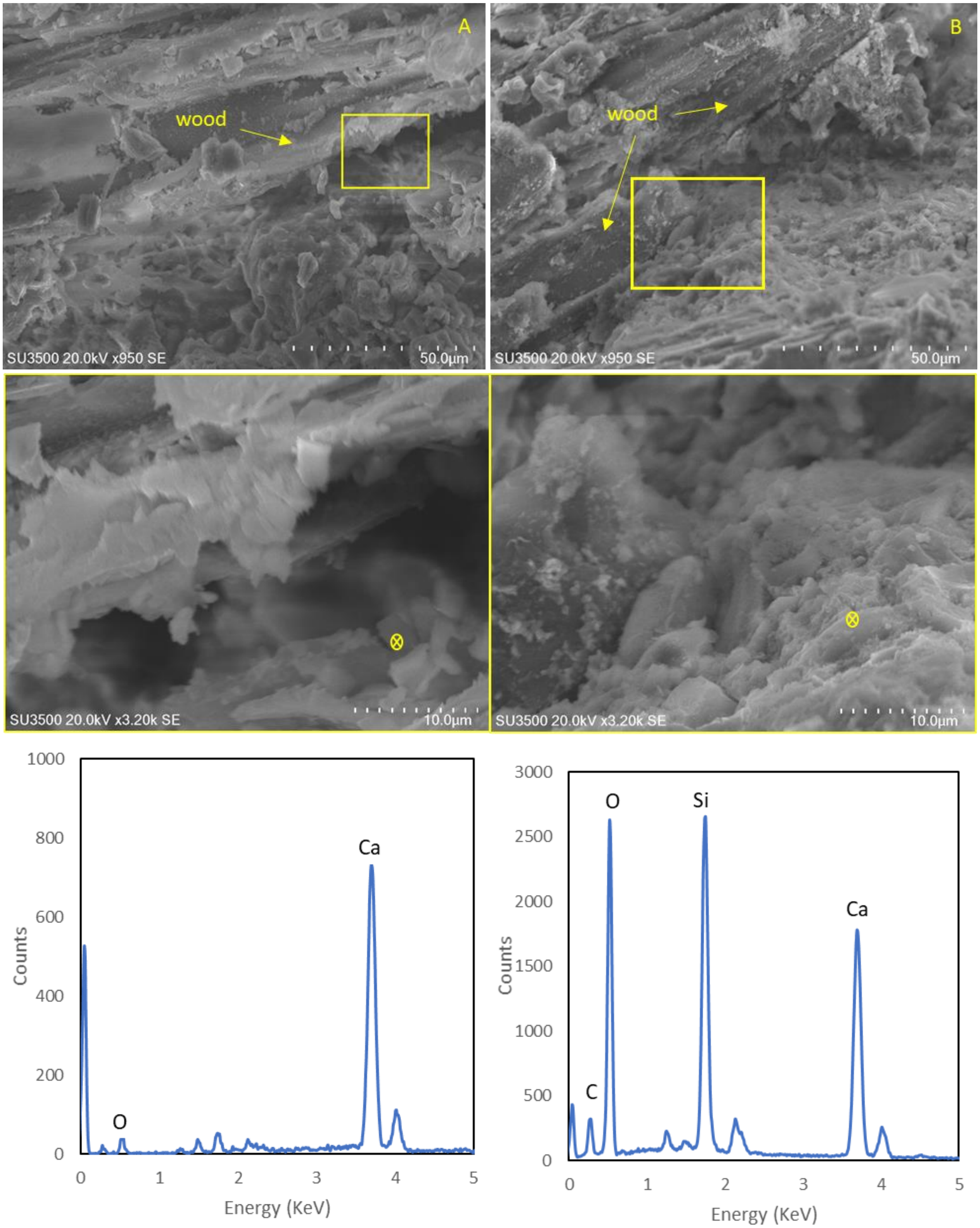

Figure 5-16 SE photomicrographs of fractured surfaces of wood-slag samples: (A) hydrated, (B) carbonated.

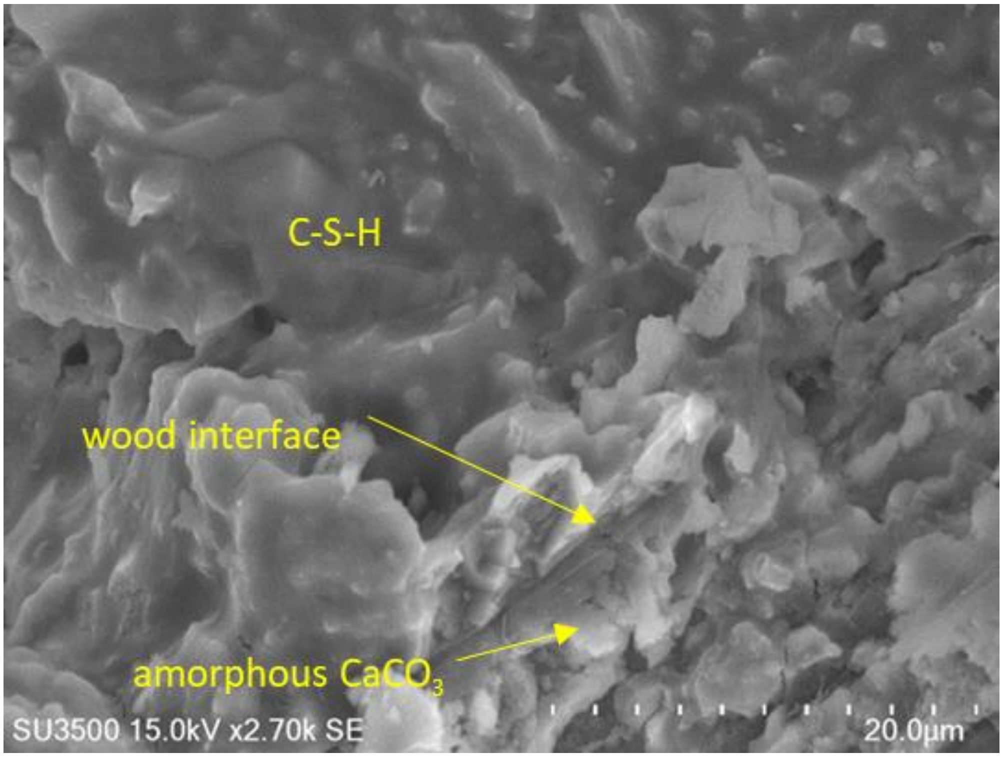

Figure 5-17 SE photomicrograph showing the interface between wood and steel slag.

6. Chapter 6 Flue Gas Carbonation of Steel Slag-Bonded Strand Board

Preface

Pure CO_2 gas separation from flue gas is an energy intensive process. Thus, pure CO_2 gas carbonation curing of common building products entails additional cost and environmental implications. To this end, in this chapter flue gas carbonation curing of steel slag bonded strand boards was studied for feasibility of utilizing kiln flue gas directly. Different carbonation temperatures were explored to optimize the flue gas carbonation process within a 24-hour carbonation window. The temperature and relative humidity inside the chamber were monitored. Microstructural tests were conducted to document the changes incurred under each curing condition. Results revealed that steel slag-bonded strand board could achieve a CO_2 uptake between 6-7 % by dry slag mass using flue gas. The mechanical performance of steel slag-bonded strand boards after a regime of carbonation and hydration curing were comparable to pure CO_2 gas carbonation. Lastly, the microstructure of steel slag bonded strand boards cured with pure and flue gas was found to be comparable after 28 days of subsequent hydration.

6.1 Introduction

Steel slag, the by-product of the steel making process, is a calcium silicate-rich material with latent hydraulic but no pozzolanic activity [1]. The weak hydraulic activity is mainly attributed to the amorphous nature of its SiO_2 content [2]. Furthermore, steel slag is rich in free CaO/MgO phases which, upon its addition to other building materials, can cause expansion and volume instability [2]. These drawbacks de-valued steel slag and limited its application as a binder. However, research has shown that carbonation curing can activate this material's early strength, giving rise to a binder of great potential [1-3]. Carbonation curing consumes free lime content thus mitigating the expansion problem [4]. Furthermore, during the curing process, CO_2 reacts with the calcium silicate phases in steel slag to form thermodynamically stable calcium carbonate ($CaCO_3$) crystals embedded within strength contributing calcium silicate hydrate (C-S-H) [1, 5, 6]. The principal reaction is given in Eq (1) [7].

$$2(2CaO \cdot SiO_2) + CO_2 + 3H_2O \rightarrow 3CaO \cdot 2SiO_2 \cdot 3H_2O + CaCO_3 \qquad (1)$$

The carbonation mechanism depends on the diffusion/permeation of CO_2 through the solid where CO_2 is dissolved in the pore spaces then hydrated to form carbonic acid (H_2CO_3). The carbonic acid subsequently ionizes to H^+, HCO_3^- and CO_3^{2-} which causes the pH to typically drop by 3 units. It is believed that the drop in pH stimulates the dissolution of calcium silicates, releasing Ca^{2+} and SiO_4^{2-} ions. This is followed by nucleation of calcium silicate hydrate (C-S-H) and the precipitation of $CaCO_3$ [7, 8]. Recent studies showed the potential of utilizing carbonation curing as an effective means of strength activation in steel slag-based building products [9],[10],[11].

Pure carbon dioxide is commonly used for carbonation curing of steel slag-based products. Research has shown that high purity gas increases the efficiency of the reaction, reduces the curing time as well as improves the CO_2 uptake [12]. Nonetheless, the flue gas purification process is energy intensive and significantly adds to the cost [13]. In this light, cleaner and more cost-effective building products could be produced if flue gas was to be used directly from the source.

Tian et al. explored the feasibility of using flue gas CO_2 in steel-making plants for the direct gas-solid carbonation of steel slag [14]. The temperature was the most important factor in carbonation conversion and reaction rate [14]. Nielsen et al. explored the influence of CO_2 concentration on the mineral carbonation of steel slag monoliths[15]. The main conclusion was that the rate of the reaction where the rate decreased with the decrease in CO_2 concentration. They also reported that for long durations of carbonation (100 hours), steel slag cured with lower concentrations of CO_2

performed better than steel slag cured at 100 % CO_2 [15]. Myers at el. reported that the mineral flue gas carbonation of basic oxygen furnace slag and electric arc furnace slag could achieve high net CO_2 uptake values within one hour [16]. Nonetheless, mineral carbonation despite its feasibility is expensive and energy intensive compared to other carbon dioxide capture and storage methods [17]. To this end, Moon et al. investigated the direct flue gas carbonation curing of a blended cement containing Portland cement and stainless-steel argon oxygen decarburization slag. However, in this study carbonation curing was extended to 28 days which is not viable for industrial production cycles.

Up to now, little attention has been given to the adoption of flue gas carbonation curing of steel slag-based building products. There are obvious advantages of flue gas utilization. Using flue gas directly from source is expected to significantly reduce the cost of manufacture which makes carbonated steel slag as binder more appealing for industrial upscale. Flue gas utilization directly as sourced would reduce emissions through re-utilization. Furthermore, the ideal scenario would be to set the production plants near the steel making plants which would also significantly cut down on the cost of transportation of both steel slag and flue gas. Nonetheless, limitations to flue gas carbonation curing need to be resolved.

The aim of this study is to use flue gas carbonation activation to develop steel slag bonded strand board within a 24-hour window to increase the likelihood of adoption by industry. The temperature and relative humidity in the curing chambers were reported. Furthermore, the carbon dioxide uptake was monitored. The mechanical and physical performance of the manufactured product were examined as per international standard requirements. Pure gas carbonation results were used as reference for comparison and overall performance assessment. Microstructural study by means of XRD, TG and FTIR was conducted to determine the products formed under each curing condition.

6.2 Experimental program

6.2.1 Materials

Steel slag used in this study was typically a ladle slag which was sourced from Harsco Environmental Quebec, Canada. Ladle slag is the by-product of the steel refining process. Its mineralogy is dependent on the appended fluxes, deoxidizing agents and cooling process. The as-received slag contained clumps that were first sieved out using an 850-µm sieve. The powder passing through the sieve was pulverized to a finer powder using a ring-and-puck mill (90 s per half-kilogram slag) to ensure homogeneity. Only slag powder that passed through a 150-µm sieve was used in this study. The major oxide components of the slag were identified by X-ray fluorescence (XRF) and results are presented in Table 6-1. The mineralogy of the powdered slag was determined by quantitative X-ray diffraction (Q-XRD) analysis using 10 % TiO_2 as an internal reference and are summarized in Table 6-2.

Poplar strands were selected for this study. Poplar trees have compelling physical characteristics for a variety of industrial applications such as board production as well as pulp and paper [18]. These trees grow fast and are moisture loving making it easier to cut strands, as the wood does not require steaming which is ideal for oriented-strand board (OSB) production. Poplar species are also known for their low densities which promote a good bond when manufacturing a composite because pressing will force the strands into close contact and thus yield a medium density-board with improved properties [18]. Table 6-3 summarizes the characteristics of the poplar strands used. The as-received strands were chopped down to a length of 5 to 10 cm to facilitate forming into lab-scale boards.

6.2.2 Production and Curing process

Table 6-4 summarizes the laboratory production parameters while the production process of a slag-bond strand board (SBSB) is illustrated in Fig. 6-1. Almost 30 % of the total mix water was used to prewet the chopped poplar strands prior to mixing. The strands were then hand mixed with steel slag and the remaining mix water for 10 min. Subsequently, the mix was evenly distributed to ensure a consistent density and placed into a 127 x 76 mm steel mold to make the board. The combined prewetting, mixing and forming process took less than 30 min. The mat was compact-formed to a thickness of 13 mm using a vibrating hammer and then pressed at pressure of 10 KPa for 1 hour to avoid spring back of strands. After pressing, the board samples were demolded and trimmed to remove any out-of-plane strands. The pressed boards were preconditioned in front of a fan for 30 minutes to evaporate almost 30 % of the water. The preconditioning step was necessary to create channels within the matrix for easier CO_2 gas penetration and ultimately higher carbonation curing efficiency. The boards were then subjected to three distinct curing scenarios to obtain: carbonated boards, combined carbonated and hydrated boards and hydrated-only boards.

For carbonated boards, the trimmed boards were transferred to a pressure chamber for carbonation curing. Several batches subjected to varying carbonation curing conditions including temperature, and CO_2 concentration were examined. Table 6-5 summarizes the curing conditions applied. Carbonation curing was conducted either with 20 % CO_2 gas used to simulate flue gas or with 100 % pure CO_2. The characteristics of the latter were adopted as reference. To control the temperature of the carbonation chamber, the chamber was placed in a water bath with a built-in heater (Tempco hydronic heating element) and a submergible pump to ensure the water circulation. The carbonation chamber was placed in the water bath one hour before the start of the curing process. The pressure inside the chamber was maintained by means of a regulator which assured that CO_2 was continuously replenished to counter the pressure drop arising from the reaction. The carbonation duration was fixed to 24 hours for all batches to maximize the reaction efficiency. The experimental apparatus used is presented in Fig. 6-2.

Half of the produced boards, referred to as SBSB-24C, were tested immediately to evaluate the properties of the carbonated-only boards. The remaining half, referred to as SBSB-24C28dH, were transferred to airtight plastic bags for subsequent hydration curing for 28 days at 22 ± 2 °C. Subsequent hydration was employed to maximize strength gain. Fig. 6-3 shows the produced SBSB.

Hydrated boards, referred to as SBSB-28dH, were placed in air-tight plastic bags immediately after demolding for 28 days of sealed curing at 24 ± 2 °C. These boards served as reference to highlight the effect of carbonation curing on the properties of produced boards.

6.2.3 Temperature and relative humidity monitoring

Temperature and relative humidity are key parameters that influence the carbonation process of steel slag. The exothermic nature of the carbonation reaction was monitored using a wireless temperature and relative humidity HOBO MX2300 data logger placed inside the carbonation chamber. The logger was configured to collect data every 30 sec during the carbonation process.

6.2.4 CO_2 uptake

CO_2 uptake was assessed on the basis of the mass gain method according to the calculation provided by Eq. 1. The carbonation reaction in calcium silicate systems resulted in mass increase of the specimens accompanying the formation of carbonation products. Therefore, specimens' mass was tracked before and after the carbonation reaction to estimate this mass-change ($Mass_{initial\ specimen}$ and $Mass_{carbonated\ specimen}$ in Eq. 1). As CO_2 reacted with raw slag, both water binding and water release took place during the reactions. The evaporated water that condensed on the internal walls of the carbonation chamber was carefully recovered using an absorbent paper and weighed ($Mass_{\text{collected water}}$ in Eq. 1). Since not all vaporized water can be collected, values obtained by the mass gain method represent a minimum conservative estimate. The net mass gain was normalized against the mass slag powder present initially in the sample ($Mass_{\text{slag powder}}$ in Eq.1).

$$CO_2 \text{ Uptake } (\%) = \frac{Mass\ carbonated\ specimen + Mass\ collected\ water - Mass\ initial\ specimen}{Mass\ slag\ powder} \qquad (1)$$

6.2.5 Mechanical Performance

Modulus of rupture (MOR) or flexural strength tests were performed as per ASTM D-1037. A three-point bending test was carried out over a span of 101 mm using an MTS-SINTECH 30/G tension and compression tester equipped with a 75 KN load cell. Tests were performed following dry and wet conditioning. A minimum of 3 specimens were tested and results averaged for each curing condition to obtain reproducible and representative results.

6.2.6 Physical Performance

Water absorption and thickness swelling tests were performed as per ASTM D-1037 requirements to evaluate the dimensional stability of the composites. Boards of various curing ages were submerged in water under ambient conditions for 2 or 24 hours. After submersion, the boards were withdrawn from water and left to drain in air for 10 min before excess surface water was dabbed with a paper towel. Water absorption values are reported as the percentage increase in weight based on the weight after conditioning. Thickness swelling of boards is expressed as percentage of conditioned thickness.

6.2.7 Microstructural Analysis

Square samples (of edge 4 cm) cut using a saw with alcohol applied as lubricant were obtained from the edge of the SBSB samples. These samples were dried at 60 °C for 24 hours and then milled using a mortar and pestle. The obtained powder was further sieved using a 200 µm sieve to separate the powder from the wood and then submitted to microstructural tests. The same powder was used for all microstructural tests.

Powder samples of SBSB subjected to various curing scenarios were analyzed by X-ray diffraction (Cu Kα radiation, scan interval 10-65° 2θ, 0.01°, and 0.5 s per step) using a Philips PW 1710 Powder Diffractometer (Philips, Amsterdam, Netherlands) to document how the mineralogy of the raw slag was modified by curing.

The thermogravimetric analysis (TG) allows the identification of constituent phases, including amorphous phases not detected by XRD, as each phase is characterized by a specific range of decomposition temperatures. To identify decomposition temperature ranges, differential thermogravimetric (DTG) curves were consulted. A thermal analyzer TG-Q500 coupled with Discover mass spectrometer (MS) detector was utilized. Approximately 30 mg of powdered sample were run under argon atmosphere (20 ml/min) over a temperature span of 30 to 1050 °C at a heating rate of 10 °C/min.

To identify the functional groups within amorphous and crystalline phases of the steel slag, Fourier transform infrared spectroscopy (FTIR) measurements were performed on a Nicolet 6700 FTIR spectrometer coupled with a Smart iTR module (FTIR-ATR). Spectra were recorded over the range of 4000 to 650 cm^{-1}.

6.3 Results and discussion

6.3.1 Temperature and relative humidity in chamber

Carbonation curing of calcium silicates is an exothermic reaction which is accompanied by water loss [19]. The temperature profiles generated by the carbonation reaction carried out at different conditions are shown in Fig. 6-4. Remarkably, stark differences were noted in the temperature profiles between different batches. A peak in temperature; nonetheless, was observed in all batches. This peak, whether periodic or single occurrence, signified the occurrence of the exothermic carbonation reaction delineated in Eq (1). The temperature curve of batch B1 which was cured at ambient temperature but elevated pressure with flue gas exhibited an increase of about 4 ℃ from ambient temperature. For B2, the temperature curve displayed a repetitive cyclic behavior where temperature appeared to fluctuate periodically between a maximum of 43 ℃ and a minimum of 37 ℃ with each cycle approximately 5 and a half hours. These cyclic fluctuations in curing chamber represent the heater cycles. Nonetheless, flue gas carbonated samples at elevated temperatures (B2 and B3) displayed the same trend where the peak temperature seemed to occur within the first 2 hours of carbonation and then decrease with the progression of the carbonation curing reaction which reflected that the reaction becomes less rigorous with time. Compared to B1, the reaction of B4 was more rigorous as reflected by the sharp increase of almost 10 ℃ with the CO_2 injection and was maintained for 1-2 hours and then dropped drastically to 22 ℃.

The relative humidity profiles are shown in Fig. 6-5. The humidity level inside the chamber increased upon CO_2 introduction and was maintained at around 90 % for all samples cured with flue gas. However, for pure gas carbonated boards B4, RH increased to a value of 75 % for 1-2 hours and then dropped and plateaued at around 65 %. With the injection of gas into the chamber, the carbonation reaction proceeded and caused water evaporation which effectively raised the RH in the chamber. In B4 samples, the RH then decreased with the deceleration in carbonation reaction rate. However, the same decrease was not seen in B1, B2 and B3 since the reaction with flue gas, although slower, was maintained with every gas replenishment cycle in the curing chamber. Also, the higher temperatures at which the reactions were carried out caused some of the water in the samples to evaporate and thus maintain a high RH.

6.3.2 Density and CO_2 uptake

Table 6-5 reports the density and CO_2 uptake of different carbonated and hydrated SBSBs. In general, carbonated boards had densities that were higher than the hydrated boards. Higher densities were attributed to the presence of carbonation reaction products, including $CaCO_3$ that is much denser than other hydration products such as C-S-H and $Ca(OH)_2$. The change in molar volume between the precipitated $CaCO_3$ and portlandite lies between 11 to 14 % depending on the nature of the $CaCO_3$ mineralogy [20]. The difference in densities was accompanied by different CO_2 uptake values in different batches. The highest density was recorded in samples cured with pure CO_2 gas at 1.39 g/cm^3 and 1.41 g/cm^3 in B4 and B5 respectively whereas the lowest density was recorded in hydrated-only SBSB and was found to be 1.21 g/cm^3. Indeed, carbonation curing is a densification process and the targeted boards acted as a sink for carbon and its permanent sequestration [21]. The CO_2 uptake recorded in B1 (6.2 %) increased to 7.3 % when the curing temperature was raised to 40 ℃. The B3 samples cured at 50 ℃ recorded a CO_2 uptake of 3.1 % by dry slag mass, almost half the CO_2 uptake recorded in B2 samples cured at 40 ℃. It seemed that higher temperatures were not favorable for the carbonation reaction. [15] revealed that higher temperatures decreased the rate of dissolution of CO_2 gas and since flue gas already has lower concentrations of CO_2 this could translate into less CO_2 dissolution and ultimately a lower reaction.

Reference samples cured with pure CO_2, recorded a CO_2 uptake of 13.4 % and 14.0 % for B4 and B5 respectively showcasing the ability of steel slag to readily react with CO_2 to form $CaCO_3$.

6.3.3 Mechanical and physical performance

MOR reflects the combined action of steel slag and wood strands, as the binder is responsible for bond stress and the wood provides tensile stress. The variability of these stresses depends on the interconnection of the strands [22] which, in turn, depends on the adhesion capabilities of the binder. Fig. 6-6 presents the MOR results recorded in boards subjected to different curing scenarios. The lowest strength was recorded in B0 where hydrated-only boards achieved a strength of 0.8 MPa after 24 hours of curing. The results highlighted that the hydrated steel slag is a weak latent hydraulic material that failed to bind the wood strands and resulted in a poor composite. In flue gas carbonated samples, the strengths recorded following 24 hours of curing were 6, 7.5 and 5 MPa in B1, B2 and B3 respectively. Evidently, carbonation curing activated the strength of steel slag and yielded a strong matrix that successfully bonded the wood strands together. The improved strength of the carbonated SBSB could be attributed to the CO_2 activation of γ-C_2S, the major constituent of the as-received slag and the mineral reported to have no hydraulic activity [23]. Increasing the curing temperature of the carbonation chamber to 40 ℃ yielded the best mechanical outcome in SBSB-24C. The counterpart pure gas carbonated samples recorded higher strength for the same curing age, of 8 and 9 MPa in B4 and B5 respectively. Flue gas carbonated boards were 1.5 MPa short of meeting the standard requirement by ASTM D1037 (9 MPa) at this age.

A subsequent 28-day sealed curing of the 24-hr carbonated strand boards led to significant increase in MOR in all boards. MOR in B0 increased to 2.6 MPa reflecting the latent hydraulic activity of the steel slag. The MOR in B1, B2 and B3 increased to 9, 11 and 8 MPa respectively. B3 samples cured at the elevated temperature of 50 ℃ failed to meet the ASTM D1037 requirement of 9 MPa.

This poor performance after elevated temperature curing could be explained by the accelerated water loss in the boards which resulted in a water-deprived composite and effectively slowed down the carbonation reaction. This is backed up by the fact that the wood strands immediately after the carbonation curing were dry and subsequently the mode of failure of these boards (B3) changed to a more brittle form.

It should be noted that the strength gain achieved by the subsequent hydration curing in carbonated boards confirmed that hydration after carbonation played a significant role in reinforcing the strength of strand boards. The early carbonation did not hinder subsequent hydration and the final strength resulted from the combined contribution of carbonation and hydration.

Water absorption (WA) and thickness swelling (TS) are physical properties that reflect the dimensional stability of boards and are key to a successful composite. Thickness swelling in boards is divided into two components: swelling induced by the wood's hygroscopic nature and swelling due to the release of compression pressure after the pressing/clamping time [24]. The latter, however, is non-recoverable when boards return to drier condition and is mostly referred to as "spring back"[24]. Results of these physical performance tests (WA and TS) performed on 24-hour cured boards are shown in Fig. 6-7 and 6-8 respectively. They were consistent with results of the mechanical performance tests. In general, carbonation-cured boards displayed superior performance than hydrated-only boards. The best performing carbonated board in terms of WA was B2 both at 2 and 24 hours following submersion with values reaching 2.7 and 6.7 % respectively. B3 performed worst among the carbonated boards with WA values reaching 8.3 and 14.7 % following 2 and 24 hours of submersion this might be, possibly due to the increased water evaporation in the sample subjected to the higher temperature creating more open pores. Nonetheless, all boards displayed values well below the standard limits of 15 and 25 % following

2 and 24 hours of submersion for WA and 2 % for TS. Conversely, the hydrated-only SBSB failed to meet the WA requirement and was marginal in TS. Hence, it was inferred that the precipitation of thermodynamically stable calcium carbonates upon carbonation curing contributed towards the superior dimensional stability of the carbonated strand boards. It could be surmised that precipitation of $CaCO_3$ in the pore solution filled the voids and limited water absorption [21]. The very low thickness swelling recorded in carbonated boards, as opposed to the very high value in hydrated boards, highlighted the ability of carbonation curing to limit the hygroscopicity of wood strands by effectively reducing the pore sizes. Also, elevating the curing temperature to 40 °C yielded the best outcome in terms of physical performance in flue gas carbonated boards.

It was interesting to note that the increase in thickness swelling between the 2 and 24-hr tests was smaller for carbonated boards (~24%) than for the hydrated-only boards (~44%), further highlighting the high dimensional stability gained by the carbonation treatment.

A further 28-day hydration of the carbonated-SBSB did not significantly improve their physical performance, implying that early carbonation curing was mostly responsible for their dimensional stability. As carbonation is a surface densification process, it contributes to porosity reduction especially at the surface [3] and thus created a less permeable barrier, preventing water seepage into the composite and promoting high dimensional stability.

6.3.4 Microstructural Analysis

XRD results revealed qualitative differences in the reactions at different temperatures and CO_2 concentrations in the carbonation curing chamber (Fig. 6-9). Freshly carbonated samples, displayed in Fig. 6-9(A), revealed a decrease in calcio-olivine and mayenite intensities to a varying degree. Comparison between samples cured under high pressure but ambient temperature using flue (B1) and pure gas (B4), respectively, revealed that carbonation curing led to higher intensities of calcite in the latter samples, consistent with the CO_2 uptake results. Increasing the carbonation temperature to 40 ℃, increased the intensity of the calcite diffraction peak (characteristic peak at 29.3 °) in both samples B2 and B5, but this increase was more prominent when using pure CO_2 gas. Increasing the temperature positively affected the CO_2 uptake capacity of samples regardless of the CO_2 concentration. Formation of calcite peaks in all samples apart from B0 was accompanied by a drop in calcio-olivine peaks (characteristic peaks at 15 °,29.6 °, 33 °) as delineated by eq. 1. Calcio-olivine displayed no hydraulic activity in sample B0, but engaged in the carbonation reactions of B1, B2, B3, B4 and B5 regardless of the carbonation conditions. Nonetheless, it was evident that calcio-olivine reacted more when the temperature was elevated to 40 ℃ compared to 22 ℃. Mayenite, however, seemed to react more in samples cured using flue gas (characteristic peak 17 °) to form higher peaks of katoite (characteristic peak 47 °). It is likely that at the low concentration of CO_2 in the flue gas this led to less carbonic acid formation in the pore solution and subsequently allowed for more aluminates to react. Interestingly, samples cured at 22 and 40 ℃ (i.e. B1 and B2) performed better than samples cured at 50 ℃. All in all, by comparing the 1-day peaks of samples cured with pure and flue gas it seemed that for this early age, pure gas performance was superior to that of flue gas.

XRD patterns appeared to be close between fresh carbonation and 28 days of subsequent hydration suggesting a vigorous mineralogical alteration in samples cured with pure CO_2. Nonetheless, subsequent hydration (Fig. 6-9 (B)) seemed to be much more significant in samples cured using flue gas where peaks of mayenite, larnite, jasmundite and periclase seemed to disappear owing to an active subsequent hydration reaction. The more vigorous subsequent hydration reaction occurring in samples subjected to an initial flue gas carbonation curing can be explained by the fact that more reactants were available to engage in subsequent hydration than in samples cured with pure CO_2 gas owing to a less vigorous initial carbonation reaction. Carbonation did not hinder subsequent hydration and seemed to promote hydration. This was confirmed by comparing the peaks of reactant minerals at 28 days. Samples B1 and B2 had lower peaks compared to hydrated-only B0. By comparing the 28-day peaks of samples cured with pure and flue gas it seemed that on this late age, flue gas performance was comparable to that of pure gas.

MS curves of detected water and CO_2 gas released during the thermal decomposition of SBSB are shown in Fig 6-10. The mass loss below 415 ℃ was associated with the decomposition of calcium aluminate hydrates (C-A-H), katoite, portlandite ($Ca(OH)_2$ and poorly crystallized calcium silicate hydrates (C-S-H) [9, 25, 26]. Above 415 ℃, de-carbonation was considered as the primary cause of mass loss induced by decomposition of amorphous $CaCO_3$, vaterite and aragonite, and well crystallized calcite [27]. The water release (MS18) profiles displayed a double peak distribution highlighting the presence of two major products: C-S-H and C-A-H at around 150 ℃ and katoite at around 350 ℃. Whereas the former was undetectable by XRD, the latter was confirmed through XRD data. The CO_2 gas (MS44) release curves showed an onset of de-carbonation at around 430 ℃. To verify the uniformity of the samples and thus the validity of the results, wood strands were submitted to TG coupled MS analysis. The thermal decomposition of wood was accompanied by the simultaneous release of water and CO_2 gas over the temperature range of 300 - 380 ℃ which overlapped with the decomposition temperature of katoite. Nonetheless, the latter released only H_2O upon decomposition. A weak bump of CO_2 release recorded at 380 ℃ revealed the presence of wood remnants in the sample; nonetheless, this peak was constant in all samples which made the comparison between samples valid.

DTG curves were plotted for each TGA of different SBSB, and the results are shown in Fig. 6-11. According to the MS curves and literature, weight loss in the peak of 700 ℃ is attributed to the decarbonation of calcium carbonates. Weight loss in dehydration of different silicate and aluminates can be observed below 380 ℃ for all samples. It was interesting to note no prominent peak due to de-hydroxylation of $Ca(OH)_2$ (380-430 ℃ [25]) which could be traced back to the poor hydraulic nature of the used steel slag. Other studies of carbonated steel slag reported similar observations [25]. It should be noted that the dearth of $Ca(OH)_2$ promotes the preservation of wood strands by providing a low alkalinity medium which prevents the long-term wood mineralization [28].

By comparing the DTG curves of samples at the age of 1-day (Fig. 6-11(A)), differences can be noted between samples cured under different conditions. Samples cured under pure gas (B4 and B5) were superior to samples cured under flue gas (B1, B2 and B3). A higher concentration of CO_2 promoted a more vigorous carbonation reaction. As surmised from the XRD results, increasing the carbonation curing temperature had a positive impact on the carbonation reaction in both samples B2 and B5 i.e., in both pure and flue gas cured samples. The decomposition temperature of formed $CaCO_3$ was the same for all samples (700 ℃) indicating that the carbonation temperature and CO_2 concentration, under the conditions adopted in this chapter, did not affect the mineralogy of $CaCO_3$s. The same however, cannot be said of carbonates formed due to weathering carbonation in hydrated-only sample (B0). These carbonates had a decomposition temperature different from those formed under carbonation curing. It should be noted that the decomposition temperature reflects the mineralogy or crystallinity of the precipitated $CaCO_3$.

The DTG curves of samples subjected to 28 days of hydration with or without initial carbonation are shown in Fig. 6-11(B). These curves revealed the formation of more hydration products in B1, B2, and B3 that decompose in the temperature range of 100-300 ℃ compared to either normal hydrated or pure gas carbonated samples indicating a more vigorous subsequent hydration reaction in flue gas carbonated samples as confirmed by XRD results.

In general, DTG results (Table 6-7) corroborated the XRD results. It is noteworthy that the hydrated-only boards (B0) recorded the highest water loss whereas their mechanical performance was 3-4 times less than carbonated boards at both ages (1-day and 28-day). This suggested that $CaCO_3$s play a major role in strengthening the amorphous C-S-H and C-A-H and ultimately contribute to the improved mechanical properties in carbonated boards. Likewise, Bukowski and Berger reported that $CaCO_3$ crystals promote the formation of a strong bonded matrix in calcium silicate systems [29].

Furthermore, the formed hydration products in samples cured with flue gas (B1, B2 and B3) were less abundant than those formed by pure gas carbonation (B4 and B5) at day 1. This trend, however, changed with subsequent hydration, as the hydration products were almost equally abundant regardless of the CO_2 concentration. The highest mass loss in hydration among the flue gas carbonated samples at both ages was recorded in boards B2 cured at 40 ℃. This observation was in alignment with the mechanical and physical performance tests where the best performance was seen in samples cured at 40 ℃. The amount of $Ca(OH)_2$ and calcium carbonate formed were estimated using the molar mass balance based on their equations and having the molar masses 18 g/mol, 100 g/mol, 44 g/mol, and 74 g/mol for H_2O, $CaCO_3$, CO_2, and $Ca(OH)_2$ respectively. Results are summarized in Table 6-8. By comparing B1, B2 and B3, it could be concluded that among the three tested temperatures, 40 ℃ performed best in terms of formed $CaCO_3$.

FTIR analyses were performed to further characterize the products formed under different curing conditions. The spectra are presented in Fig. 6-12. The peaks occurring at 711, 871, and 1048 cm^-

^{1} corresponding to the stretching vibration of C-O [30] were evidence of carbonate formation by carbonation curing. These peaks were strongest in samples cured with pure CO_2 (B4 and B5) which corroborated the results obtained by TG and XRD. The prominent peak at 848 cm^{-1} was attributed to calcio-olivine. This peak was the highest in hydrated-only samples, demonstrating its non-hydraulic nature. This peak decreased upon carbonation curing such that the lowest intensity was seen in B4 and B5. Hence, increasing the curing temperature to 40 ℃ improved the carbonation reaction of calcio-olivine as confirmed by TG and XRD. The broad hump observed between 3000-3650 cm^{-1} was associated with the stretching vibration of O-H in amorphous C-S-H. The intensity of this O-H bond was highest in pure gas carbonated samples (B4 and B5), indicating the deposition of more products. The broad peaks, with maxima between 920 and 1050 cm^{-1}, could be attributed to the asymmetric and symmetric stretching vibration of the Si-O bonds [31]. This C-S-H phase was present in hydrated and carbonated samples albeit at varying contents. It was interesting to note that the C-S-H formed in samples cured by flue gas and normal hydrated samples had the same wavenumber; but this wavenumber shifted to higher frequencies upon carbonation with pure gas (B4 and B5). The increase in intensity and wavenumber suggested an increasing polymerization of C-S-H in pure gas carbonated samples compared to flue gas carbonated samples. The very weak shoulder at 3650 cm^{-1} could be attributed to the O-H bond in some hydration products such as portlandite [30]. Interestingly, this peak was almost of invariant intensity for all samples which further reinforced the observation that steel slag is a weakly hydraulic material, and that carbonation does not hinder subsequent hydration.

Subsequent hydration results displayed in Fig. 6-12(B), revealed an increase in formed hydration products reflected in an increase in the intensity of the peak located between 3000-3650 cm^{-1}. The subsequent hydration reaction minimized the differences between pure and flue gas carbonated samples, results that complied well with the results of the TG and XRD analyses. This phenomenon was more prominent in samples cured at the elevated temperature of 40 °C. These findings further stress that subsequent hydration was necessary to optimize the performance and reduce the differences between pure and flue gas carbonated samples.

6.4 Conclusion

In this chapter, the results of the study on the feasibility of using flue gas to replace pure CO_2 gas in the carbonation curing of slag-bonded strand boards were reported. Renewable wood strands mixed with steel slag were formed into boards and subjected to various curing temperatures and CO_2 concentrations to optimize the flue gas carbonation process. The following conclusions can be drawn from this study:

1. Flue gas can be utilized to cure slag bonded strand boards. The CO_2 uptake in flue gas carbonated boards was less than that in pure gas carbonated boards, but the strength after 28 days of subsequent hydration was comparable.
2. The formation of C-S-H and $CaCO_3$ by flue gas carbonation curing led to boards that could display good mechanical and physical performance. Nevertheless, subsequent hydration was necessary for boards to conform with ASTM C1185 and ASTM D1037 requirements.
3. XRD, TGA, and FTIR analyses confirmed that carbonation does not hinder subsequent hydration. On the contrary, carbonation seemed to promote more hydration in flue gas carbonated samples.
4. Increasing the carbonation temperature to 40 °C yielded the best outcome, in terms of mechanical performance and CO_2 uptake, in both pure and flue gas carbonated samples. For flue gas carbonated samples at 50 °C, it was found that this temperature was not favorable for the overall performance of slag bonded strand board. The microstructure of

steel slag bonded strand boards cured with pure and flue gas was found to be comparable after 28 days of subsequent hydration.

5. The innovative slag-bonded wood composite displayed comparable performance to commercial wood-cement composites while preserving natural resources, recycling industrial wastes, promoting carbon negativity, and serving as a means of carbon storage.
6. In conclusion, flue gas can be utilized directly from source points to cure steel slag bonded strand boards. Direct utilization of flue gas can be beneficial for economic and environmental reasons through the reduction of CO_2 emissions and energy consumption. This would contribute towards a cleaner production in steel slag-based products and improve the sustainable development.

References

1. Mahoutian, M., Y. Shao, A. Mucci, and B. Fournier, *Carbonation and hydration behavior of EAF and BOF steel slag binders.* Materials and Structures, 2015. **48**(9): p. 3075-3085.
2. Humbert, P.S. and J. Castro-Gomes, *CO_2 activated steel slag-based materials: A review.* Journal of cleaner production, 2019. **208**: p. 448-457.
3. Ghouleh, Z., R.I. Guthrie, and Y. Shao, *High-strength KOBM steel slag binder activated by carbonation.* Construction and Building Materials, 2015. **99**: p. 175-183.
4. Abu-Eishah, S.I., A.S. El-Dieb, and M.S. Bedir, *Performance of concrete mixtures made with electric arc furnace (EAF) steel slag aggregate produced in the Arabian Gulf region.* Construction and Building Materials, 2012. **34**: p. 249-256.
5. Johnson, D., *Accelerated carbonation of waste calcium silicate materials*. 2000: Society of Chemical Industry Science Lecture Series.
6. Ghouleh, Z., M. Celikin, R.I. Guthrie, and Y. Shao, *Microstructure of carbonation-activated steel slag binder.* Journal of Materials in Civil Engineering, 2018. **30**(9): p. 04018217 DOI: https://doi.org/10.1061/(asce)mt.1943-5533.0002421
7. Young, J., R. Berger, and J. Breese, *Accelerated curing of compacted calcium silicate mortars on exposure to CO_2.* Journal of the American Ceramic Society, 1974. **57**(9): p. 394-397.
8. Bertos, M.F., S. Simons, C. Hills, and P. Carey, *A review of accelerated carbonation technology in the treatment of cement-based materials and sequestration of CO_2.* Journal of Hazardous Materials, 2004. **112**(3): p. 193-205.
9. Zod, N., A. Mucci, O. Bahn, R. Provençal, and Y. Shao, *Steel slag-bonded strand board as a carbon-negative building product.* Construction and Building Materials, 2022. **340**: p. 127695 DOI: https://doi.org/10.1016/j.conbuildmat.2022.127695

10. Mahoutian, M. and Y. Shao, *Production of cement-free construction blocks from industry wastes.* Journal of Cleaner Production, 2016. **137**: p. 1339-1346 DOI: https://doi.org/10.1016/j.jclepro.2016.08.012

11. Monkman, S., Y.X. Shao, and C.J. Shi, *Carbonated Ladle Slag Fines for Carbon Uptake and Sand Substitute.* Journal of Materials in Civil Engineering, 2009. **21**(11): p. 657-665 DOI: https://doi.org/10.1061/(asce)0899-1561(2009)21:11(657)

12. He, Z., S. Wang, M. Mahoutian, and Y. Shao, *Flue gas carbonation of cement-based building products.* Journal of CO_2 Utilization, 2020. **37**: p. 309-319 DOI: https://doi.org/10.1016/j.jcou.2020.01.001

13. Madejski, P., K. Chmiel, N. Subramanian, and T. Kuś, *Methods and Techniques for CO_2 Capture: Review of Potential Solutions and Applications in Modern Energy Technologies.* Energies, 2022. **15**(3): p. 887 DOI: https://doi.org/10.3390/en15030887

14. Tian, S., J. Jiang, X. Chen, F. Yan, and K. Li, *Direct Gas–Solid Carbonation Kinetics of Steel Slag and the Contribution to In situ Sequestration of Flue Gas CO_2 in Steel-Making Plants.* ChemSusChem, 2013. **6**(12): p. 2348-2355 DOI: https://doi.org/10.1002/cssc.201300436

15. Nielsen, P., M.A. Boone, L. Horckmans, R. Snellings, and M. Quaghebeur, *Accelerated carbonation of steel slag monoliths at low CO_2 pressure-microstructure and strength development.* Journal of CO_2 Utilization, 2020. **36**: p. 124-134 DOI: https://doi.org/10.1016/j.jcou.2019.10.022

16. Myers, C.A., T. Nakagaki, and K. Akutsu, *Quantification of the CO_2 mineralization potential of ironmaking and steelmaking slags under direct gas-solid reactions in flue gas.*

International Journal of Greenhouse Gas Control, 2019. **87**: p. 100-111 DOI: https://doi.org/10.1016/j.ijggc.2019.05.021

17. Mouedhen, I., N. Kemache, L.-C. Pasquier, E. Cecchi, J.-F. Blais, and G. Mercier, *Effect of pCO_2 on direct flue gas mineral carbonation at pilot scale.* Journal of Environmental Management, 2017. **198**: p. 1-8 DOI: https://doi.org/10.1016/j.jenvman.2017.04.048

18. Balatinecz, J.J. and D.E. Kretschmann, *Properties and utilization of poplar wood.* Poplar Culture in North America, 2001(Part A): p. 277-291.

19. Zhan, B., C. Poon, and C. Shi, *CO_2 curing for improving the properties of concrete blocks containing recycled aggregates.* Cement and Concrete Composites, 2013. **42**: p. 1-8 DOI: https://doi.org/10.1016/j.cemconcomp.2013.04.013

20. Shah, V., K. Scrivener, B. Bhattacharjee, and S. Bishnoi, *Changes in microstructure characteristics of cement paste on carbonation.* Cement and Concrete Research, 2018. **109**: p. 184-197.

21. Pizzol, V., L. Mendes, L. Frezzatti, H. Savastano Jr, and G. Tonoli, *Effect of accelerated carbonation on the microstructure and physical properties of hybrid fiber-cement composites.* Minerals Engineering, 2014. **59**: p. 101-106.

22. Caprai, V., F. Gauvin, K. Schollbach, and H. Brouwers, *MSWI bottom ash as binder replacement in wood cement composites.* Construction and Building Materials, 2019. **196**: p. 672-680.

23. Ashraf, W. and J. Olek, *Carbonation behavior of hydraulic and non-hydraulic calcium silicates: potential of utilizing low-lime calcium silicates in cement-based materials.* Journal of Materials Science, 2016. **51**(13): p. 6173-6191 DOI: https://doi.org/10.1007/s10853-016-9909-4

24. Halligan, A., *A review of thickness swelling in particleboard.* Wood Science and Technology, 1970. **4**(4): p. 301-312 DOI: https://doi.org/10.1007/bf00386406

25. Ghouleh, Z., R.I.L. Guthrie, and Y.X. Shao, *High-strength KOBM steel slag binder activated by carbonation.* Construction and Building Materials, 2015. **99**: p. 175-183 DOI: https://doi.org/10.1016/j.conbuildmat.2015.09.028

26. Mahoutian, M., Z. Ghouleh, and Y.X. Shao, *Carbon dioxide activated ladle slag binder.* Construction and Building Materials, 2014. **66**: p. 214-221 DOI: https://doi.org/10.1016/j.conbuildmat.2014.05.063

27. Zhang, D., X.H. Cai, and B. Jaworska, *Effect of pre-carbonation hydration on long-term hydration of carbonation-cured cement-based materials.* Construction and Building Materials, 2020. **231**: p. 117122 DOI: https://doi.org/10.1016/j.conbuildmat.2019.117122.

28. Toledo Filho, R.D., K. Ghavami, G.L. England, and K. Scrivener, *Development of vegetable fibre–mortar composites of improved durability.* Cement and Concrete Composites, 2003. **25**(2): p. 185-196 DOI: https://doi.org/10.1016/s0958-9465(02)00018-5

29. Bukowski, J.M. and R.L. Berger, *Reactivity and Strength Development of CO_2 Activated Non-Hydraulic Calcium Silicates.* Cement and Concrete Research, 1979. **9**(1): p. 57-68 DOI: https://doi.org/10.1016/0008-8846(79)90095-4

30. Xian, X.P. and Y.X. Shao, *Microstructure of cement paste subject to ambient pressure carbonation curing.* Construction and Building Materials, 2021. **296**: p. 123652 DOI: https://doi.org/10.1016/j.conbuildmat.2021.123652

31. Xian, X., D. Zhang, and Y. Shao, *Flue gas carbonation curing of cement paste and concrete at ambient pressure.* Journal of Cleaner Production, 2021. **313**: p. 127943 DOI: https://doi.org/10.1016/j.jclepro.2021.127943.

Tables

Table 0-1Chemical composition of raw ladle slag.

XRF analysis (wt. %)								
SiO_2	Al_2O_3	Fe_2O_3	MnO	MgO	CaO	Na_2O	K_2O	LOI
23.37	4.02	7.71	1.208	11.09	46.59	0.04	< 0.01	3.53

Table 0-2 Mineral composition of as-received ladle slag.

Q-XRD Rietveld analysis (wt. %)		
Mineral Compound	Chemical formula	
Calcio-olivine	γ-Ca_2SiO_4	53.1
Mayenite	$Ca_{5.65}Al_7O_{16.15}$	15.3
Periclase	MgO	10.0
Jasmundite	$Ca_{10.5}Mg_{0.5}$ Si_4 SO_{18}	9.7
Larnite	β-Ca_2SiO_4	3.0
Cuspidine	$Ca_4(Si_2O_7)F_2$	1.0
Portlandite	$Ca(OH)_2$	n.d.
Calcite	$CaCO_3$	n.d.
Amorphous		7.9

Table 0-3 Wood strand characteristics.

Wood-Strands			
Physical Specifications (mm)			
Length			100
Width		1.73	
Thickness		0.16	
Density (g/cm^3)	0.42		
Moisture Content (%)	0		
Water Absorption (%)	118.7		

Table 0-4 Laboratory production parameters of SBSB.

Manufacture parameters		Value
Length of board	(cm)	12.7
Width of board	(cm)	7.6
Thickness of board	(cm)	1.3
Wood to slag ratio		0.17
Water to slag ratio		0.35

Table 0-5 Carbonation curing schemes.

Batch	Curing	CO_2 Concentration	Carbonation Pressure	Carbonation Temperature	Curing Duration
B0	Hydration	N.A.	N.A.	N.A.	24 hours
B1	Carbonation	20 %	350 KPa	22 ℃	24 hours
B2	Carbonation	20 %	350 KPa	40 ℃	24 hours
B3	Carbonation	20 %	350 KPa	50 ℃	24 hours
B4	Carbonation	99.9 %	350 KPa	22 ℃	24 hours
B5	Carbonation	99.9 %	350 KPa	40 ℃	24 hours

*N.A. not applicable

Table 0-6 Oven-dried density and CO_2 uptake of carbonated and hydrated SBSB at 28 days.

Batch		B0	B1	B2	B3	B4	B5
Density	(g/cm^3)	1.21	1.36	1.30	1.27	1.39	1.41
CO_2 Uptake	(%)	-	6.26	7.25	3.06	13.35	14.02

Table 0-7 TG analysis of slag-bonded strand boards at 1 and 28 days.

Age	Batch	Mass loss in hydration products	Mass loss in $Ca(OH)_2$	Mass loss in $CaCO_3$
1-day	B0	4.63	0.42	0.84
	B1	3.40	0.43	8.12
	B2	3.31	0.40	8.22
	B3	4.34	0.64	8.29
	B4	3.67	0.73	12.87
	B5	4.50	0.84	13.8
28-day	B0	5.73	0.40	0.70
	B1	4.40	0.46	8.35
	B2	4.57	0.58	8.82
	B3	4.39	0.48	6.94
	B4	4.97	0.95	14.43
	B5	5.27	1.11	14.48

Table 0-8 Formed products in SBSBs subjected to various curing conditions by TG analysis.

Age	Batch	Formed $Ca(OH)_2$	Formed $Ca(CO)_3$
1-day	B0	1.73	1.91
	B1	1.77	18.45
	B2	1.64	18.68
	B3	2.63	18.84
	B4	3.00	29.25
	B5	3.45	31.36
28-day	B0	1.64	1.59
	B1	1.89	18.98
	B2	2.38	20.05
	B3	1.97	15.77
	B4	3.91	32.8
	B5	4.56	32.91

Figures

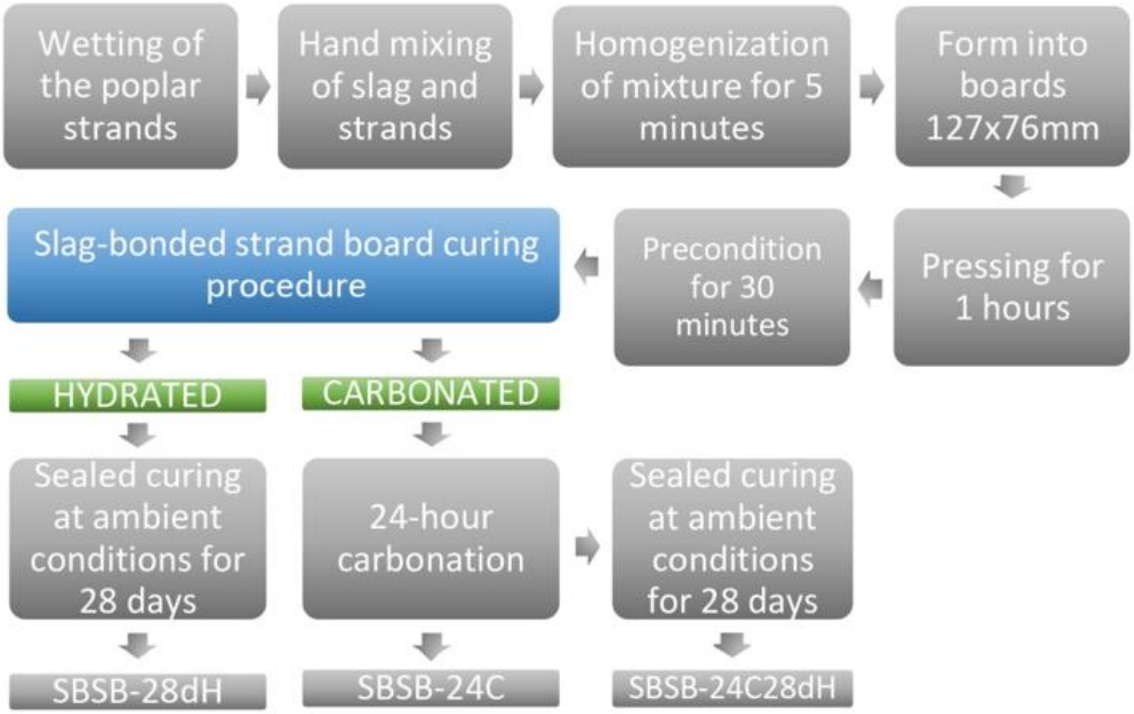

Figure 0-1 Production process of SBSB.

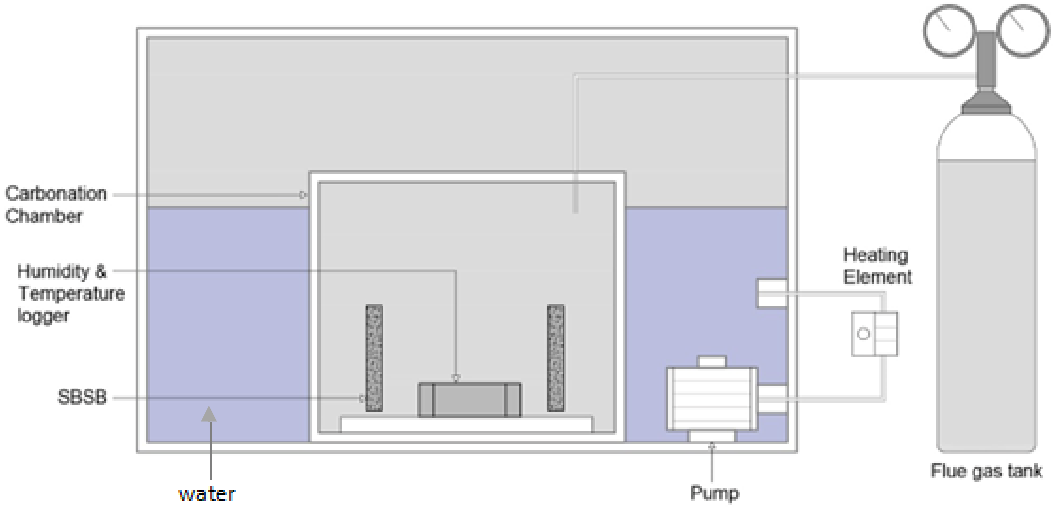

Figure 0-2 Carbonation setup for different SBSB samples.

*Figure 0-3 Photo of slag bonded strand board (12.7 * 7.6 *1.3 cm).*

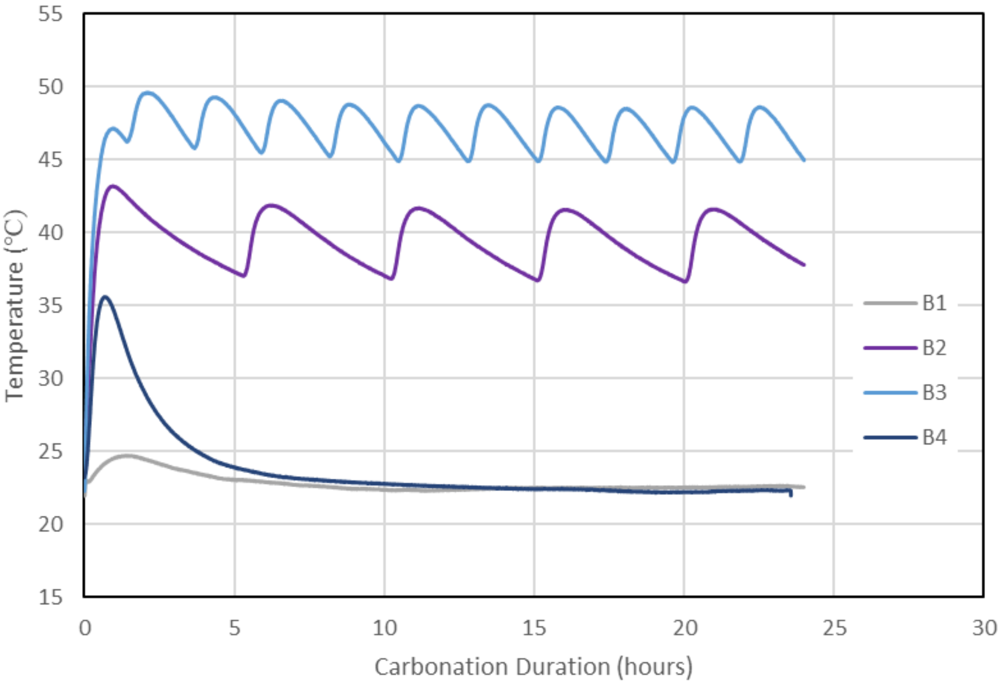

Figure 0-4 Fluctuations of temperature in carbonation chamber.

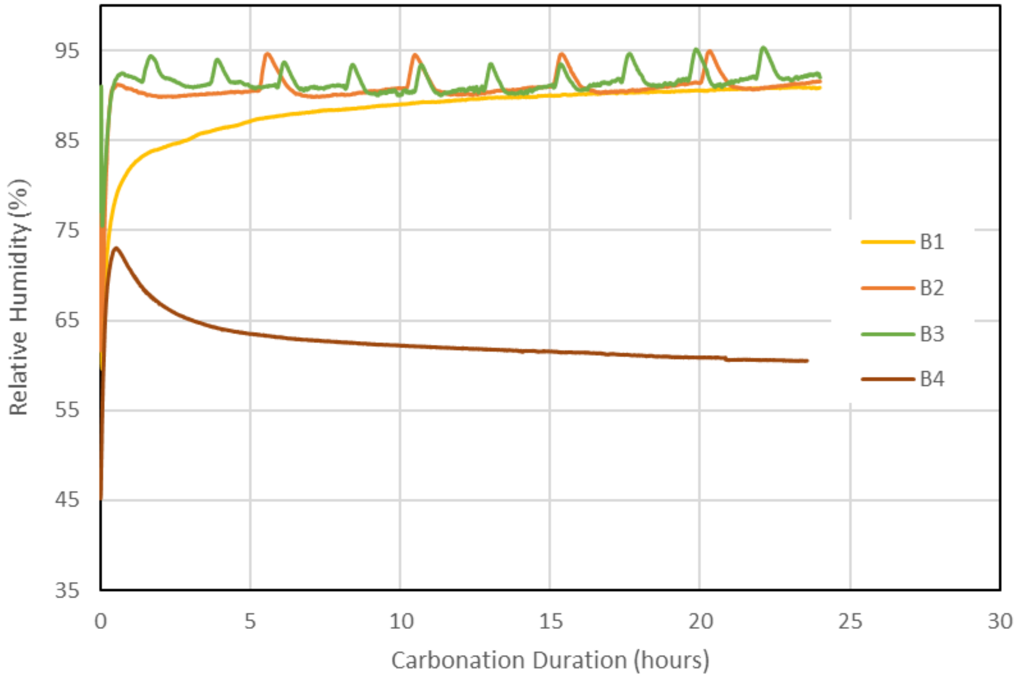

Figure 0-5 Changes in relative humidity in the carbonation chamber.

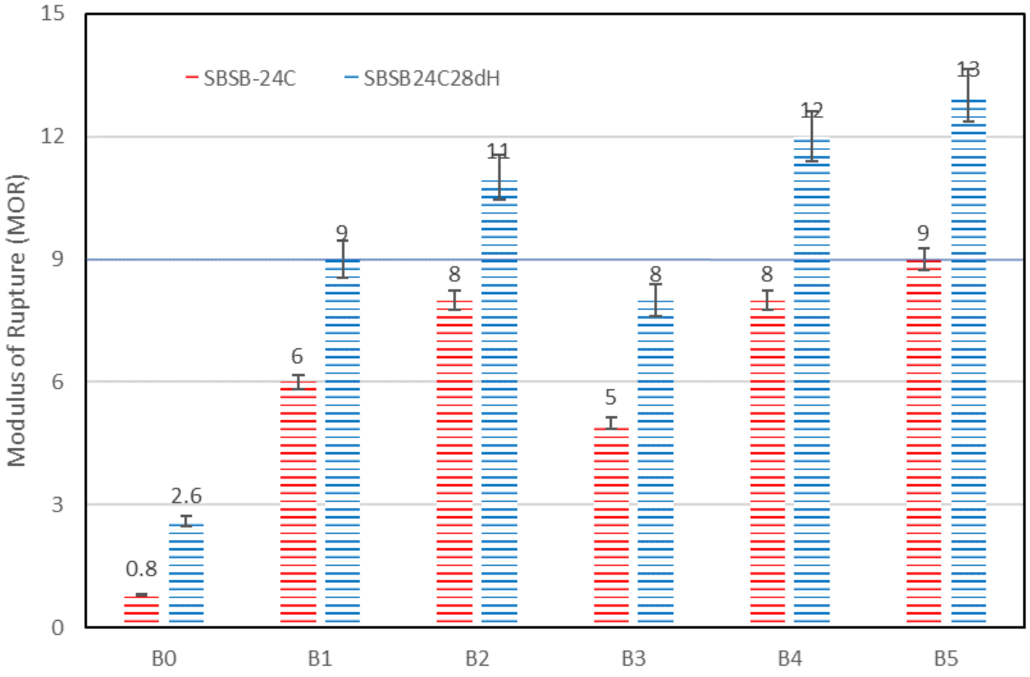

Figure 0-6 Mechanical performance of SBSB.

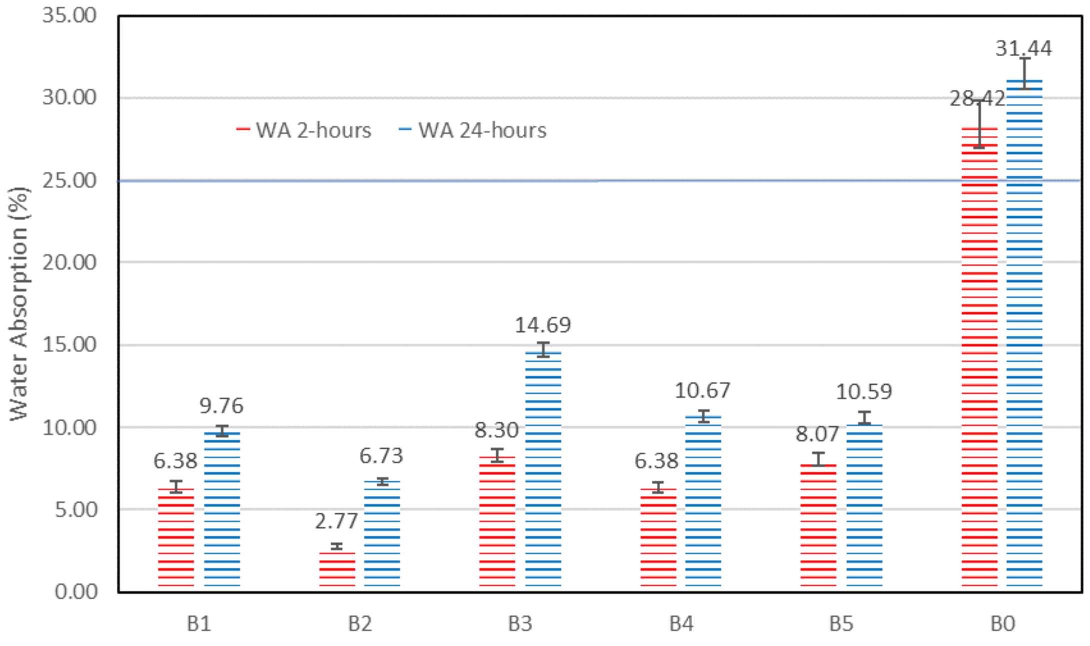

Figure 0-7 Water absorption performance of 1-day carbonated and 28-day hydrated SBSB after 2 and 24-hour submersion.

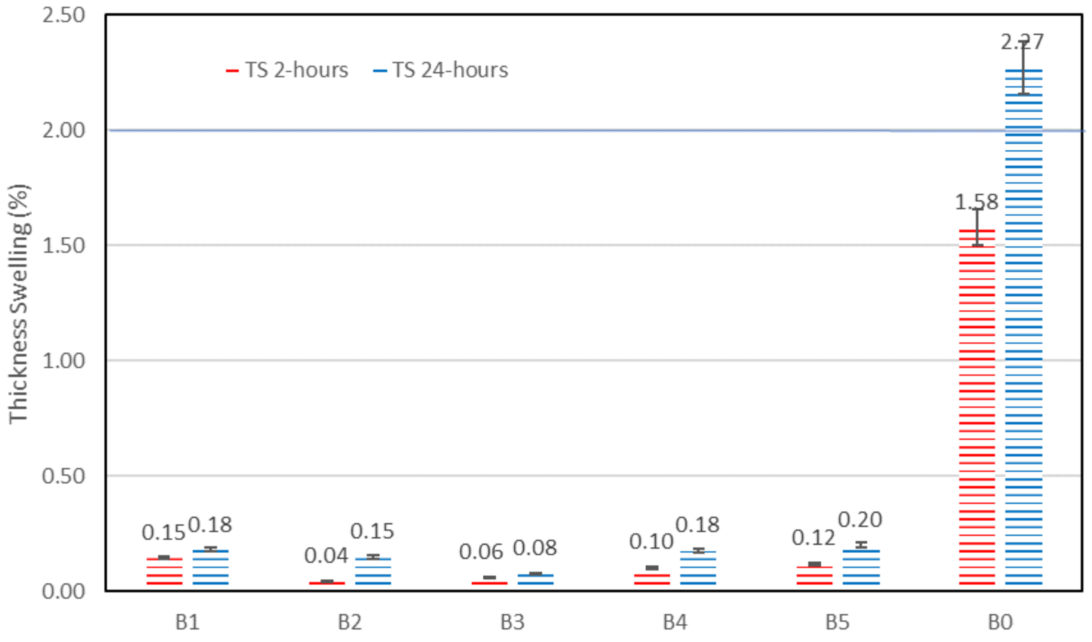

Figure 0-8 Thickness swelling in 1 -day carbonated and 28-day hydrated SBSB after 2 and 24-hour submersion.

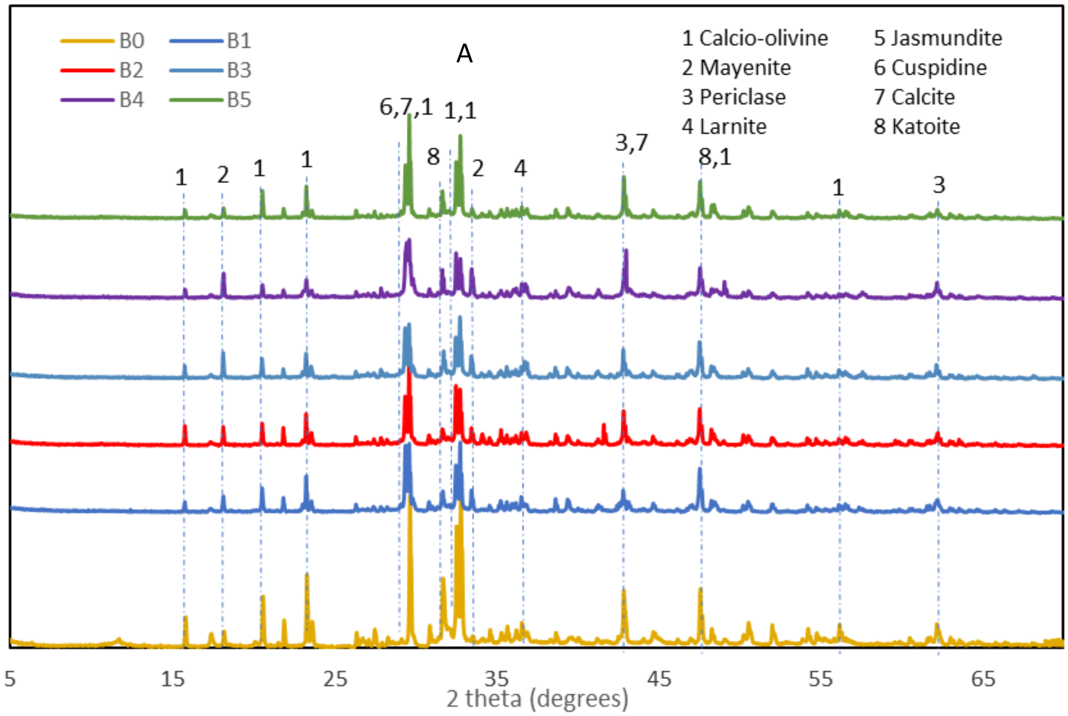

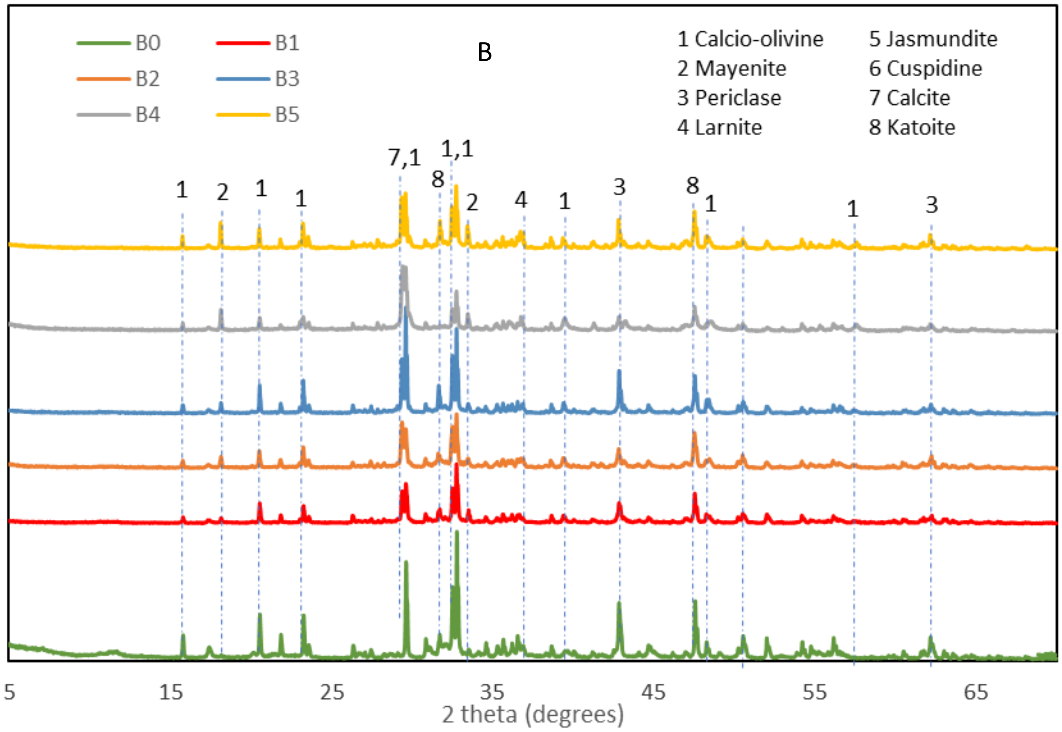

Figure 0-9 XRD curves of SBSB subjected to various curing scenarios: (A) 1-day aged samples, (B) 28-day aged samples.

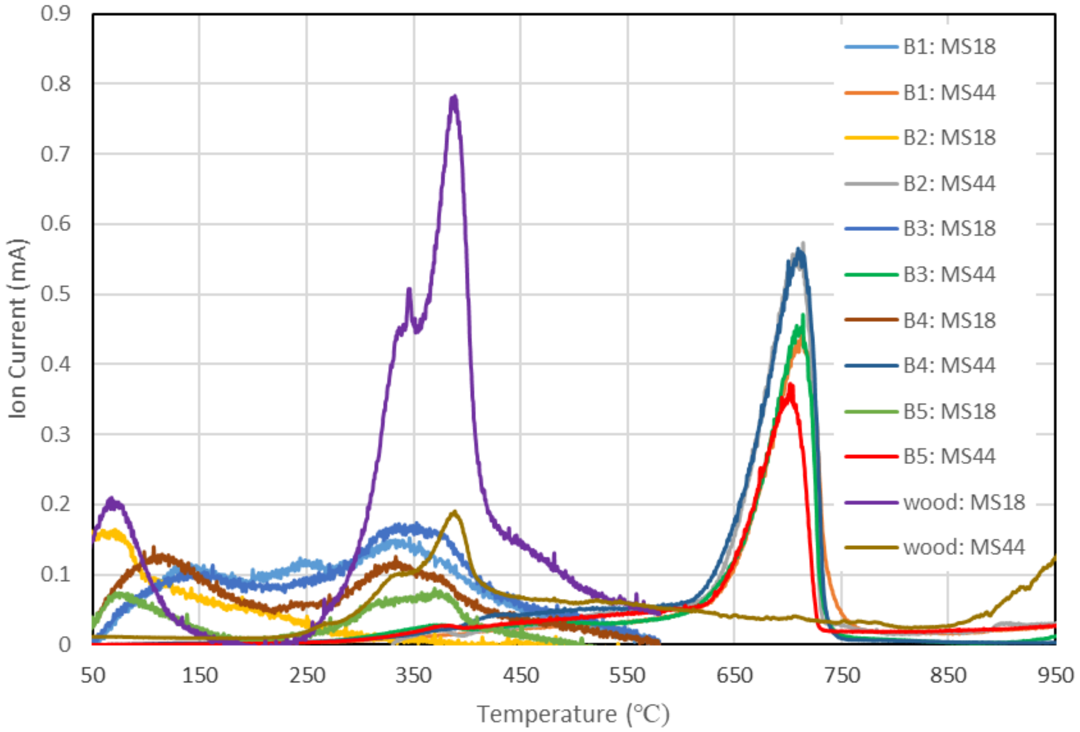

Figure 0-10 MS curves for water (MS18) and CO_2 gas (MS44) released during the thermal analysis of SBSB subjected to various curing scenarios following 24 hours of curing.

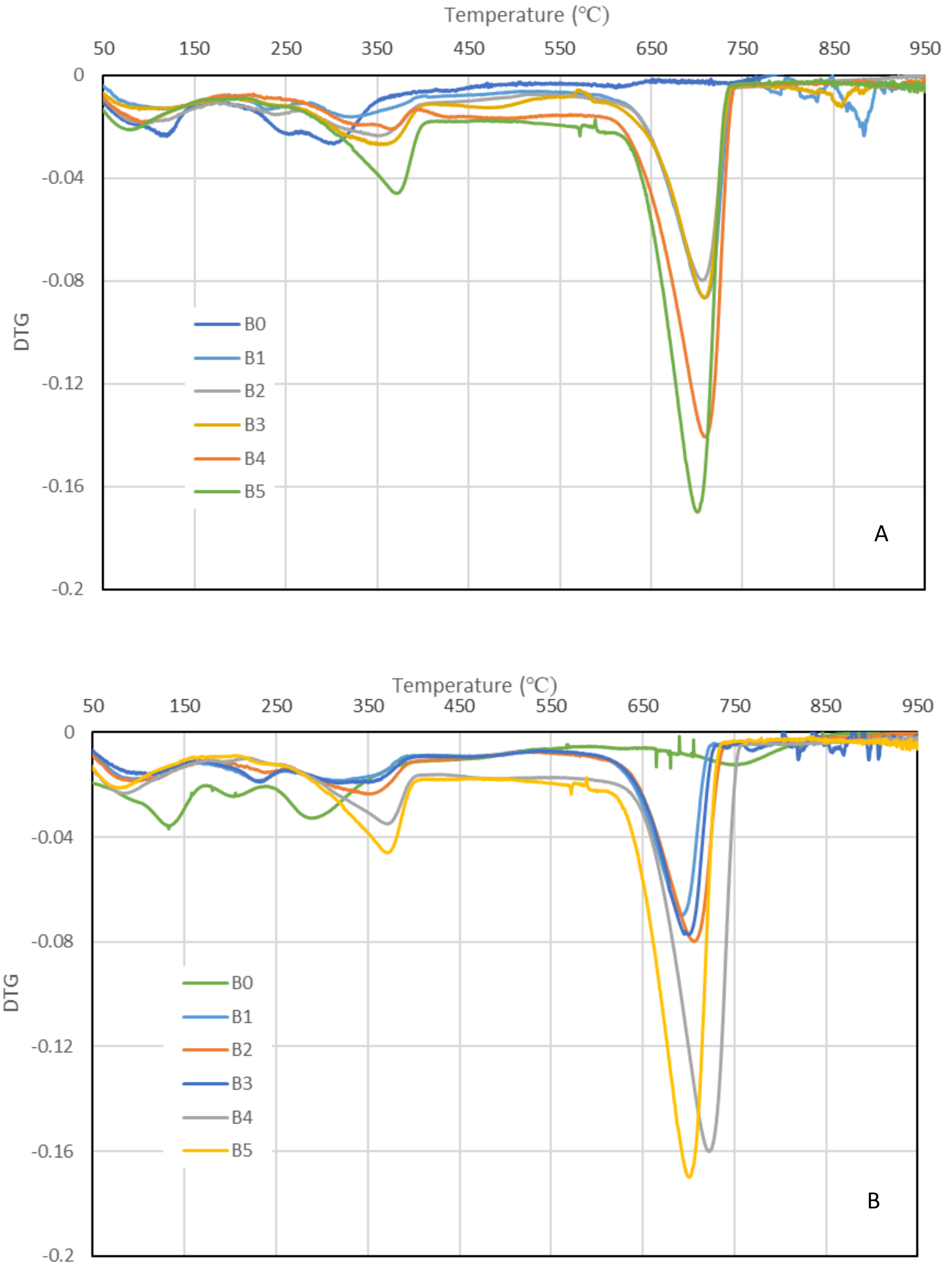

Figure 0-11 DTG curves of SBSB subjected to various curing scenarios: (A) 1-day aged samples, (B) 28-day aged samples.

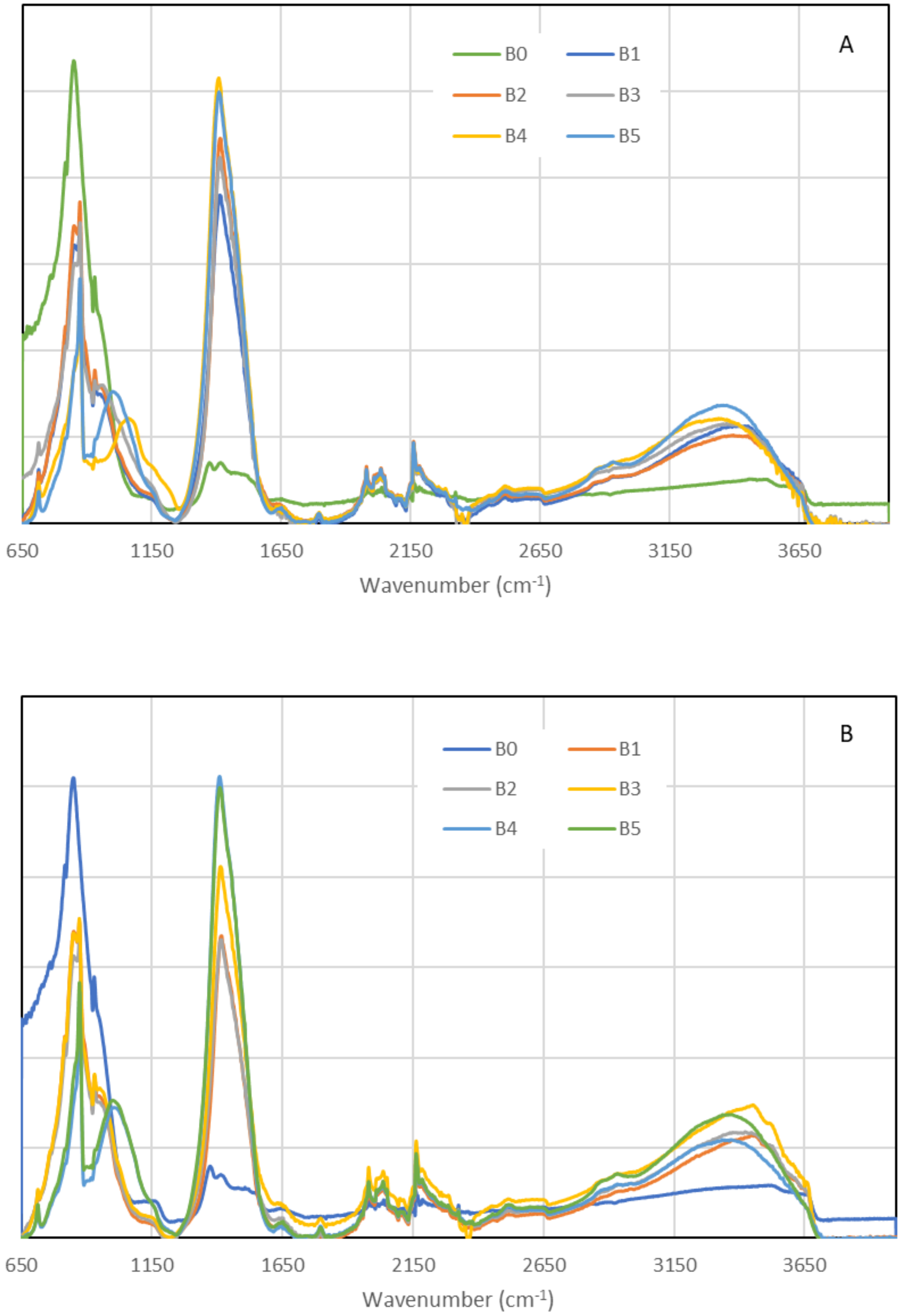

Figure 0-12 FTIR spectra of different SBSB: (A) 1-day cured samples, (B) 28-day cured samples.

7. Chapter 7 Conclusions

7.1 Conclusions

Steel slag, a by-product of steel industry, was investigated for binder innovation purposes. The carbonation and hydration activity were initially evaluated, and the mechanism of strength gain was investigated. Realizing that prolonged carbonation followed by subsequent hydration curing contributed substantially to strength, the combined carbonation-hydration curing scenario proposed in Chapter 3 was adopted in all subsequent chapters. The characteristics of the steel slag paste reported in Chapter 3 were used towards the development of wood-steel slag products. Chapter 4 explored the feasibility of manufacturing carbon-negative slag-bonded strand boards. In Chapter 5, the effect of wood replacement ratios and carbonation durations on production of wood-steel slag masonry units were studied. Lastly, Chapter 6, examined the feasibility of producing slag bonded strand boards using flue gas. Based on results of this study, the following conclusions were derived:

1. Steel slag displayed a weak hydraulic latent activity with an ultimate strength of 17 MPa recorded after 28 days of hydration curing. However, carbonation curing valorized the steel slag and a compressive strength of 46.8 MPa was recorded following 24 hours of carbonation curing. Subsequent hydration for 27 days further enhanced the strength and an ultimate strength of 70 MPa was achieved following a combined carbonation-hydration curing regime.
2. The strength of steel slag paste compacts increased with the increase in carbonation curing duration. Furthermore, the strength enhancement induced by subsequent hydration also increased with the increase in carbonation duration. These findings contrast with the performance of OPC paste compacts reported in the literature where it was found that the

strength was on the same order of magnitude regardless of the initial carbonation duration and that the strength enhancement induced by subsequent hydration decreased with the increase in carbonation duration. These revelations were explained by the microstructural changes induced by carbonation reaction in steel slag. Steel slag is a latent hydraulic material with weak activity and is mostly dominated by non-hydraulic minerals. Thus, when carbonation was introduced in the early stages this led to the formation of calcium silicate hydrate and calcium carbonates. With the increase in carbonation duration, the formed products were found to be a hybrid of calcium carbonates and gel phase (calcium silicate hydrate and calcium modified silica gel). Furthermore, increasing the carbonation duration induced these calcium carbonates to act as seeds promoting hydration and contributing towards an over-all higher strength. Thus, steel slag carbonation curing for prolonged durations, up to 24 hours, can improve the mechanical properties of steel slag. This strength enhancement effect would significantly reduce the production cost of steel slag-building products through eliminating the need to apply chemical or mechanical activation, as means to improve the strength.

3. Tests on steel slag-wood products revealed that wood can be used in a steel slag matrix to produce products that were performance equivalent and even superior to cement-based products.
4. Carbonation curing owed to the calcium carbonate precipitation contributed towards a slag bonded strand board with superior physical and mechanical performance.
5. The durability of wood-slag composites was explored through multiple tests performed on carbonated and on hydrated slag-bonded strand boards. It was revealed that carbonation curing limited the weathering carbonation induced by soak/dry cycles. Also, the weak

hydraulic activity of steel slag preserved the low alkaline medium induced by carbonation curing which led to an overall suitable medium for the long-term preservation of wood.

6. The innovative slag-bonded wood composite displayed comparable performance to commercial wood-cement composites while preserving natural resources, recycling industrial wastes, promoting carbon negativity, and serving as a means of carbon storage. A typical 2400 x 600 slag bonded strand board of thickness 12 mm could sequester approximately 1.62 kg of CO_2 through the carbonation curing process. A carbon balance analysis revealed that the end product was carbon negative.
7. Cost analysis showed that carbonated slag-bonded strand boards can be produced at a lower cost than commercial cement bonded strand board while offering greater environmental benefits.
8. Carbonation curing of steel slag masonry units incorporating recycled wood revealed that wood used even at 50 % by volume replacement of fine aggregates could meet the performance requirements of masonry units. It should be noted that literature survey of wood used as a partial replacement of any of the components showed that wood failed to meet the requirements for loadbearing uses and was deemed applicable for low grade applications only. Thus, this innovative masonry unit not only valorized steel slag but also recycled wood and resulted in a superior end product that combined the elements of performance and sustainability.
9. Carbonation curing of steel slag masonry units, also revealed that wood, owing to its geometry and compartmentalized structure, allowed for more CO_2 diffusion and ultimately more CO_2 sequestration and permanent storage. An ultimate CO_2 uptake of 16 % by dry slag mass was achieved in wood incorporating 50 % by volume of recycled wood.

10. The density of slag masonry units reduced almost 30 % when 50 % of the fine aggregates were replaced by wood particles. The developed wood-slag masonry units offer high performance while maintaining low densities.
11. Knowing that the interfacial transition zone (ITZ) is a main contributor towards mechanical performance, the study also examined the ITZ of wood-slag. It was revealed that the ITZ was devoid of cracks and pores, as carbonation products were deposited in the ITZ between the wood and slag. The ITZ of hydrated wood-slag was dominated by epoxy resin accounting for the poor bond and loose structure, while the matrix was dominated by voids and cracks. The Ca/Si of calcium silicate hydrate in the bulk carbonated matrix was almost the same as that in the wood-slag ITZ.
12. Flue gas can be utilized directly to cure slag-bonded strand boards. Direct utilization from source points can be beneficial for economic and environmental reasons.
13. Subsequent hydration was found essential in compensating the strength deficiency caused by the substitution of pure CO_2 gas by flue gas. Microstructural tests revealed that flue gas carbonation could promote more hydration. The best performance was achieved when the carbonation temperature was raised to 40 °C.

7.2 Suggestions for Future Work

1. The performance of steel slag paste was only studied for relatively short carbonation durations deemed acceptable for industry applications. It would be interesting to study the performance of steel slag when subjected to longer periods of carbonation namely 7 and 28 days, especially, to monitor the morphology and composition of reaction products.
2. More studies should be done on the formed products by carbonation curing to clearly identify the different phases formed through nanoindentations. Also, the elastic modulus and hardness of each phase should be reported.
3. Tests revealed that some minerals in steel slag were relatively inert in the carbonation process. More studies should be performed to try to activate these phases to make full use of the minerals present in as-received slag. A thorough analysis of the activity of minerals found in raw steel slag should be performed in order to provide the steel industry with suggestions as to what deoxidizing agents and cooling processes could promote cementitious phases in steel slag.
4. Durability performance tests of wood slag composites did not include an examination of the porosity changes. It would be more informative to do MIP tests to further support the findings of this study.
5. This study showed that slag-bonded strand boards upon ageing had rust deposits forming on them. De-ironizing the steel slag, using magnetic separation techniques to reduce the ferrous content prior to use, could be a possible solution. This should be further investigated to promote the likelihood of industrial adoption and commercialization.

6. More tests should be performed on the developed wood-slag masonry units. As this study only targeted lab-scale samples which simulated the web of the masonry unit, tests should be done on full scale commercial units to validate the performance.
7. Although, literature survey revealed that carbonation curing can effectively improve the resistance of concrete to elevated temperatures. A fire performance test on wood-slag masonry units is necessary and would bring the developed product one step closer towards industrial acceptance and commercialization.
8. The developed wood slag masonry units utilized wood chips only. It would be interesting to explore other types of wood residues such as saw dust or wood ash. It is important to study the effect of carbonation on different material systems as this is relatively new and knowledge on this topic is relatively limited.